

Flexible structure and solid-state transformation in silver(I) coordination polymers



Feifan Lang

A Thesis submitted to the University of Sheffield in partial fulfilment of the requirements for the degree of Master of Philosophy

April 2017

Department of Chemistry, University of Sheffield, Brook Hill, Sheffield S3 7HF

Abstract

Coordination polymer chemistry is a very active research field as it acts as a cross-linking subject between all branches of chemistry and also overlaps with physics, biology and materials science. With potential applications such as in catalysis, luminescence and molecular storage, the extensive involvement in industry and technology has made coordination polymers more attractive to scientists in developing novel functional materials. Meanwhile, the increasing recognition of green chemistry stimulates the combination of solid-state chemistry and coordination polymer chemistry at either the synthetic stage or the practical application where the guest adsorption/release involving the solid-state might be the most significant part.

The thesis describes research on families of silver(I)-perfluorocarboxylate coordination polymers with diimine ligands and contains four chapters.

Chapter 1 provides an overview of the basic characteristics of coordination polymers, and their synthesis, followed by an introduction to solid-state transformations and a brief summary of previous studies on a series of silver(I)-perfluorocarboxylate coordination polymers with diimine ligands that provide the foundation for the current project.

Chapter 2 describes the syntheses, characterisations and solid-state transformation studies of a series of silver(I)-perfluoroalkylcarboxylate coordination polymers with quinoxaline ligands. This project demonstrates a rare solid-state topological transformation from 4:4:4 ratio structures to 4:4:3 ratio structures by losing one coordinating quinoxaline ligand in the structure (4:4:x refers to the ratio of silver: perfluorocarboxylate: quinoxaline ligand in these coordination polymers).

Chapter 3 describes the syntheses and characterisations of a series of silver(I)-perfluoroalkylcarboxylate coordination polymers with 2-methylquinoxaline ligands. The aim of this part of the project was to test whether slight modification on the diimine ligand would cause differences to the structure formed. The results have shown many new structures and several of the compounds demonstrate the effect on the structures of trapping arene solvent molecules during syntheses.

Chapter 4 provides a brief summary of the main findings of the thesis project and some thoughts on possible future work.

Acknowledgements

My deepest gratitude goes first and foremost to Professor Lee Brammer, my supervisor, for his constant encouragement and guidance on a foreign student who is not majored in chemistry in the first place. He walked me through all the stages of this project patiently and scholarly and without his consistent and illuminating instruction, this thesis could not have reached its present form.

The Brammer group is a wonderful family with strong relationships and academic atmosphere. I would like to deserve my great thanks to all the members: Jamie Wright, Tom Roseveare, Elliot Carrington, Rebecca Smith and Daniel Watkins – for their kind advice, patient help and academic guidance. I would also send my gratitude to all the people who helps me through the project: Harry Adams and Craig Robertson for crystallography support, Mark Warren and Stephen Thompson for data collection at Diamond Light Source.

Last my thanks would go to my beloved family for their considerations and great confidence in me all through these years. I also owe my sincere gratitude to my friends here and the lovely British people for this wonderful period.

Author's declaration

The work described in this thesis is the original work of the author carried out in the Department of Chemistry, University of Sheffield or at Diamond Light Source between October 2015 and April 2017 and has not been submitted for any other degree before. Some data from previous studies necessary for full discussion of the research are included in the Chapter 2 and are referenced. The views expressed in this Thesis are entirely those of the author and not the University of Sheffield.

Feifan Lang

April 2017

Abbreviations

2-Me-Quin – 2-methyl-quinoxaline

2,3-dime-Quin – 2,3-dimethyl-quinoxaline

DCM – dichloromethane

DMF – *N,N*-dimethylformamide

***m*-xyl** – *m*-xylene

***o*-xyl** – *o*-xylene

***p*-xyl** – *p*-xylene

Quin – quinoxaline

SBU – Secondary Building Unit

SCSC – Single-Crystal-to-Single-Crystal

tol –toluene

TMP – 2,3,5,6-tetramethylpyrazine

Phen – Phenazine

SCXRD –Single Crystal X-ray Diffraction

PRXD –Powder X-ray Diffraction

Table of contents

1.Introduction	3
1.1 Coordination polymers– A review.....	3
1.1.1 Porous structures and metal-organic frameworks (MOFs).....	3
1.1.2 Applications.....	6
1.2 Synthesis of coordination polymers.....	10
1.2.1 Solvothermal processes.....	10
1.2.2 Diffusion.....	11
1.2.3 Solid-state synthesis.....	13
1.3 Solid-state chemistry with coordination polymers.....	15
1.3.1 Solid-state transformations.....	15
1.3.2 Potential applications of solid-state transformations.....	17
1.4 Silver(I)-based coordination polymers.....	19
1.4.1 Review of silver(I) coordination polymers.....	20
1.4.2 Coordination polymers from silver(I) perfluorocarboxylates combined with diamines/diimines.....	22
1.4.3 Project overview.....	27
1.5 References.....	29
2. Structures and solid-state transformations of coordination polymers containing silver perfluorocarboxylates combined with quinoxaline	33
2.1 Introduction.....	33
2.2 Experimental.....	35
2.2.1 Synthesis.....	35
2.2.2 Single Crystal X-ray Diffraction (SCXRD).....	38
2.2.3 Powder X-ray Diffraction (PXRD).....	42
2.2.4 Thermogravimetric analyses (TGA).....	47
2.2.5 In situ PXRD heating studies.....	53
2.2.6 Dielectric constant test.....	64
2.3 Results and Discussion.....	64
2.3.1 Synthesis and Crystal Structures.....	64

2.3.2 Solid-state transformation of 4:4:4 [Ag ₄ (O ₂ C(CF ₂) _n CF ₃) ₄ (Quin) ₄] to 4:4:3 [Ag ₄ (O ₂ C(CF ₂) _n CF ₃) ₄ (Quin) ₃]	73
2.3.4 Dielectric constant test	86
2.4 Conclusions	88
2.5 References	89
3. Coordination polymers containing silver perfluoroalkylcarboxylates combined with 2-methylquinoxaline: structures and solvent effects	91
3.1 Introduction	91
3.2 Experimental	94
3.2.1 Synthesis	94
3.2.2 Single Crystal X-ray Diffraction (SCXRD)	97
3.2.3 Powder X-ray Diffraction (PXRD)	102
3.2.4 Thermogravimetric analyses (TGA)	105
3.3 Results and Discussion	107
3.3.1 Structure determination	107
3.3.2 PXRD data collections	120
3.3.3 Thermogravimetric analyses (TGA)	123
3.4 Conclusion	125
3.4 Reference	126
4. Conclusions	127
4.1 Conclusion	127
4.2 Future work	130
4.3 References	130

1.Introduction

1.1 Coordination polymers- A review

The study of coordination polymers has taken an important place in chemical research since they were first discovered. Tens of thousands of coordination polymers have now been reported¹ and their potential applications have covered a wide range of scientific areas, including catalysis, molecular adsorption and storage, pharmaceuticals and the development of a new generation of advanced materials. Along with the development in related subjects such as supramolecular chemistry, X-ray crystallography and materials science, coordination chemistry has become a new tool in discovering novel functional materials.²

Coordination polymers consist of architectures formed from metal-ions and ligand molecules, which crystallise along with the guest molecules in some cases. Different preferences in coordination geometry for metal ions lead to different spatial preferences in the networks formed by coordination polymers. Coordination polymers can form one-, two- or three-dimensional networks of a variety of topologies. 2D and 3D networks can lead to coordination polymers that exhibit porosity, resulting in a number of interesting properties. Also, intermolecular interactions play an important role in stabilizing the structures of coordination polymers. Several types of intermolecular interactions such as hydrogen bonds³, π - π stacking⁴ and halogen bonds⁵ exist in certain types of coordination polymers, but coordination bonds, obviously, lay the solid foundation for all these compounds.

1.1.1 Porous structures and metal-organic frameworks (MOFs)

The structures of porous coordination polymers are affected by the choices of different metal ions, organic ligands, solvents, etc. Internal pores exist in these one-, two- or three-dimensional architectures or can be formed by the intermolecular-networks. Porous coordination polymers are generally referred to as metal-organic frameworks (MOFs).⁶ A wide varieties of functional groups inside the pores or channels or designed flexible structures endow MOFs with great potential in post-synthetic modification and crystal engineering.

The first coordination polymer framework was reported by Hoskins and Robson in 1989 (**Figure 1.1**). This infinite metal-organic framework, $[\text{Cu}\{\text{C}(\text{C}_6\text{H}_4\text{CN})_4\}]^+$, established the new possibility of designing and synthesizing new types of molecular-sized cavities by linking metal ions and organic ligands.⁷

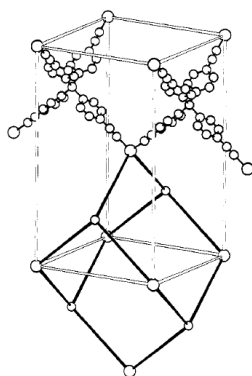


Figure 1.1 Structure of the infinite $[\text{Cu}\{\text{C}(\text{C}_6\text{H}_4\text{CN})_4\}]^+$ diamondoid network. (Figure reproduced from ref. 7).

Yaghi and coworkers made early developments of MOFs such as MOF-5 (**Figure 1.2**),⁸ which has an extremely high non-framework space (>80% of the structure), as well as good thermal stability, and exhibits favourable absorption of a number of gases.

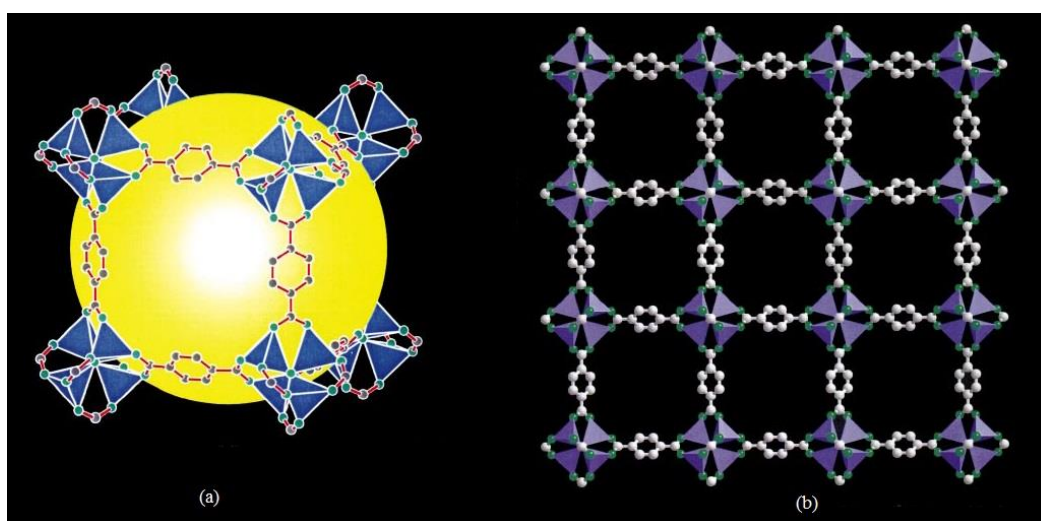


Figure 1.2 (a) One of the cavities in the $[\text{Zn}_4(\mu_4\text{-O})(\text{BDC})_3]$ (MOF-5). (b) The layer structure of MOF-5 extending along the a -axis and the pore size. (Figure reproduced from ref. 8)

Moreover, based on the nature of the linking ligands and the backbone of the architecture itself, some coordination polymers are able to undergo pore-size transformations, known as “breathing”, which depends on whether guest molecules are entrapped or not. These types of microporous coordination polymers are generally called flexible MOFs. Kitagawa has defined MOFs according to different generations, based on their response to guest removal/uptake, as illustrated in **Figure 1.3**.⁹ The 1st generation MOFs have an irreversible breakdown of the frameworks once they lose their guests. The 2nd generation MOFs are rigid and have open pores on loss of guests, and the 3rd generation have reversible flexibility of the

whole structure on guest loss and uptake. This significant discovery has guided research in coordination polymers to flourish by focusing on the development of their applications based on suitable frameworks.

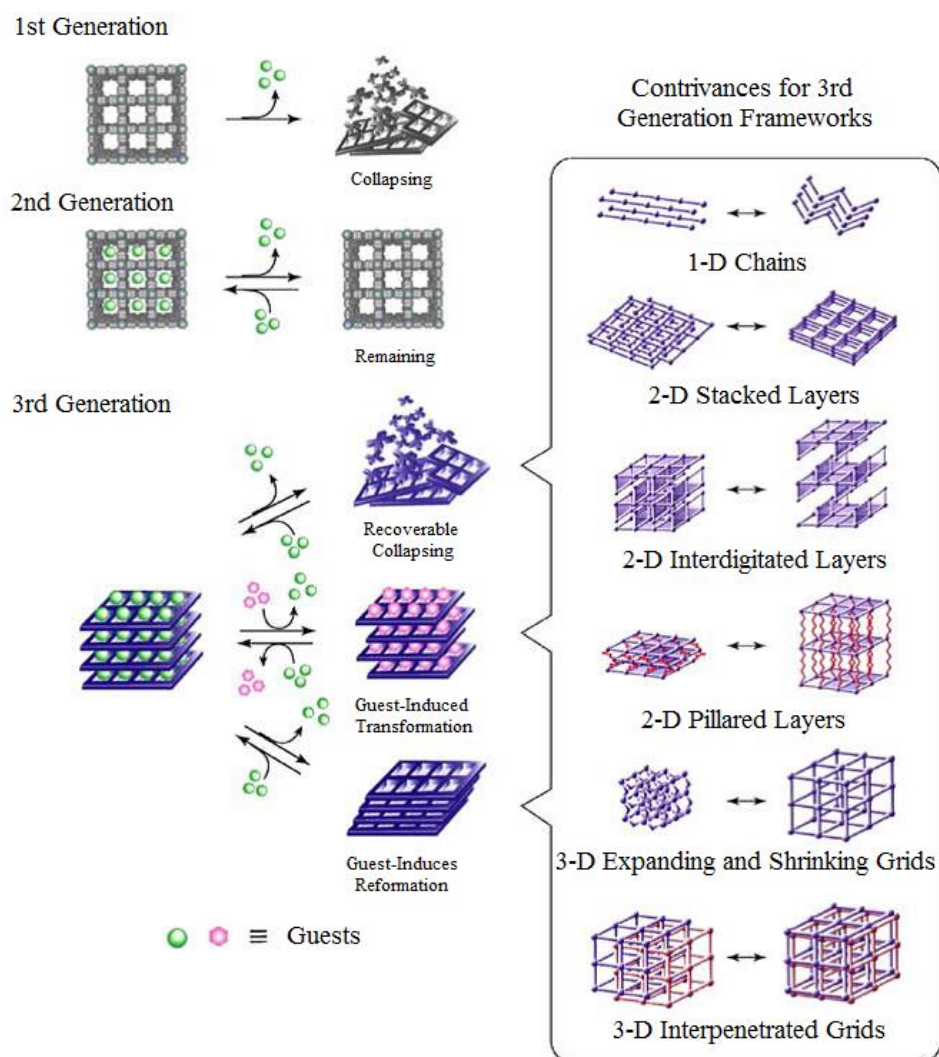


Figure 1.3 Illustration of the three generations of microporous coordination polymers with their characteristics. (Figure reproduced from ref. 9).

Since MOFs were first discovered, scientists have made great efforts in understanding and utilizing their void structures for practical applications.

1.1.2 Applications

With amazingly rich combinations of metal ions and ligands, there is almost no limit to the discovery of new materials from coordination polymers. Meanwhile, structures of coordination polymers, as well as the sizes of pores or channels, can be controlled with the chemical environments and various ligands to a certain extent. Such properties may endow coordination polymers with molecular recognition capabilities. The idea is that high accuracy and efficiency of molecular recognition can be artificially achieved by post-synthetic modification of functional groups inside or around the pores and channels within the coordination polymers. The related host-guest chemistry is highly based on the design and synthesis of the molecular-recognizable polymers which lays a firm foundation for important areas. For example, energy science might benefit from those MOFs which could store and release energetic compounds (e.g. nitrogen-containing anions) under ambient conditions.¹⁰

Small molecule entrapment / separation/ exchange

Strong molecular recognition forces can lead to the formation of some promising MOFs which have high selectivity for one type of molecule over others in a mixture. Comparing MOFs to molecular sieves, which are more limited and hard-to-control in their pore sizes,¹¹ coordination polymers have shown prospective advantages in both synthesis and practical applications.

Due to the increasing CO₂ emission from consumption of coal and natural gas sources, one of the most active fields for molecular entrapment is CO₂ capture. Coordination polymers, especially MOFs, are now considered to be one of the potential next-generation CO₂ capture materials.¹² An example of a family of highly-selective MOFs ([Cu(bpy-1)₂(SiF₆)] and [Cu(bpy-2)₂(SiF₆)]), reported by Zaworotko et al.,¹³ allowed CO₂ uptake in preference to CH₄ and N₂, as shown in **Figure 1.4**. Under the condition of 298 K and 1 atm, the highest experimental uptake for CO₂ over CH₄ could achieve 10.5:1 for [Cu(bpy-1)₂(SiF₆)] and 8:1 for [Cu(bpy-2)₂(SiF₆)] with larger pores and surfaces.

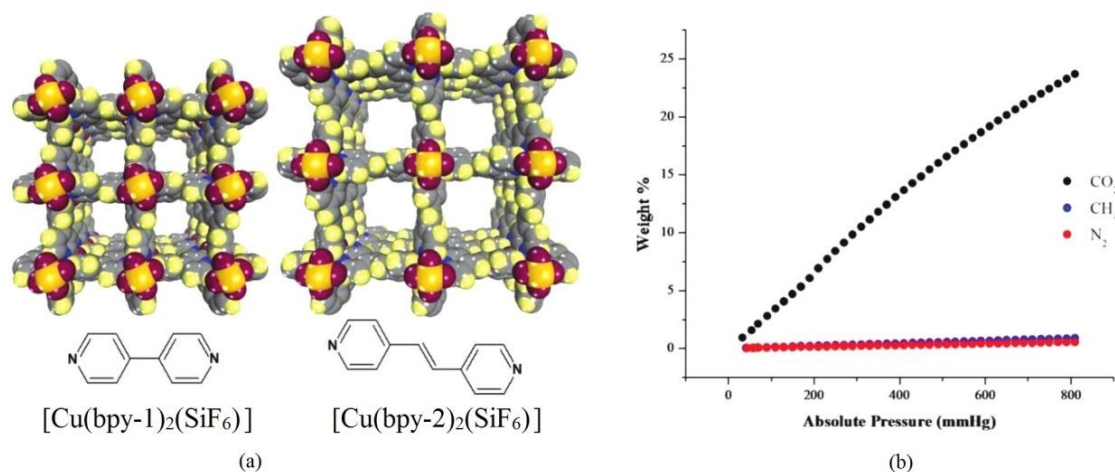


Figure 1.4 (a) Crystal structures of [Cu(bpy-1)₂(SiF₆)] and [Cu(bpy-2)₂(SiF₆)] showing channels along their *c*-axes and exposed fluoride groups of the SiF₆²⁻ pillars. **(b)** Single component gas adsorption which reveals high selectivity of CO₂ versus CH₄ and N₂ for [Cu(bpy-1)₂(SiF₆)] (Figure reproduced from ref. 13).

Although coordination polymers with larger micro-pores can absorb more guest molecules, the pore size can also affect the strength of interaction between the guest and framework and influence selectivity. In fact, the actual adsorption sites are more important. Zhou and co-workers synthesized the MOF [Cu₆(H₂O)₆(TATB)₄ DMA · 12H₂O] (PCN-6, **Figure 1.5**), which has a doubly-interpenetrated architecture with the repeating unit PCN-6' (the non-interpenetrated counterpart). The pore size was reduced by the interpenetration in PCN-6, but the Langmuir surface area is 41% larger than the PCN-6' due to the catenation (new adsorption sites and small pores are formed), which indicated a higher apparent surface area, and gas sorption.¹⁴

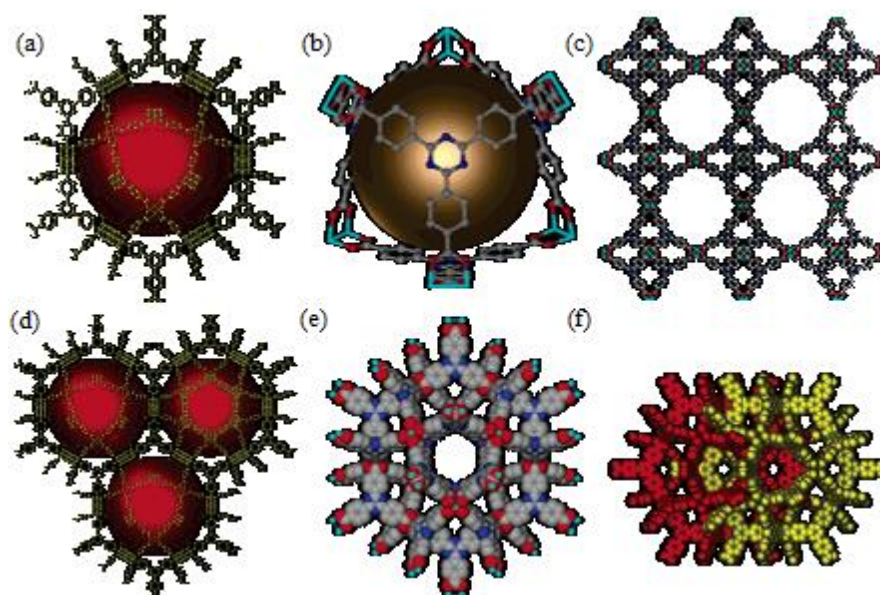


Figure 1.5 The MOF PCN-6 showing (a) the cuboctahedral cage, (b) the Td-octahedral cage, (c) view along the [001] direction, (d) view along the [111] direction, (e) one independent net of PCN-6', (f) the doubly-interpenetrated architecture of PCN-6. (Figure reproduced from ref. 14).

Catalysis

With the booming development in materials and applied chemistry, the increasing demand for highly efficient catalysts has led to new ideas from coordination polymers and in particular MOFs.^{15,16} Specifically designed porous structures can promote reactions and increase the selectivity against other reactions. The field has developed considerably since Fujita et al. reported the first coordination polymer with catalytic selectivity.¹⁷ Many areas such as oxidation¹⁸, organic reactions¹⁹ and chiral synthesis²⁰ are now being advanced by developments in coordination polymers.

Treatments of pollutant gases have now become an urgent challenge in many areas. For example, the automotive industry is now seeking cheap materials in exhaust gas treatments. Xu and coworkers reported a coordination polymer, [Cu(5-methylisophthalate)] (**Figure 1.6**), which exhibited favourable and stable activity toward catalysing the oxidation of CO to CO₂. With the open Lewis acid sites associated with the Cu₂(O₂CR) paddlewheel clusters in the microporous framework, this material had a nearly 100% conversion of CO compared to another { [Na₂₀-(Ni₈L₁₂)(H₂O)₂₈](H₂O)₁₃(CH₃OH)₂ }_n material (3%) which was also reported by Xu's group.²¹

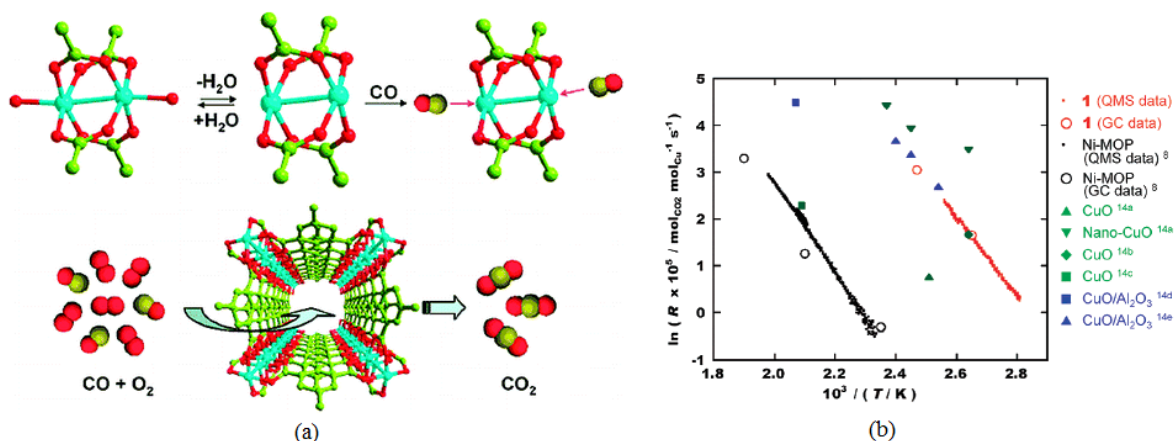


Figure 1.6 (a) Cu₂ clusters unit and the paddle-wheel open channel architectures with CO catalytic pathway. (b) Arrhenius plots of CO oxidation for [Cu(5-methylisophthalate)] and other reported materials (Figure reproduced from ref. 21).

Meanwhile, in addition to high catalyst efficiency and highly specialized catalysts, great interest and effort has also been placed in research on multi-functional catalysts, especially since the discovery of multiple metal-based catalytic centres in enzymes.²² Li and coworkers reported a Cu(I)/Cu(II)-salen coordination polymer ([Cu^{II}(SalImCy)](Cu^I)₂ DMF, (SalImCy = *N,N'*-bis-[(imidazol-4-yl)methylene]cyclo-hexane-1,2-diamine), which had good bimetallic catalytic activities for three-component Strecker reactions (Figure 1.7.b). It could also function as the catalyst of photo-degradation for several organic dyes. Figure 1.7.c shows the different dye degradation rates under different condition for this compound.²³

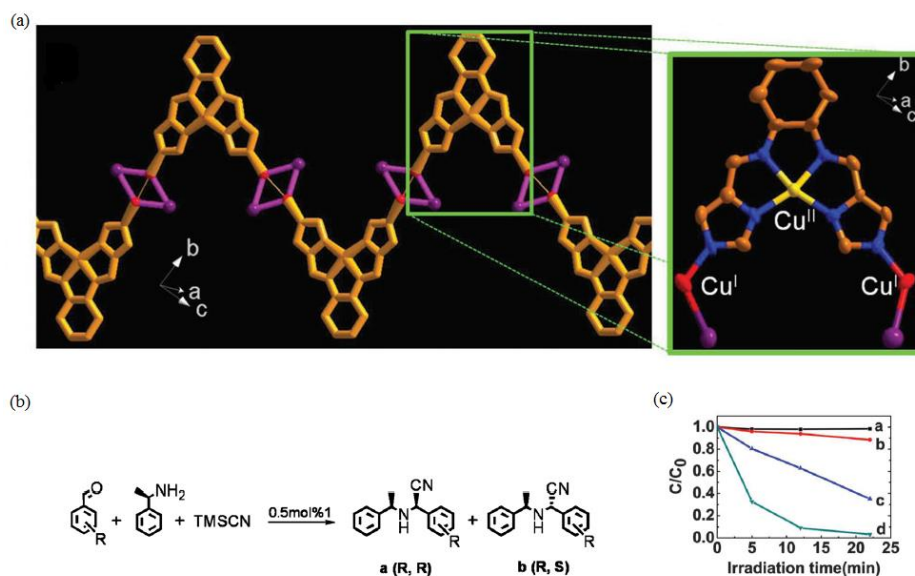


Figure 1.7 (a) The zigzag chain of the Cu(I)/Cu(II)-salen coordination polymer and the asymmetric unit. (b) The equation of the three-component Strecker reactions. (c) The degradation of methylene blue, which is dependent on the irradiation time under different conditions. (Figure reproduced from ref. 23).

In summary, coordination polymers are now playing an increasingly important role, not only due to the availability of post-synthetic modification of their architectures but also their application to a number of fields. Apart from the general fields introduced above, some other areas (such as conductivity and magnetism) are benefited with the development of coordination polymers.²⁴ With the demand of seeking new materials from coordination polymers, the next section will be an overview of several different methods frequently used in preparing coordination polymers.

1.2 Synthesis of coordination polymers

Coordination polymers are generally synthesized from isolated metal ions and organic linkers and a variety of synthetic methods are developed for the preparation of coordination polymers. Common routes including solvothermal synthesis, solvent diffusion methods and different approaches offered by solid-state and mechanochemical syntheses will be discussed in this section. Also, it should be noted that with the recent development on new technologies, several novel ways for synthesizing coordination polymers are starting to be used. Examples include microwave-assisted synthesis, which is based on the interaction of electromagnetic waves and mobile electric charges, and electrochemical synthesis, which has been aimed at forming better MOF thin films.²⁵

1.2.1 Solvothermal processes

Solvothermal synthesis is one of the most widely used methods of synthesizing coordination polymers, especially for growing single crystals. The idea is that solid-state compounds are prepared under high temperature and pressure in an enclosed aqueous environment (i.e. hydrothermal synthesis), the motivation for which comes from how minerals are formed under natural environment. To date, a huge number of different reactions for synthesizing coordination polymers and ligands have been reported by utilizing this method.^{26,27}

The main advantages of the solvothermal synthesis are, obviously, the one-pot synthesis and possibility in achieving different structures. An example of a series of controlled syntheses forming different structures from same the reactants was reported by Loiseau's group.²⁸ The thorium-terephthalate coordination polymers synthesized in a DMF/H₂O solvent system tend

to form two phases, $[\text{Th}_6\text{O}_4(\text{OH})_4(\text{H}_2\text{O})_6(\text{bdc})_6] \cdot 6\text{DMF} \cdot 12\text{H}_2\text{O}$ and $[\text{Th}(\text{bdc})_2(\text{DMF})_2]$ (bdc = 1,4-benzenedicarboxylate or terephthalate). However, if a low amount of water present in the synthesis, a third phase $[\text{Th}(\text{bdc})_2]$ forms (**Figure 1.8**).

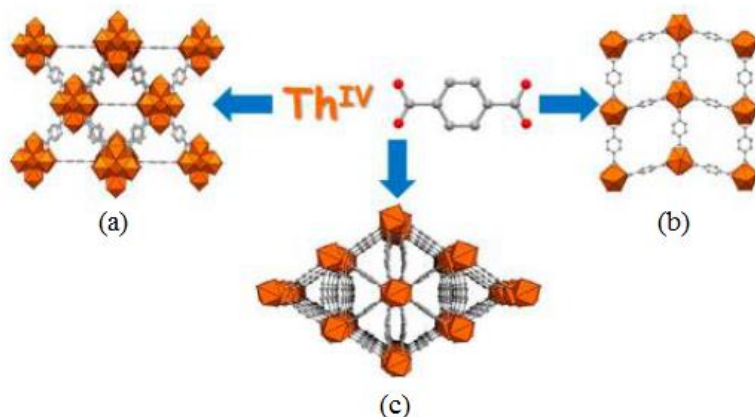


Figure 1.8 The three different phases of thorium-terephthalate coordination polymers prepared by solvothermal synthesis in a DMF-water solvent system: **(a)** $[\text{Th}_6\text{O}_4(\text{OH})_4(\text{H}_2\text{O})_6(\text{bdc})_6] \cdot 6\text{DMF} \cdot 12\text{H}_2\text{O}$, **(b)** $[\text{Th}(\text{bdc})_2(\text{DMF})_2]$ and **(c)** $[\text{Th}(\text{bdc})_2]$. (Figure reproduced from ref. 28).

However, solvothermal processes are obviously not viable for thermally sensitive reactants and products and some reactions do not require high temperature for motivation. Here diffusion method can be an easier way to set up and avoid these problems.

1.2.2 Diffusion

Being different from solvothermal synthesis which is based on the change of the temperature, diffusion methods focus more on changing the solubility by slowly mixing different solvents. Generally, molecules prefer the transportation from a region with a higher concentration to one with a lower concentration. With utilizing this principle, a direction-controlled diffusion can be achieved which facilitates the formation of the coordination polymers under mild conditions. Two common diffusion-involved methods, vapour-phase and solvent diffusion, are illustrated in **Figure 1.9**. In a vapour-phase diffusion, one solvent (in which the product is less soluble) is slowly transported into the solution which contains the reactants. It creates a gradually insoluble environment for the product to form crystals. Similarly, solvent diffusion forms a contact surface for different materials with two solvent layers with different densities. Either miscible or immiscible solvents can be used as crystals generally form at the contact interface.

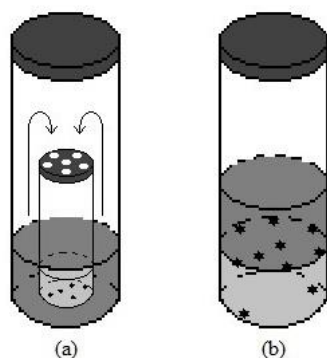


Figure 1.9 Two types of diffusion processes used in coordination polymer synthesis: (a) vapour diffusion and (b) solvent diffusion.

Diffusion can also be achieved by using substrates to provide a surface area for the coordination polymer crystallization (**Figure 1.10**). Ceramic or silica substrates²⁹ have been used universally in synthesis, whereas Wang and coworkers initiated a new method, *contra-diffusion*, which produced ZIF-8 (zeolitic imidazolate framework-8) on flexible nylon substrates. With the expected interaction between the ligand of ZIF-8 and the nylon polymer, the two solutions diffused through the nylon membrane in-between and slowly formed ZIF-8 on both sides with different speeds. The product was confirmed by PXRD.³⁰

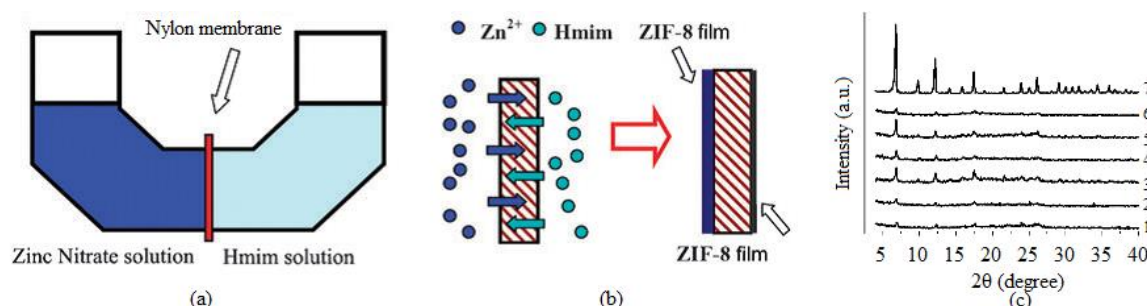


Figure 1.10 (a) Cell designed for the contra-diffusion. (b) The template formation of ZIF-8 on both sides of the membrane with different environments. (c) The PXRD collected for the ZIF-8 films for Zn side (1, 2, 5) and Hmim (= 2-methylimidazolate) side (2, 4, 6) with increasing time compared to the pure ZIF-8 powder (7). (Figure reproduced from ref. 30).

Although liquid-phase reactions are often quicker and easier in preparation, they are not always suitable for all cases such as special reactions or products with high water-sensitivity or polymorphism. In these cases, solid-state reactions can be another choice in discovering new routes for syntheses.

1.2.3 Solid-state synthesis

Solid-state reactions can be more convenient and controllable than solution-phase synthesis, as well as lead to a higher product yield by avoiding material loss from solution, although solid-state synthesis is not applicable to all reactions. Solid-state reactions have been well-defined by Schmalzried,³¹ who suggested that the mechanism is linked to migration of the point defects governed the mass transport in crystals. Mechanisms for a simple $AX+BX \rightarrow ABX_2$ reactions in ionic solids can be complicated as shown below in **Figure 1.11**. The three cases partially indicate that the ions in the reactant crystals might separate and migrate in different ways.

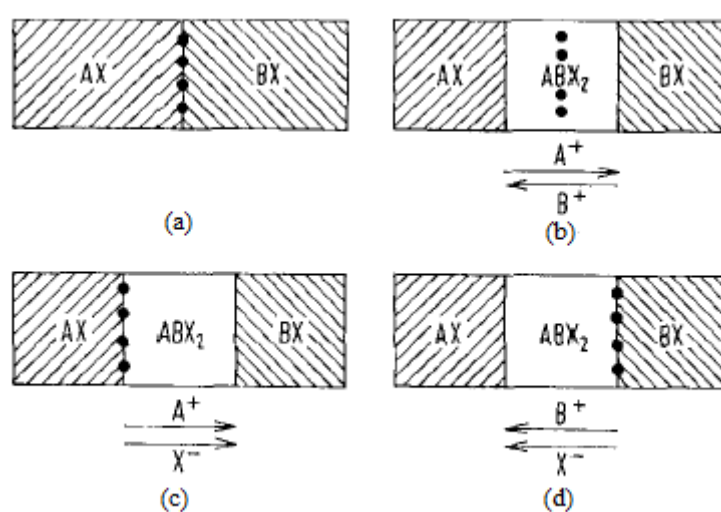


Figure 1.11 Different self-diffusion mechanisms for a typical solid-state reaction. (Figure reproduced from ref. 31).

Mechanochemistry, which utilizes the mechanical force to conduct chemical transformations in the solid state, has also been used to expand the methods for synthesizing coordination polymers.^{32,33} The most simple solvent-free mechanochemical synthesis only requires grinding the mixture of the reactants in a simple way, such as in a pestle and mortar. Lang and coworkers reported a two-step ambient temperature solid-state synthesis of a 2D coordination polymer $[Pb(Tab)_2(4,4'\text{-bipy})](PF_6)_2$ ($4,4'\text{-bipy}$ = 4,4'-bipyridine; Tab = 4-(trimethylammonio)benzenethiolate) (see **Figure 1.12**).³⁴ The reaction only required simple procedures and mild conditions but is high in efficiency.

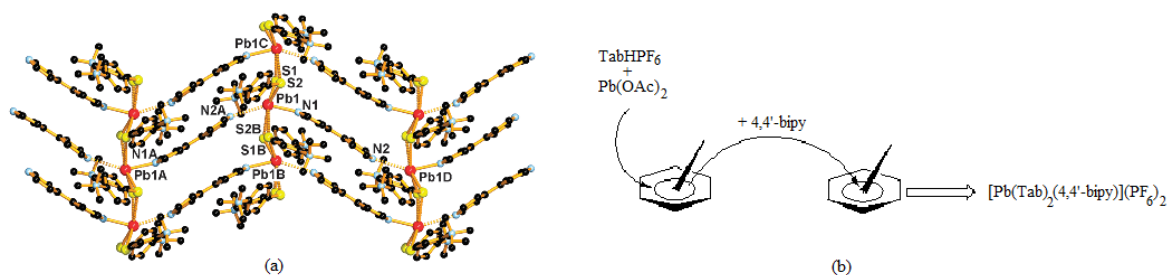


Figure 1.12 (a) The wave-like 2D framework of $[\text{Pb}(\text{Tab})_2(4,4'\text{-bipy})](\text{PF}_6)_2$. (b) The procedure for the two-step solid-state synthesis in one mortar. (Figure adapted from ref. 34).

On the foundation of simple solid-state mechanochemical synthesis, many new technologies have been developed for reaching the required parameters (e.g. grinding speed) during the reaction. Also, the different input of kinetic energy has effects on local melting, particle size reduction and formation of new polymorphs.³⁵ Thus, novel types of mechanical grinding methods (**Figure 1.13**) like ball mills have been introduced for achieving reactions which are highly controlled.³⁶

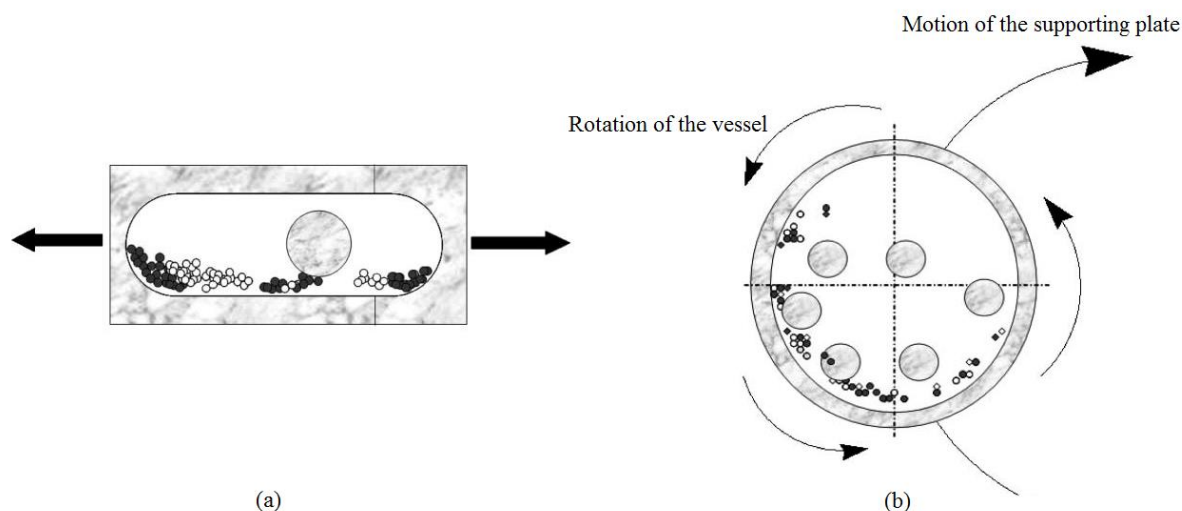


Figure 1.13 Two types of mechanical-grinding mills: (a) shaker mill; (b) planetary mill. (Figure reproduced from ref. 36).

In summary, synthesis is an important component of research involving coordination polymers. There continues to be interest in developing effective and efficient synthetic methods or protocols and there are demands for routes towards the synthesis of specific coordination polymers. In the light of developments in green chemistry, the development of solid-state chemistry, especially the solid-state synthesis is becoming increasingly important.

1.3 Solid-state chemistry with coordination polymers

Solid-state chemistry is a large subdiscipline of chemistry which closely links to coordination polymers. The reasons for and categories of solid-state phase transformation are very complex.³⁷ Current interests focus on developing theories and methods, understanding of interactions and reactions in solid-phase, which may potentially benefit some of the crystal engineering and syntheses which are not good enough in other phases.³⁸ From a reaction point of view, as the molecules are restricted within a fixed area based on the structure, the reactants are less mobile and the reactions are often slow. However, this makes some special syntheses possible such as products formed with regioselectivity.³⁹ In the next section, solid-state transformations related to coordination polymers will be discussed.

1.3.1 Solid-state transformations

Solid-state transformations can be caused, macroscopically, by changes in temperature, pressure, field, light, or even the interaction with other molecules. For coordination polymers, some of these transformations can be achieved in a single-crystal-to-single-crystal (SCSC) manner.⁴⁰⁻⁴² Such transformations may involve changes in the coordination number of the metal centres, rearrangement of the structure or spatial architecture, thermally driven associations or dissociations or interactions with ligand/guest molecules. From a structural perspective, solid-state transformations involve the direct or staged transformation among 0D, 1D, 2D and 3D structures.³⁹

The most common reason for solid-state transformations in coordination polymers is a change in temperature, leading to the movement of guest molecules and change in network architecture. Sheu and co-workers reported a reversible 1D-to-2D transformation for a Zn(II) coordination polymer, $[\text{Zn}(\text{HBTC})(\text{DPE})_{0.5}(\text{H}_2\text{O})]_n \cdot n\text{H}_2\text{O}$ (HBTC²⁻ = dianion of trimesic acid, DPE = 1,2-bis-(4-pyridyl)ethane), by dehydration in the solid state at 180 °C and re-hydration with water vapour (**Figure 1.14.**). The O-H \cdots O hydrogen bonds were shown as red dashed lines between carboxylate groups and coordinated water in hydrated version. By removing the water, the hydrogen bonds shift to the Zn-O coordination bonds shown as black dashed lines.⁴³

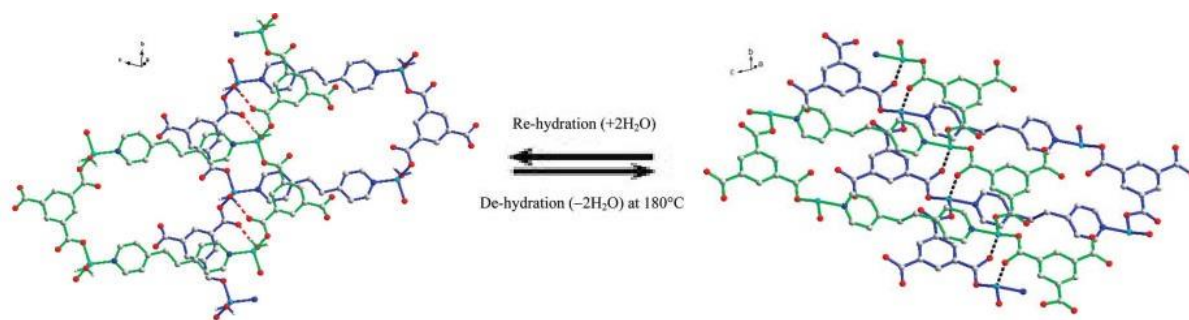


Figure 1.14 The 1D-to-2D solid-state transformation of the $[\text{Zn}(\text{HBTC})(\text{DPE})_{0.5}(\text{H}_2\text{O})]_n \cdot n\text{H}_2\text{O}$. (Figure reproduced from ref. 43).

Also, the possible flexibility and multiple choices in the metal coordination geometry make structure transformations possible for coordination polymers. By changing the structure and components, the behaviour of MOFs when interacting with other molecules can be affected as well. This behaviour makes flexible MOFs more attractive than rigid-pore MOFs in certain areas. Recent work by Kaskel and co-workers on the MOF, DUT-49,⁴⁴ provided the first report of a phenomenon referred as a "negative gas adsorption" transition. When the pressure applied to the MOF reached a certain level, the highly porous architecture (**Figure 1.15.a**: asymmetric unit, **b**: unit cell) underwent a dramatic transformation into a significantly compressed structure (**Figure 1.15.c**: asymmetric unit, **d**: unit cell) and partly squeezed out the entrapped gas molecules (**Figure 1.15.ef**). This interesting new property might pave the way for the further developments in areas such as stimuli-responsive systems.⁴⁵

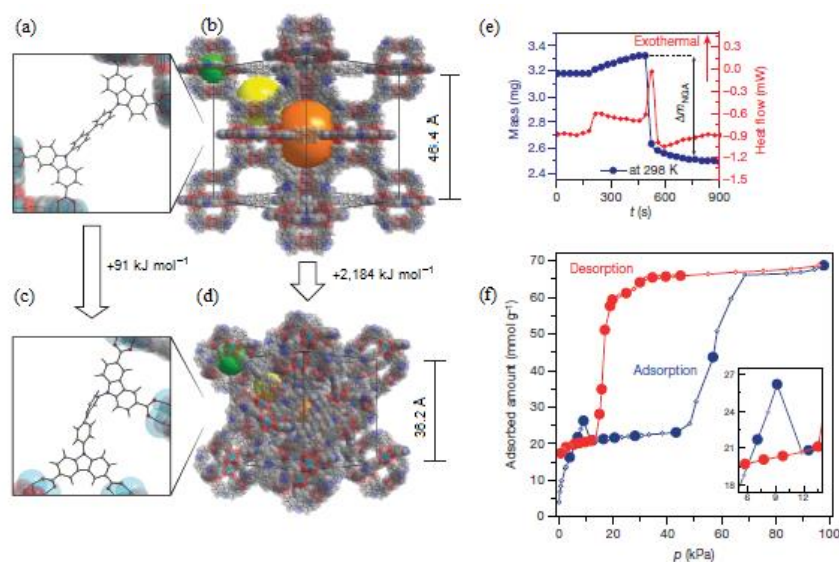


Figure 1.15 Illustration of the transformation for DUT-49 from **(a)** to **(c)**, or **(b)** to **(d)**, with the crystal structures viewed along [110]. **(e)** Plot showing the methane release by the gravimetric adsorption with dynamic scanning calorimetry. **(f)** Plot showing the *in situ* methane adsorption and desorption isotherms at 111 K. (Figure reproduced from ref. 45).

Solid-state transformation has its pros and cons. For example, it may have significant effects on the parameters of certain reactions, which open up new synthetic routes for some reactions. In certain cases, reaction temperature can be significantly reduced which was considered as reducing the system energy by the re-organization of the product in the solid-state.⁴⁶ On the other hand, solid-state transformations of the product might lead to different physical, chemical and biological properties and could potentially cause huge problems. Particularly for pharmaceutical industry, determining and controlling the solid-state transformation of the products is very important.⁴⁷ On balance, the understanding of solid-state transformations can be beneficial in certain areas.

1.3.2 Potential applications of solid-state transformations

The properties of adsorbing and releasing small molecules by coordination polymers have opened new doors in green technology, such as reversible gas storage, and introduction of an efficient and safe way for separating, transporting and releasing the target gas, rather than physical separation and storage tanks. Again CO₂ capturing is one of the major areas of interest in this field. Takamizawa and co-workers reported a series of coordination polymers based on $[M^{II}_2(bza)_4(Rpyz)]_n$ ($M^{II} = Rh, Cu$; bza = benzoate; R = H, 2-methyl or 2,3-dimethyl; pyz = pyrazine). All of these complexes adsorb CO₂ very well at 195 K with ratio of two or three CO₂ molecules per M₂ unit. The absorption is accompanied by a structure transformation of the host skeletons (**Figure 1.16**). Analogous manners of adsorption for H₂, N₂, O₂ and Ar gases were identified for these coordination polymers as well.⁴⁸

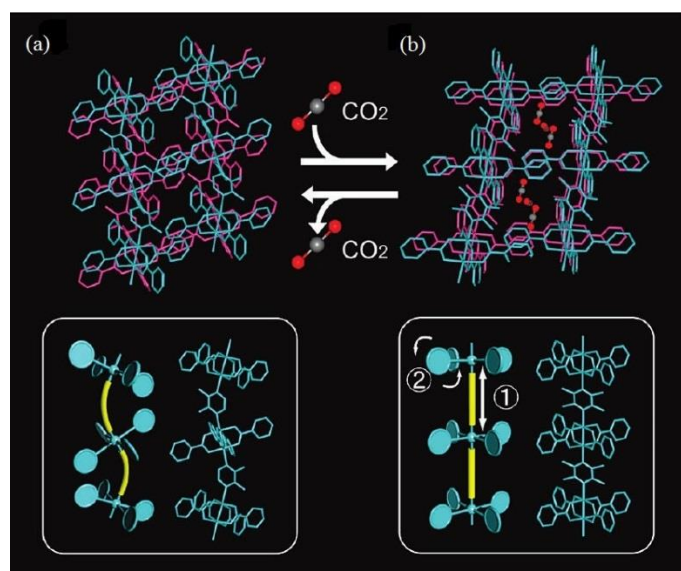


Figure 1.16 Scheme showing the reversible structure transformation for $[Rh^{II}_2(bza)_4(Rpyz)]_n$ between (a) and (b) by adsorbing/releasing CO₂ molecules with the change of the coordination polymer backbone (2-methylpyrazine were modelled disordered in two/four positions in each case). (Figure reproduced from ref. 48).

Beyond simple guest entrapment, solid-state transformations might also raise new ideas in discovering new porous materials that have potential usages in the semiconductor area. The entrapped guest molecules might induce electron transfer in the structure which leads to a totally different conductivity from that of the material without guests. Lan and coworkers designed a new solid-state transformation on a non-interpenetrated coordination polymer $[(\text{Zn}_4\text{O})_2(\text{L})_3] \cdot 10\text{H}_2\text{O} \cdot 4\text{DMA}$ (IFMC-68, H_4L = methanetetra(tetrakis[4-(carboxyphenyl)oxamethyl]-methane acid) which enabled its conversion into a self-interpenetrated analogue $[(\text{Zn}_4\text{O})_2(\text{L})_3\text{H}_2\text{O}] \cdot \text{H}_2\text{O} \cdot 4\text{DMA}$ (IFMC-69). In IFMC-68, the Zn_4O cluster formed a classic $[\text{Zn}_4\text{O}(\text{CO}_3)_6]$ SBU (secondary building unit). But in IFMC-69 each pair of units were further coordinated with a water molecule into a $[\text{Zn}_4\text{O}(\text{CO}_3)_6\text{H}_2\text{O}]$ SBU (**Figure 1.17.a**). IFMC-69 exhibits much greater stability in air and stronger capability in absorbing CO_2 and iodine than IFMC-68 (**Figure 1.17.b**). The I_2 -absorbed material $\text{I}_2@$ IFMC-69 showed 2.24×10^7 times higher electrical conductivity ($2.80 \times 10^{-6} \text{ S cm}^{-1}$) than IFMC-69 which potentially could be used in semiconductors.⁴⁹

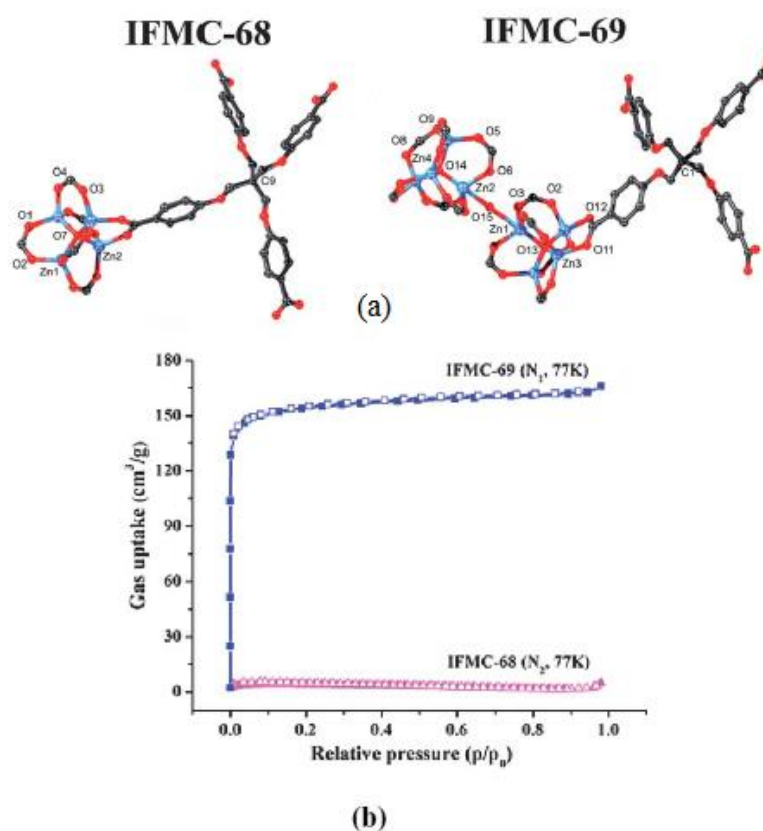


Figure 1.17 The coordination environment (a) and the nitrogen sorption isotherms (b) for IFMC-68 and IFMC-69. (Figure reproduced from ref. 49).

With increasing numbers of studies being carried out, the field of coordination polymers with solid-state transformation properties is rapidly expanding. Combining thermal analyses and X-ray diffraction techniques, the exact transformation can be studied more effectively, which triggers discovery of novel materials. In particular, silver(I)-containing coordination polymers have attracted interest due to their structural flexibility shown in many areas including solid-state transformations.

1.4 Silver(I)-based coordination polymers

Silver(I)-based coordination polymers have driven much interest due to the flexibility and lability in coordination geometry of Ag(I) ions. The d^{10} configuration, with zero crystal field stabilisation energy,⁵⁰ gives the Ag(I) ion various choices of coordination numbers and coordination geometry. In general, Ag(I) ion has a coordination number around two to four and prefers linear, trigonal and tetrahedral geometry.⁵¹ Thus, many different ligands can form weak coordinative bonds with Ag(I) in variety of combinations of coordination number and geometry.⁵²

Silver-silver interactions, usually referred to as an argentophilic interaction, may also need to be considered. According to the research in past decades, argentophilicity is considered to involve interaction between Ag(I) centres in close proximity because the energy levels for 5s and 5p orbitals are similar to those of the 4d orbital in Ag(I) ions. This results in the specific but systematic geometric structures for ligands surrounding around the silver centres, which are shown in **Figure 1.18**.⁵³

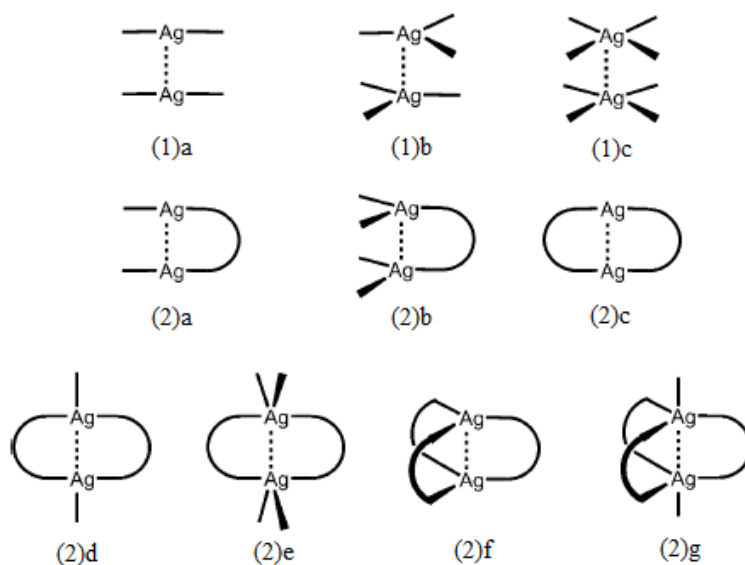


Figure 1.18 The unsupported (1) types of argentophilic interactions without ligands and supported (2) types with the ligands. (Figure reproduced from ref. 53).

1.4.1 Review of silver(I) coordination polymers

Based on the aforementioned principles for the Ag(I) centres, the high flexibility in structure and high compatibility with different ligands have led to interest in silver-containing coordination polymers in materials science,⁵⁴ pharmaceutical science⁵⁵ and many other areas.

Silver and silver-containing compounds have been used as antibiotics since centuries ago. With the strong ability to interact with the microbial cell membranes, proteins, enzymes and DNA in light concentrations without harming human cells, silver compounds have come back to the field after more microbes developed strong resistance to general antibiotics.⁵⁶ Nomiya and co-workers suggested that the bonds between Ag(I) and nitrogen atoms could endow these Ag(I)-containing compounds with potential antimicrobial activity towards several microbes.⁵⁷ So far some coordination polymers with different nitrogen-containing organic ligands have been synthesized and exhibited remarkable antimicrobial activity. Fromm's group tested a series of Ag(I)-N coordination polymers formed with "Ln" ligands (L stood for the bis-nicotinic acid compounds and the additional number "n" was added for showing the length of the ligand, **Figure 1.19**). They showed good antibiotic activity against species such as *Escherichia coli* and *Staphylococcus epidermidis*, as well as probability in coating the surfaces of metallic substrates.⁵⁶

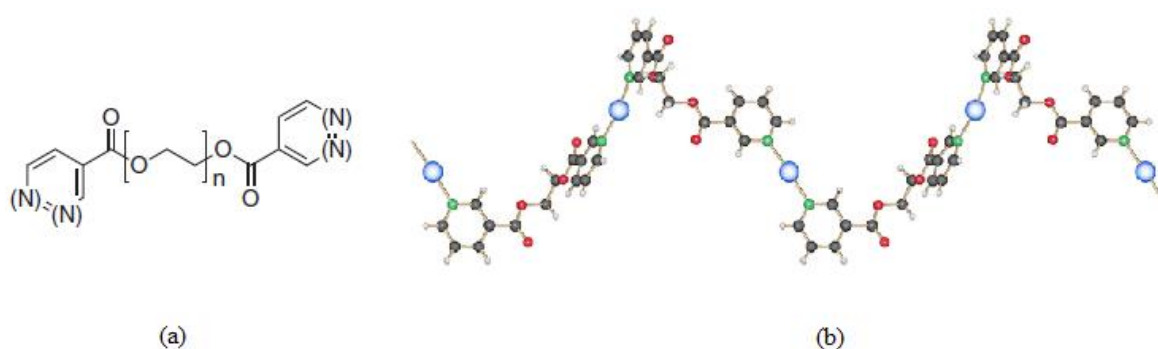


Figure 1.19 (a) The "Ln" ligand family ($n = 1-4, 6, 8, 10, 12, >100$); (b) The 1-D helical coordination structure formed by $[Ag(L1)NO_3]_n$ (Figure reproduced from ref. 56).

Silver(I)-containing materials also have promising luminescent properties, as do many other d^{10} -ion-containing compounds.⁵⁸ Luminescence is the light emission of the material by the photoexcitation under certain wavelength of light, which now widely used in several areas such as biomedical analyses.⁵⁹ A novel coordination polymer, $[Ag_4(C_5O_5)_2(H_2O)_2]_n$, ($C_5O_5^{2-}$ = croconate dianion) was reported by Bu's group. This tetranuclear Ag(I) coordination polymer had two types of silver(I) coordination geometries (tetrahedral 4-coordinate or square-pyramidal 5-coordinate) and exhibits green luminescent emission at room temperature, when excited by 380 nm light (**Figure 1.20**).⁶⁰

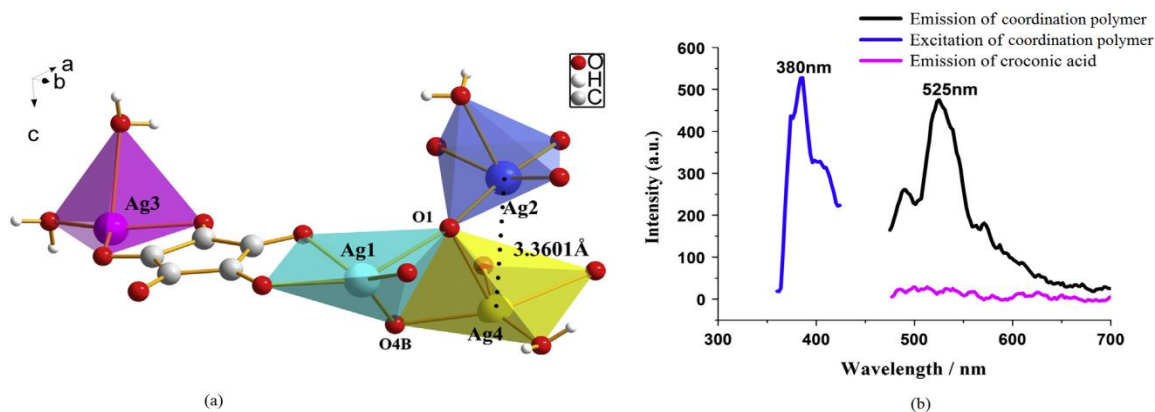


Figure 1.20 (a) The different coordination geometries for Ag(I) ions in $[Ag_4(C_5O_5)_2(H_2O)_2]_n$; (b) The fluorescence spectra in the solid state for $[Ag_4(C_5O_5)_2(H_2O)_2]_n$. (Figure reproduced from ref. 60).

Meanwhile, the unique catalytic activity of Ag(I) coordination polymers may give them a place in the next generation of catalysts. Lang and co-workers reported a 1D coordination polymer, $[Ag_4(NO_3)_4(dpppda)]_n$ (dpppda = 1,4-N,N,N',N'-tetra(diphenylphosphanyl)methyl)-benzene diamine) that could degrade nitroaromatics in water under UV irradiation to yield CO_2 , NO_3^- , NH_4^+ and possibly N_2 as degradation products, which gave options other than semiconductors in industrial waste water treatment (**Figure 1.21**).⁶¹

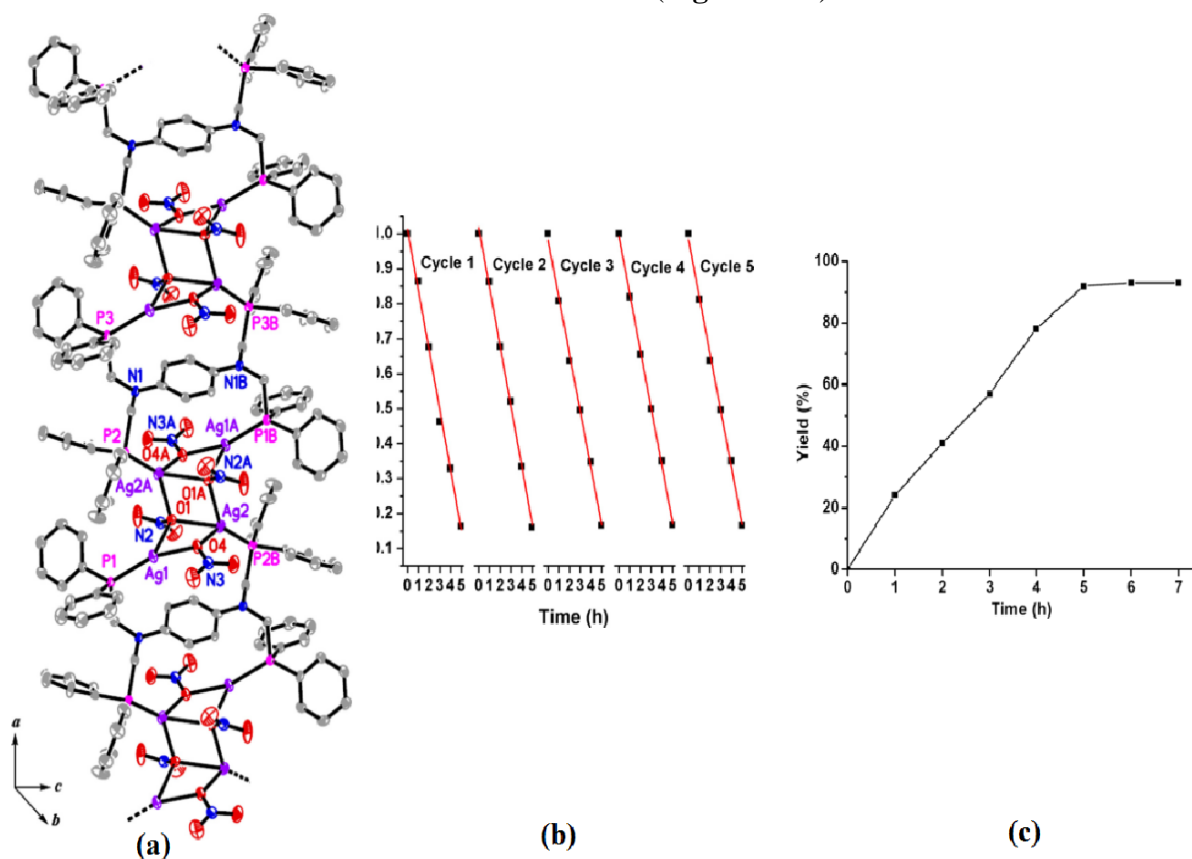


Figure 1.21 (a) The 1-D linear array of $[Ag_4(NO_3)_4(dpppda)]_n$ extending along the a axis; (b) its recycled performance for the photodegradation of nitrobenzene in water upon UV light irradiation; (c) the yield of CO_2 generated from the photodegradation of nitrobenzene catalysed by this complex within 7h. (Figure reproduced from ref. 61).

In short, Ag(I) coordination polymers with Ag(I)-N interactions have shown a variety of applications and attracted interest in the development of new materials. In the next section, a brief description of the previous work with Ag(I) coordination polymers by the Brammer group will be made as this provides the most direct introduction to the current project.

1.4.2 Coordination polymers from silver(I) perfluorocarboxylates combined with diamines/diimines

The Brammer group's studies on the Ag(I)-perfluorocarboxylate coordination polymers first started from an approach in which they could form supramolecular synthons analogous to hydrogen-bonded carboxylic acid dimers but involving Ag^+ ions rather than H^+ ions. **Figure 1.22** illustrates the single crystal structures for trifluoroacetic acid ($\text{CF}_3\text{CO}_2\text{H}$) and silver trifluoroacetate (AgO_2CCF_3), demonstrating this analogy.⁶²

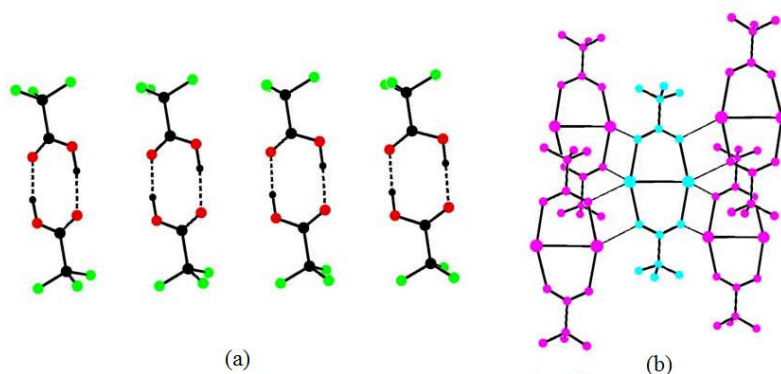


Figure 1.22 The comparison between the single crystal structures of (a) $\text{CF}_3\text{CO}_2\text{H}$ and (b) AgO_2CCF_3 . (Figure reproduced from ref. 62).

This series of structures provided the basic backbones for coordination polymers constructed from combining Ag(I)-perfluorocarboxylates with linear diimines or diamine.⁶² The results showed that these coordination polymers preferred the formation of 1D-tape chain or 2D-layer networks composed of Ag(I)-carboxylate dimer nodes linked by diimine ligand bridges. This approach utilized a soft secondary building unit (SBU) for achieving potential flexible coordination polymers (**Figure 1.23**).⁶³ For better illustration, different parts of the compounds are shown in different colours: silvers are in black, perfluorocarboxylates are in red and ligands are in blue. Silver atoms are coordinated to the oxygen atoms from the carboxylates and also coordinated to the nitrogen atoms from the bridging ligands. Most of them share similar basic 2D structure but different ligands lead to slight differences among

the structure, such as the ligand orientation. The perfluoroalkyl chains are generally interdigitated in between the spaces of neighbouring layers.

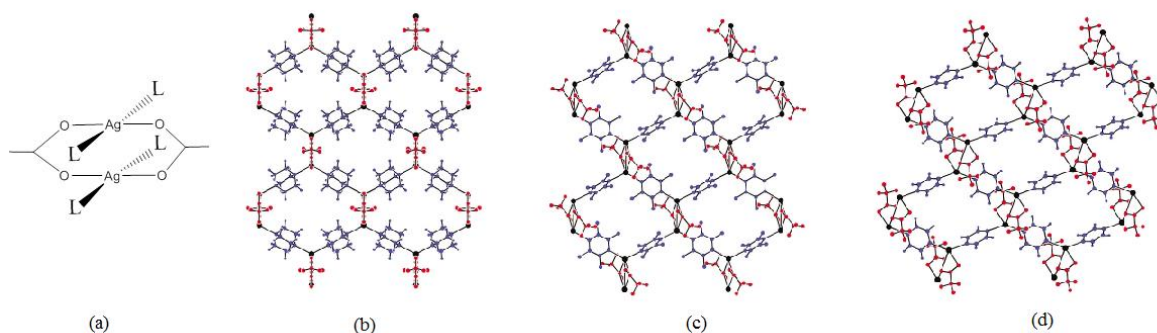


Figure 1.23 (a) A typical Ag(I)-dimer node for a series of 2D layered coordination polymers $[\text{Ag}\{\text{O}_2\text{C}(\text{CF}_2)_n\text{CF}_3\}(\text{L})]$. Structures of single layers of such coordination polymers (here with $n = 0$) with different ligands, L: (b) 1,4-diazabicyclooctane, (c) tetramethylpyrazine, (d) pyrazine. (Figure reproduced from ref. 63).

Some of the coordination polymers (e.g. $[\text{Ag}_4(\text{O}_2\text{C}(\text{CF}_2)_2\text{CF}_3)_4(\text{TMP})_3]_n$ (TMP = 2,3,5,6-tetramethylpyrazine))^{64,65} were then discovered to perform interesting solid-state transformations which allowed inclusion and release of small molecules such as alcohols (**Figure 1.24.a**). This compound could undergo single-crystal-to-single-crystal (SCSC) transformations by exposing the crystal to alcohol vapour to take up the alcohol molecules, then heating it to release the alcohol. This SCSC transformation was also shown to be reversible. Different alcohols can be taken up and released in sequence with one single crystal (**Figure 1.24.b**).

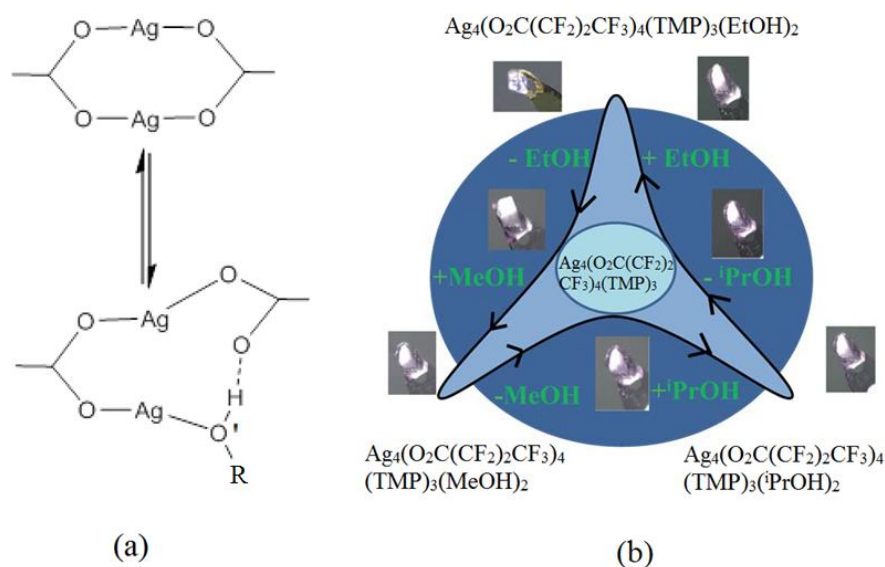


Figure 1.24 (a) Scheme for the alcohol uptake and release in the coordination polymer subunit; (b) Illustration of the SCSC cycle of the alcohol uptake and release for $[\text{Ag}_4(\text{O}_2\text{C}(\text{CF}_2)_2\text{CF}_3)_4(\text{TMP})_3]$. (Figure adapted from refs. 64 and 65).

The reversible SCSC transformation reported for $[\text{Ag}_4(\text{O}_2\text{C}(\text{CF}_2)_2\text{CF}_3)_4(\text{TMP})_3]$ involves the absorption and release of alcohol molecules in vapour phase through its non-porous architecture. The coordinated alcohol molecules are inserted into Ag-O bonds and stabilized by the newly formed Ag-O' bonds and hydrogen bonds between alcohol and carboxylate group (**Figure 1.24a**). The hypothesis for the guest movement pathway in the structure is that this is permitted by the gaps between the (disordered) interdigitated fluorinated chains along a certain planes in the crystals. This hypothesis is supported by the observation of cracks formed along these planes in the single crystal during the transformations (**Figure 1.25.a**). Further heating of $[\text{Ag}_4(\text{O}_2\text{C}(\text{CF}_2)_2\text{CF}_3)_4(\text{TMP})_3]$, which has a composition with 4:4:3 ratio of Ag:perfluorocarboxylate:TMP, showed that it could undergo an additional, irreversible solid-state transformation by losing one TMP ligand per formula unit to generate a coordination polymer with a 2D-layered structure (**Figure 1.25.b**) and a 4:4:2 ratio composition.⁶⁶

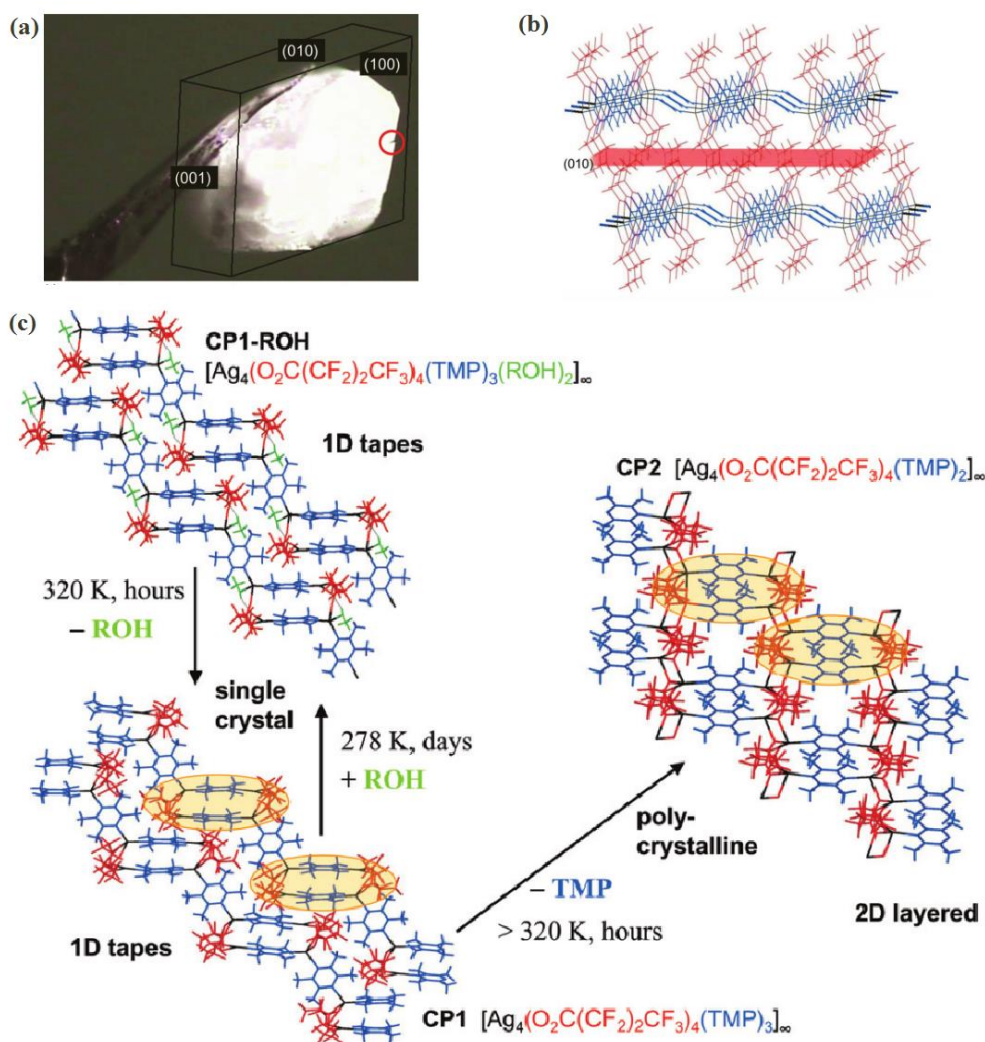


Figure 1.25 View of (a) the crack formed along (010) plane after transformation from $[\text{Ag}_4(\text{O}_2\text{C}(\text{CF}_2)_2\text{CF}_3)_4(\text{TMP})_3(\text{MeOH})_2]$ to $[\text{Ag}_4(\text{O}_2\text{C}(\text{CF}_2)_2\text{CF}_3)_4(\text{TMP})_3]$, (b) the (010) plane from SCXRD structure and (c) The full solid-state transformation scheme including structure determination for $[\text{Ag}_4(\text{O}_2\text{C}(\text{CF}_2)_2\text{CF}_3)_4(\text{TMP})_3]$ which indicates the reversible alcohol uptake/release and irreversible loss of one TMP ligand. (Figure adapted from ref. 66).

Another diimine ligand, phenazine, was examined by forming series of similar coordination polymers of the form $[\text{Ag}_4(\text{O}_2\text{CR})_4(\text{phenazine})_2]$. Thereafter, $[\text{Ag}_4(\text{O}_2\text{C}(\text{CF}_2)_2\text{CF}_3)_4(\text{phenazine})_2]$ was shown as another good example of solid-state transformation with its different manners when interacted with toluene or xylene. These aromatic compounds were used as solvents and themselves were also acting as the bridging ligands between coordination layers and these molecules could be lost by heating under solid-state. The structures of coordination polymers formed in these two solvents were different. They have similar 1D tape structure but in the xylene version the neighbouring tapes have 90° rotation to each other (**Figure 1.26.ab**). The toluene version formed one type of desolvated structure (**Figure 1.26.c**) and the xylene versions formed a mixture of minor portion of this structure and a major portion of another desolvated structure (**Figure 1.26 (d)**). For those desolvated 4:4:2 polymorphs, they have similar architectures to the original compounds with solvents, thus it might suggest the role of the pre-organization of the products and the inter-conversion between these polymorphs, as well as the relationships among all coordination polymers in this family that they share similar structures.⁶⁷

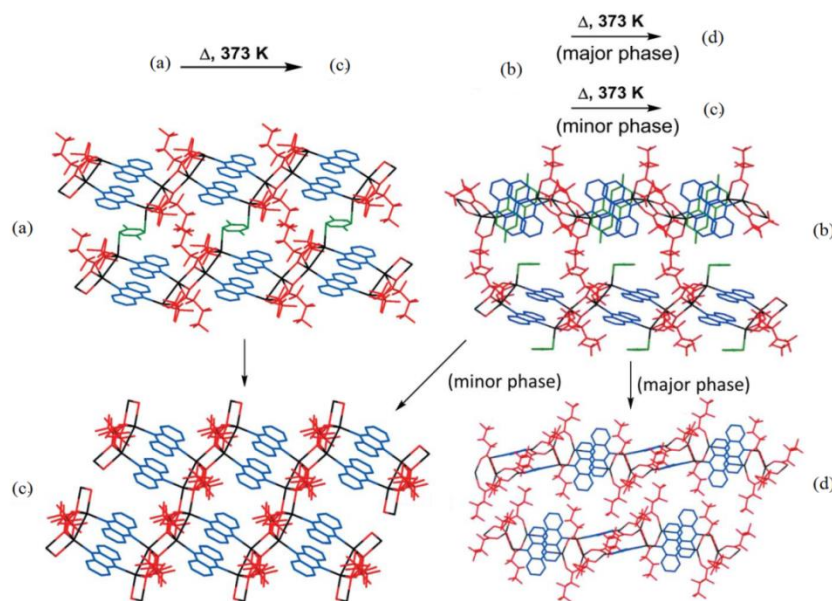


Figure 1.26 Structural transformations by loss of aromatic hydrocarbon guest: $[\text{Ag}_4(\text{O}_2\text{C}(\text{CF}_2)_2\text{CF}_3)_4(\text{phenazine})_2] \cdot 2(\text{toluene})$ (**a**) to $[\text{Ag}_4(\text{O}_2\text{C}(\text{CF}_2)_2\text{CF}_3)_4(\text{phenazine})_2]$ (**c**); two polymorphs (**c**) and (**d**) formed from $[\text{Ag}_4(\text{O}_2\text{C}(\text{CF}_2)_2\text{CF}_3)_4(\text{phenazine})_2] \cdot 2(p\text{-xylene})$ (**b**). (Figure reproduced from ref. 67).

The phenazine coordination polymers have also been proved to have solvent selectivity among different types of arenes. A series of coordination polymers, $[\text{Ag}_4(\text{O}_2\text{CCF}_3)_4(\text{phen})_3]$ phen arene (phen=phenazine; arene=toluene, *p*-xylene or benzene) and $[\text{Ag}_4(\text{O}_2\text{CCF}_3)_4(\text{phen})_2]$, were synthesized in mix phases of different combination of these solvents and determined the major phase formed. The result shown a solvent selectivity

preference: *p*-xylene>toluene≈benzene>*o*-xylene>*m*-xylene. The compounds formed in the first three arenes were sharing a very similar 4:4:3 ratio structure and solvent sites. The compounds formed in *o*-xylene and *m*-xylene had the same 4:4:2 ratio structure and no xylene taken in the structure (**Figure 1.27.a**).⁶⁸

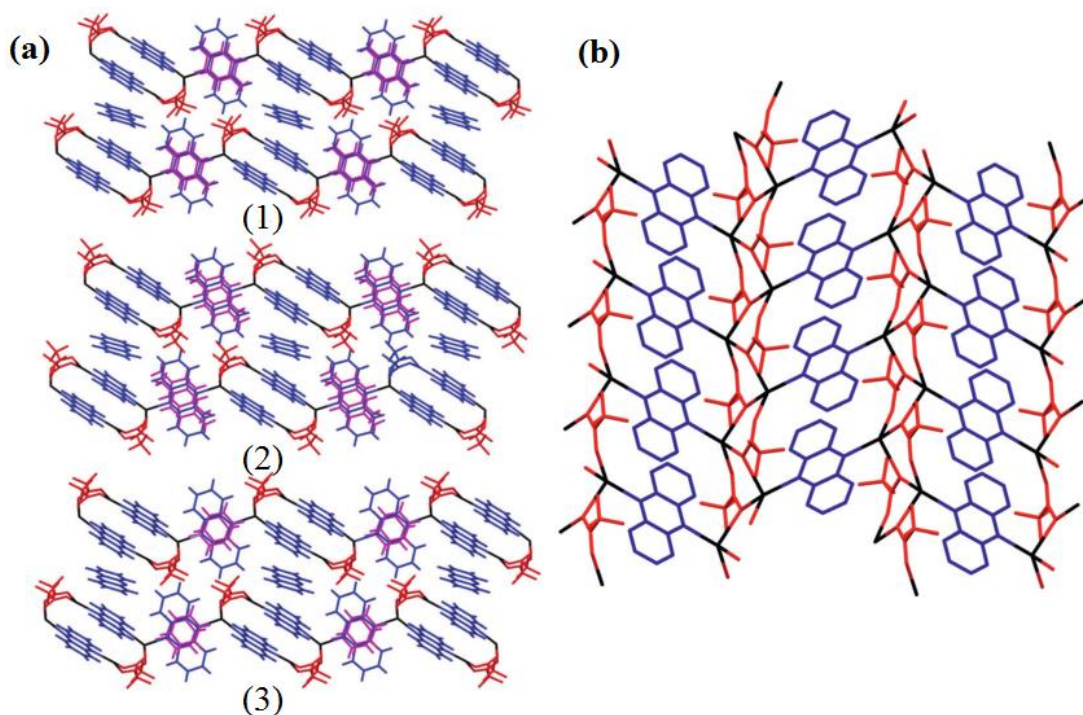


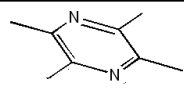
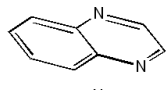
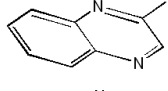
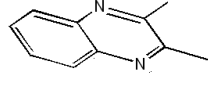
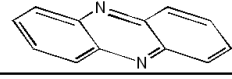
Figure 1.27 View of the structure of $[\text{Ag}_4(\text{O}_2\text{CCF}_3)_4(\text{phen})_3]$ phen arene (phen=phenazine; arene=toluene (1), *p*-xylene (2) or benzene (3)) **(a)** and the solvent-free structure $[\text{Ag}_4(\text{O}_2\text{CCF}_3)_4(\text{phen})_2]$ formed in *o*-xylene and *m*-xylene **(b)**. (Picture reproduced from ref.68)

In summary, Ag(I)-perfluorocarboxylate-diimine coordination polymers seem to share similar basic structures and potential properties in molecule absorption via solid-state transformations. These initial successes suggest there is still scope to expand these families of coordination polymers by employing related diimine ligands and carboxylates with longer perfluoroalkyl chains. Such studies are fully described in Chapters 2 and 3.

1.4.3 Project overview

As outlined above, series of Ag(I)-perfluorocarboxylate coordination polymers with different diimine ligands (e.g. TMP and phenazine) have been studied in our group. Most of them have shown similar and high flexibility in their topological structures, involving either thermally driven solid-state structure transformation, or small molecule capture and release. In order to fully understand the subtle dependence of these processes on the choice of diimine ligand, several families of quinoxaline-based Ag(I)-perfluorocarboxylate coordination polymers have been investigated in this thesis. These ligands lie in between the TMP and phenazine ligands already studied in terms of steric requirements, and will have slightly different electronic contributions. The selected ligands are shown in **Table 1.1**. Chapter 2 focuses on coordination polymers that use the quinoxaline ligand, whereas Chapter 3 will include studies of coordination polymers involving 2-methyl-quinoxaline.

Table 1.1 Comparison between the studied and planned diimine ligands.

Ligand Name	Properties	Structure	Studied or not
tetramethylpyrazine	solid, white		Studied
quinoxaline	solid, pale yellow		Chapter 2
2-methyl-quinoxaline	liquid, red		Chapter 3
2,3-dimethyl-quinoxaline	solid, colourless		On-going project
phenazine	solid, pale yellow		Studied

Silver(I)-perfluorocarboxylate-quinoxaline coordination polymers

Based on the previous research on solid-state transformation with Ag(I)-perfluorocarboxylate-diimine coordination polymers suggested above, a rough hypothesis has been reached on their common behaviours. Further studies will be focused on some selected coordination polymers in order to look for more detailed evidence to contribute to the overall understanding of the behaviour of these materials. Based on some preliminary

work in the Brammer group there is evidence that coordination polymers based on the combination of silver perfluorocarboxylate with quinoxaline can adopt structures with 4:4:4 or 4:4:3 ratios for Ag(I) ions, perfluorocarboxylate ligand and diimine ligands. This work aims to establish whether there is a well-defined direct synthetic method with different conditions (such as concentration of the reactants or solvent types) to prepare phase-pure products with these different stoichiometries or other stoichiometries. Further investigation aims to establish whether solid-state transformations between these different coordination polymers can be established and if so whether these can be studied by different experimental techniques including *in situ* X-ray diffraction.

Silver(I)-perfluorocarboxylates-2-methyl-quinoxaline coordination polymers

In order to fully understand the behaviour of the Ag-perfluorocarboxylate-diimine coordination polymers, it is of interest to introduce new diimine ligands that involve small changes from the ligands already studied, but may be able to form analogous coordination polymers. The ligand 2-methyl-quinoxaline fulfils this requirement and can be thought to lie between phenazine and quinoxaline in structure. It would be valuable to find out whether slight modifications of the ligands would greatly change the characteristics of the coordination polymers. New coordination polymers containing these ligands will be synthesised by combination with a silver perfluoroalkylcarboxylates of different alkyl chain lengths. These coordination polymers will be fully characterised, including by X-ray crystallography and their potential to undergo structural transformations and/or guest uptake/release will be investigated where possible.

1.5 References

- 1 M. J. Zaworotko, *J. Am. Chem. Soc.*, 2010, **132**, 7821–7822.
- 2 L. Brammer, *Chem. Soc. Rev.*, 2004, **33**, 476–489.
- 3 S. Kitagawa and K. Uemura, *Chem. Soc. Rev.*, 2005, **34**, 109–119.
- 4 H. W. Roesky and M. Andruh, *Coord. Chem. Rev.*, 2003, **236**, 91–119.
- 5 P. Politzer and J. S. Murray, *ChemPhysChem*, 2013, **14**, 278–294.
- 6 S. R. Batten, N. R. Champness, X.-M. Chen, J. Garcia-Martinez, S. Kitagawa, L. Öhrström, M. O’Keeffe, M. P. Suh and J. Reedijk, *CrystEngComm*, 2012, **14**, 3001–3004.
- 7 B. Hoskins and R. Robson, *J. Am. Chem. Soc.*, 1989, **111**, 5962–5964.
- 8 H. Li, M. Eddaoudi, M. O’Keeffe and O. M. Yaghi, *Nature*, 1999, **402**, 276–279.
- 9 K. Uemura, R. Matsuda and S. Kitagawa, *J. Solid State Chem.*, 2005, **178**, 2420–2429.
- 10 J. Zhang, Y. Du, K. Dong, H. Su, S. Zhang, S. Li and S. Pang, *Chem. Mater.*, 2016, **28**, 1472–1480.
- 11 R. Kitaura, K. Fujimoto, S. I. Noro, M. Kondo and S. Kitagawa, *Angew. Chem.*, 2002, **41**, 133–135.
- 12 K. Sumida, D. L. Rogow, J. A. Mason, T. M. McDonald, E. D. Bloch, Z. R. Herm, T. Bae and R. Long, *Chem. Rev.*, 2012, **112**, 724–781.
- 13 S. D. Burd, S. Ma, J. A. Perman, B. J. Sikora, R. Q. Snurr, P. K. Thallapally, J. Tian, L. Wojtas and M. J. Zaworotko, *J. Am. Chem. Soc.*, 2012, **134**, 3663–3666.
- 14 S. Ma, D. Sun, M. Ambrogio, J. A. Fillinger, S. Parkin and H. C. Zhou, *J. Am. Chem. Soc.*, 2007, **129**, 1858–1859.
- 15 J. Lee, O. K. Farha, J. Roberts, K. A. Scheidt, S. T. Nguyen and J. T. Hupp, *Chem. Soc. Rev.*, 2009, **38**, 1450–1459.
- 16 M. Yoon, R. Srirambalaji and K. Kim, *Chem. Rev.*, 2012, **112**, 1196–1231.
- 17 M. Fujita, Y. J. Kwon, S. Washizu and K. Ogura, *J. Am. Chem. Soc.*, 1994, **116**, 1151–1152.
- 18 Z. Li, N. M. Schweitzer, A. B. League, V. Bernales, A. W. Peters, A. B. Getsoian, T. C. Wang, J. T. Miller, A. Vjunov, J. L. Fulton, J. A. Lercher, C. J. Cramer, L. Gagliardi, J. T. Hupp and O. K. Farha, *J. Am. Chem. Soc.*, 2016, **138**, 1977–1982.
- 19 M. Yoshizawa, M. Tamura and M. Fujita, *Science.*, 2006, **312**, 251–255.
- 20 C. Wu, A. Hu, L. Zhang and W. Lin, *J. Am. Chem. Soc.*, 2005, **127**, 8940–8941.

- 21 R. Q. Zou, H. Sakurai, S. Han, R. Q. Zhong and Q. Xu, *J. Am. Chem. Soc.*, 2007, **129**, 8402–8403.
- 22 L. Que and W. B. Tolman, *Nature*, 2008, **455**, 333–340.
- 23 Y. Hou, R. W. Sun, X. Zhou, J. Wang and D. Li, *Chem. Commun.*, 2014, **50**, 2295–7.
- 24 C. Janiak, *Dalt. Trans.*, 2003, 2781–2804.
- 25 Y. Sun and H.-C. Zhou, *Sci. Technol. Adv. Mater.*, 2015, **16**, 54202.
- 26 X.-M. M. Chen and M.-L. L. Tong, *Acc. Chem. Res.*, 2007, **40** VN-r, 162–170.
- 27 X. M. Zhang, *Coord. Chem. Rev.*, 2005, **249**, 1201–1219.
- 28 C. Falaise, J. S. Charles, C. Volkringer and T. Loiseau, *Inorg. Chem.*, 2015, **54**, 2235–2242.
- 29 D. Jiang, X. Huang, F. Qiu, C. Luo and L. L. Huang, *Macromolecules*, 2010, **43**, 71–76.
- 30 J. Yao, D. Dong, D. Li, L. He, G. Xu and H. Wang, *Chem. Commun.*, 2011, **47**, 2559–2561.
- 31 H. Schmalzried, *Angew. Chem.*, 1963, **2**, 31–34.
- 32 J. G. Hernandez and T. Friscicé, *Tetrahedron Lett.*, 2015, **56**, 4253–4265.
- 33 S. L. James, C. J. Adams, C. Bolm, D. Braga, P. Collier, T. Friščić, F. Grepioni, K. D. M. Harris, G. Hyett, W. Jones, A. Krebs, J. Mack, L. Maini, a G. Orpen, I. P. Parkin, W. C. Shearouse, J. W. Steed and D. C. Waddell, *Chem. Soc. Rev.*, 2012, **41**, 413–47.
- 34 F. Wang, C. Y. Ni, Q. Liu, F. L. Li, J. Shi, H. X. Li and J. P. Lang, *Chem. Commun.*, 2013, **49**, 9248–9250.
- 35 C. Suryanarayana, *Prog. Mater. Sci.*, 2001, **46**, 1–184.
- 36 A. L. Garay, A. Pichon and S. L. James, *Chem. Soc. Rev.*, 2007, **36**, 846.
- 37 C. Wayman, *Annu. Rev. Mater. Sci.*, 1971, **1**, 185–218.
- 38 K. Biradha and R. Santra, *Chem. Soc. Rev.*, 2013, **42**, 950–967.
- 39 G. K. Kole and J. J. Vittal, *Chem. Soc. Rev.*, 2013, **42**, 1755–1775.
- 40 J. M. Falkowski, C. Wang, S. Liu and W. Lin, *Angew. Chem.*, 2011, **50**, 8674–8678.
- 41 R. J. Marshall, S. L. Griffin, C. Wilson and R. S. Forgan, *J. Am. Chem. Soc.*, 2015, **137**, 9527–9530.
- 42 Q. Q. Li, C. Y. Ren, Y. Y. Huang, J. L. Li, P. Liu, B. Liu, Y. Liu and Y. Y. Wang, *Chem. Eur. J.*, 2015, **21**, 4703–4711.
- 43 C. C. Wang, C. C. Yang, C. T. Yeh, K. Y. Cheng, P. C. Chang, M. L. Ho, G. H. Lee, W. J. Shih and H. S. Sheu, *Inorg. Chem.*, 2011, **50**, 597–603.

- 44 U. Stoeck, S. Krause, V. Bon, I. Senkovska and S. Kaskel, *Chem Commun*, 2012, **48**, 10841–10843.
- 45 S. Krause, V. Bon, I. Senkovska, U. Stoeck, D. Wallacher, D. M. Töbrens, S. Zander, R. S. Pillai, G. Maurin, F.-X. Coudert and S. Kaskel, *Nature*, 2016, 1–5.
- 46 L. Xu, F. Bu, M. Hu, C. Jin, D. Jiang, Z. Zhao, Q. Zhang and J. Jiang, *Chem. Commun.*, 2014, **50**, 13849–13852.
- 47 A. Heinz, C. J. Strachan, K. C. Gordon and T. Rades, *J. Pharm. Pharmacol.*, 2009, **61**, 971–988.
- 48 S. Takamizawa, E. I. Nataka, T. Akatsuka, R. Miyake, Y. Kakizaki, H. Takeuchi, G. Maruta and S. Takeda, *J. Am. Chem. Soc.*, 2010, **132**, 3783–3792.
- 49 P. Shen, W. He, D. Du, H. Jiang, S. Li, Z. Lang, Z. Su, Q. Fu and Y. Lan, *Chem. Sci.*, 2014, **5**, 1368.
- 50 A. N. Khlobystov, A. J. Blake, N. R. Champness, D. A. Lemenovskii, A. G. Majouga, N. V. Zyk and M. Schroder, *Coord. Chem. Rev.*, 2001, **222**, 155–192.
- 51 Y. L. Wang, Q. Y. Liu and L. Xu, *CrystEngComm*, 2008, **10**, 1667.
- 52 S. Kitagawa, R. Kitaura and S. Noro, *Angew. Chem.*, 2004, **43**, 2334–2375.
- 53 H. Schmidbaur and A. Schier, *Angew. Chem.*, 2015, **54**, 746–784.
- 54 Z. Xu, *Coord. Chem. Rev.*, 2006, **250**, 2745–2757.
- 55 M. I. Azócar, G. Gómez, P. Levín, M. Paez, H. Muñoz and N. Dinamarca, *J. Coord. Chem.*, 2014, **67**, 3840–3853.
- 56 K. M. Fromm, *Appl. Organomet. Chem.*, 2013, **27**, 683–687.
- 57 K. Nomiya, K. Tsuda, T. Sudoh and M. Oda, *J. Inorg. Biochem.*, 1997, **68**, 39–44.
- 58 G. Chakkaradhari, Y. T. Chen, A. J. Karttunen, M. T. Dau, J. Janis, S. P. Tunik, P. T. Chou, M. L. Ho and I. O. Koshevoy, *Inorg. Chem.*, 2016, **55**, 2174–2184.
- 59 J. Heine and K. Müller-Buschbaum, *Chem. Soc. Rev.*, 2013, **42**, 9232–9242.
- 60 S. M. Zhang, T. L. Hu, J. R. Li, J. L. Du and X. H. Bu, *CrystEngComm*, 2008, **10**, 1595–1604.
- 61 X. Y. Wu, H. X. Qi, J. J. Ning, J. F. Wang, Z. G. Ren and J. P. Lang, *Appl. Catal. B Environ.*, 2015, **168–169**, 98–104.
- 62 L. Brammer, M. D. Burgard, M. D. Eddleston, C. S. Rodger, N. P. Rath and H. Adams, *CrystEngComm*, 2002, **4**, 239–248.
- 63 L. Brammer, M. D. Burgard, C. S. Rodger, J. K. Swearingen and N. P. Rath, *Chem. Commun.*, 2001, 2468–2469.
- 64 S. Libri, M. Mahler, G. Míguez Espallargas, D. C. N. G. Singh, J. Soleimannejad, H. Adams, M. D. Burgard, N. P. Rath, M. Brunelli and L. Brammer, *Angew. Chem.*, 2008, **47**, 1693–1697.

- 65 I. J. Vitórica-Yrezabal, G. Múñez Espallargas, J. Soleimannejad, A. J. Florence, A. J. Fletcher and L. Brammer, *Chem. Sci.*, 2013, **4**, 696–708.
- 66 I. J. Vitórica-Yrezabal, S. Libri, J. R. Loader, G. Múñez Espallargas, M. Hippler, A. J. Fletcher, S. P. Thompson, J. E. Warren, D. Musumeci, M. D. Ward and L. Brammer, *Chem. Eur. J.*, 2015, **21**, 8799–8811.
- 67 J. S. Wright, I. J. Vitórica-Yrezabal, H. Adams, S. P. Thompson, A. H. Hill and L. Brammer, *IUCrJ*, 2015, **2**, 188–197.
- 68 J. S. Wright, I. J. Vitórica-Yrezabal, S. P. Thompson and L. Brammer, *Chem. Eur. J.*, 2016, **22**, 13120–13126.

2. Structures and solid-state transformations of coordination polymers containing silver perfluorocarboxylates combined with quinoxaline

2.1 Introduction

Quinoxaline ($C_8H_6N_2$) is an organic compound in which nitrogen atoms replace two carbon atoms (C1 and C4) of naphthalene. It and its derivatives have received recent attention in the pharmaceutical industry because of the wide-spectrum antimicrobial properties.¹ However, quinoxaline-based ligands have not been very common choices in synthesizing coordination polymers and there are only few silver-containing coordination polymer examples reported in the literature. Kocunov and co-workers have reported a coordination polymer of silver(I) perrhenate with quinoxaline ($[Ag(Quin)](ReO_4)$, Quin: quinoxaline). The basic coordination environment for quinoxaline is similar to the previous diimine-containing coordination polymers discussed in **Chapter 1**. Quinoxaline ligands are bridging in between every two silvers along one direction, which gives an see-saw Ag coordination centre. However two Ag-Quin chains are connected by the perrhenate ions and result in a 1D double Ag-Quin polymer, which is different from the 1D tape structure we studied. As observed in many other silver(I) coordination polymers, this compound is luminescent.²

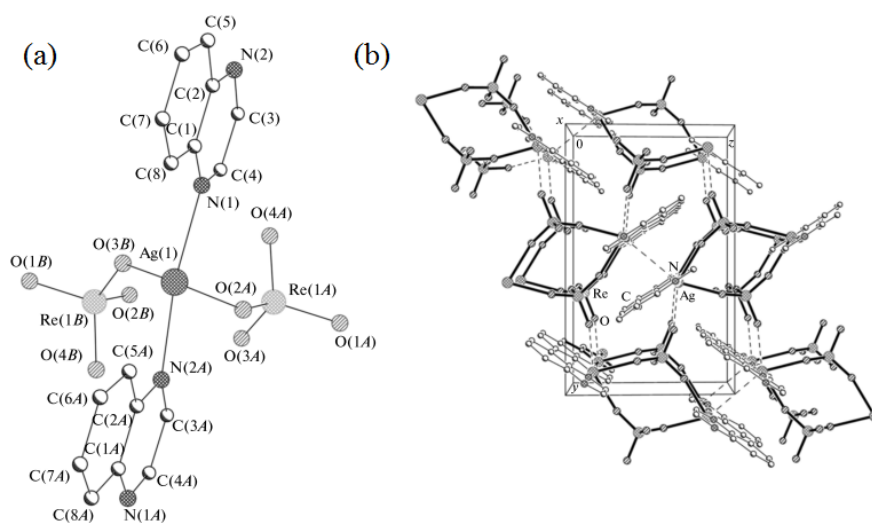


Figure 2.1 Crystal structures of $[Ag(Quin)](ReO_4)$ showing (a) see-saw coordination environment of Ag centre and (b) crystal packing along $[100]$. (Figure reproduced from ref. 2)

Abu-Youssef and co-workers have reported a coordination polymer of silver nitrate with quinoxaline, $[Ag(Quin)](NO_3)$, which again has similar coordination environment for silver but further connected into a 2D layer structure. According to the test (broth microdilution method against selected standard microorganisms), this compound has a wide spectrum against bacteria (either Gram+ or Gram-) and yeasts.³

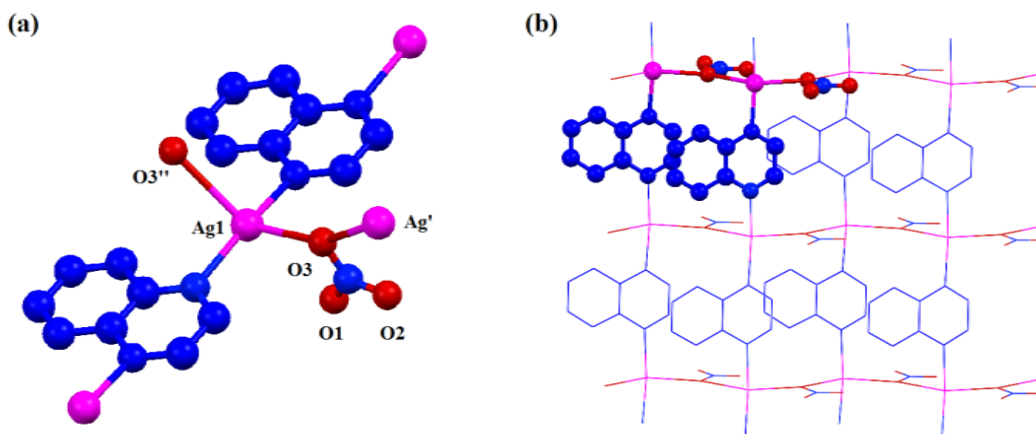


Figure 2.2 Crystal structures of $[\text{Ag}(\text{Quin})](\text{NO}_3)$ showing (a) see-saw coordination environment of Ag centre and (b) the 2D layer structure. (Figure reproduced from ref. 3)

In recent years solid-state transformations of coordination polymers has become quite an active area in inorganic and materials chemistry.⁴ Among them, there are some interesting studies of solid-state transformation of silver-containing coordination polymers. For example, Vittal and co-workers have reported a multiple-step solid-state transformation of $[\text{Ag}(\mu\text{-bpe})(\text{H}_2\text{O})](\text{CF}_3\text{CO}_2)\text{CH}_3\text{CN}$ ($\mu\text{-bpe}$ = 4,4'-bipyridylethylene). The transformation starts from the desolvation of the single crystal (**Figure 2.3.a**) and the linear 1D structure starts to collapse. After a phase-rebuilding process an intermediate crystalline phase (**Figure 2.3.b**) can be found, followed by the completion of the phase transformation with a stable 1D ladder-like structure (**Figure 2.3.c**). This structure can undergo a further photodimerized transformation into another zig-zag structure (**Figure 2.3.d**).⁵

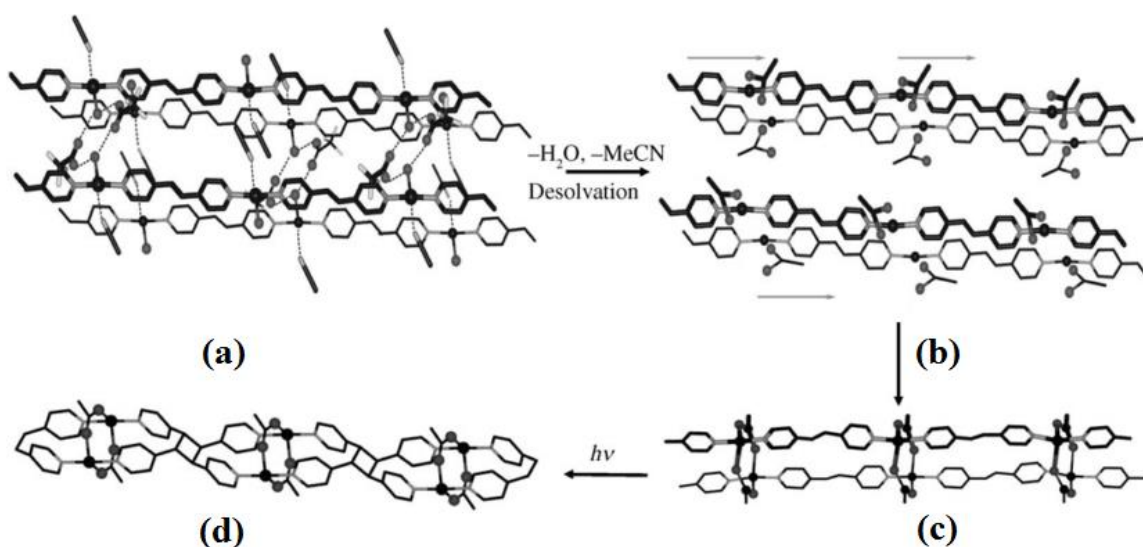


Figure 2.3 Scheme of the transformation of $[\text{Ag}(\mu\text{-bpe})(\text{H}_2\text{O})](\text{CF}_3\text{CO}_2)\text{CH}_3\text{CN}$ upon desolvation (a) 1D linear structure before desolvation, (b) Intermediate phase after desolvation, (c) 1D ladder-like structure after transformation, (d) structure of photodimerized product (Figure reproduced from ref. 5)

In past few years, the Brammer group have been studying the solid-state transformation of Ag(I)-perfluorocarboxylate-diimine coordination polymers, which is described in Chapter 1. These coordination polymers can undergo single-crystal-to-single-crystal transformation by taking up and releasing different alcohol molecules reversibly.⁶ Staged solid-state transformations are common for these coordination polymers by losing the coordinated solvent or ligand molecules under heating.⁷ It has also been shown that the likely pathway for the molecular transportation during the solid-state transformation involves the spaces in between the interdigitated perfluoroalkyl chains.⁸ We are seeking a more complete understanding the scope of solid-state transformations in these Ag(I)-perfluorocarboxylate-diimine coordination polymers. Thus, further studies will be focused on some selected related materials in order to look for more detailed evidence to develop the full picture. Previous materials of this type, have been shown to undergo solid-state transformations in which a diimine ligand is lost.⁸ The study described in this chapter sets out to establish the generality of these coordination polymer structures when different perfluoroalkyl carboxylates are used and to determine whether conversion between coordination polymers can be achieved via loss of quinoxaline ligands in a solid-state chemical reaction. Previous work in our group^{9,10} has established that reaction of silver(I) perfluoroalkylcarboxylates with quinoxaline has the potential to lead to coordination polymers of the general formula $[\text{Ag}_4(\text{O}_2\text{CR}_f)_4(\text{quin})_4]$ or $[\text{Ag}_4(\text{O}_2\text{CR}_f)_4(\text{quin})_3]$ (R_f = perfluoroalkyl group; quin = quinoxaline). These studies have been added to in this work in order to clearly establish the behaviour of these materials (Some unpublished results from previous group members are included in this section to enable a full discussion. Such inclusions are denoted by an asterisk).

2.2 Experimental

2.2.1 Synthesis

All the reactants were purchased from Sigma Aldrich, Alfa Aesar or Fluorochem and used as received. Elemental analyses were carried out by the University of Sheffield, Department of Chemistry elemental analysis service, using a Perkin–Elmer 2400 CHNS/O Series II elemental analyzer.

All the coordination polymers were prepared using a similar method, referred to as "layering synthesis" (**Figure 2.4**). For the series of coordination polymers, solution A, in which quinoxaline was dissolved, was the bottom layer while solution B, which contained the silver perfluorocarboxylate salts, was the top layer. The middle buffer layer was prepared by separately layering the two solvents, which were used in preparing the two reactant solutions, onto the solution A. The idea for using layering synthesis was to slow down the reaction by generating slow diffusion between two reactants in order to improve the chance of forming single crystals rather than powders. Generally, thin plate-like crystals formed either on the

surface of the solution, or on the wall and/or bottom of the vial. In a few reactions, cloudy powders would form first after several hours and then crystals formed from the powder later.

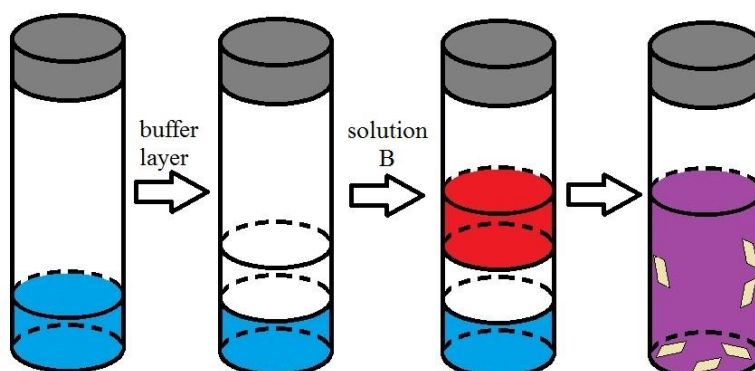


Figure 2.4 Illustration of the layering synthesis (blue: solution A; white: buffer layer; red: solution B).

Preparation of $[\text{Ag}_4(\text{O}_2\text{CCF}_3)_4(\text{Quin})_4]$ (1**).** Quinoxaline (6.5 mg, 0.05 mmol) was dissolved in ethyl acetate (1.0 mL) in a 20 mL glass vial and gently layered with ethyl acetate (2 mL) and then acetone (2 mL) onto this solution. Then an acetone solution (1.0 mL) of silver(I) trifluoroacetate (10 mg, 0.045 mmol) was carefully layered onto the buffer layer. The vial was tightly capped and stored in a dark cupboard to minimize the possibility of light degradation of silver ions. Yellow crystals of **1** were formed within one week. Yield: 14.6 mg (93%). Anal. Calcd. (%) for $\text{C}_{40}\text{H}_{24}\text{Ag}_4\text{F}_{12}\text{N}_8\text{O}_8$: C 34.22; H 1.72; N 7.98; found (%): C 34.01; H 1.67; N 7.82%.

Preparation of $[\text{Ag}_4(\text{O}_2\text{CCF}_2\text{CF}_3)_4(\text{Quin})_4]$ (2**).** An analogous layering synthesis to that used for **1** was applied for preparing **2**, using a methanol solution (1.0 mL) of quinoxaline (32 mg, 0.246 mmol), a methanol solution (1.0 mL) of silver(I) pentafluoropropanoate (30 mg, 0.11 mmol) and without applying a buffer layer. Yellow crystals of **2** were generated within 3 days. Yield: 9.5 mg (21%). Anal. Calcd. (%) for $\text{C}_{44}\text{H}_{24}\text{Ag}_4\text{F}_{20}\text{N}_8\text{O}_8$: C 32.92; H 1.50; N 6.98; found (%): C 32.72; H 1.78; N 6.75%.

Preparation of $[\text{Ag}_4(\text{O}_2\text{C}(\text{CF}_2)_2\text{CF}_3)_4(\text{Quin})_4]$ (3**).** An analogous layering synthesis to that used for **1** was applied for preparing **3**, using an ethyl acetate solution (1.0 mL) of quinoxaline (13 mg, 0.10 mmol), a buffer solution of ethyl acetate (2 mL) and acetone (2 mL) and an acetone solution (1.0 mL) of silver(I) heptafluorobutanoate (29 mg, 0.09 mmol). Pale yellow crystals of **3** were formed within 5 days. Yield: 18.7 mg (46%). Anal. Calcd. (%) for $\text{C}_{44}\text{H}_{24}\text{Ag}_4\text{F}_{20}\text{N}_8\text{O}_8$: C, 31.95; H, 1.33; N, 6.21%; found (%): C, 31.87; H, 1.20; N, 6.31%.

Preparation of [Ag₄(O₂C(CF₂)₃CF₃)₄(Quin)₄] (4). An analogous layering synthesis to that used for **1** was applied for preparing **4**, using an ethyl acetate solution (1.0 mL) of quinoxaline (13 mg, 0.1 mmol), a buffer solution of ethyl acetate (2 mL) and acetone (2 mL) and an acetone solution (1.0 mL) of silver(I) nonafluoropentanoate (16.5 mg, 0.045 mmol). Pale yellow crystals of **4** were afforded within 4 days. Yield: 11 mg (48%). Anal. Calcd. (%) for C₅₂H₂₄Ag₄F₃₆N₈O₈: C 31.16; H 1.21; N 5.59; found (%): C 31.24; H 1.43; N 5.52%.

Preparation of [Ag₄(O₂C(CF₂)₄CF₃)₄(Quin)₄] (5). An analogous layering synthesis to that used for **1** was applied for preparing **5**, using an ethyl acetate solution (4.0 mL) of quinoxaline (64 mg, 0.4 mmol), a buffer solution of ethyl acetate (0.5 mL) and acetone (0.5 mL) and an acetone solution (4.0 mL) of silver(I) undecafluorohexanoate (151.2 mg, 0.36 mmol). Yellow crystals were produced after 1 day and gradually turned into yellow crystals of **5** within 2 days. Yield: 126 mg (64%). Anal. Calcd. (%) for C₅₆H₂₄Ag₄F₄₄N₈O₈: C 30.52; H 1.10; N 5.08; found (%): C 30.60; H 1.46; N 5.17%.

Preparation of [Ag₄(O₂CCF₃)₄(Quin)₃] (6). An analogous layering synthesis to that used for **1** was applied for preparing **6**, using an ethyl acetate solution (1.0 mL) of quinoxaline (6.5 mg, 0.05 mmol), a buffer solution of ethyl acetate (2 mL) and acetone (2 mL) and an acetone solution (1.0 mL) of silver(I) trifluoroacetate (20 mg, 0.09 mmol). Pale yellow crystals of **6** were formed within 2 days. Yield: 6.5 mg (60%). Anal. Calcd. (%) for C₃₂H₁₈Ag₄F₁₂N₆O₈: C 30.15; H 1.41; N 6.60; found (%): C 30.14; H 1.70; N 6.56%.

Preparation of [Ag₄(O₂CCF₂CF₃)₄(Quin)₃] (7). An analogous layering synthesis to that used for **1** was applied for preparing **7**, using an ethyl acetate solution (1.0 mL) of quinoxaline (6.0 mg, 0.046 mmol), a buffer solution of ethyl acetate (2 mL) and acetone (2 mL) and an acetone solution (1.0 mL) of silver(I) pentafluoropropanoate (16.8 mg, 0.062 mmol). Off-white crystals of **7** were turned formed within 3 days. Yield: 5.1 mg (23%). Anal. Calcd. (%) for C₃₆H₁₈Ag₄F₂₀N₆O₈: C 29.35; H 1.22; N 5.70; found (%): C 29.29; H 1.12; N 5.62%.

Preparation of [Ag₄(O₂C(CF₂)₂CF₃)₄(Quin)₃] (8). An analogous layering synthesis to that used for **1** was applied for preparing **8**, using an ethyl acetate solution (2.0 mL) of quinoxaline (13.0 mg, 0.10 mmol), a buffer solution of ethyl acetate (2 mL) and acetone (2 mL) and an acetone solution (2.0 mL) of silver(I) heptafluorobutanoate (58.0 mg, 0.18 mmol). Off-white crystals of **8** were formed within 3 days. Yield: 30 mg (58%). Anal. Calcd. (%) for C₄₀H₁₈Ag₄F₂₈N₆O₈: C 28.68; H 1.08; N 5.02; found (%): C 28.92; H 1.10; N 5.06%.

Syntheses for potential 4:4:3 coordination polymers, $[\text{Ag}_4(\text{O}_2\text{C}(\text{CF}_2)_3\text{CF}_3)_4(\text{Quin})_3]$ (**9**) and $[\text{Ag}_4(\text{O}_2\text{C}(\text{CF}_2)_4\text{CF}_3)_4(\text{Quin})_3]$ (**10**), were attempted using analogous layering syntheses with different combinations of different concentrations of the two reactants but failed. **9** could not be directly synthesized in solution even with low concentrations of quinoxaline, as **4** was always formed as the sole product. Preparing **10** in solution proved to be difficult even when using low concentrations of quinoxaline. The synthesis always yielded white crystals first, which were different from the yellow needle-like crystals for compound **5**. These white, thin and tape-like crystals are not mechanically robust as general crystals and could be easily bent when moving them in the oil under the microscope. This phenomenon is popular in some organic crystals due to the high anisotropic nature in their structure as reported by Desiraju and co-workers.^{11,12} Unfortunately, the SCXRD data sets collected in Sheffield were not good enough for solving the structure. These white crystals turned into yellow crystals within 1-2 days, which were then identified to be compound **5**. Thus, combining with the results reported from the previous members in our group, we roughly assume that 4:4:4 phases are the thermodynamically-driven products and the 4:4:3 phases are the kinetically-driven products in the liquid phase.

2.2.2 Single Crystal X-ray Diffraction (SCXRD)

Single-crystal X-ray data were collected at 150 K for **1**, **3-6** and **8**, 120 K for **2** and 100 K for **7**, on a Bruker D8 *VENTURE* diffractometer, equipped with a PHOTON 100 CMOS detector (using Cu- K_α radiation, $\lambda = 1.54178 \text{ \AA}$) or a Bruker APEX-II diffractometer (using Mo- K_α radiation, $\lambda = 0.71073 \text{ \AA}$). The crystal structures were solved with Direct methods or Patterson method using the *SHELXTL*¹³ or *Olex2*¹⁴ suites of programs. All the structures were refined against all F^2 values and a multi-scan method (*SADABS*)¹⁵⁻¹⁷ was used for absorption correction. All non-H atoms were applied anisotropically and hydrogen atoms were added at their calculated positions. Disordered parts in some compounds were modelled with reasonable occupancies for all those atoms and all these atoms were refined isotropically. Disorder of one CF_3 group in compound **7** was modelled with two orientations related by rotation (occupancy for two orientations in each compound: 0.67(4)/0.33(4)). Disorder of the four CF_3 groups in compound **6** was modelled with two orientations related for each (occupancy for two orientations in each compound: 0.50(3), 0.54(4)/0.46(4), 0.60(6)/0.40(6) and 0.66(6)/0.34(6)). Disorder of the $\text{CF}_2(\text{CF}_2)_4\text{CF}_3$ chains in compound **5** was modelled with two orientations (occupancy for two orientations: 0.58(1)/0.42(1)). Disorder of two out of total four $\text{CF}_2(\text{CF}_2)_2\text{CF}_3$ chains in compound **8** was modelled with two orientations (occupancy for two orientations in each chain: 0.59(2)/0.41(2) and 0.52(2)/0.48(2)). Details of crystal data, structure solution and refinement parameters for compounds **1-8** can be found in **Table 2.1**.

Table 2.1 Crystal Data, Structure Solution and Refinement Parameters

	[Ag ₄ (O ₂ CCF ₃) ₄ (quin) ₄] (1)	[Ag ₄ (O ₂ CCF ₂ CF ₃) ₄ (quin) ₄] (2)	[Ag ₄ (O ₂ C(CF ₂) ₂ CF ₃) ₄ (quin) ₄] (3)
Crystal colour	Yellow	Colourless	Yellow
Crystal size (mm)	0.22 x 0.26 x 0.05	0.20 x 0.14 x 0.04	0.34 x 0.22 x 0.13
Crystal system	Orthorhombic	Triclinic	Monoclinic
Space group, <i>Z</i>	<i>Pbcm</i> , 1	<i>P</i> -1, 1	<i>P</i> 2 ₁ / <i>c</i> , 1
<i>a</i> (Å)	11.7575(3)	13.3405(9)	14.5530(7)
<i>b</i> (Å)	6.6483(2)	6.6186(4)	6.6729(4)
<i>c</i> (Å)	14.4311(4)	14.3831(11)	14.3152(6)
α (°)	90	90.191(5)	90
β (°)	90	102.636(5)	96.466(3)
γ (°)	90	80.249(5)	90
<i>V</i> (Å ³)	1128.04(5)	1220.55(15)	1381.32(12)
Density (Mg.m ⁻³)	2.067	2.182	2.169
Wavelength (Å)	0.71073	1.54178	0.71073
Temperature (K)	150	120	150
μ (Mo-K α /Cu-K α) (mm ⁻¹)	1.822	13.973	1.554
Θ range (°)	2.82 to 27.39	3.151 to 52.184	2.86 to 29.05
Reflns collected	10513	6712	11045
Independent reflns (<i>R</i> _{int})	1351 (0.0277)	2633 (0.0613)	3682 (0.0279)
Reflns used in refinement, <i>n</i>	1351	2633	3682
L.S. parameters, <i>p</i>	90	379	216
No. of restraints, <i>r</i>	0	1	0
<i>R</i> 1 (<i>F</i>) ^[a] <i>I</i> > 2.0 σ (<i>I</i>)	0.0223	0.0630	0.0391
<i>wR</i> 2(<i>F</i> ²) ^[a] , all data	0.0601	0.1765	0.1260
<i>S</i> (<i>F</i> ²) ^[a] , all data	1.051	1.029	1.018

Table 2.1 (continued)

	[Ag ₄ (O ₂ C(CF ₂) ₃ CF ₃) ₄ (quin) ₄] (4)	[Ag ₄ (O ₂ C(CF ₂) ₄ CF ₃) ₄ (quin) ₄] (5)	[Ag ₄ (O ₂ CCF ₃) ₄ (quin) ₃] (6)
Crystal colour	Pale yellow	Yellow	Yellow
Crystal size (mm)	0.34 x 0.19 x 0.02	0.38 x 0.10 x 0.07	0.25 x 0.14 x 0.04
Crystal system	Monoclinic	Monoclinic	Monoclinic
Space group, <i>Z</i>	<i>P</i> 2 ₁ / <i>c</i> , 1	<i>P</i> 2 ₁ / <i>c</i> , 1	<i>P</i> 2 ₁ / <i>n</i> , 4
<i>a</i> (Å)	17.0394(8)	17.0199(16)	10.3394(3)
<i>b</i> (Å)	6.6746(3)	6.6761(6)	16.3000(5)
<i>c</i> (Å)	14.2268(6)	14.3243(16)	23.2981(8)
α (°)	90	90	90
β (°)	109.915(3)	94.823(7)	97.9921(19)
γ (°)	90	90	90
<i>V</i> (Å ³)	1521.42(12)	1638.9(3)	3888.24(2)
Density (Mg.m ⁻³)	2.178	2.225	2.176
Wavelength (Å)	0.71073	0.71073	1.54178
Temperature (K)	150	150	150
μ ((Mo-K α /Cu-K α) (mm ⁻¹))	1.440	1.36	16.988
Θ range (°)	2.873 to 26.816	3.19 to 26.62	3.32 to 52.06
Reflns collected	12678	12736	21617
Independent reflns (<i>R</i> _{int})	3280 (0.0466)	3659 (0.0495)	4261 (0.0628)
Reflns used in refinement, <i>n</i>	3280	3659	4261
L.S. parameters, <i>p</i>	243	250	549
No. of restraints, <i>r</i>	0	55	0
<i>R</i> 1 (<i>F</i>) ^[a] <i>I</i> > 2.0 σ (<i>I</i>)	0.0414	0.0861	0.0620
<i>wR</i> 2(<i>F</i> ²) ^[a] , all data	0.1264	0.2614	0.1574
<i>S</i> (<i>F</i> ²) ^[a] , all data	1.032	1.039	1.057

Table 2.1 (continued)

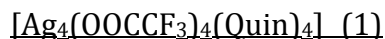
	[Ag ₄ (O ₂ CCF ₂ CF ₃) ₄ (quin) ₃] (7)	[Ag ₄ (O ₂ C(CF ₂) ₂ CF ₃) ₄ (quin) ₃] (8)
Crystal colour	Yellow	White
Crystal size (mm)	0.14 x 0.07 x 0.03	0.18 x 0.14 x 0.03
Crystal system	Orthorhombic	Monoclinic
Space group, <i>Z</i>	<i>P</i> ₂ ₁ ₂ ₁ ₂ , 2	<i>P</i> ₂ ₁ / <i>n</i> , 4
<i>a</i> (Å)	10.5119(5)	10.6884(11)
<i>b</i> (Å)	16.3803(8)	16.4660(16)
<i>c</i> (Å)	12.3916(6)	27.817(3)
α (°)	90	90
β (°)	90	91.547(5)
γ (°)	90	90
<i>V</i> (Å ³)	2133.69(18)	4893.8(9)
Density (Mg.m ⁻³)	2.294	2.272
Wavelength (Å)	1.54178	0.71073
Temperature (K)	100	150
μ ((Mo-K α /Cu-K α) (mm ⁻¹))	15.886	1.743
Θ range (°)	3.57 to 50.36	2.47 to 27.44
Reflns collected	11113	37133
Independent reflns (<i>R</i> _{int})	1918 (0.0630)	10782 (0.0700)
Reflns used in refinement, <i>n</i>	1918	10782
L.S. parameters, <i>p</i>	312	760
No. of restraints, <i>r</i>	24	46
<i>R</i> 1 (<i>F</i>) ^[a] <i>I</i> > 2.0 σ (<i>I</i>)	0.0531	0.0391
<i>wR</i> 2(<i>F</i> ²) ^[a] , all data	0.1333	0.1260
<i>S</i> (<i>F</i> ²) ^[a] , all data	1.047	1.210

$$[a] RI(F) = \Sigma(|F_o| - |F_c|) / \Sigma|F_o|; wR2(F^2) = [\Sigma w(F_o^2 - F_c^2)^2 / \Sigma w F_o^4]^{1/2}; S(F^2) = [\Sigma w(F_o^2 - F_c^2)^2 / (n + r - p)]^{1/2}$$

2.2.3 Powder X-ray Diffraction (PXRD)

Powder X-ray diffraction data for phase purity checks were either recorded in University of Sheffield (for compound **5**, **6**, **7** and **8**) or Diamond Light Source Synchrotron (for compounds **1**, **2**, **3** and **4**). The Bruker D8 ADVANCE X-ray powder diffractometer in University of Sheffield was fitted with a focusing Göbel mirror optic and a high-resolution energy-dispersive Lynxeye XE detector and operated in a capillary mode or flat-plate mode and using Cu-K α radiation ($\lambda = 1.54178 \text{ \AA}$). For the capillary mode, the sample was packed in a 0.7 mm borosilicate capillary, whereas in the flat plate mode each sample was loaded on a 14 mm silicon zero-background sample disc. Each sample was rotated at 30 rot min^{-1} to average the sample exposure and scanned at room temperature (collected as 4 sec step^{-1} and $0.02^\circ \text{ step size}$). The beamline I11 at Diamond Light Source was equipped with a wide angle (90°) PSD detector comprising 18 Mythen-2 modules ($\lambda = 0.82562 \text{ \AA}$). The samples were packed into 0.7 mm borosilicate capillaries and five pairs of scans were collected for 10 sec per pattern (2x10s per pair), as well as one 1 sec scan at both the start and the end of each pair for checking the exposure damage. These patterns were summed to offer the final collection pattern.

All the patterns were collected at room temperature and diffraction patterns were indexed and fitted by Pawley refinement¹⁸ using the *TOPAS-Academic* program.¹⁹



The unit cell parameters of **1** were used as a starting point for Pawley refinement, employing 444 parameters (6 background, 1 zero error, 5 profile, 3 cell, 429 reflections). Pawley refinement converged to $R_{wp} = 0.0675$, $R_{wp}' = 0.193$. [$a = 14.6765$ (3) \AA , $b = 11.7985$ (3) \AA , $c = 6.7539$ (2) \AA , $V = 1169.51$ (6) \AA^3].

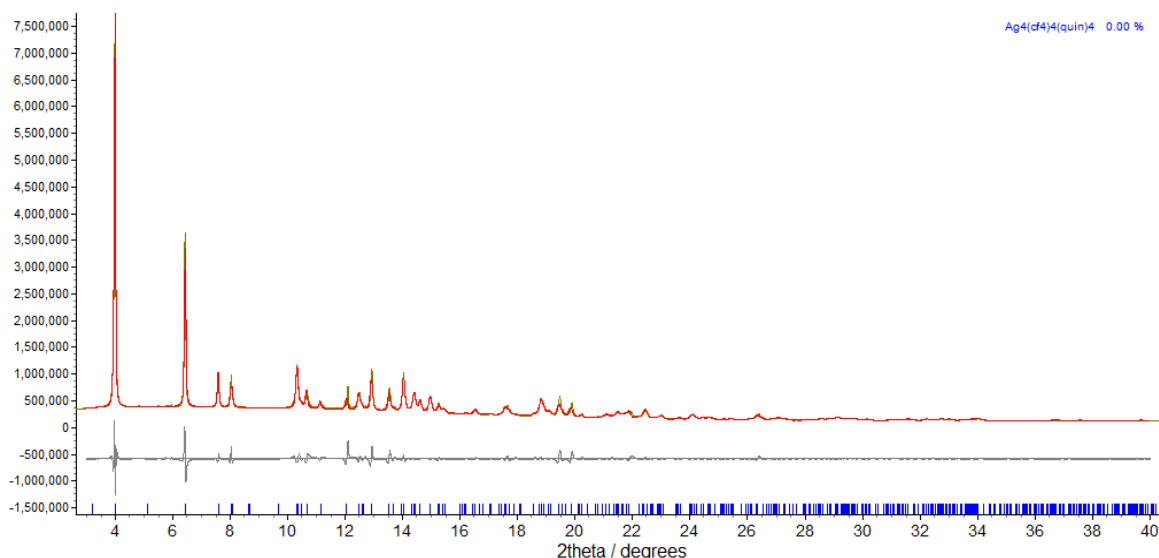


Figure 2.5 Observed (green) and calculated (red) profiles and difference plot [$I_{\text{obs}} - I_{\text{calc}}$] (grey) of the Pawley refinement. (2θ range 3.0 - 40 °, $d_{\text{min}} = 1.21$ Å).



The unit cell parameters of **2** were used as a starting point for Pawley refinement, employing 3111 parameters (6 background, 1 zero error, 5 profile, 6 cell, 3093 reflections). Pawley refinement converged to $R_{\text{wp}} = 0.0445$, $R_{\text{wp}'} = 0.118$. [$a = 22.1969$ (9) Å, $b = 11.2486$ (4) Å, $c = 25.9702$ (7) Å, $\alpha = 85.446$ (3) °, $\beta = 135.633$ (2) °, $\gamma = 83.814$ (3) °, $V = 4392.2$ (3) Å³].

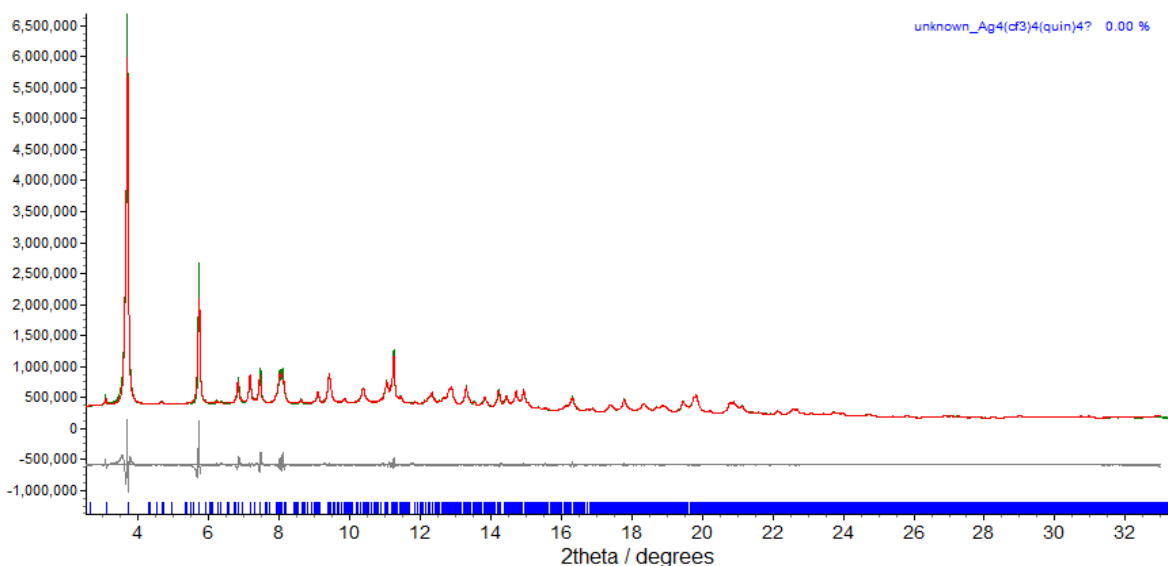


Figure 2.6 Observed (green) and calculated (red) profiles and difference plot [$I_{\text{obs}} - I_{\text{calc}}$] (grey) of the Pawley refinement. (2θ range 2.5 - 33 °, $d_{\text{min}} = 1.45$ Å).

[Ag₄(OOC(CF₂)₂CF₃)₄(Quin)₄] (3)*

The unit cell parameters of compound **3** were used as a starting point for the Pawley refinement, employing 338 parameters (6 background, 1 zero error, 5 profile, 4 cell, 322 reflections). Pawley refinement converged to $R_{wp}=0.0692$, $R_{wp}'=0.112$. [$a = 14.6410$ (2) Å, $b = 6.7869$ (1) Å, $c = 14.3907$ (2) Å, $\beta = 96.842$ (2) °, $V = 1419.78$ (4) Å³].

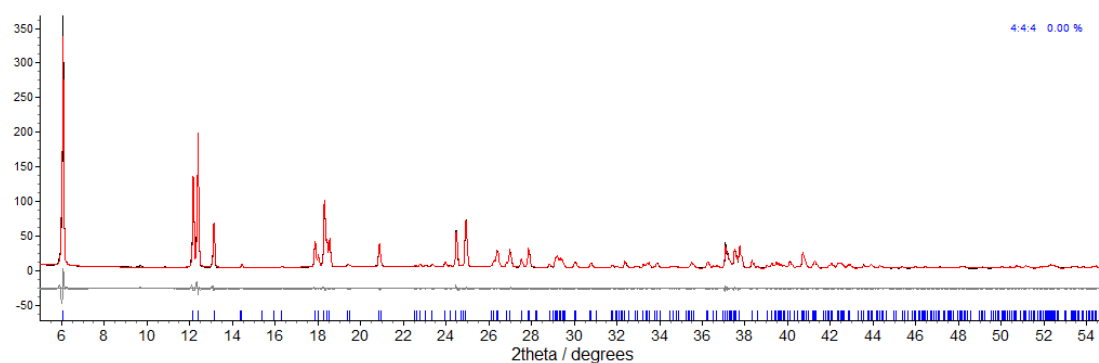


Figure 2.7 Observed (black) and calculated (red) profiles and difference plot [$I_{\text{obs}}-I_{\text{calc}}$] (grey) of the Pawley refinement for compound **1** (2θ range 6.0 - 55 °, $d_{\text{min}} = 0.89$ Å).

[Ag₄(OOC(CF₂)₃CF₃)₄(Quin)₄] (4)*

The unit cell parameters of **4** were used as a starting point for Pawley refinement, employing 1825 parameters (6 background, 1 zero error, 5 profile, 4 cell, 1809 reflections). Pawley refinement converged to $R_{wp} = 0.06956$, $R_{wp}' = 0.181$. [$a = 18.3750$ (3) Å, $b = 6.78303$ (7) Å, $c = 14.3382$ (1) Å, $\beta = 61.400$ (1) °, $V = 1569.03$ (4) Å³].

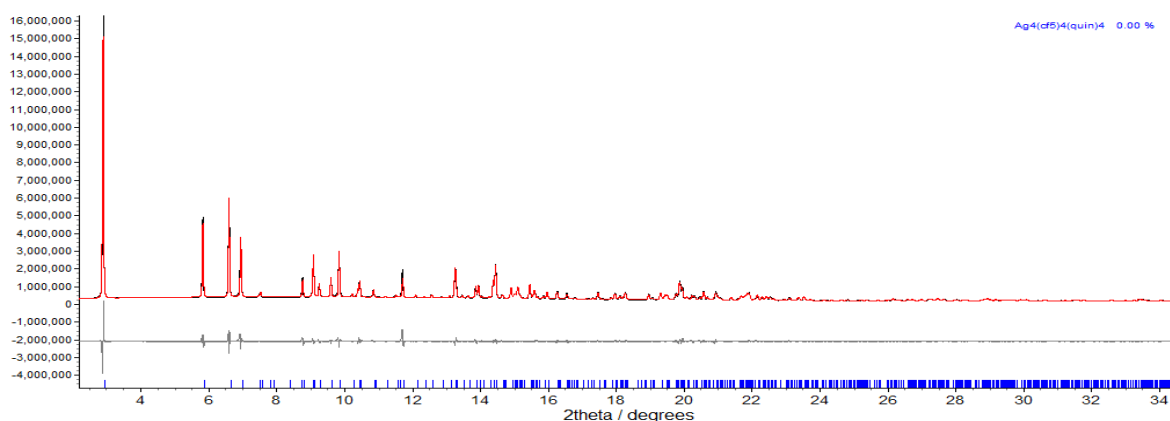


Figure 2.8 Observed (black) and calculated (red) profiles and difference plot [$I_{\text{obs}}-I_{\text{calc}}$] (grey) of the Pawley refinement. (2θ range 2.0 - 35 °, $d_{\text{min}} = 1.37$ Å).

[Ag₄(OOC(CF₂)₄CF₃)₄(Quin)₄] (5)

The sample was scanned at a rate of 1 sec step⁻¹, with each detector step size being 0.02 °. The unit cell parameters of **5** were used as a starting point for Pawley refinement, employing 480 parameters (14 background, 1 zero error, 5 profile, 4 cell, 456 reflections). Pawley refinement converged to $R_{wp}=0.051$, $R_{wp}'=0.157$. [$a = 17.288$ (9) Å, $b = 6.883$ (1) Å, $c = 14.479$ (6) Å, $\beta = 95.18$ (2) °, $V = 1715.9$ (12) Å³].

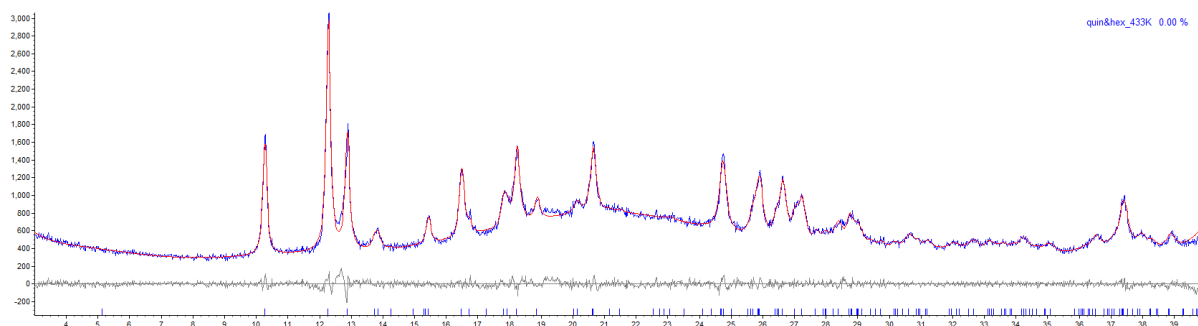


Figure 2.9 Observed (blue) and calculated (red) profiles and difference plot [$I_{obs}-I_{calc}$] (grey) of the Pawley refinement. (2θ range 3 - 40 °, $d_{min} = 2.25$ Å).

[Ag₄(OOCF₃)₄(Quin)₃] (6)

The sample was scanned at a rate of 1 sec step⁻¹, with each detector step size being 0.02 °. The unit cell of **6** from single crystal data were used as a starting point for a Pawley refinement, employing 384 parameters (6 background, 1 zero error, 5 profile, 4 cell, 368 reflections), resulting in final indices of fit $R_{wp}=0.0674$, $R_{wp}'=0.281$. [$a = 10.164$ (4) Å, $b = 16.239$ (3) Å, $c = 23.582$ (3) Å, $\beta = 99.27$ (4) °, $V = 3841$ (2) Å³].

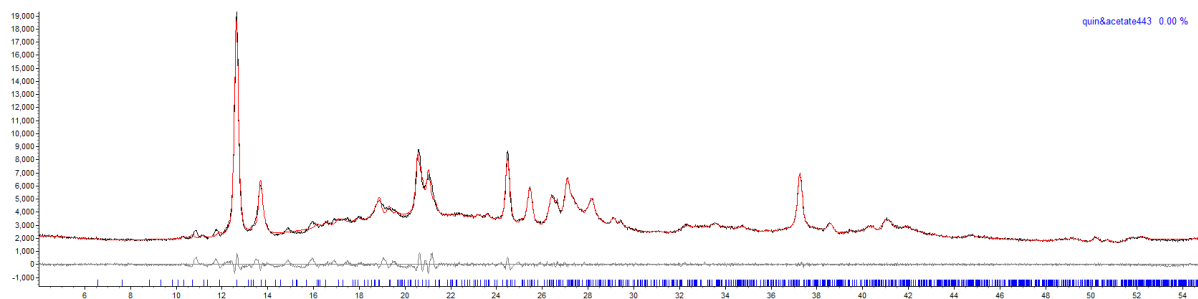


Figure 2.10 Observed (black) and calculated (red) profiles and difference plot [$I_{obs}-I_{calc}$] (grey) of the Pawley refinement. (2θ range 4 - 55 °, $d_{min} = 1.67$ Å).

[Ag₄(OOCF₂CF₃)₄(Quin)₃] (7)

The sample was scanned at a rate of 1.5 sec step⁻¹, with each detector step size being 0.02 °. The unit cell parameters of **7** were used as a starting point for the Pawley refinement, employing 420 parameters (15 background, 1 zero error, 5 profile, 4 cell, 395 reflections). Pawley refinement converged to $R_{wp}=0.0750$, $R_{wp}'=0.111$. [$a=10.649(9)$ Å, $b=16.49(1)$ Å, $c=12.715(2)$ Å, $V=2232(2)$ Å³].

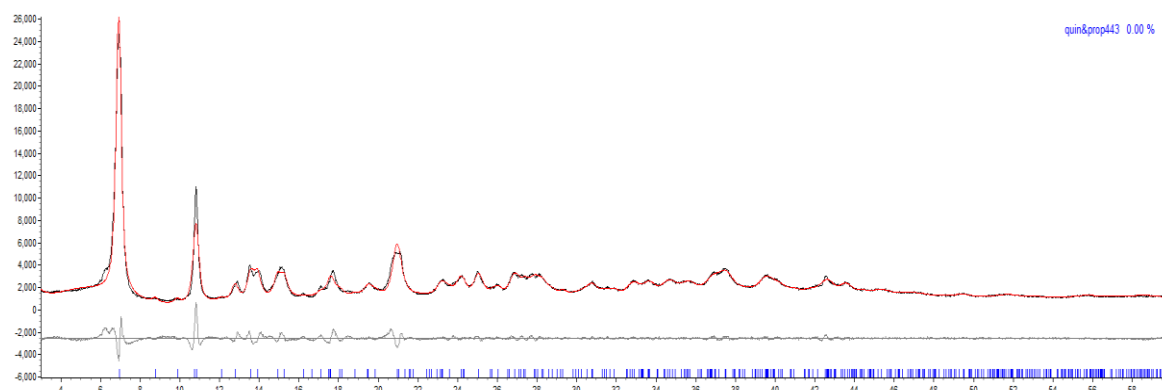


Figure 2.11 Observed (black) and calculated (red) profiles and difference plot [$I_{\text{obs}}-I_{\text{calc}}$] (grey) of the Pawley refinement. (2θ range 3.0 - 60 °, $d_{\text{min}}=1.54$ Å).

[Ag₄(OOC(CF₂)₂CF₃)₄(Quin)₃] (8)

The sample was scanned at a rate of 1.5 sec step⁻¹, with each detector step size being 0.02 °. The unit cell parameters of **8** were used as a starting point for the Pawley refinement, employing 1453 parameters (15 background, 1 zero error, 5 profile, 4 cell, 1428 reflections). Pawley refinement converged to $R_{wp}=0.0513$, $R_{wp}'=0.0891$. [$a=10.6996(9)$ Å, $b=16.312(1)$ Å, $c=27.977(2)$ Å, $\beta=92.364(7)$ °, $V=4878.8(7)$ Å³].

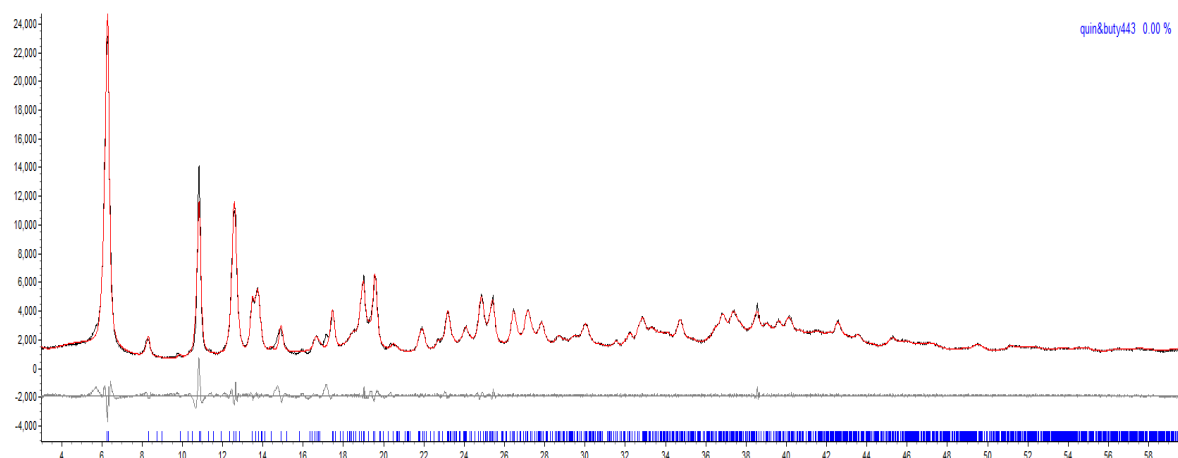
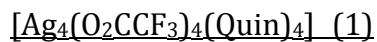


Figure 2.12 Observed (black) and calculated (red) profiles and difference plot [$I_{\text{obs}}-I_{\text{calc}}$] (grey) of the Pawley refinement. (2θ range 3.0 - 60 °, $d_{\text{min}}=1.54$ Å).

2.2.4 Thermogravimetric analyses (TGA)

Thermogravimetric analyses were recorded on a Perkin-Elmer Pyris1 TGA model thermogravimetric analyser. Samples were heated under a flow of dry N₂ gas.



Temperature sweep TGA: The sample (6.91 mg) was held at 25 °C for 5 mins and then heated to 500 °C at a rate at 2.5 °C/min, followed by holding the temperature at 500 °C for another 5 mins.

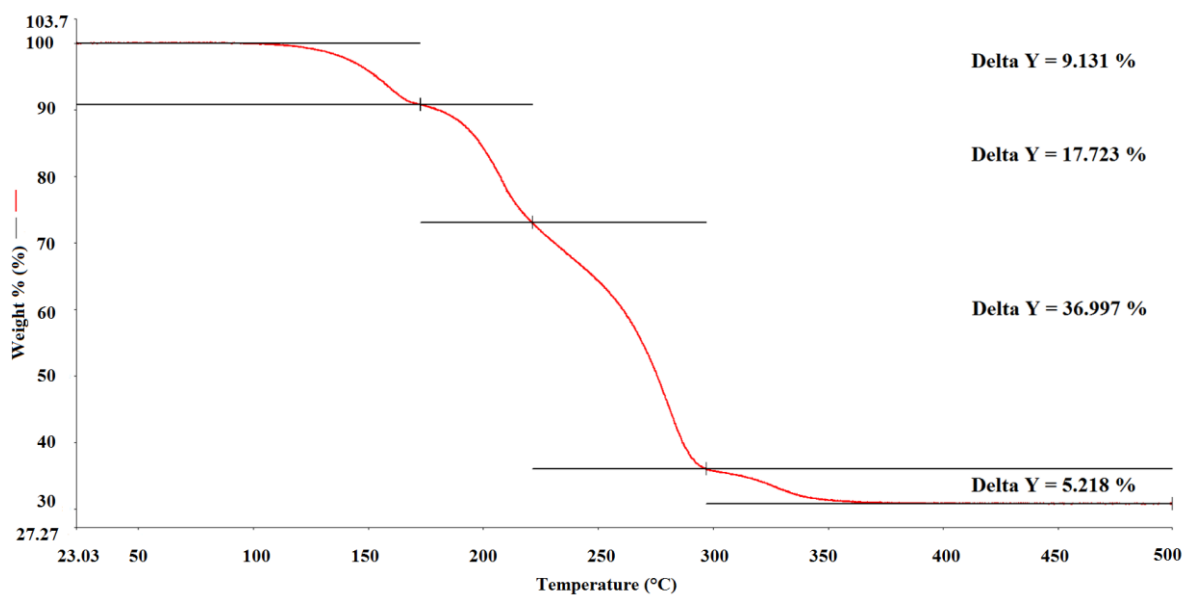


Figure 2.13 TGA for [Ag₄(O₂CCF₃)₄(Quin)₄] at a scan rate of 5 °C/min

Isothermal TGA: Sample (5.23 mg) was heated to 135 °C with a heating rate of 10 °C/min and then held at this temperature for 180 mins.

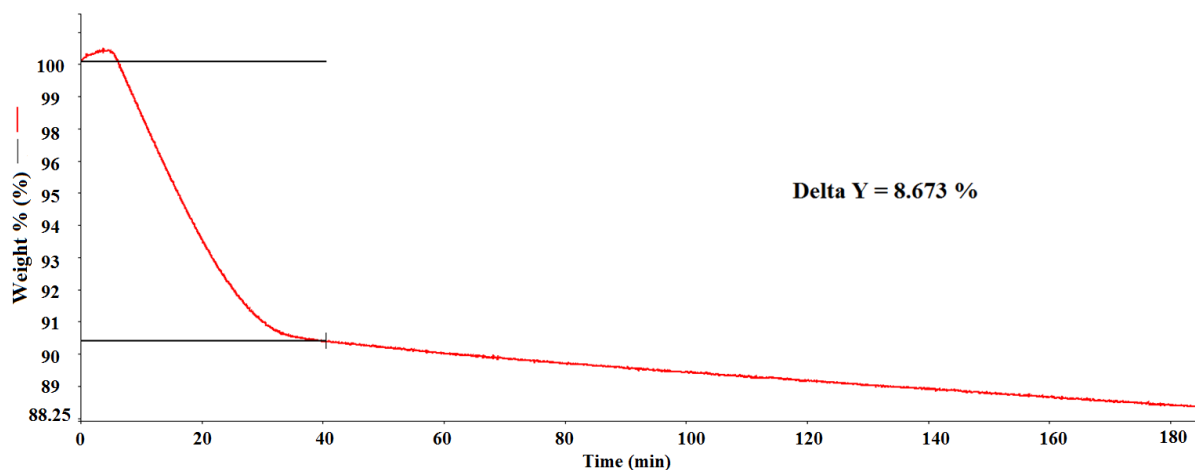


Figure 2.14 TGA for [Ag₄(O₂CCF₃)₄(Quin)₄] at a constant temperature of 135 °C



Temperature sweep TGA: Sample (3.31 mg) was held at 25 °C for 5 mins and then heated to 480 °C at a rate at 2.5 °C/min, followed by holding the temperature at 480 °C for another 5 mins.

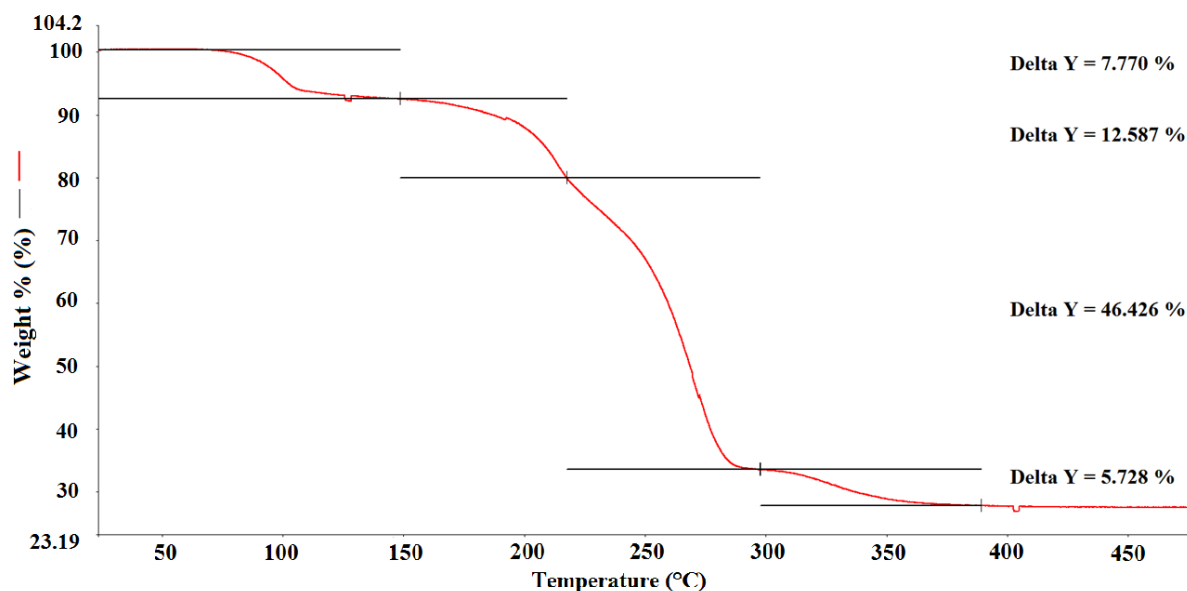


Figure 2.15 TGA for [Ag₄(O₂CCF₂CF₃)₄(Quin)₄] at a scan rate of 2.5 °C/min

Isothermal TGA: Sample (6.12 mg) was heated to 95 °C with a heating rate of 10 °C/min and then held at this temperature for 120 mins.

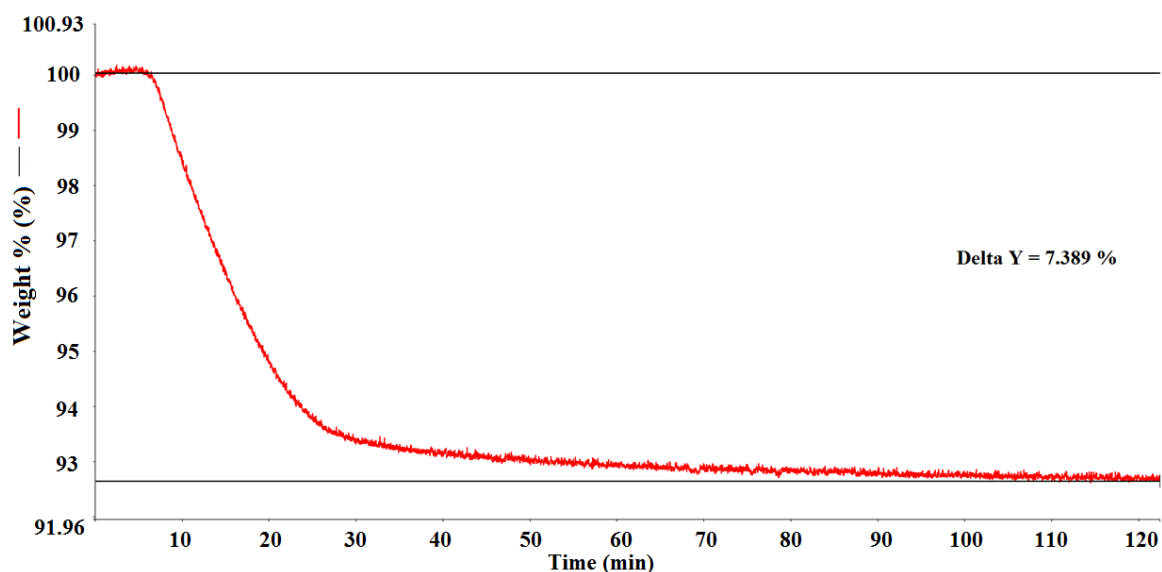


Figure 2.16 TGA for [Ag₄(O₂CCF₂CF₃)₄(Quin)₄] at a constant temperature of 95 °C



Temperature sweep TGA: Sample (4.16 mg) was held at 25 °C for 5 mins and then heated to 480 °C at a rate at 2.5 °C/min followed by holding the temperature at 480 °C for another 5 mins.

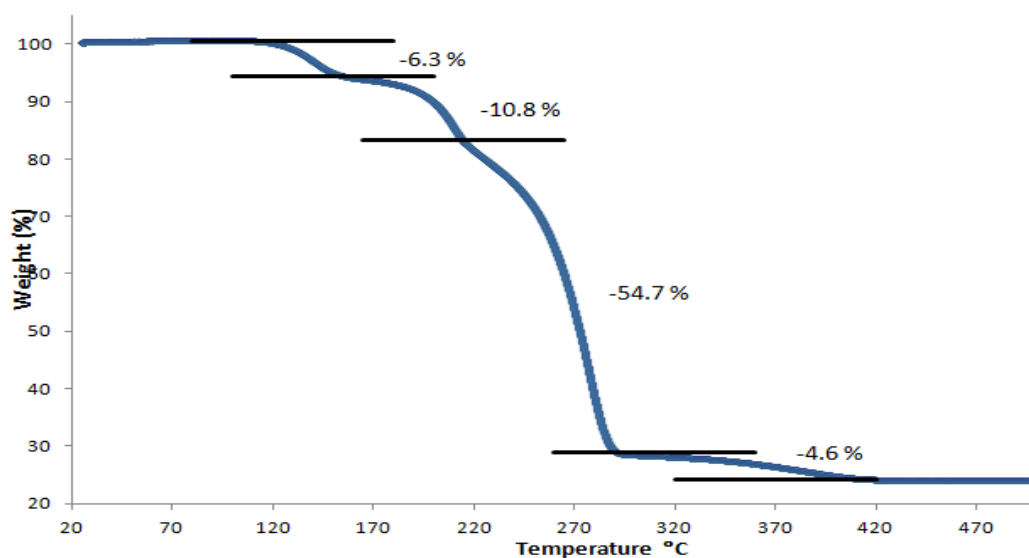


Figure 2.17 TGA for $[Ag_4(O_2C(CF_2)_2CF_3)_4(Quin)_4]$ at a scan rate of 2.5 °C/min

Isothermal TGA: Sample (3.85 mg) was heated to 120 °C with a heating rate of 10 °C/min and then held at this temperature for 140 mins.

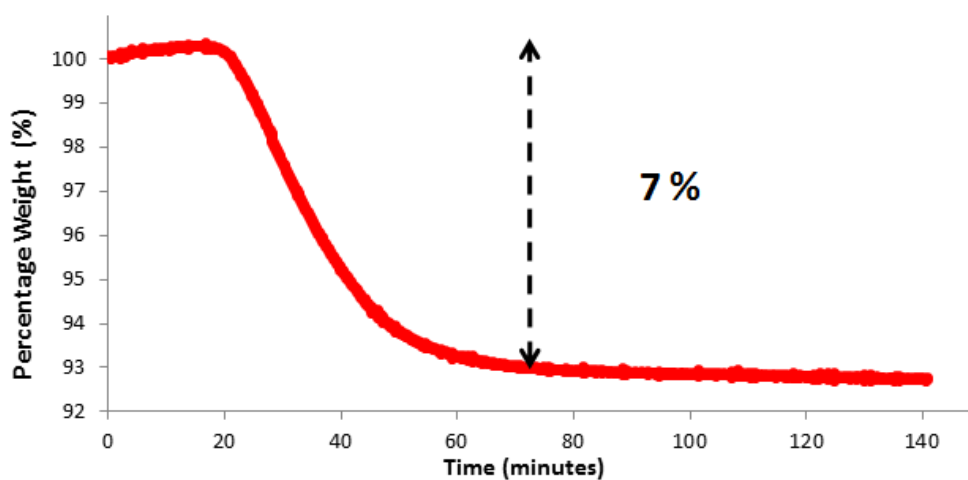


Figure 2.18 TGA for $[Ag_4(O_2C(CF_2)_2CF_3)_4(quin)_4]$ at constant temperature of 120 °C



Temperature sweep TGA: Sample (5.83 mg) was held at 25 °C for 5 mins and then heated to 550 °C at a rate at 2.5 °C/min followed by holding the temperature at 550 °C for another 5 mins.

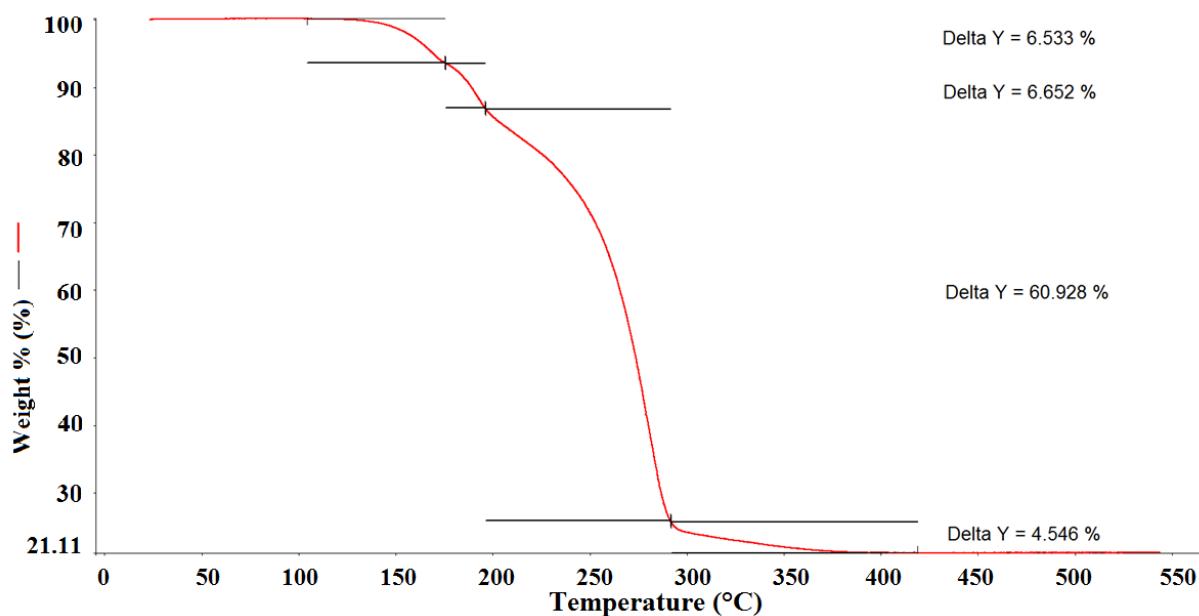


Figure 2.19 TGA for [Ag₄(O₂C(CF₂)₃CF₃)₄(Quin)₄] at a scan rate of 2.5 °C/min

Isothermal TGA: Sample (7.08/7.15/6.87 mg) was heated to 130/120/115 °C with a heating rate of 10 °C/min and then held at this temperature for 180/300/400 mins.

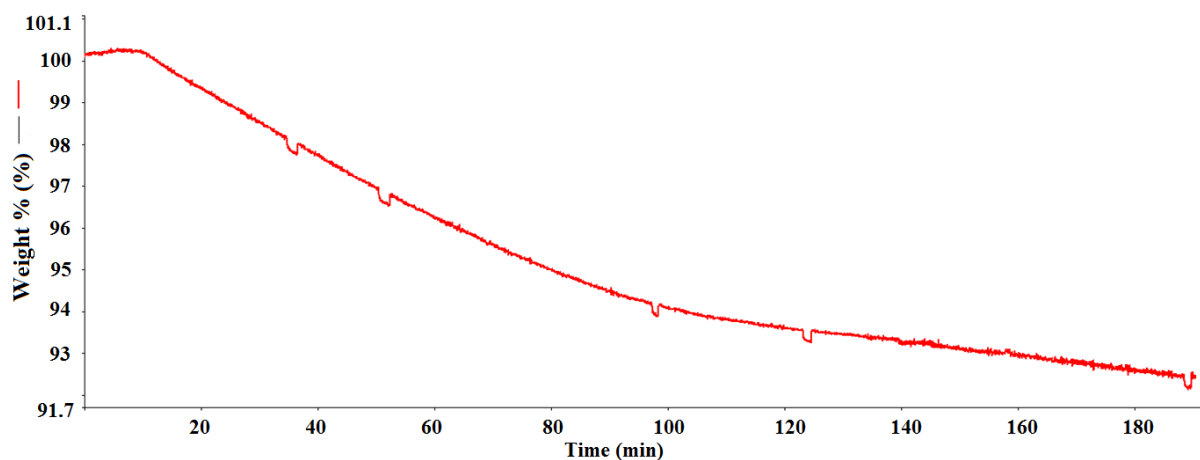


Figure 2.20a TGA for [Ag₄(O₂C(CF₂)₃CF₃)₄(Quin)₄] at a constant temperature of 130 °C

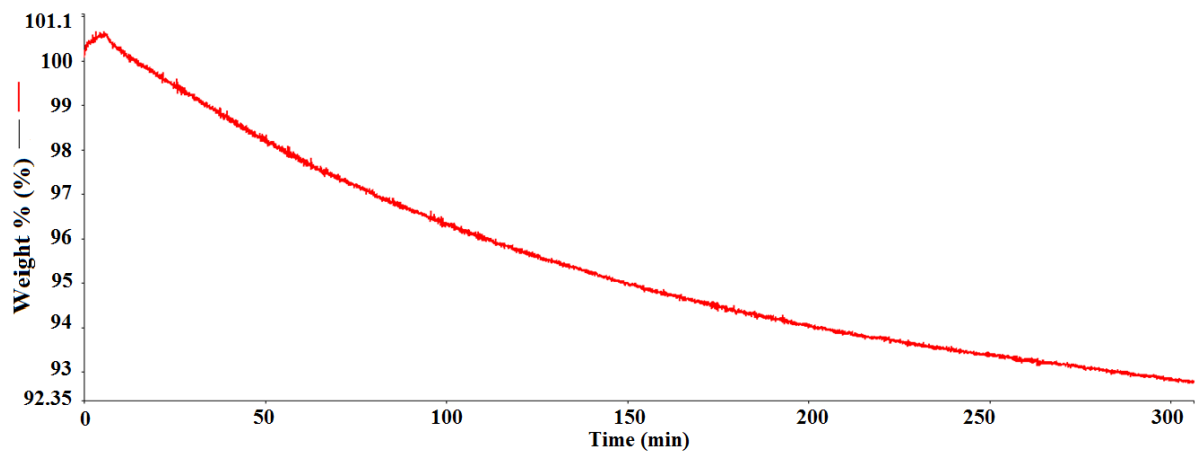


Figure 2.20b TGA for $[\text{Ag}_4(\text{O}_2\text{C}(\text{CF}_2)_3\text{CF}_3)_4(\text{Quin})_4]$ at a constant temperature of 120 °C

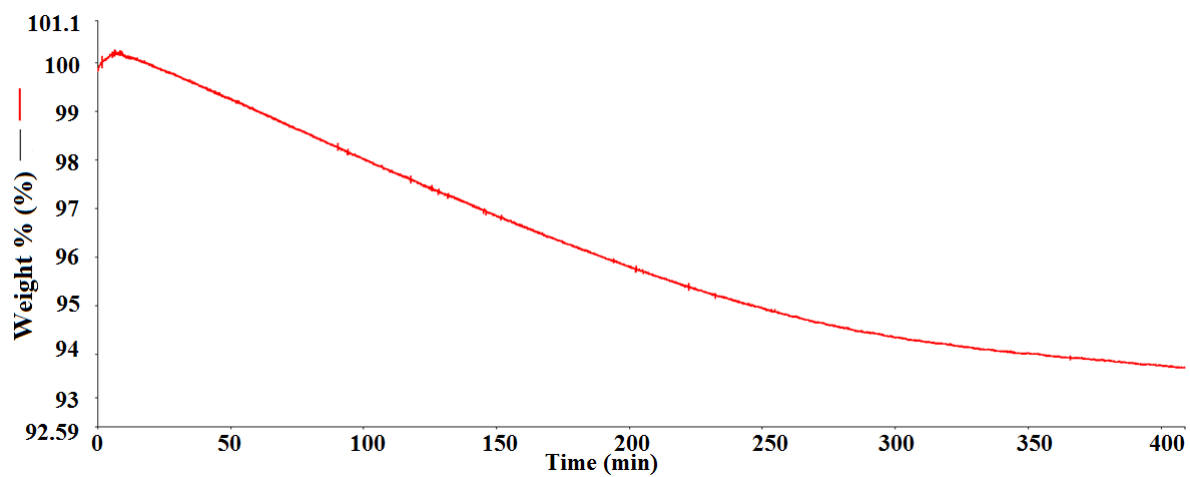


Figure 2.20c TGA for $[\text{Ag}_4(\text{O}_2\text{C}(\text{CF}_2)_3\text{CF}_3)_4(\text{Quin})_4]$ at a constant temperature of 115 °C



Temperature sweep TGA: Sample (7.45 mg) was held at 25 °C for 5 mins and then heated to 500 °C at a rate at 5 °C/min followed by holding the temperature at 500 °C for another 5 mins.

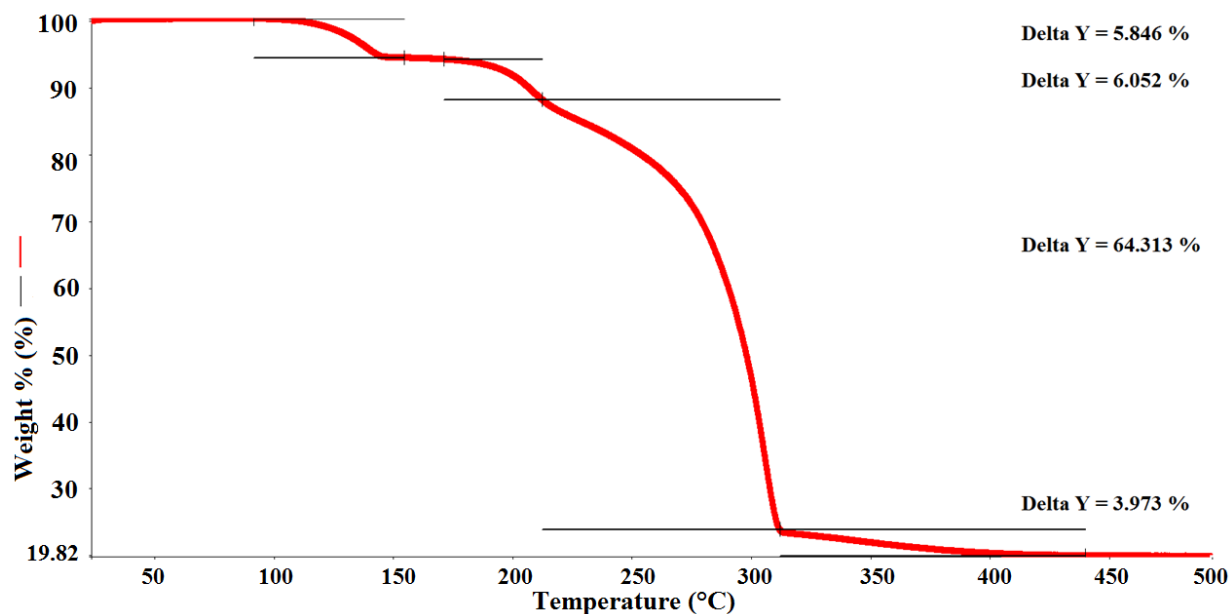


Figure 2.21 TGA for [Ag₄(O₂C(CF₂)₄CF₃)₄(Quin)₄] at a scan rate of 5 °C/min

Isothermal TGA: Sample (5.97 mg) was heated to 120 °C with a heating rate of 10 °C/min and then held at this temperature for 120 mins.

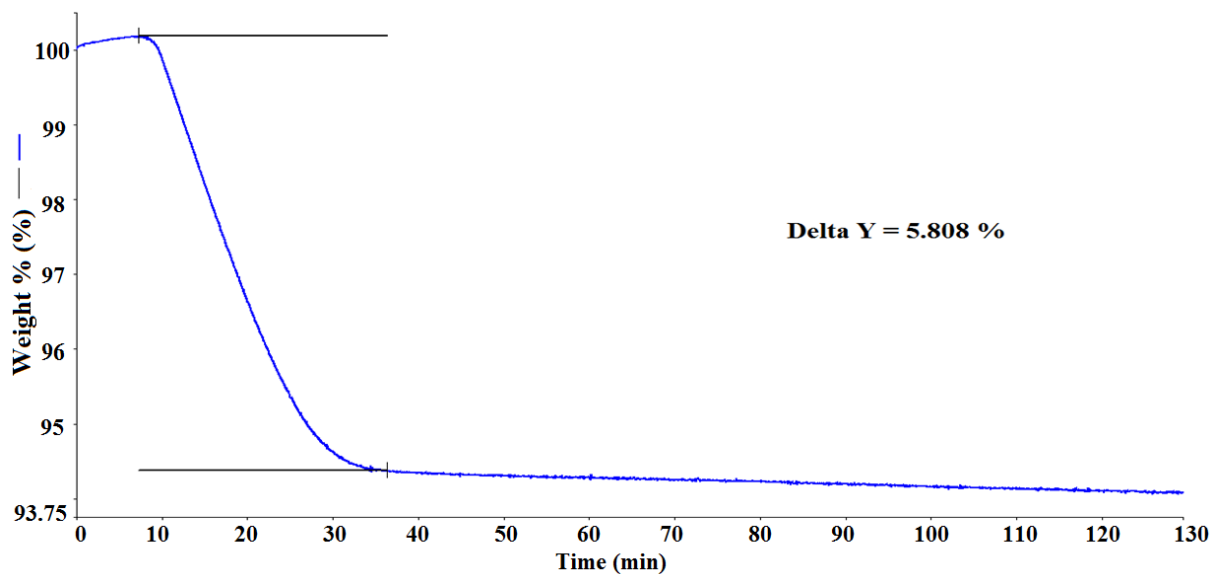
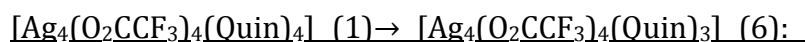


Figure 2.22 TGA for [Ag₄(O₂C(CF₂)₄CF₃)₄(Quin)₄] at a constant temperature of 120 °C

2.2.5 In situ PXRD heating studies

In situ PXRD heating studies were recorded on a Bruker D8 ADVANCE X-ray powder diffractometer equipped with a focusing Göbel mirror optic and a high-resolution energy-dispersive Lynxeye XE detector. Samples were loaded in a 0.7 mm borosilicate capillary which was open at both ends and was spun about its axis at a rate of 30 rev min⁻¹. Measurements started with a collection at 298 K and then the samples were heated up to 433 K with an Oxford Cryosystems Cryostream Plus device for several more collections, followed by a final collection after cooling back to 298 K. The patterns were indexed and fitted using Pawley¹³ and Rietveld refinement²⁰ using the *TOPAS Academic* program. Only representative patterns are shown below with the fitting parameters (other patterns are provided in the Appendix).



For the measurements at 298 K, a scan was collected for phase purity check in the range $6 \leq 2\theta \leq 50^\circ$ using a step size of 0.015° and step time of 2.5 s, giving a total exposure time of 94 mins. No scans were collected during the heating process to 433K. For the measurements at 433 K, scans were collected in the range $3 \leq 2\theta \leq 40^\circ$ using a step size of 0.015° and step time of 0.5 s, giving a total exposure time of 19 mins each. The patterns were compared to the calculated PXRD patterns from the single crystal structures of **1** and **6** and fitted using Pawley and Rietveld refinement. A stack of the original powder patterns representing the overall transformation is shown in (Figure 2.23). The starting material and the final product at 293K were confirmed to be phase-pure **1** and **6**, respectively.

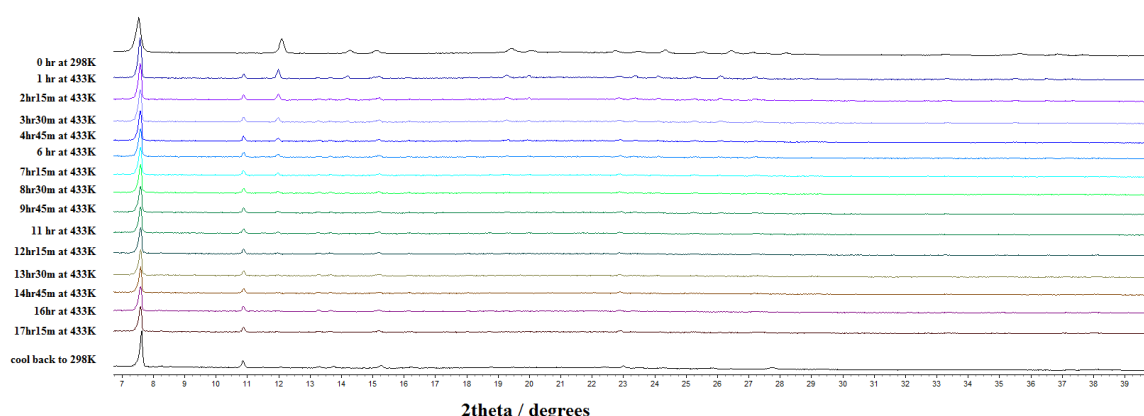


Figure 2.23 *In situ* X-ray powder patterns from the transformation of **1** to **6** shown in the range $7 \leq 2\theta \leq 40^\circ$ (patterns before 7° were cut due to the misplacement of the beam-stop). On the left the heating temperature and time interval between patterns are noted.

Initial pattern at 298 K

The pattern was indexed, and a unit cell resembling that of **1** obtained from single-crystal X-ray data at 150 K was found. This unit cell was used as the starting point for a Pawley refinement, employing 130 parameters (10 background, 1 zero error, 5 profile, 3 cell, 111 reflections), resulting in final indices of fit $R_{wp} = 0.0445$, $R_{wp'} = 0.162$. [[**1**]: $a = 11.7080(7)$ Å, $b = 6.7367(7)$ Å, $c = 14.6158(9)$ Å, $V = 1152.8(2)$ Å³].

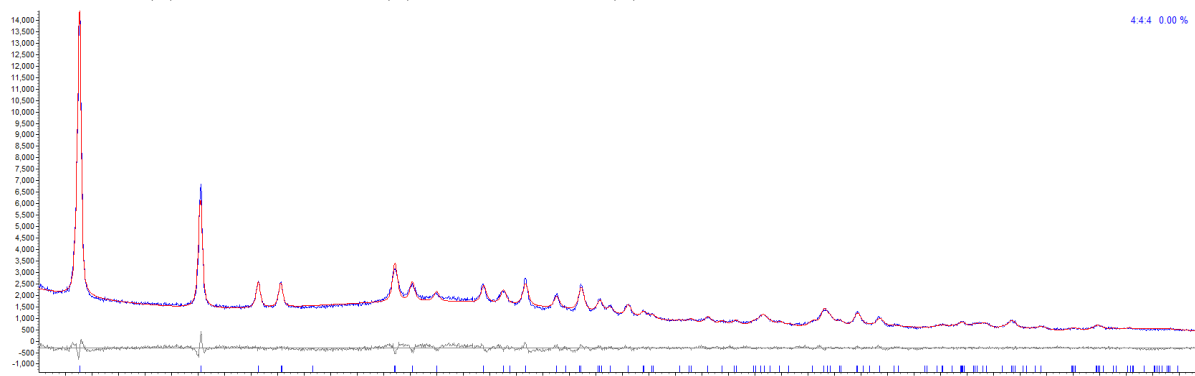


Figure 2.24 Observed (blue) and calculated (red) profiles and difference plot [$I_{obs} - I_{calc}$] (grey) of the Pawley refinement. (2θ range 7 - 50 °, $d_{min} = 1.82$ Å).

After 1 hour at 433 K

The sample was heated to 433 K and allowed to equilibrate at this temperature for one hour before the pattern was recorded. Visible inspection and comparison of the data indicated the presence of both **1** and **6**. The unit cells of the 4:4:4 phase (**1**) from the refinement at 298 K and that of the 4:4:3 phase (**6**) from a later point in the study at 433 K (when it was the only phase present) were used as the starting points for a mixed-phase Pawley refinement, employing 452 parameters (8 background, 1 zero error, 9 profile, 7 cell, 427 reflections), resulting in final indices of fit $R_{wp} = 0.0670$, $R_{wp'} = 0.166$. [**1**]: $a = 11.848(2)$ Å, $b = 6.783(2)$ Å, $c = 14.620(5)$ Å, $V = 1174.8(5)$ Å³; [[**6**]: $a = 10.1389(11)$ Å, $b = 16.244(2)$ Å, $c = 23.6611(12)$ Å, $\beta = 99.249(6)$ °, $V = 3846.3(6)$ Å³].

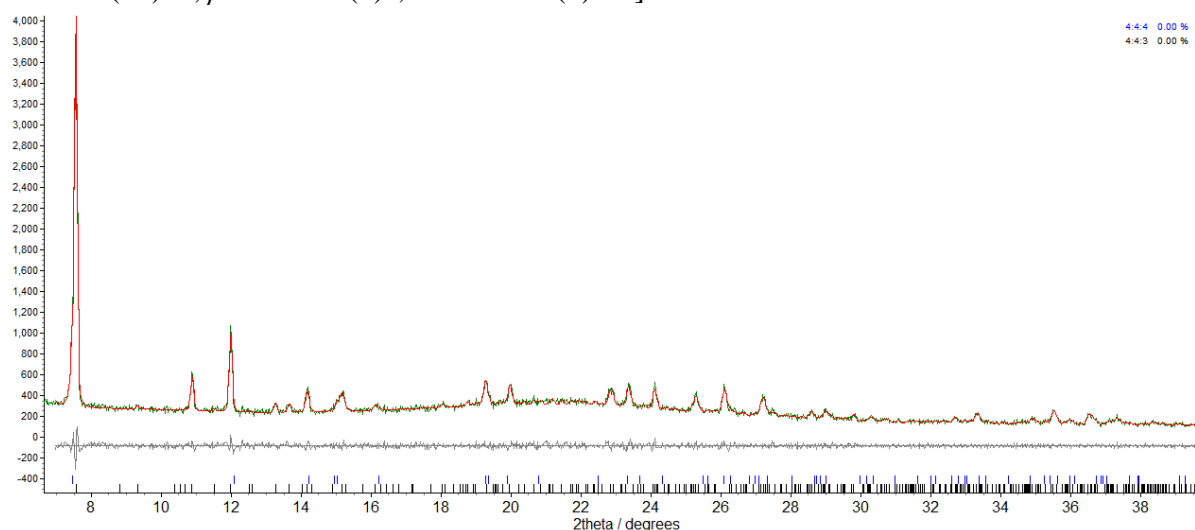


Figure 2.25 Observed (green) and calculated (red) profiles and difference plot [$I_{obs} - I_{calc}$] (grey) of the Pawley refinement. (2θ range 7 - 40 °, $d_{min} = 2.25$ Å).

After 8 hours 30 min at 433 K

The sample was kept at 433 K for another 8 hours and 30 mins. The pattern was recorded again. Visual inspection of the data suggested that the only remaining phase was **6**. The unit cell of the 4:4:3 phase from the previous refinement was used as the starting point for a Pawley refinement, employing 386 parameters (8 background, 1 zero error, 5 profile, 4 cell, 368 reflections), resulting in final indices of fit $R_{wp} = 0.0801$, $R_{wp'} = 0.286$. [[**6**]: $a = 10.170(3)$ Å, $b = 16.255(2)$ Å, $c = 23.643(2)$ Å, $\beta = 99.23(2)^\circ$, $V = 3857.9(11)$ Å³].

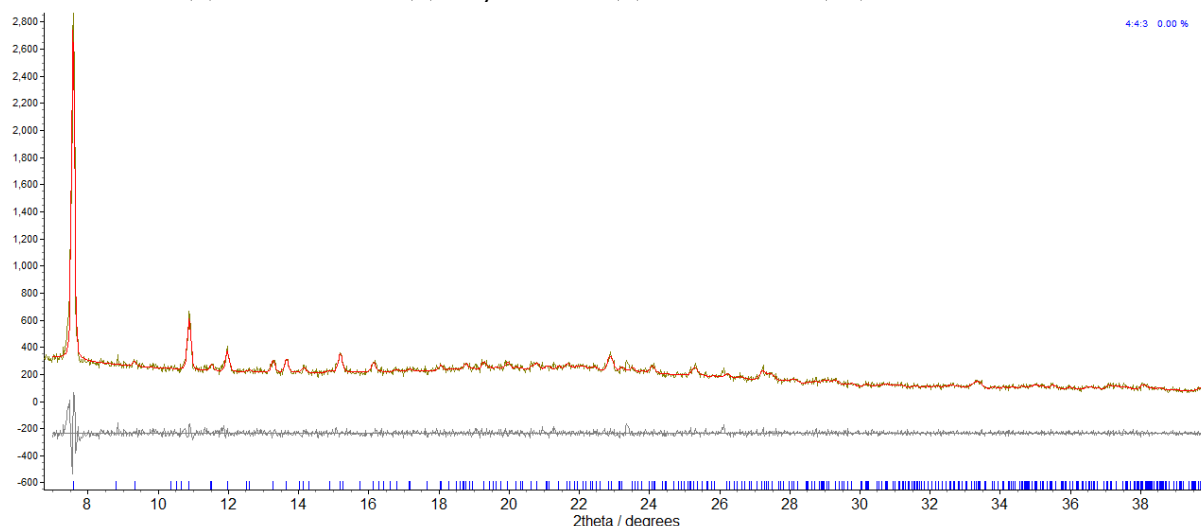


Figure 2.26 Observed (gold) and calculated (red) profiles and difference plot [$I_{obs} - I_{calc}$] (grey) of the Pawley refinement. (2θ range 6 - 40 °, $d_{min} = 2.25$ Å).

After returning to 298 K

The sample was allowed to cool back to 298 K, and was allowed to stay at 298 K for two hours, before recording the pattern again, at a longer exposure. The peak corresponding to the unknown phase at $2\theta = 8.25^\circ$ was shown, in addition to the appearance of a smaller peak at $2\theta = 8.55^\circ$. This region was therefore excluded from the refinement. The pattern was indexed, and a unit cell resembling that of **6** obtained from single-crystal X-ray data at 150 K was identified. This unit cell was used as the starting point for a Pawley refinement, employing 386 parameters (8 background, 1 zero error, 5 profile, 4 cell, 368 reflections), resulting in final indices of fit $R_{wp} = 0.0361$, $R_{wp'} = 0.140$. [[**6**]: $a = 10.0347(12)$ Å, $b = 16.2603(11)$ Å, $c = 23.4602(9)$ Å, $\beta = 99.150(8)^\circ$, $V = 3779.2(5)$ Å³].

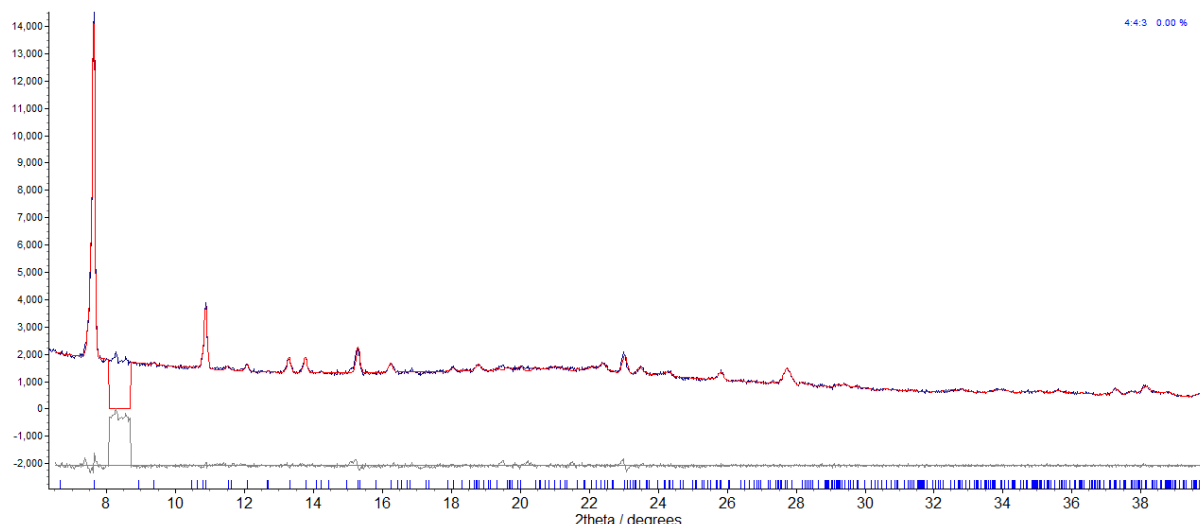
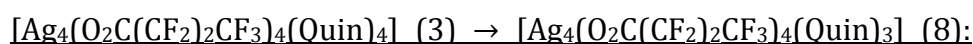


Figure 2.27 Observed (blue) and calculated (red) profiles and difference plot [$I_{\text{obs}} - I_{\text{calc}}$] (grey) of the Pawley refinement. (2θ range 7 - 40°, $d_{\text{min}} = 2.25$ Å).



For the measurements at 298 K, scans were collected in the range of $3 \leq 2\theta \leq 40^\circ$ using a step size of 0.015° and step time of 1.0 s, giving a total exposure time of 41 mins. No scans were collected during the heating process to 433 K. For the measurements at 433 K, scans were collected in the range $3 \leq 2\theta \leq 40^\circ$ using a step size of 0.015° and step time of 0.5 s, giving a total exposure time of 21 mins. The patterns were compared to the calculated PXRD patterns from the single-crystal structures of **3** and **8** and fitted using Pawley and Rietveld refinement.

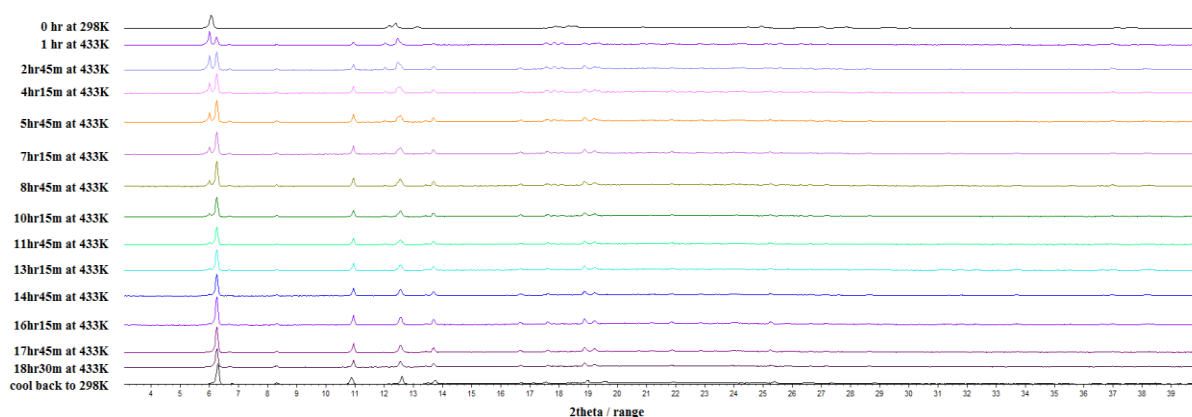


Figure 2.28 *In situ* X-ray powder patterns from the transformation of $[\text{Ag}_4(\text{O}_2\text{C}(\text{CF}_2)_2\text{CF}_3)_4(\text{Quin})_4]$ (**3**) to $[\text{Ag}_4(\text{O}_2\text{C}(\text{CF}_2)_2\text{CF}_3)_4(\text{Quin})_3]$ (**8**) shown in the range of $3 \leq 2\theta \leq 13^\circ$. On the left the heating temperature and time interval between patterns are noted.

Initial pattern at 298 K

The pattern was indexed, and a unit cell resembling that of **3** obtained from single-crystal X-ray data at 150 K was identified. This unit cell was used as the starting point for a Pawley refinement, employing 154 parameters (13 background, 1 zero error, 5 profile, 4 cell, 131 reflections), resulting in final indices of fit $R_{wp} = 0.0610$, $R_{wp}' = 0.148$. [[**3**]: $a = 14.6269(11)$ Å, $b = 6.7864(6)$ Å, $c = 14.3807(9)$ Å, $\beta = 96.82(1)^\circ$; $V = 1417.4(2)$ Å³].

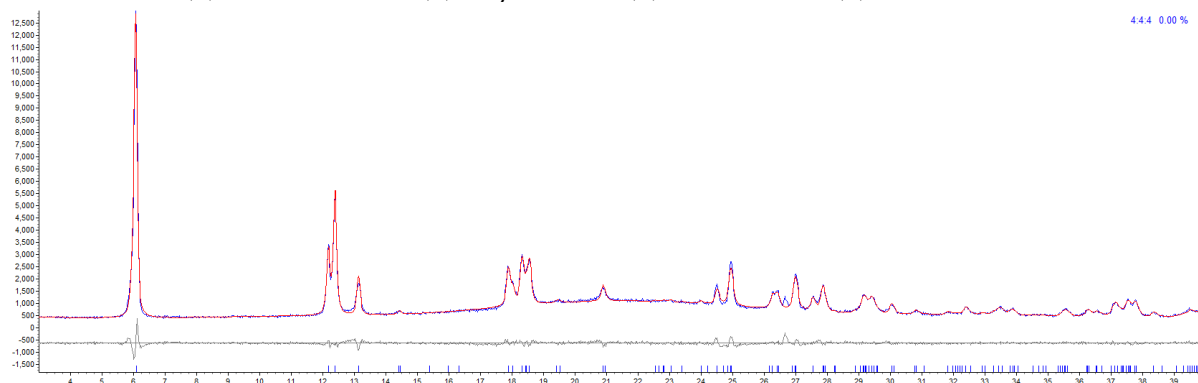


Figure 2.29 Observed (blue) and calculated (red) profiles and difference plot [$I_{\text{obs}} - I_{\text{calc}}$] (grey) of the Rietveld refinement. (2θ range 3 - 40°, $d_{\text{min}} = 2.25$ Å).

After 1 hour at 433 K

The sample was heated to 433 K and allowed to stay at this temperature for a period of one hour. The pattern was recorded again. Visual inspection and comparison of the data indicated the presence of **3** and **8**. The appearance of a new peak at $2\theta = 6.69^\circ$ was also observed, which did not correspond to either of these two phases, and thus was excluded from the refinement. The unit cell of **3** from the refinement at 298 K and that of **8** from a later point in the study at 433 K (when it is the only phase present) were used as the starting point for a mixed-phase Pawley refinement, employing 648 parameters (12 background, 1 zero error, 9 profile, 8 cell, 618 reflections), resulting in final indices of fit $R_{wp} = 0.0494$, $R_{wp}' = 0.239$. [[**3**]: $a = 14.7853(9)$ Å, $b = 6.7542(9)$ Å, $c = 14.2912(8)$ Å, $\beta = 96.75(1)^\circ$; $V = 1417.3(2)$ Å³; [**8**]: $a = 11.2818(9)$ Å, $b = 16.1521(9)$ Å, $c = 28.2213(14)$ Å, $\beta = 92.779(6)^\circ$; $V = 5136.6(5)$ Å³].

Attempts at a Rietveld refinement to determine the relative ratio of the two phases present, using the structural models of **3** and **8** obtained from single-crystal X-ray data at 150 K were, however, unsuccessful. Rietveld refinement was therefore not attempted for other patterns at 433 K.

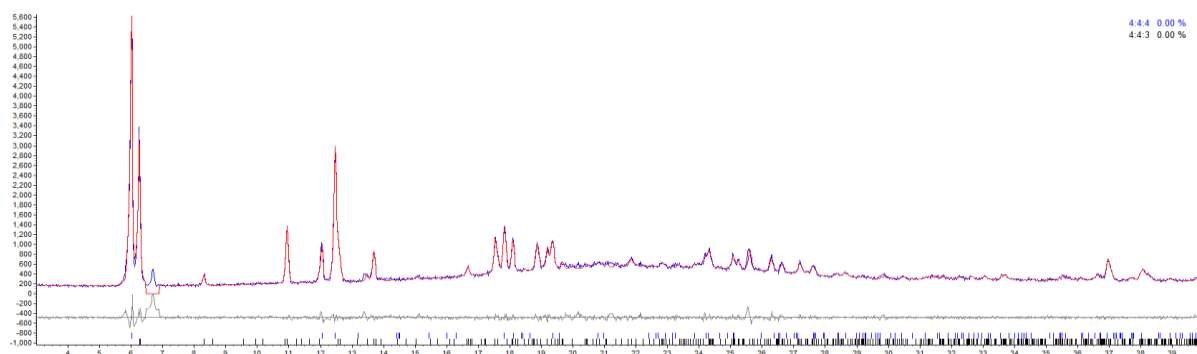


Figure 2.30 Observed (blue) and calculated (red) profiles and difference plot [$I_{\text{obs}}-I_{\text{calc}}$] (grey) of the Pawley refinement. (2θ range 3 - 40 °, $d_{\text{min}} = 2.25$ Å).

After 18 hours 30 mins at 433 K

The sample was kept at 433 K for another 18 hour and 30 minutes and the patterns were recorded again. The peak corresponding to the unknown phase at $2\theta = 6.69^\circ$ remained, and was excluded from refinement. The unit cell of the 4:4:3 phase (**8**) from the previous refinement was used as the starting point for a Pawley refinement, employing 503 parameters (8 background, 1 zero error, 5 profile, 4 cell, 485 reflections), resulting in final indices of fit $R_{\text{wp}} = 0.0876$, $R_{\text{wp}'} = 0.205$. [[**8**]: $a = 11.3076(13)$ Å, $b = 16.1428(9)$ Å, $c = 28.1989(14)$ Å, $\beta = 91.887(8)^\circ$, $V = 5144.5(7)$ Å³].

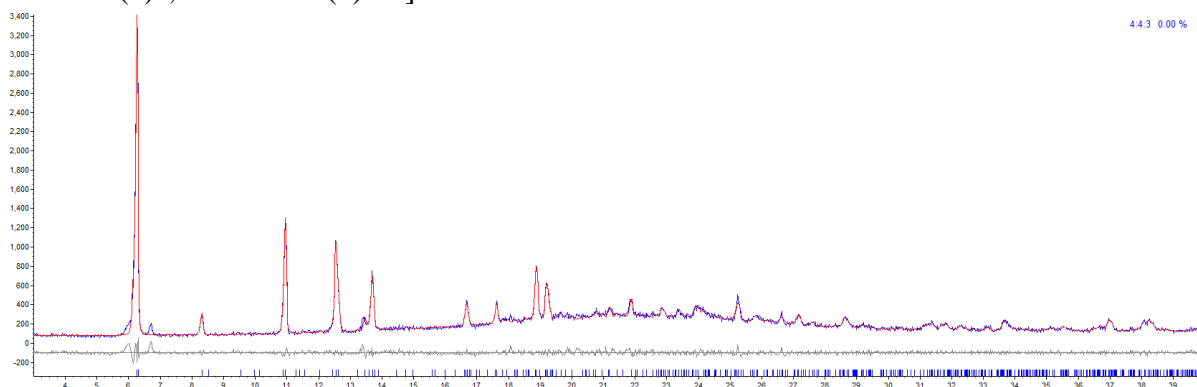


Figure 2.31 Observed (brown) and calculated (red) profiles and difference plot [$I_{\text{obs}}-I_{\text{calc}}$] (grey) of the Pawley refinement. (2θ range 3 - 40 °, $d_{\text{min}} = 2.25$ Å).

After returning to 298 K

The sample was allowed to cool back to 298 K, and was kept at 298 K for four hours, before recording the pattern again. The peak corresponding to the unknown phase at $2\theta = 6.69^\circ$ remained, and was excluded from the refinement. The pattern was indexed, and a unit cell resembling that of **8** (as determined by single-crystal X-ray diffraction at 150 K) was identified and used as the starting point for a Pawley refinement, employing 507 parameters (10 background, 1 zero error, 5 profile, 4 cell, 487 reflections), resulting in final indices of fit $R_{\text{wp}} = 0.0709$, $R_{\text{wp}'} = 0.199$. [[**8**]: $a = 11.2892(8)$ Å, $b = 16.1561(9)$ Å, $c = 28.203(2)$ Å, $\beta = 92.629(7)^\circ$, $V = 5138.4(6)$ Å³].

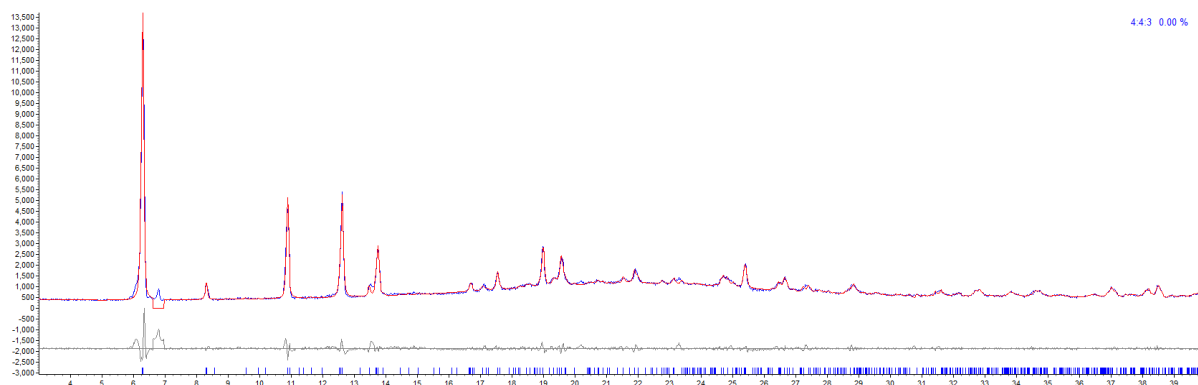


Figure 2.32 Observed (blue) and calculated (red) profiles and difference plot [$I_{\text{obs}} - I_{\text{calc}}$] (grey) of the Pawley refinement. (2θ range 3 - 40°, $d_{\text{min}} = 2.25$ Å).

[Ag₄(O₂C(CF₂)₄CF₃)₄(Quin)₄] (5) → Several unknown phases:

General: For the measurements at 298 K, scans were collected in the range of $3 \leq 2\theta \leq 40^\circ$ using a step size of 0.015° and step time of 1.0 s, giving a total exposure time of 58 mins. No scans were collected during the heating process to 433 K. For the measurements at 433 K, scans were collected in the range of $3 \leq 2\theta \leq 40^\circ$ using a step size of 0.015° and step time of 0.5 s, giving a total exposure time of 21 mins. The patterns were compared to the calculated PXRD patterns from the single crystal structure of **5**. The stacking plot in **Figure 2.33** shows a completed single phase change after about 6 hours of heating.

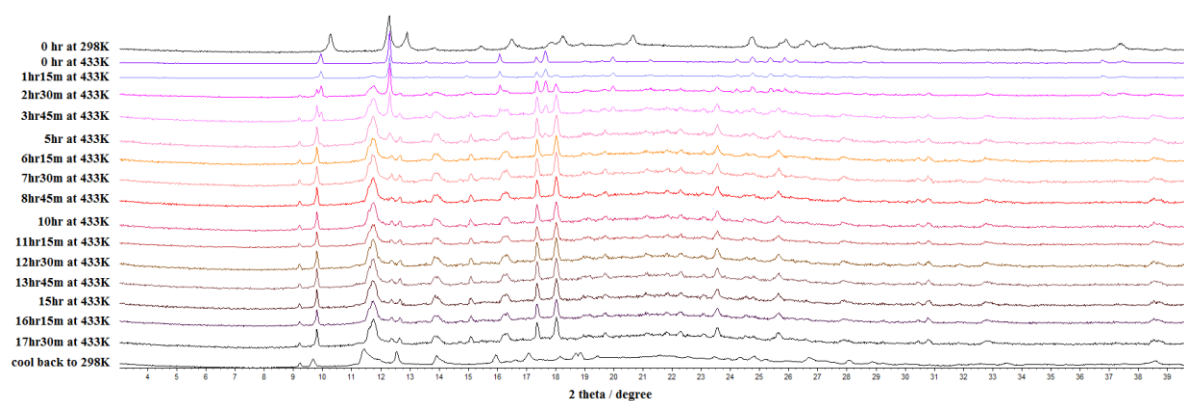


Figure 2.33 *In situ* X-ray powder patterns of the transformation shown in the range of $9 \leq 2\theta \leq 15.5^\circ$. On the left the heating temperature and time interval between patterns are noted.

Initial pattern at 298 K

The pattern was indexed, and a unit cell resembling that of **5** (obtained from single-crystal X-ray data at 150 K) was identified. Unit cell parameters from SCXRD were used as the starting point for a Pawley refinement, employing 177 parameters (10 background, 1 zero error, 5 profile, 4 cell, 157 reflections), resulting in final indices of fit $R_{wp} = 0.0507$, $R_{wp'} = 0.161$. [[**5**]: $a = 17.246(2)$ Å, $b = 6.8761(6)$ Å, $c = 14.4452(8)$ Å, $\beta = 95.146(10)$ °, $V = 1706.1(2)$ Å³].

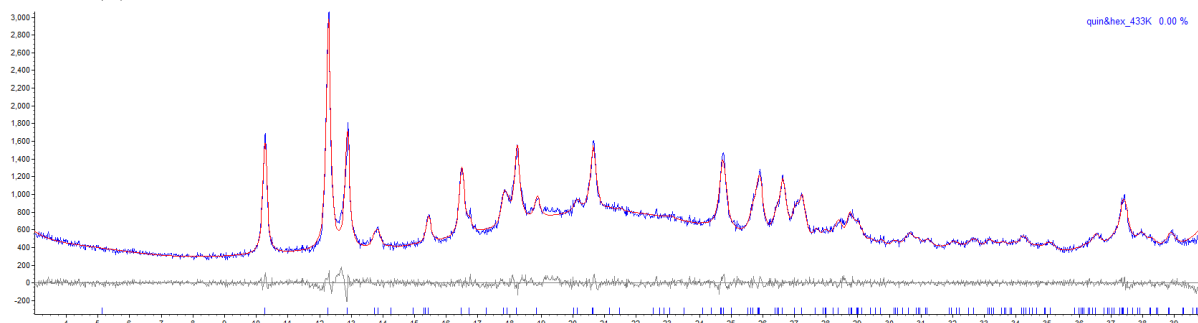


Figure 2.34 Observed (blue) and calculated (red) profiles and difference plot [$I_{obs} - I_{calc}$] (grey) of the Pawley refinement. (2θ range 3 - 40 °, $d_{min} = 2.25$ Å).

Sample upon reaching 433 K

The sample was heated to 433 K at a rate of 360 °C hr⁻¹, and when the sample reached 433 K, the diffraction pattern was immediately recorded. Visual inspection of the data indicated that the material had transformed into a new crystalline phase. The pattern was indexed to give a unit cell which did not match or resemble any known phases for either 4:4:4 or 4:4:3 composition materials. This unit cell was used as the starting point for a Pawley refinement, employing 90 parameters (15 background, 1 zero error, 5 profile, 3 cell, 66 reflections), resulting in final indices of fit $R_{wp} = 0.0440$, $R_{wp'} = 0.138$. [["**unknown HT phase B**"]: $a = 35.580(1)$ Å, $b = 7.3470(3)$ Å, $c = 7.020(2)$ Å, $V = 1835.0(1)$ Å³].

Attempts to determine the structure of this unknown phase (herein referred to as "**unknown HT phase B**") by direct space methods using simulated annealing were unsuccessful.

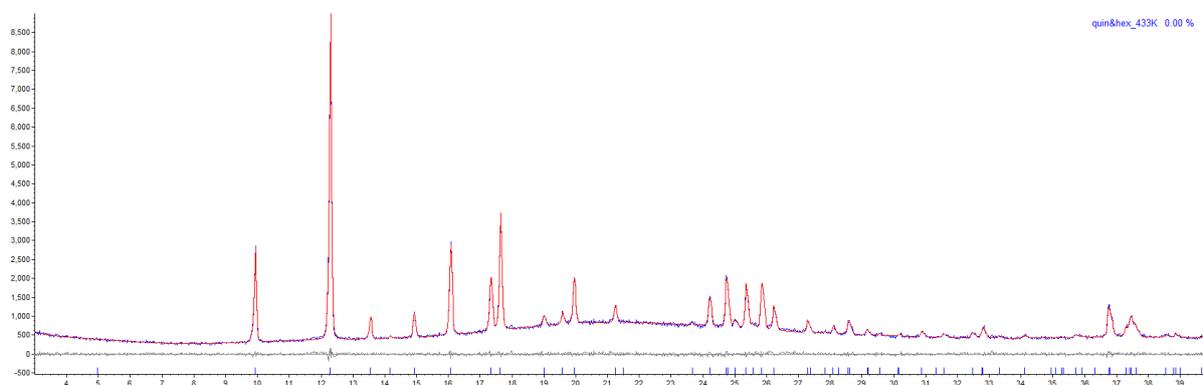


Figure 2.35 Observed (blue) and calculated (red) profiles and difference plot [$I_{obs} - I_{calc}$] (grey) of the Pawley refinement. (2θ range 3 - 40 °, $d_{min} = 2.25$ Å).

After 1 hour and 15 mins at 433 K

The sample was kept at 433 K for a further one hour and 15 mins, and the diffraction pattern was recorded again. Visual inspection of the data indicated the growth of broad peaks corresponding to another new crystalline phase(s), which again did not match or resemble any known phase for the 4:4:4 or 4:4:3 composition materials. The new peaks could not be successfully indexed to a single unit cell (even at later points in the study where they become more prominent and numerous). The unit cell of "**unknown HT phase B**" from the previous refinement was used as the starting point for a Pawley refinement, employing 82 parameters (8 background, 1 zero error, 5 profile, 3 cell, 65 reflections), resulting in final indices of fit $R_{wp} = 0.0808$, $R_{wp} = 0.324$. ["**unknown HT phase B**": $a = 35.577(4)$ Å, $b = 7.3464(7)$ Å, $c = 7.0180(6)$ Å, $V = 1834.3(3)$ Å³]. These indices of fit are necessarily high as the new phase is not included in the fit.

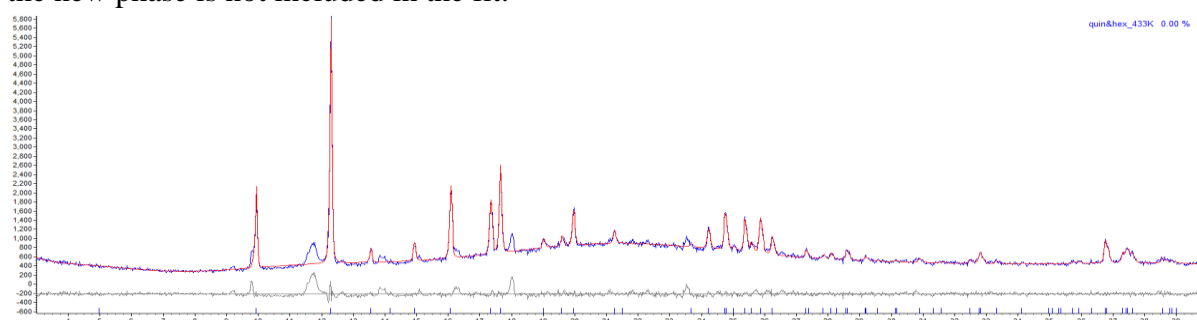


Figure 2.36 Observed (blue) and calculated (red) profiles and difference plot [$I_{obs}-I_{calc}$] (grey) of the Pawley refinement. (2θ range 3 - 40 °, $d_{min} = 2.25$ Å).

After 2 hour and 30 mins at 433 K

The sample was held at 433 K for a further one hour and 15 mins, and the diffraction pattern was recorded again. Peaks corresponding to the new un-indexed crystalline phase(s) developed further, and those corresponding to "**unknown HT phase B**" further decreased in intensity. The unit cell of "**unknown HT phase B**" derived from the previous refinements was used as the starting point for a Pawley refinement, employing 82 parameters (9 background, 1 zero error, 5 profile, 3 cell, 64 reflections), resulting in final indices of fit $R_{wp} = 0.126$, $R_{wp} = 0.614$. ["**unknown HT phase B**": $a = 35.56(1)$ Å, $b = 7.344(2)$ Å, $c = 7.016(2)$ Å, $V = 1832.4(8)$ Å³]. These indices of fit are necessarily higher than that for the previous pattern as the new phase is not included in the fit.

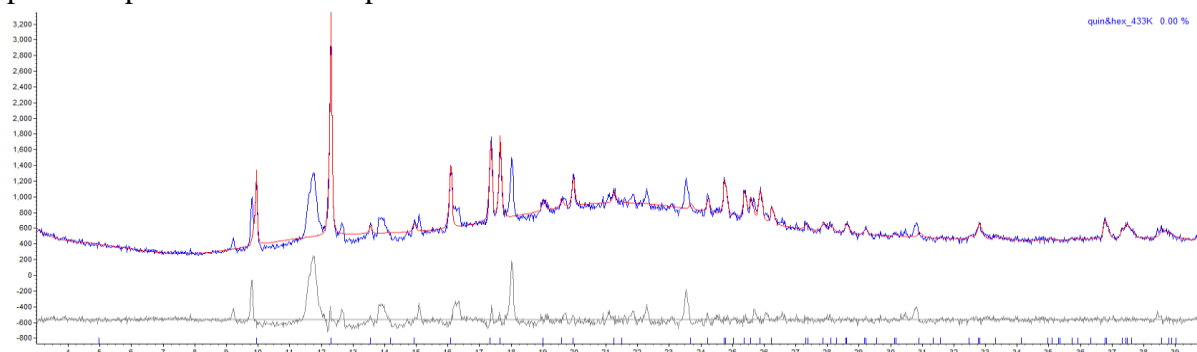


Figure 2.37 Observed (blue) and calculated (red) profiles and difference plot [$I_{obs}-I_{calc}$] (grey) of the Pawley refinement. (2θ range 9 - 40 °, $d_{min} = 2.25$ Å).

Overlap of peaks corresponding to the "**unknown HT phase B**" and the new un-indexed crystalline phase(s) meant that further meaningful refinement of the unit cell parameters of "**unknown HT phase B**" was no longer possible. As such, further fitting was not performed on subsequent diffraction patterns in this study.

293K→433K: The sample of **5** was heated from 293 K to 433 K in steps of 20 K at a rate of $360\text{ }^{\circ}\text{C hr}^{-1}$. A pattern was measured after each 20 K temperature rise while the temperature was held during the measurement. Each scan was collected in the range $3 \leq 2\theta \leq 25^{\circ}$ using a step size of 0.015° and step time of 0.1 sec, giving a total exposure time of 58 mins. The data were compared to the calculated PXRD pattern from the single crystal structure of **5**.

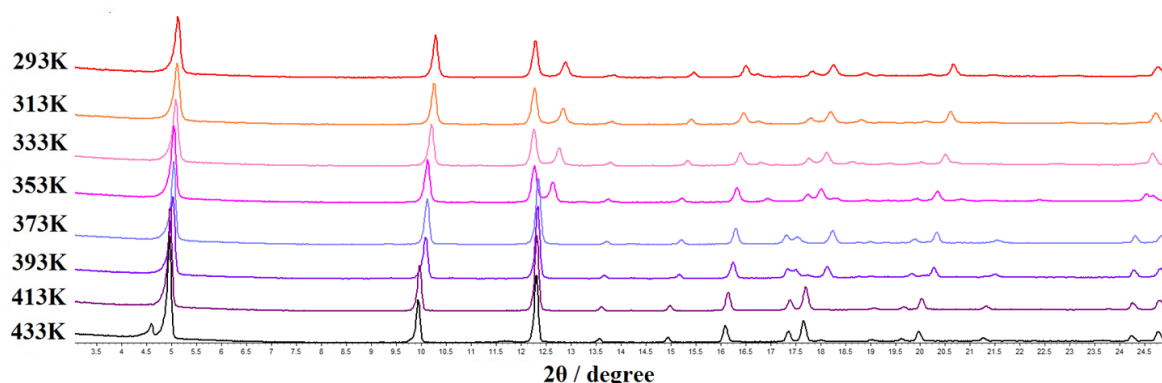


Figure 2.38 *In situ* X-ray powder patterns of the transformation started from **5** shown in the range of $3 \leq 2\theta \leq 25^{\circ}$. On the left the heating temperatures are noted.

Pattern at 373 K

The pattern was indexed to a single phase with a new unit cell that was different from that of the "**unknown HT phase B**"; this new phase will be referred to as "**unknown HT phase A**". This unit cell was used as the starting point for a Pawley refinement, employing 47 parameters (15 background, 1 zero error, 5 profile, 3 cell, 23 reflections), resulting in final indices of fit $R_{wp} = 0.0571$, $R_{wp}' = 0.107$. [{"**unknown HT phase A**"}: $a = 7.3301(3)\text{ \AA}$, $b = 34.939(2)\text{ \AA}$, $c = 6.9508(4)\text{ \AA}$, $\beta = 87.01(1)^{\circ}$, $V = 1777.7(2)\text{ \AA}^3$].

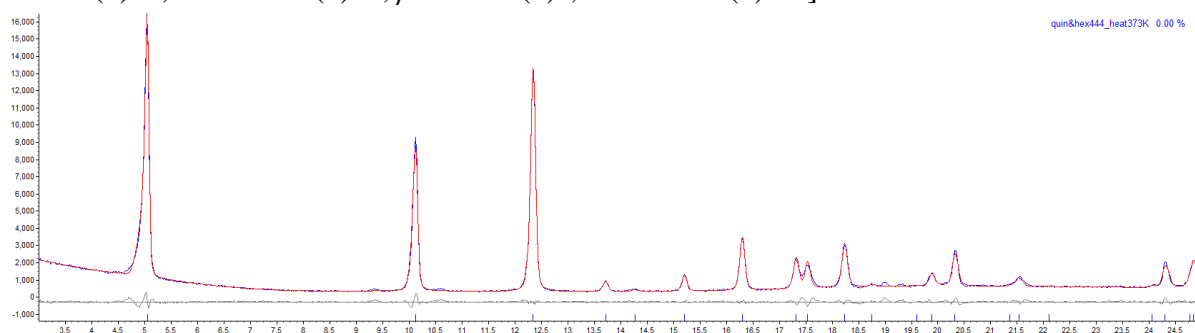


Figure 2.39 Observed (blue) and calculated (red) profiles and difference plot [$I_{\text{obs}} - I_{\text{calc}}$] (grey) of the Pawley refinement. (2θ range 3 - 25° ; $d_{\text{min}} = 3.56\text{ \AA}$).

Patterns at 413 K

The unit cell of "unknown HT phase B" was used as the starting point for a Pawley refinement, employing 47 parameters (15 background, 1 zero error, 5 profile, 3 cell, 23 reflections), resulting in final indices of fit $R_{wp} = 0.0547$, $R_{wp'} = 0.102$. ["unknown HT phase B"]: $a = 35.4334(9) \text{ \AA}$, $b = 7.3325(2) \text{ \AA}$, $c = 6.9834(3) \text{ \AA}$, $V = 1814.4(1) \text{ \AA}^3$.

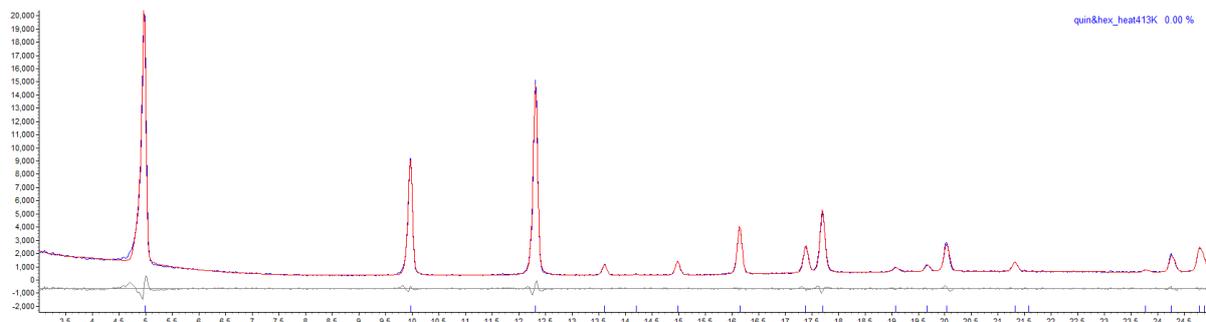


Figure 2.40 Observed (blue) and calculated (red) profiles and difference plot [$I_{obs} - I_{calc}$] (grey) of the Pawley refinement. (2θ range 3 - 25 °, $d_{min} = 3.56 \text{ \AA}$).

Patterns at 433 K

The unit cell of "unknown HT phase B" from the previous refinement was used as the starting point for a Pawley refinement, employing 47 parameters (15 background, 1 zero error, 5 profile, 3 cell, 23 reflections), resulting in final indices of fit $R_{wp} = 0.106$, $R_{wp'} = 0.208$. ["unknown HT phase B"]: $a = 35.559(4) \text{ \AA}$, $b = 7.342(6) \text{ \AA}$, $c = 7.011(8) \text{ \AA}$, $V = 1830.3(3) \text{ \AA}^3$. Some new peaks were increasing in intensity around 4.75° and 11.75° which no longer fitted to this phase suggesting that a further transformation may be beginning.

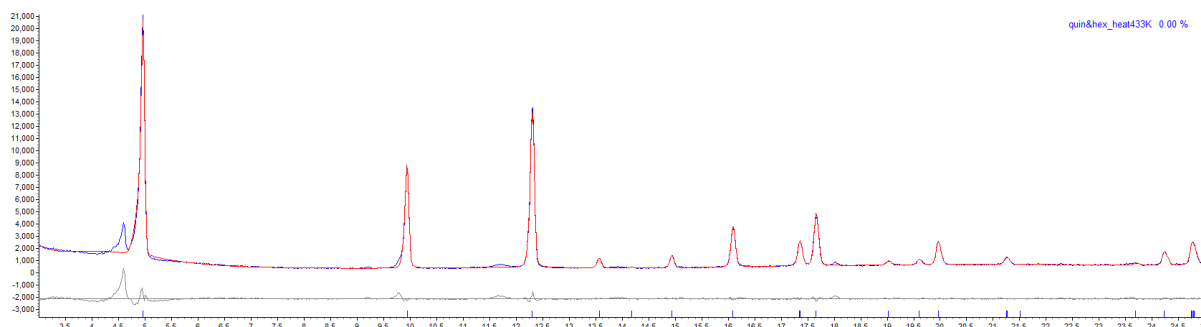


Figure 2.41 Observed (blue) and calculated (red) profiles and difference plot [$I_{obs} - I_{calc}$] (grey) of the Pawley refinement. (2θ range 3 - 25 °, $d_{min} = 3.56 \text{ \AA}$).

2.2.6 Dielectric constant test

Samples (0.1g each) were ground into powders and compressed into round plates (d=13mm) by using IR plate moulds. Both upper and lower surfaces of samples were coated with silver paint and dried before measurements, which aims to smooth the surface of the plates and reduce the error. Dielectric constants and losses at different frequencies (1-10⁶ Hz) were measured on a broadband dielectric spectrometer (Novocontrol Concept 80, Germany) in Soochow University, China.

2.3 Results and Discussion

2.3.1 Synthesis and Crystal Structures

Two series of coordination polymers have been synthesised from reaction of silver(I) perfluoroalkyl carboxylates with quinoxaline (Quin), [Ag₄(O₂C(CF₂)_nCF₃)₄(Quin)₄] **1** (n=0), **2** (n=1), **3** (n=2), **4** (n=3), **5** (n=4), [Ag₄(O₂C(CF₂)_nCF₃)₄(Quin)₃] **6** (n=0), **7** (n=1), **8** (n=2). These will be referred to as "4:4:4" or "4:4:3" phases, which refers to the ratio of Ag(I) centres, perfluoroalkyl carboxylate ligands and quinoxaline ligands in these materials. All have been characterised by single-crystal X-ray diffraction and, where possible, composition and phase purity has been confirmed by elemental analysis and powder X-ray diffraction. In figures all in the atoms are coloured by element: Silver (magenta), oxygen (red), perfluoroalkyl groups (green), quinoxaline (blue).

2.3.1.1 4:4:4 [Ag₄(O₂C(CF₂)_nCF₃)₄(Quin)₄] structures

The basic coordination environments for all these compounds are nearly the same. Thus compound **3** (middle chain length) will be described as an illustration. Compound **3** crystallizes in the monoclinic space group *P*2₁/*c* and consists of 1/4 of the [Ag₄(O₂C(CF₂)₂CF₃)₄(Quin)₄] moiety in its asymmetric unit. Each Ag centre is four-coordinated with two N-atoms from two Quin ligands and two O-atoms from two heptafluorobutanoates, resulting in an uncommon see-saw-shaped geometry (**Figure 2.42a**). Two O-atoms from each heptafluorobutanoate connect two Ag centres in a $\mu:\kappa^1,\kappa^1$ -bridging mode to form a [Ag₂(O₂C(CF₂)₂CF₃)₂] S-shaped unit. This unit is then further linked to its equivalent ones by $\mu:\kappa^1,\kappa^1$ -O₂C(CF₂)₂CF₃ ligands, yielding 1D zigzag backbone chains extending along the *b*-axis (**Figure 2.42b**).

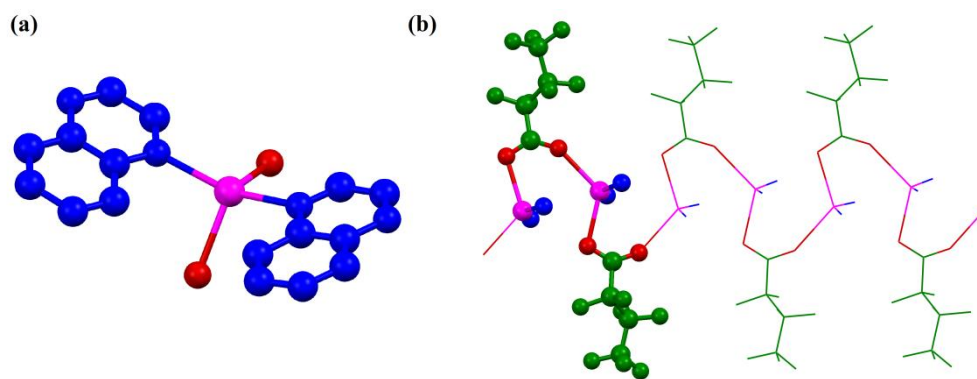


Figure 2.42 Crystal structures of **3** showing (a) see-saw coordination environment of Ag centre and (b) the S-shaped $[\text{Ag}_2(\text{O}_2\text{C}(\text{CF}_2)_2\text{CF}_3)_2]$ unit (shown in ball and stick) and the 1D zigzag backbone chains structure.

The chains are interconnected to their equivalent ones by the double Quin bridges to form a 2D herringbone structure propagated in the bc plane (**Figure 2.43a**). As the van der Waals distance between two silver(I) centres is around 3.44 \AA^{21} and the $\text{Ag} \cdots \text{Ag}$ distance in compound **3** is $3.4302(2) \text{ \AA}$, it suggests no significant Ag-Ag argentophilic interaction.²² The Quin ligands in between backbones are face-to-face aligned with an interplanar distance of 3.17 \AA , indicating strong π - π stacking interactions. Neighbouring 2D layers are stacked with a distance of 14.4604 \AA (**Figure 2.43b**).

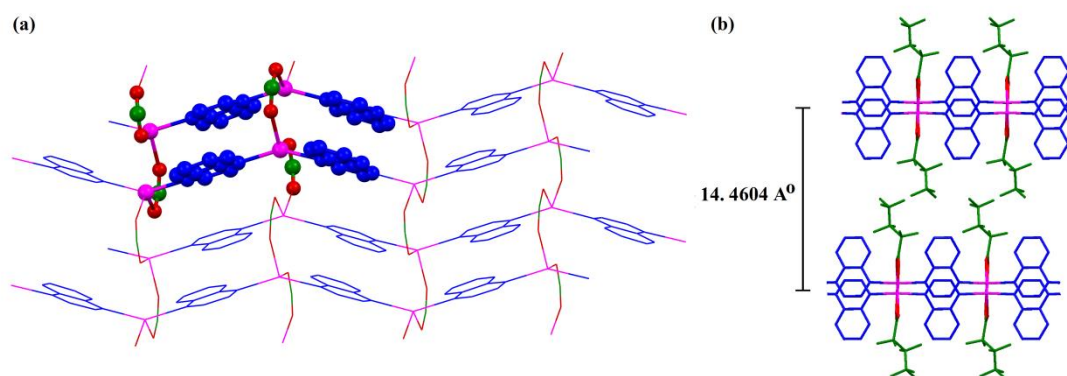


Figure 2.43 Crystal structures of **3** showing (a) the 2D herringbone structure along bc plane (perfluorobutanoate chains are simplified as green balls for clarity) and (b) the stacking fashion with interplaner distance.

The crystal structures of all the 4:4:4 phase coordination polymers (**1-5**) are shown in **Figure 2.44-46**. All the coordination polymers are very similar 2D layer structures (*bc*-plane) in which the perfluoroalkyl chains from adjacent layers are interdigitated in the space between these layers. Longer chain lengths lead to the increased interlayer space which is represented by an increase in the *a*-axis length (**Figure 2.44**). Viewing from *c*-axis (**Figure 2.45**) shows nearly same structures for all compounds.

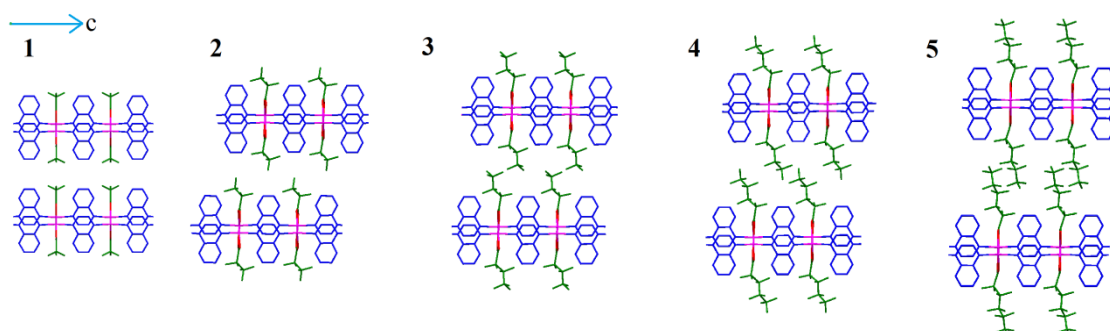


Figure 2.44 Crystal structures of 4:4:4 phase coordination polymers **1-5** viewed along the *b*-axis.

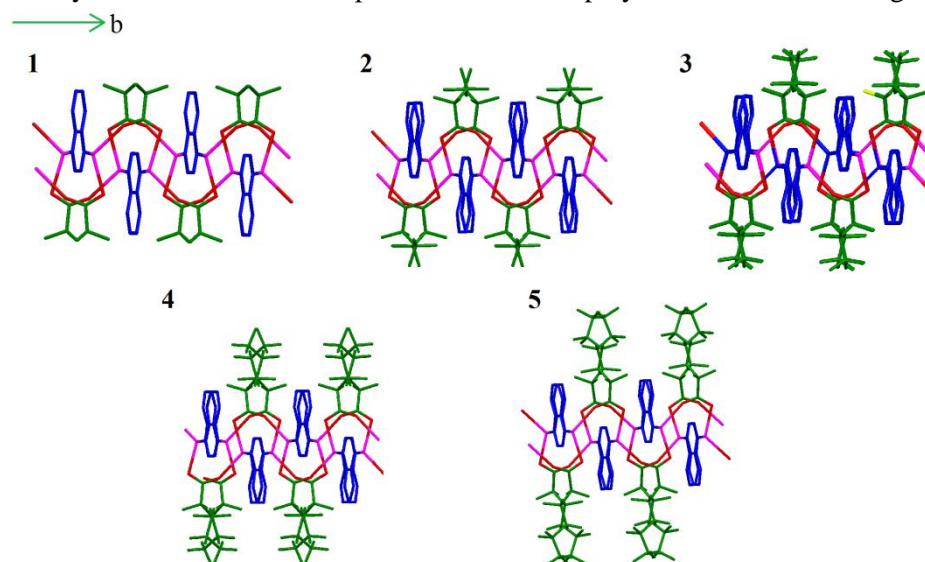


Figure 2.45 Crystal structures of 4:4:4 phase coordination polymers **1-5** viewed along the *c*-axis.

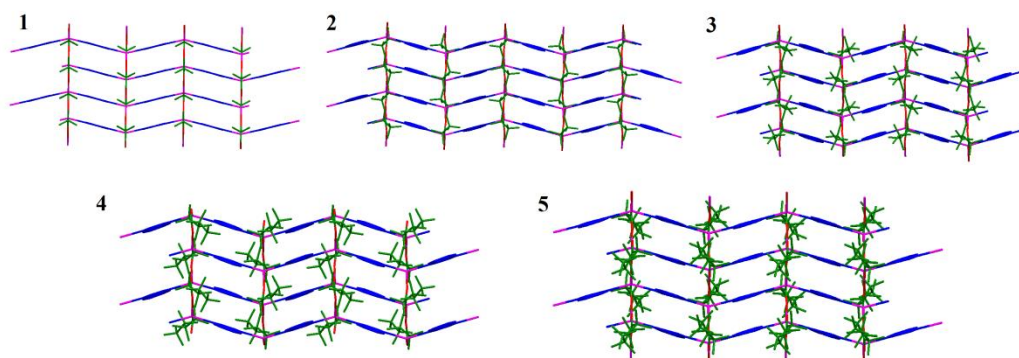


Figure 2.46 Structure viewing along the *a**-axis for all 4:4:4 phase coordination polymers.

When viewed along the a^* -axis (**Figure 2.46**), it can be seen that the layer structures for all these 4:4:4 structures extend along the b -axis (Ag-O chains via bridging carboxylate ligands) and c -axis (Ag-Quin tapes via bridging quinoxaline ligands). The increasing length of the perfluoroalkyl chains does not have a significant effect on the length along these two axes (the single-crystal data suggest only the a -axis is increasing significantly along with the chain length, **Table 2.2**). This is because the coordination environments for Ag-O (~3.3 Å) and Ag-N (~2.3 Å) do not change with the increasing chain length. The increases in the interplanar spaces for all these compounds are reasonably regular except in compound **4** and **5**. This phenomenon can be explained as in compound **5**, the interdigitation of perfluoroalkyl chains is deeper than in compound **4** along the a -axis (**Figure 2.42**) but a smaller β -angle in compound **5** results in a larger actual spacing between layers for the longer chains.

Table 2.2 Unit cell parameters for compound **1** to **5**

	1	2	3	4	5
a (Å)	11.7575(3)	13.3405(9)	14.5530(7)	17.0394(8)	17.0199(16)
b (Å)	6.6483(2)	6.6186(4)	6.6729(4)	6.6746(3)	6.6761(6)
c (Å)	14.4311(4)	14.3831(11)	14.3152(6)	14.2268(6)	14.3243(16)
α (°)	90	90.191(5)	90	90	90
β (°)	90	102.636(5)	96.466(3)	109.915(3)	94.823(7)
γ (°)	90	80.249(5)	90	90	90
V (Å ³)	1128.04(5)	1220.55(15)	1381.32(12)	1521.42(12)	1638.9(3)
Interplanar distance (Å)	11.7575	13.0174	14.4604	16.0204	16.9596

2.3.1.2 4:4:3 [Ag₄(O₂C(CF₂)_nCF₃)₄(Quin)₃] structures

The basic coordination environment for compounds **6-8** are almost the same. Thus, compound **8** will be described to illustrate this coordination environment. Compound **8** crystallizes in the monoclinic space group $P2_1/n$ and its asymmetric unit contains one discrete [Ag₄(O₂C(CF₂)₂CF₃)₄(Quin)₃] unit. Ag(I) atoms in this unit have two different coordination geometries (**Figure 2.47**). The first type of silver centre, referred as Ag1 and Ag3 in each unit, is tetrahedrally coordinated with two N-atoms from two Quin ligands and two O-atoms from two heptafluorobutanoate chains and is the same see-saw shaped coordination environment as in 4:4:4 structures. The second type of silver centre, referred as Ag2 and Ag4, displays a

T-shaped geometry, coordinated with two O-atoms from two heptafluorobutanoate ligands and only one N from one Quin ligand.

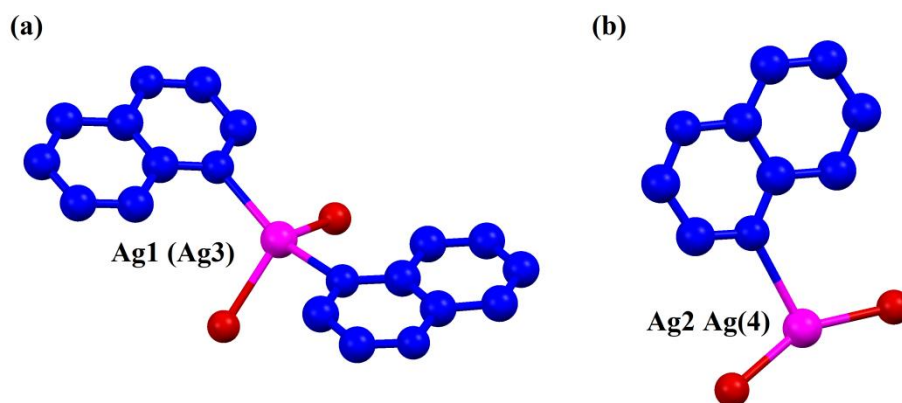


Figure 2.47 Crystal structures of **8** showing (a) see-saw coordination environment of Ag centre and (b) the T-shape Ag centre.

Four $\mu:\kappa^1, \kappa^1$ -bridged $\text{O}_2\text{C}(\text{CF}_2)_2\text{CF}_3$ ligands in **8** links two different Ag centres to form two $[\text{Ag}_2(\text{O}_2\text{C}(\text{CF}_2)_2\text{CF}_3)_2]$ ring units and connected by two Quin ligands into a V-shaped unit (**Figure 2.48a-b**). Every two V-shaped units are connected with an extra Quin ligand between Ag2 and Ag4' and forming a 4:4:3 1D zigzag tape along *b*-axis (**Figure 2.48c**). The double-bridging Quin ligands are face-to-face aligned with the distance of 3.520 Å. But the orientations of the extra Quin ligands are opposite to the doubly-bridging Quin pairs in the V-shaped units.

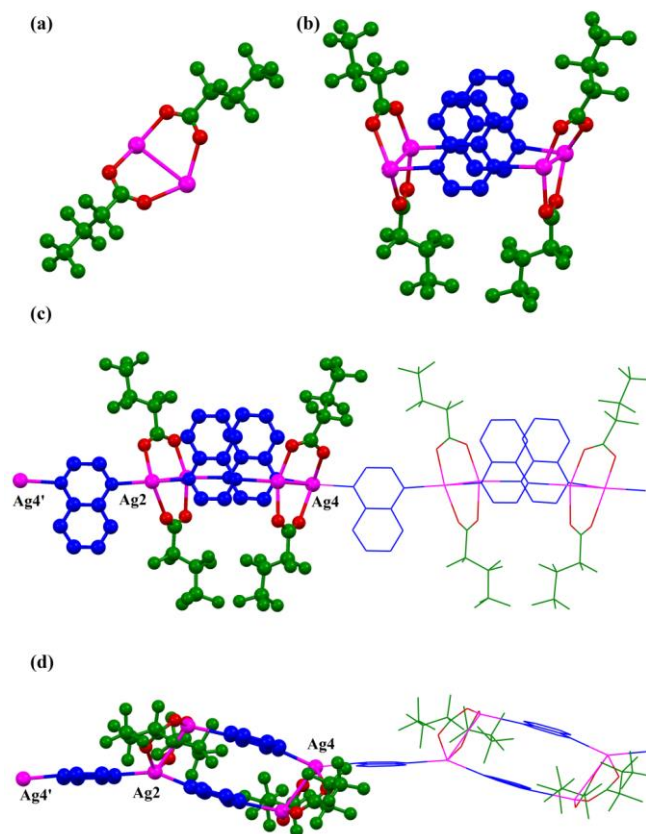


Figure 2.48 Crystal structures of **8** showing (a) $[Ag_2(O_2C(CF_2)_2CF_3)_2]$ ring unit; (b) the v-shape unit; (c) the 4:4:3 1D tape connection viewing from *a*-axis and (d) from *c*-axis.

These 4:4:3 1D tapes are then stacking along *a*-axis in an anti-parallel way by weak Ag...Ag interactions, which looks like a slightly collapsed version of 4:4:4 layers (**Figure 2.49**). The V-shaped units are joined together by argentophilic interactions (3.088 Å and 3.097 Å), which notably stronger than the Ag-Ag contacts (3.155 Å and 3.194 Å) inside the V-shape units and what in compound **3**. This results the formation of a layer extending along the *ab* plane. Neighbouring layers are arranged with a distance of 14.4604 Å.

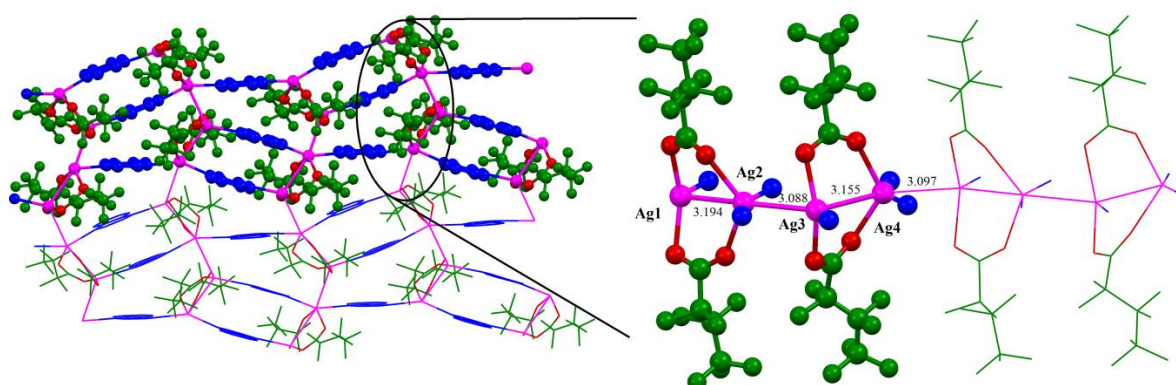


Fig. 2.49 View of the structure unit and (b)/(c) the 2D structure of compound **8**.

The crystal structures of the 4:4:3 phase coordination polymers **6**, **7** and **8** are shown in **Figures 2.50-52**. These coordination polymers are all the 4:4:3 phases are 1D tape structures (which further formed into layers by weak Ag...Ag interactions) which is different from the 4:4:4 2D-layers. First of all, the layers are no longer flat along the plane but wave-like (**Figure 2.50**). This also changes the way that the perfluoroalkyl chains interdigitate to each other. As discussed in compound **8**, instead of facing directly, now they are in a “V” shaped orientation and not perpendicular to the layer. This kind of interdigitation fills the interplanar spaces more and can be the reason for smaller interlayer spaces compared to the 4:4:4 structures with same chains lengths (**Table 2.3**).

Table 2.3 Unit cell parameters for compounds **6** to **8**

	6	7	8
<i>a</i> (Å)	10.3394(3)	10.5119(5)	10.6884(11)
<i>b</i> (Å)	16.3000(5)	16.3803(8)	16.4660(16)
<i>c</i> (Å)	23.2981(8)	12.3916(6)	27.817(3)
α (°)	90	90	90
β (°)	97.9921(19)	90	91.547(5)
γ (°)	90	90	90
<i>V</i> (Å ³)	3888.24(2)	2133.69(18)	4893.8(9)
<i>Z</i>	4	2	4
<i>V</i> per 4:4:3 unit, <i>V</i> / <i>Z</i> (Å ³)	972.1	1066.8	1223.5
Interplanar distance (Å) $d = c * \sin(180-\beta) / (Z/2)$	11.5359	12.3916	13.9034
d for 444 structures in same chain lengths (Å)	11.7575	13.0174	14.4604

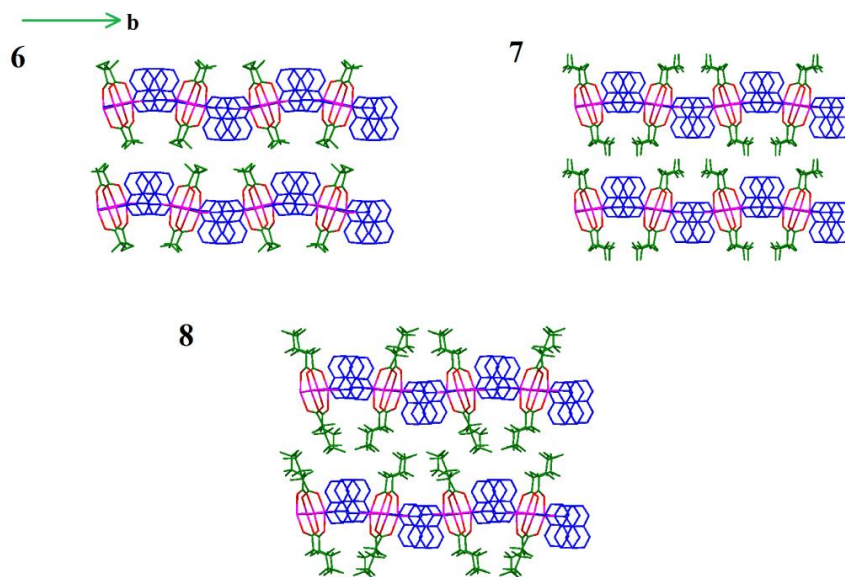


Figure 2.50 Structure viewing along the a -axis for all 4:4:3 phase coordination polymers.

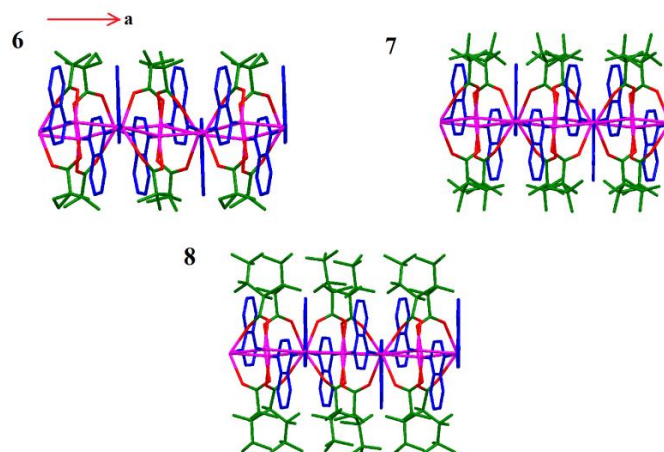


Figure 2.51 Structure viewing along the b -axis for all 4:4:3 phase coordination polymers.

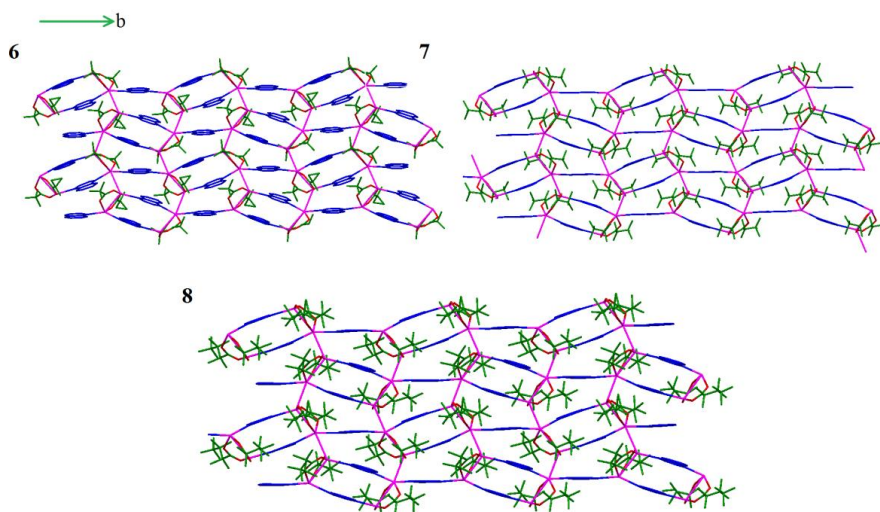


Figure 2.52 Structure viewing along the c^* -axis for all 4:4:3 phase coordination polymers.

Several 4:4:3 phase coordination polymers have been previously reported by our group such as $[\text{Ag}_4(\text{O}_2\text{C}(\text{CF}_2)_2\text{CF}_3)_4(\text{TMP})_3]$ and $[\text{Ag}_4(\text{O}_2\text{CCF}_3)_4(\text{Phen})_3]$, and they are all 1D- tape structures and further stacking into a layer. The differences of their structures are illustrated in **Figure 2.53**. Obviously, the Quin 4:4:3 phases are much different from the other two formed from TMP and Phenazine ligands as the 1D tapes are stacking in an anti-parallel way as others are parallel. The formation of the weak $\text{Ag}\dots\text{Ag}$ interaction can be the explanation as no such interaction can be suggested in other 4:4:3 structures. However, this also leads to slightly larger spaces between each tape in the other 4:4:3 layers which allow the extra singly-bridging ligands to rotate a certain angle within the space (which can further result in π - π stacking with the arene solvents in some cases).

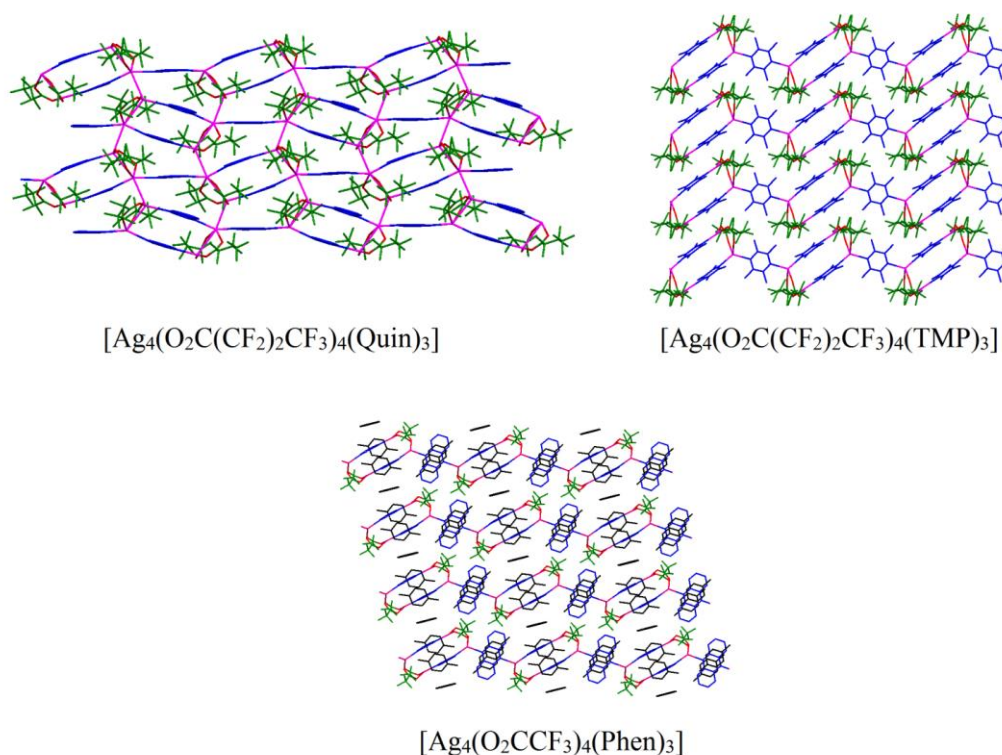
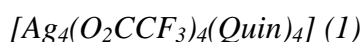


Figure 2.53 Illustration of different structures of 4:4:3 layers formed by different ligands.

2.3.2 Solid-state transformation of 4:4:4 [Ag₄(O₂C(CF₂)_nCF₃)₄(Quin)₄] to 4:4:3 [Ag₄(O₂C(CF₂)_nCF₃)₄(Quin)₃]

2.3.2.1 Thermogravimetric analyses (TGA)

As mentioned in the introduction section, this series of coordination polymers has potential to undergo thermal solid-state transformations by losing one or more ligands. In order to provide a preliminary insight into possible ligand-loss for all these compounds, two types of thermogravimetric analyses were applied to all the 4:4:4 phase coordination polymers. Temperature-sweep TGA, which heats the sample to a certain high temperature with a fixed heating rate, gave an overall view of how the products perform under increasing temperatures. Isothermal TGA in which the compounds are held at a certain temperature for a fixed period of time was used to establish the thermal stability of secondary products. Temperature-sweep TGA plots are shown for compounds **1-5** in Figures 2.13, 2.15, 2.17, 2.19 and 2.21, respectively. Analysis of the mass changes observed is provided in Tables 2.4-2.8. Isothermal TGA plots for **1-5** are shown in Figures 2.14, 2.16, 2.18, 2.20 and 2.22, respectively.



Temperature-sweep TGA (5 °C/min) for **1** (Fig. 2.13) shows mass losses at 125 °C and 175 °C consistent with sequential losses of Quin ligands, followed by degradation of the remaining material to a mixture of AgCO₃ and Ag₂O, finally to silver metal (see **Table 2.4**).

Table 2.4 Temperature-sweep TGA mass losses for [Ag₄(O₂CCF₃)₄(Quin)₄]

Onset Temperature (°C)	Lost Component	Calculated Mass Contribution (%)	Observed Mass Contribution (%)	Residue
125	Quin	9.27	9.131	[Ag ₄ (O ₂ CCF ₃) ₄ (Quin) ₃]
175	2Quin	18.54	17.723	[Ag ₄ (O ₂ CCF ₃) ₄ (Quin)]
225	Quin, 2COCF ₃ , 2(CF ₃), CO ₂	36.01	36.997	Ag ₂ O, Ag ₂ CO ₃
290	CO ₂ , O ₂	5.41	5.218	Ag

An isothermal TGA study (Figure 2.14) was conducted at 135 °C to more closely examine the first mass loss observed in the temperature-sweep TGA. The observed mass loss (8.67 %) is consistent with the mass loss calculated for one Quin ligand per formula unit (9.3 %) and confirms the transformation from 4:4:4 coordination polymer $[Ag_4(O_2CCF_3)_4(Quin)_4]$ to 4:4:3 coordination polymer $[Ag_4(O_2CCF_3)_4(Quin)_3]$. It is also confirmed that the $[Ag_4(O_2CCF_3)_4(Quin)_3]$ material is not thermally stable at the 135 °C as there is a further slow mass loss.



There are mass losses in agreement with sequential loss of Quin ligands, followed by decomposition of the remaining material to $AgCO_3$ and finally to a mixture of $AgCO_3$ and Ag_2O (see Table 2.5).

Table 2.5 Temperature-sweep TGA mass losses for $[Ag_4(O_2CCF_2CF_3)_4(Quin)_4]$

Onset Temperature (°C)	Lost Component	Calculated Mass Contribution (%)	Observed Mass Contribution (%)	Residue
85	Quin	8.12	7.770	$[Ag_4(OOCCF_2CF_3)_4(Quin)_3]$
150	1.5Quin	12.17	12.587	$[Ag_4(OOCCF_2CF_3)_4(Quin)_{1.5}]$
210	1.5Quin, 2CO CF ₂ CF ₃ , 2(CF ₂ CF ₃)	46.49	46.426	2Ag ₂ CO ₃
300	2CO ₂	5.49	5.728	2Ag ₂ O

Again an isothermal TGA study (Figure 2.16) was conducted at 95 °C. The observed mass loss (7.39%) is close to the mass loss calculated for one Quin ligand per formula unit (8.12%), which verifies the transformation from 4:4:4 phase to 4:4:3 phase. It is also confirmed that the 4:4:3 phase is thermally stable at 95 °C.



There are mass losses in agreement with sequential loss of Quin ligands, followed by decomposition of the remaining material to $AgCO_3$ and finally to a residue of Ag_2O (see **Table 2.6**).

Table 2.6 Temperature-sweep TGA mass losses for $[Ag_4(O_2C(CF_2)_2CF_3)_4(Quin)_4]$

Onset Temperature (°C)	Lost component	Calculated Mass Contribution (%)	Observed Mass Contribution (%)	Residue
85	quin	7.2	6.3	$Ag_4(OOC(CF_2)_3CF_3)_4(quin)_3$
150	1.5quin	10.8	10.8	$Ag_4(OOC(CF_2)_3CF_3)_4(quin)_{1.5}$
210	1.5quin, 2CO (CF_2) ₂ CF ₃ , 2((CF_2) ₂ CF ₃)	53.0	54.7	$2Ag_2CO_3$
290	2CO ₂	4.8	4.6	$2Ag_2O$

The isothermal TGA study (at 120 °C) was conducted to more closely examine the first mass loss observed in the temperature-sweep TGA. The observed mass loss (7 %) is consistent with the mass loss calculated for one quinoxaline ligand per formula unit (7.2 %) and confirms the transformation from 4:4:4 coordination polymer $[Ag_4(O_2C(CF_2)_2CF_3)_4(Quin)_4]$ to 4:4:3 coordination polymer $[Ag_4(O_2C(CF_2)_2CF_3)_4(Quin)_3]$ which is thermally stable at 120 °C.



There are mass losses compatible with sequential loss of Quin ligands, followed by the degradation of the remaining material to AgCO₃ and finally to Ag₂O (see **Table 2.7**).

Table 2.7 Temperature-sweep TGA mass losses for [Ag₄(O₂CCF₂CF₃)₄(Quin)₄]

Onset Temperature (°C)	Lost Component	Calculated Mass Contribution (%)	Observed Mass Contribution (%)	Residue
125	Quin	6.49	6.533	[Ag ₄ (OOC(CF ₂) ₃ CF ₃) ₄ (Quin) ₃]
175	Quin	6.49	6.652	[Ag ₄ (OOC(CF ₂) ₃ CF ₃) ₄ (Quin) ₂]
195	2CO, 4((CF ₂) ₄ CF ₃) ₄ , 2Quin	59.50	60.928	2Ag ₂ CO ₃
290	2CO ₂	4.39	4.546	2Ag ₂ O

Several runs of individual isothermal TGA studies at different temperatures (130/120/115 °C) were done leading to similar results. None of the runs showed a clear step for a single Quin ligand loss but instead a continuous mass loss process. Combining this with the failure in attempted direct synthesis of the silver/nonafluoropentanoate/Quin coordination polymer in a 4:4:3 ratio, we assumed that this 4:4:3 ratio coordination polymer could not form or is very unstable in solution.



There are mass losses corresponding to sequential loss of Quin ligands, followed by the degradation of the residual material to AgCO₃ and finally to Ag₂O (see **Table 2.8**).

Table 2.8 Temperature-sweep TGA mass losses for $[\text{Ag}_4(\text{O}_2\text{C}(\text{CF}_2)_4\text{CF}_3)_4(\text{Quin})_4]$

Onset Temperature (°C)	Lost Component	Calculated Mass Contribution (%)	Observed Mass Contribution (%)	Residue
100	Quin	5.91	5.846	$[\text{Ag}_4(\text{OOC}(\text{CF}_2)_4\text{CF}_3)_4(\text{Quin})_3]$
170	Quin	5.91	6.052	$[\text{Ag}_4(\text{OOC}(\text{CF}_2)_4\text{CF}_3)_4(\text{Quin})_2]$
220	2CO, 4((CF ₂) ₄ CF ₃) ₄ , 2Quin	63.18	64.313	2Ag ₂ CO ₃
315	2CO ₂	3.99	3.972	2Ag ₂ O

The isothermal TGA study (120 °C) was conducted to more closely inspect the first mass loss observed in the temperature-sweep TGA. The observed mass loss (5.81 %) amounts to the mass loss calculated for one Quin ligand per formula unit (5.91 %) and backs up the transformation from the 4:4:4 coordination polymer $[\text{Ag}_4(\text{O}_2\text{C}(\text{CF}_2)_4\text{CF}_3)_4(\text{Quin})_4]$ to the 4:4:3 coordination polymer $[\text{Ag}_4(\text{O}_2\text{C}(\text{CF}_2)_4\text{CF}_3)_4(\text{Quin})_3]$, which is thermally stable at 120 °C.

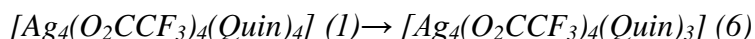
Above all, all the TGA data suggest that these coordination polymers have similar mass-loss trends when heated up to a certain temperature. Combining with the experimental data obtained in our group, all the studied Quin-based 4:4:4 ratio coordination polymers (up to undecafluorohexanoate) share a similar initial single-ligand-loss stage based on the calculation, which was then supported by the isothermal TGA studies. Surprisingly, a secondary ligand-loss stage was also observed, and which indicated the presence of a possible 4:4:2 phase coordination polymer in compounds with longer chains. The increasing chain length could contribute to the increased difficulty in removing other Quin ligands after the first one (**Table 2.9**). The calculation of second mass loss stages for compound **1** to **5** suggest the increasing of the chain length lead to fewer Quin ligands leaving in the second stage. It is reasonable as longer chains may more easily block the pathway for quinoxaline to leave due to stronger interdigitation between layers. This interlayer region is the pathway for transport of ligands and other small molecules suggested from previous work.⁸ Due to the failure of direct synthesis in some of the 4:4:3 phase coordination polymers with longer perfluoroalkyl chain lengths (i.e. **9** and **10**), these TGA results suggested the possibility of preparing these compounds by solid-state transformation. This has been investigated by *in situ* PXRD studies.

Table 2.9 List of the secondary ligand loss after first Quin loss for each compound

Chain length (Number of carbon)	Calculated Mass Contribution (%)	Observed Mass Contribution (%)	Number of quinoxaline molecules
2	18.54	17.2	2
3	12.17	12.6	1.5
4	10.80	10.8	1.5
5	6.49	6.7	1
6	5.91	5.9	1

2.3.2.2 In situ PXRD heating study

In order to inspect the actual structure transformation for these compounds in solid state, *in situ* PXRD heating studies were employed after it was established that single crystals were not robust enough to survive in an *in situ* SCXRD heating study. The idea is to heat the sample or maintain a certain temperature and collect PXRD patterns at several time points, which enable the determination of the structure changes over the whole study. This type of study is becoming more common in monitoring solid-state transformations involving solvent uptake and release.^{23,24} Our group have also been previously utilizing this powerful tool in understanding the solvent and ligand loss in silver-perfluoroalkylcarboxylate-diimine coordination polymers.⁶⁻⁸



The study shown in **Figure 2.53** was successful in demonstrating the solid-state conversion of compound **1** into **6** by loss of a single Quin ligand. Pawley fitting of the patterns for the starting material and the final product identify the unit cell parameters of the phase pure compounds **1** and **6** (**Figures 2.24** and **2.27**). The stacking patterns clearly suggest that only one phase transformation occurred during the heating study.

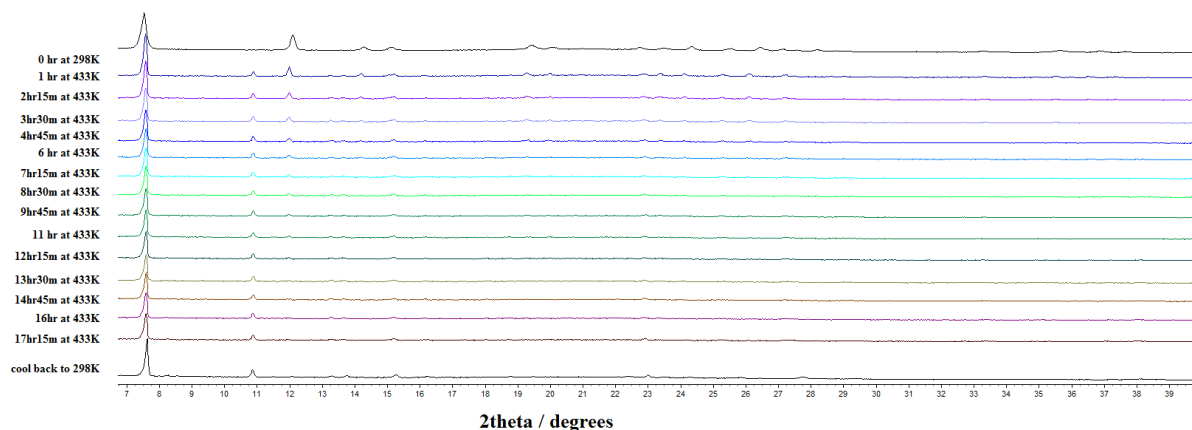


Figure 2.53 *In situ* X-ray powder patterns from the transformation of **1** to **6** shown in the range $7 \leq 2\theta \leq 40^\circ$. On the left the heating temperature and time interval between patterns are noted.

By zooming out typical ranges of the patterns (**Figure 2.54**), it is obvious that the intensity of the peaks around 12.01° for the 4:4:4 phase shifts to 11.96° and continuously weakened over the time and the transformation finishes after about 9 hours (red arrows) and a new peak shows at 10.88° at the same time (red arrows). A single phase change also means that there are no polymorphs formed for compound **1** or **6** by structure transformation under high temperature. This is different from the previous work reported on similar coordination polymers with TMP ligands, such as $[\text{Ag}_4(\text{O}_2\text{C}(\text{CF}_2)_2\text{CF}_3)_4(\text{TMP})_3]$ which has a high-temperature polymorph with different structure from its room temperature phase.⁶ The reason may be that the trifluoroacetate chains in compound **1** are far less variable (bending) than the heptafluorobutanoate chains in the TMP-containing coordination polymer.

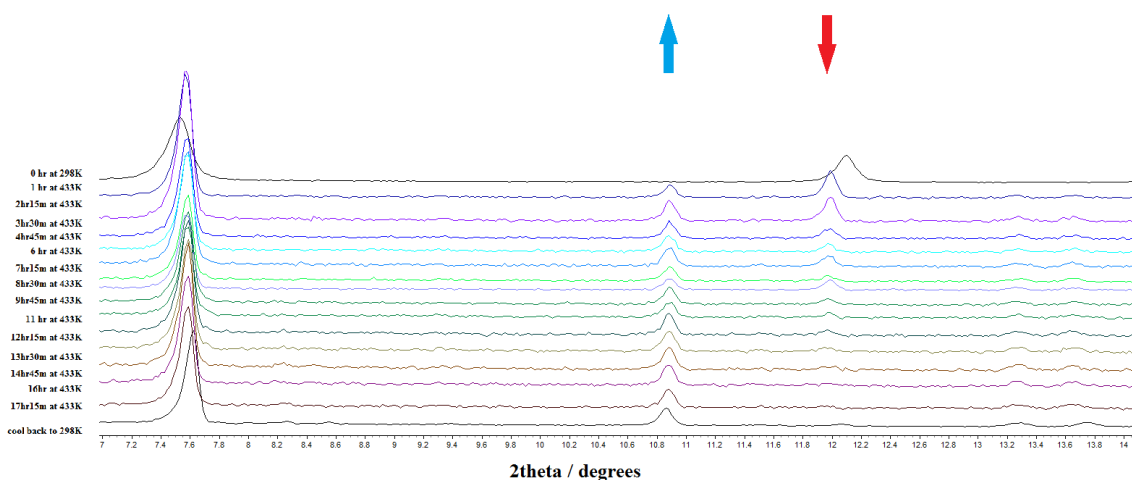
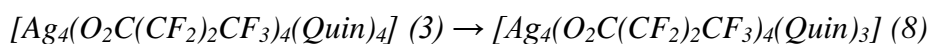


Figure 2.54 *In situ* X-ray powder patterns from the transformation of **1** to **6** shown in the range $7.4 \leq 2\theta \leq 12^\circ$ (obvious change around 12°).



The study shown in **Figure 2.55** shows the solid-state conversion of compound **3** into **8** by loss of a single Quin ligand is again successful as phase purity was also proved for the final product.

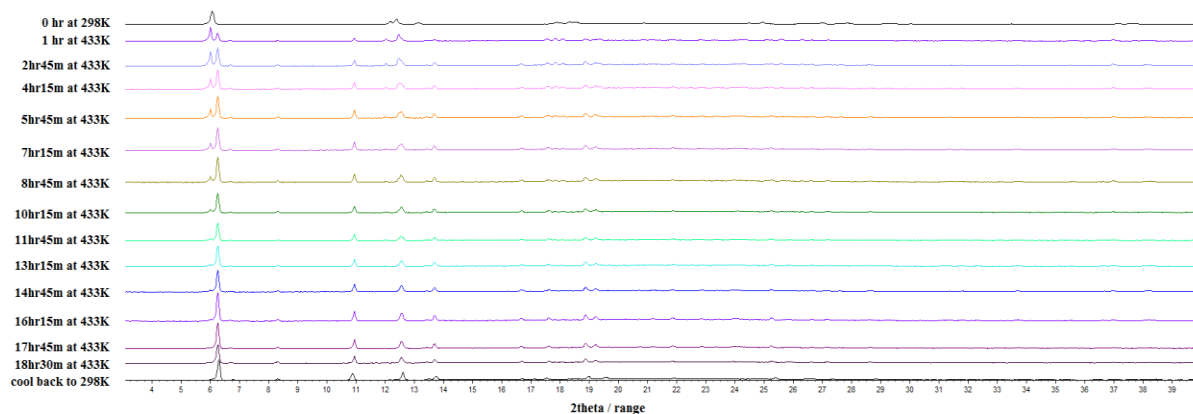


Figure 2.55 *In situ* X-ray powder patterns from the transformation of $[Ag_4(O_2C(CF_2)_2CF_3)_4(Quin)_4]$ (**3**) to $[Ag_4(O_2C(CF_2)_2CF_3)_4(Quin)_3]$ (**8**) shown in the range of $3 \leq 2\theta \leq 13^\circ$. On the left the heating temperature and time interval between patterns are noted.

Similar single phase transformation could be easily observed by zooming patterns (**Figure 2.56**). Two significant peak intensities show at 6.06° and 12.15° first and shift slightly to 5.99° and 12.02° with decrease along the time (red arrows). Three peak intensities show up at 6.26° , 10.95° and 13.69° and increase over the time (blue arrows). The actual phase change period is estimated to be 15 hours based on the patterns, which is slower than the transformation of **1**→**6**, which echo to the hypothesis from TGA that longer chain length will result in a tougher pathway for ligands to leave.

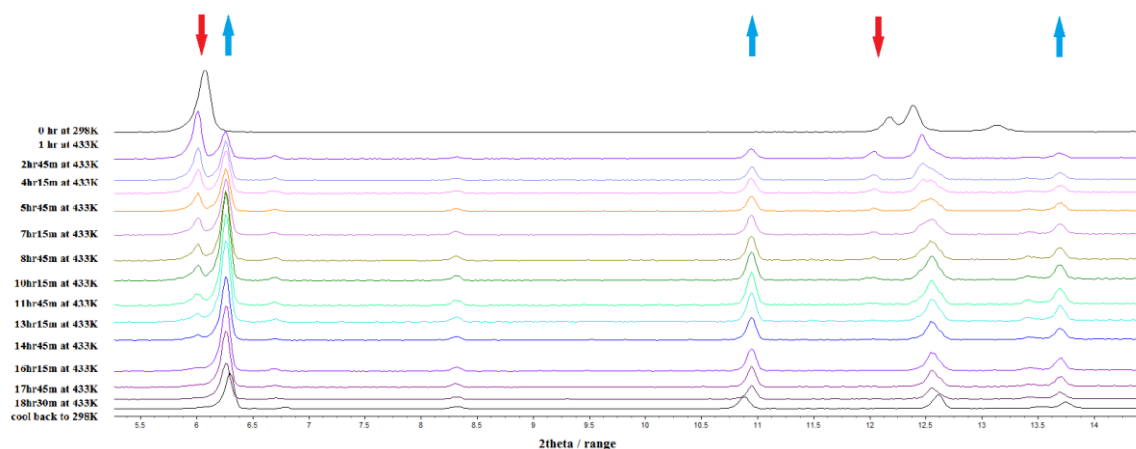


Figure 2.56 Zoomed-in *In situ* X-ray powder patterns from the transformation of $[Ag_4(O_2C(CF_2)_2CF_3)_4(Quin)_4]$ (**3**) to $[Ag_4(O_2C(CF_2)_2CF_3)_4(Quin)_3]$ (**8**) shown in the range of $6 \leq 2\theta \leq 14.5^\circ$.

$[Ag_4(O_2C(CF_2)_4CF_3)_4(Quin)_4]$ (**5**) \rightarrow Several unknown phases

In order to fully understand the complicated TGA results, compound **5** was examined with two *in situ* PXRD heating studies. The first study is an isothermal study at 433 K shown in **Figure 2.57**. Pawley fitting of an initial pattern obtained at 298 K confirmed the presence of only compound **5**. The sequence of patterns in Figure 2.54 begins with a pattern measured after heating the sample to 433 K at $360\text{ }^\circ\text{C hr}^{-1}$.

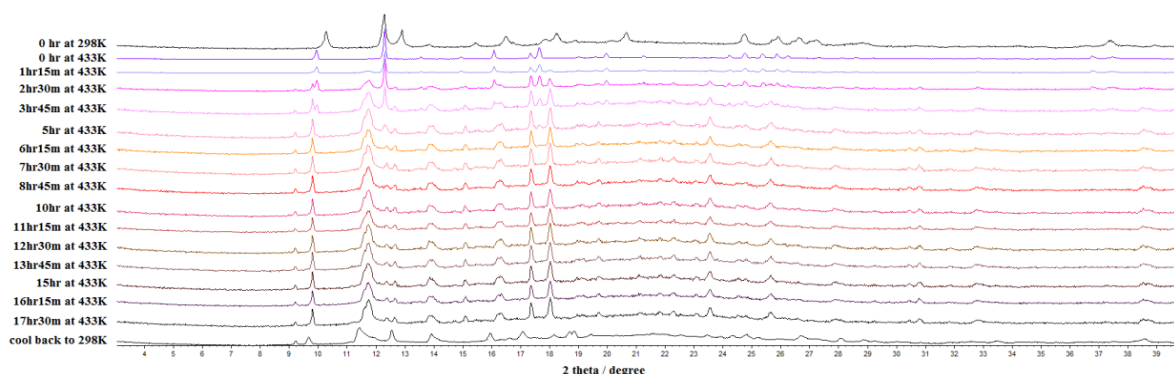


Figure 2.57 *In situ* X-ray powder patterns of the transformation shown in the range of $9 \leq 2\theta \leq 15.5^\circ$. Pawley fitting of the first 433K pattern showed the presence of a new phase when reaching 433K, and which does not fit to any known unit cells in this series of 4:4:4 or 4:4:3 coordination polymers, and I have referred to as "**unknown HT phase B**". This implies that a phase change has already occurred before 433 K. Comparison between the patterns of starting material and this **phase B** are shown in **Figure 2.58**. Two patterns are similar to each other and only peak shifts and few peak changes can be observed, which may indicate they are polymorphs under different temperature.

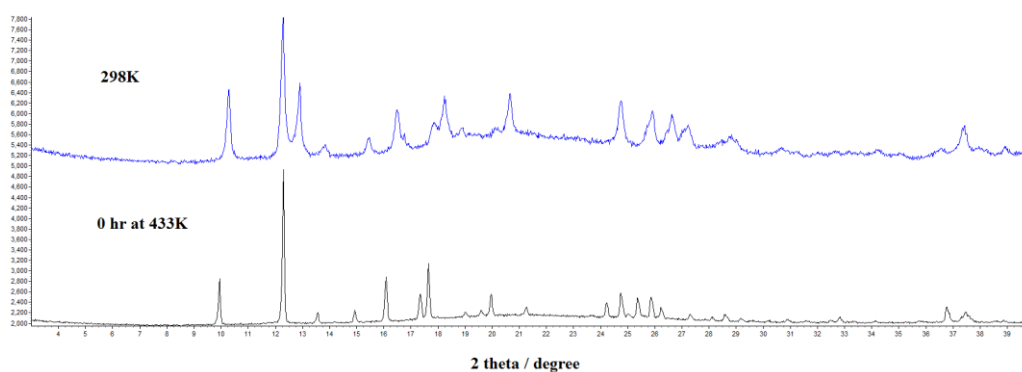


Figure 2.58 Comparison of the PXRD patterns of the starting material (4:4:4 phase) and the new phase shown when just reached 433K.

By visual inspection, however, it is clear that peaks corresponding to the "unknown HT phase B" material eventually disappear over the time at 433 K, leaving a new phase(s) which is could not be indexed with a reasonable unit cell. After keeping the temperature at 433 K for a further 6 hours, peaks corresponding to "unknown HT phase B" are no longer observed. The peaks corresponding to the new unindexed phase(s) shift to higher angles upon cooling back to 298 K.

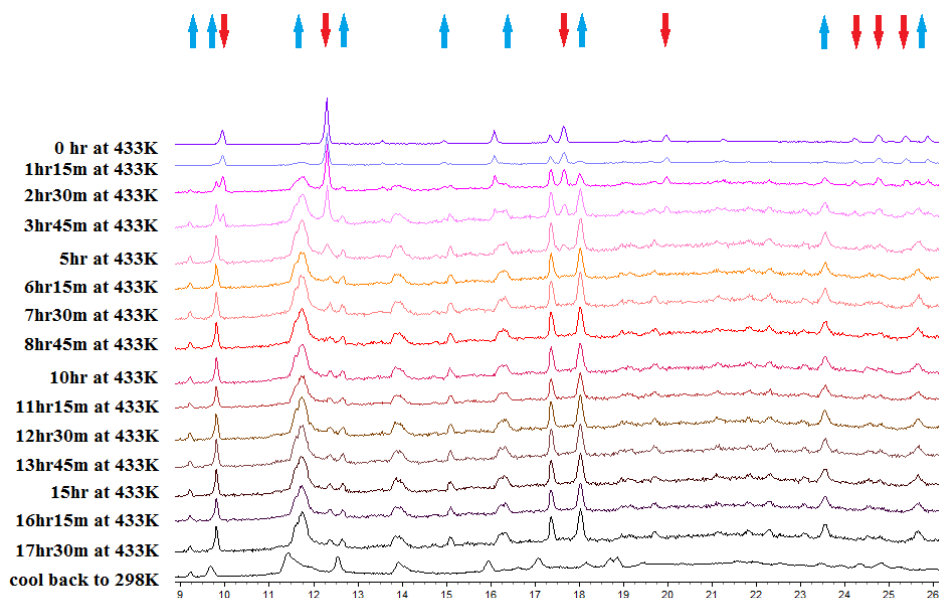


Figure 2.59 Zoomed-in *In situ* X-ray powder patterns from the transformation of $[Ag_4(O_2C(CF_2)_4CF_3)_4(Quin)_4]$ (**5**) shown in the range of $9 \leq 2\theta \leq 26^\circ$.

Based on the results on this isothermal study, a second study was carried out to collect a series of patterns during the period of raising the temperature to 433 K. This was aimed at monitoring the phase-change during the heating process. The stacking patterns are shown below (**Figure 2.60**). Two completed phase transformations and one on-going transformation are observed.

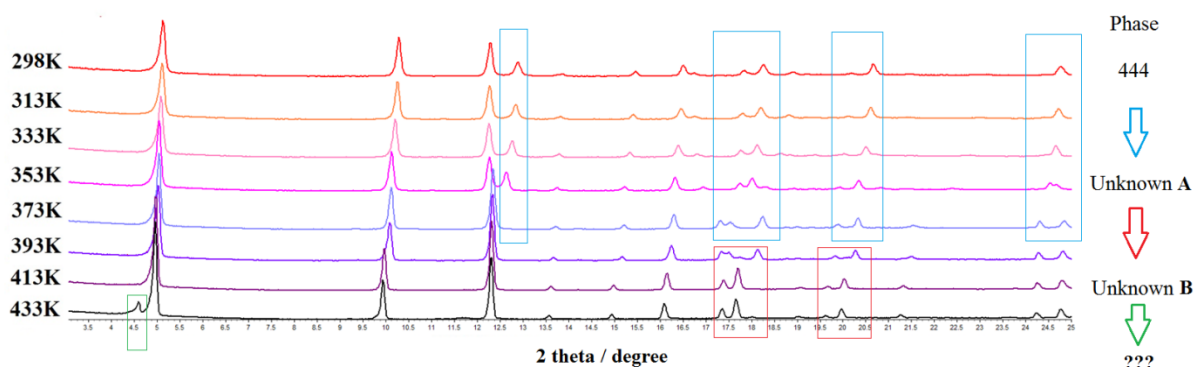


Figure 2.60 *In situ* X-ray powder patterns of the transformation starting from **5** shown in the range of $3 \leq 2\theta \leq 25^\circ$. Blue box: shifting from 4:4:4 phase (**5**) to phase **Unknown A**; red box: shifting from phase **Unknown A** to phase **Unknown B**, Green box: phase **Unknown B** to new un-indexed crystalline phase(s).

The first phase change occurs between 353 K and 373 K. The pattern at 373 K was indexed and fitted into another new unit cell, referred to as "**unknown HT phase A**". The second phase change occurs between 393 K and 413 K. The 413 K pattern was then compared with the first 433 K pattern in the first study, proved as the same "**unknown HT phase B**"

According to the TGA result, there are two identical Quin ligand loss stages occurring around 373 K and 443 K for **5**. It could somehow be an explanation of this multiple phase transformation. However, by comparing all the unit cell parameters for three phases together with that of the crystal structure of **5** at 150 K (**Table 2.10**), a different conclusion is suggested.

Table 2.10 Comparison between the four unit cell parameters under different temperatures

	4:4:4 phase (150 K)	4:4:4 phase (273 K)	Unknown phase A (373 K)	Unknown phase B (413 K)
<i>Space gp</i>	<i>P2₁/c</i>	<i>P2₁/c</i>	<i>Cc</i>	<i>C222₁</i>
<i>a</i> (Å)	17.02	17.35	7.33	35.56
<i>b</i> (Å)	6.68	6.86	34.94	7.34
<i>c</i> (Å)	14.32	14.52	6.95	7.01
α (°)	90	90	90	90
β (°)	94.82	94.82	87.01	90
γ (°)	90	90	90	90
<i>V</i> (Å ³)	1638.9	1723.1	1777.7	1830.30

Notably, the unit cell volumes are increasing significantly and regularly along with the temperature, which is inconsistent with these phases being formed by losing Quin ligands, as the cell volume should decrease. The decrease in cell volume on loss of Quin ligand is confirmed by the two studies above (**1**→**6**: 1169→960 Å³, **3**→**8**: 1419→1219 Å³), as well as for loss of TMP in previous TMP-ligand coordination polymers (1429→1157 Å³).^{6,8} Rate of increase of the cell volume with temperature is linear (**Figure 2.61**). Thus, we assume that the study does not suggest the supposed solid-state transformation by loss of Quin ligands but solid-state phase transformation of compound **5** into two high temperature polymorphs, in a similar manner to that previously observed for a TMP-containing coordination polymer.⁸

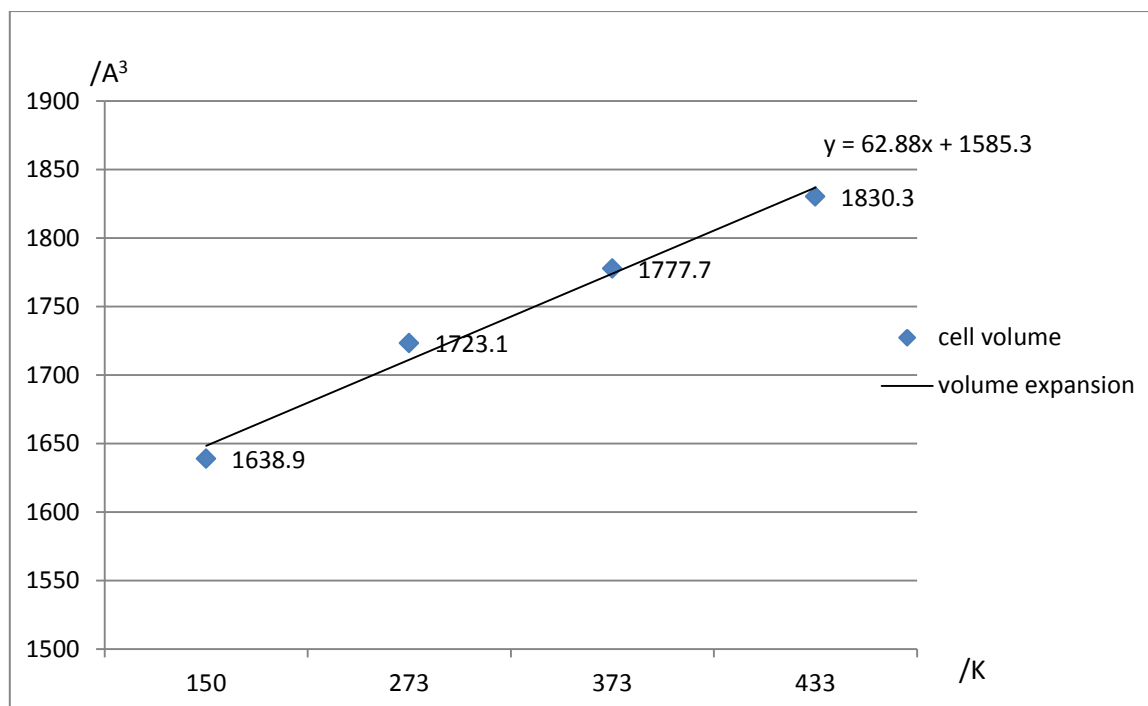


Figure 2.61 Linear correlation of unit cell volume with temperature for compounds in Table 2.10.

To conclude all three studies, *in situ* PXRD heating studies have shown that single Quin-ligand loss by heating the 4:4:4-phase coordination polymers **1** and **3** into 4:4:3 phases (**6** and **8**) in a solid-state transformation. For compound **5** the 4:4:3 phase is not found during the PXRD heating study, although it is possible that the unindexed phase formed at the end of isothermal 433 K study is the 4:4:3 phase. Combining all the *in situ* PXRD heating studies and TGA studies done so far in the group, we notice that the speed of the solid-state transformation depends on how samples are exposed to the heat. In TGA, samples are in an open environment (ceramic pan) when heated with nitrogen flow. However, samples are packed in a capillary during *in situ* PXRD heating studies. Even if the capillary open at both ends, it may still be difficult for the ligand to leave the capillary. This could build up the ligand pressure inside of the sample and lead to a solid-vapour equilibrium with the 4:4:4 phase site, which slows down the conversion to the 4:4:3 phase.

2.3.2.3 Discussion of chemical and structural transformation

By carefully comparing those two types of structures, the actual structure transformation from 4:4:4 to 4:4:3 is found to be far more complicated than simply losing one quinoxaline (**Figure 2.62**).

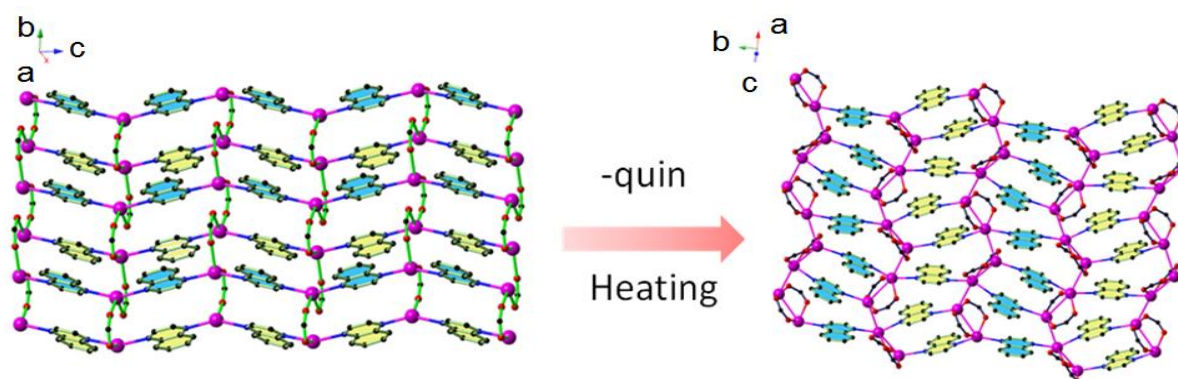


Figure 2.62 Loss of a Quin ligand leads to the topological structural change from 4:4:4 phase (**1**) to 4:4:3 phase (**6**). Different colours are used in showing different directions of Quin ligands (blue: toward inside of the paper; yellow: outside of the paper).

The Ag-N and Ag-O bonds around these Ag centres experience a rare process of dissociation and reformation. The demonstration of the presumed transformation process is illustrated in **Figure 2.63** below. First of all this process needs cleaving two Ag⁺-N bonds due to the single Quin ligand loss in between two [Ag₂(O₂R)₂] zigzag backbones which results in two Ag centre shift from four-coordination to three-coordination. This is followed by cleaving one Ag⁺-N bond of the remained Quin ligand in this pair and reform a new Ag-N bond crossing to the Ag three-coordination centre. Also, one of the Quin ligand in the neighbouring Quin pairs undergoes a 180° rotation (light blue into blue in the figure) which now alternates to the same direction as another ligand in the pair.

For Ag-O bonds, half of the perfluorocarboxyl groups rotates to their neighbouring one by breaking down the [Ag₂(O₂R)₂] zigzag backbone into [Ag₂(O₂R)₂] ring units. This is achieved by cleaving one Ag⁺-O bond in each of these half of the perfluorocarboxyl groups and reforming a new Ag⁺-O bond with the Ag⁺ centre two Ag atoms away. After the rings formed, due to the position of the Quin ligands, two rings are pushed into the V-shaped unit. Also, as mentioned in the crystal structure part, the Ag-Ag distance is much shorter after shifting to 4:4:3 phases thus these V shaped units are connected by stronger Ag...Ag interactions along where the [Ag₂(O₂R)₂] zigzag backbone used to be. This kind of complicated topological structure transformation in the solid-state is very rare for coordination polymers as most of the literatures are related to the solvents in the structure. Thus it would be in interest to take further studies than only structure determination for these compounds.

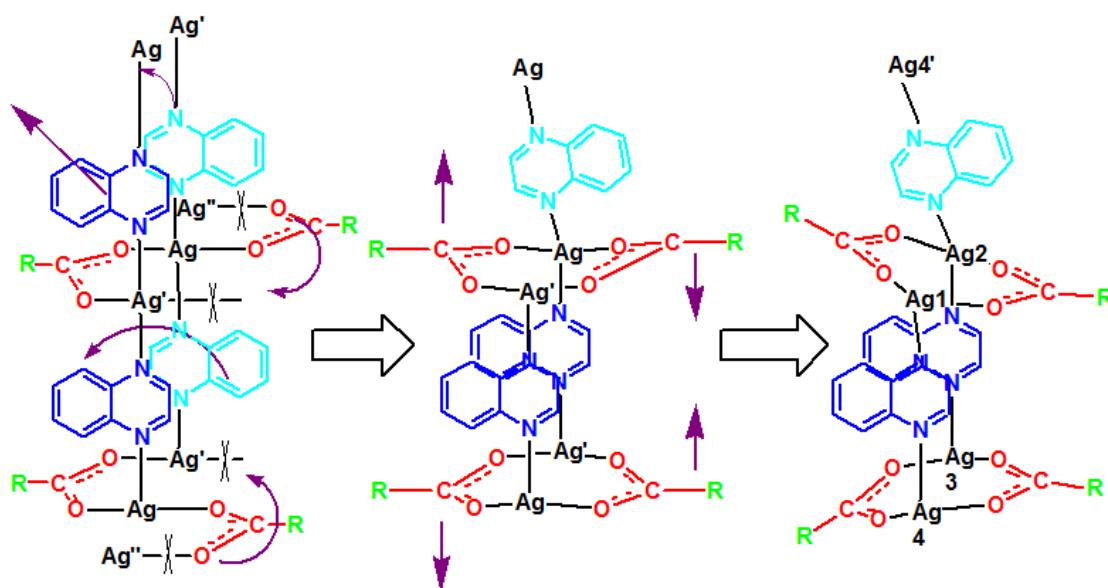


Figure 2.63 Illustration of the presumed transformation from 4:4:4 phase to 4:4:3 phase under heat.

2.3.4 Dielectric constant test

High dielectric constant materials (high- k materials) have received increasing interest over the years due to their potential applications in modern electronic and electrical power systems. To date, there have been a vast number of studies for these purposes on organic polymers, organic/inorganic hybrids, polymer nanocomposites, coordination polymers and so on.

Organic polymers are playing significant roles in the dielectric capacity industry. Although biaxially oriented poly-propylene (BOPP) is one of the industrial standard polymers, it is still facing the problem that its dielectric permittivity is low. Polystyrene with different oligoanilines can overcome the problem and reach a dielectric permittivity of 1690 F/m (at 1 kHz) or 70 F/m (at 1 MHz) with high dielectric losses²⁵ or 5 F/m (1 MHz) / 25 F/m (1 kHz) with low dielectric loss.²⁶

Ferroelectric metal oxides are widely used as fillers in high dielectric permittivity materials. Ferroelectric polymer nanocomposites with TiO₂ have dielectric constant values in the range of 5-45 F/m (at 1 kHz) dependent on the temperature and percentage volume fraction of TiO₂.²⁷ Ferroelectric polymer composites induced by a metal-semiconductor Zn-ZnO core-shell structure can even reach ~115 F/m (1 kHz) by adjusting the thickness of the shell structure.²⁸

Metal-organic coordination polymers are now being examined in the field of high dielectric constant materials. A channel coordination polymer with water molecules, such as [Ln₂Cu₃-(IDA)₆] nH₂O (Ln = La, Nd, Sm, Gd, Ho, Er; IDA = [NH(CH₂COO)₂]²⁻; n ≈ 9), has extremely high dielectric constants at high temperatures (100-200 F/m at room temperature and >1000 F/m at 400K, all at 10 kHz).²⁹ [(CH₃)₂NH₂]Zn(HCOO)₃ shows a changing

dielectric constant from 2.5-20 F/m based on an order-disorder phase transition under different temperatures.³⁰ A similar ferroelectric transition has been reported in the metal-formate framework, $[\text{NH}_4][\text{Zn}(\text{HCOO})_3]$, which has a dramatic increase in dielectric constant (~ 600 F/m at 0.1 kHz and >300 F/m at 1 MHz) at temperatures around 190 K compared to low dielectric constants at other temperatures in the test range (140-250K).³¹

Due to the limited access to the instrument, only the dielectric performance of compound **3** and **8** has been investigated. The results reveal a significant difference in their dielectric behaviour at room temperature. Shown in **Figure 2.64a**, two phases of coordination polymers present totally different dielectric constant (ϵ) in the range of 1 Hz to 1MHz. **8** has an remarkably high ϵ (376.1) at 1 Hz and drops quickly (7.29 at 1MHz) when increasing the frequency, which is suitable to function as high- k materials. On the other hand, **3** does not show distinct changes in ϵ (7.58-7.07) and is always lower than **8** within the range, which may be due to the fact that **3** has a more asymmetric structure than **8**.

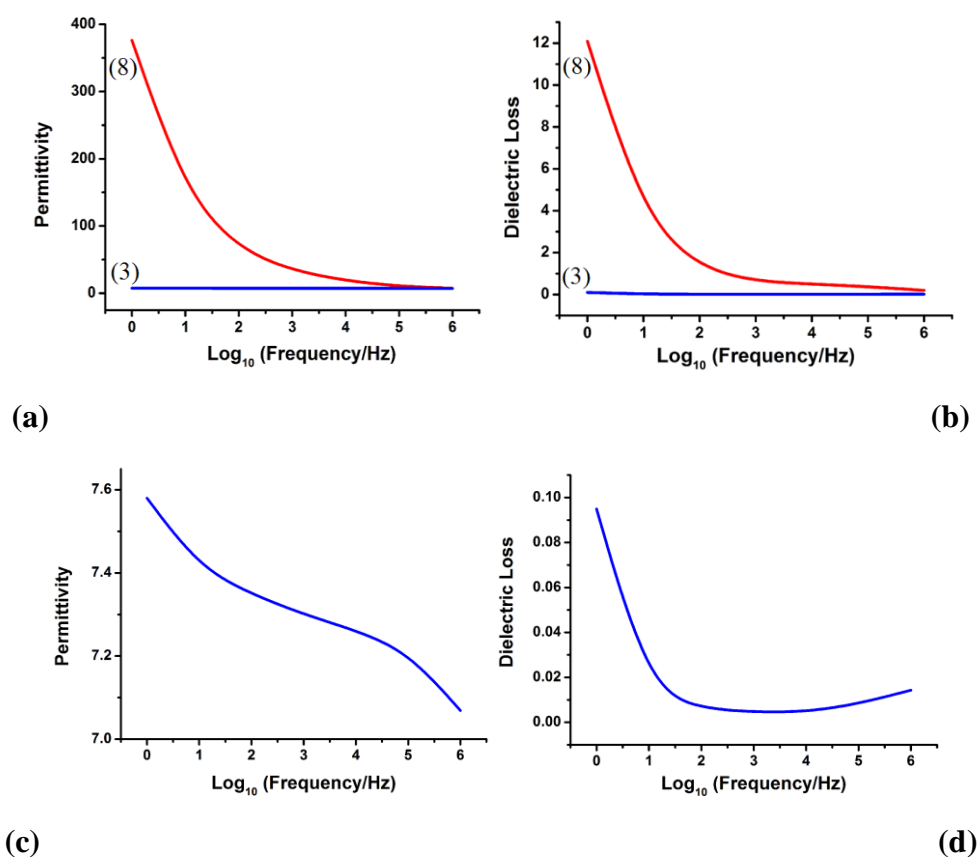


Figure 2.64 (a) Frequency-dependent dielectric permittivity (ϵ) of **3** and **8** under room temperature. (b) Frequency-dependent dielectric loss (DL) of **3** and **8** at ambient temperature. (c) Enlarged plot of the frequency-dependent dielectric permittivity (ϵ) of **3** at ambient temperature showed in (a). (d) Enlarged plot of the frequency-dependent dielectric loss (DL) of **3** at ambient temperature showed in (b).

In terms of dielectric loss (DL , which is denoted as the energy loss inside of the dielectric materials), the curve of **8** quickly drops from 12.08 to 1.24 below 100 Hz and then decelerates slowly then (**Figure 2.64**). On the opposite, the DL of **3** decreases first and then slightly rises with the increasing frequency, exhibiting a nearly frequency-independent behaviour with a magnitude of about 10^{-3} in the range of 10^2 - 10^5 Hz. Though, the value is still much smaller than that of **8**. In short, the results demonstrate that **8** can be a good candidate used as a high- k material in the range of low frequencies at room temperature.

2.4 Conclusions

In summary, it has been demonstrated that several 2D layered coordination polymers $[\text{Ag}_4(\text{O}_2\text{C}(\text{CF}_2)_n\text{CF}_3)_4(\text{Quin})_4]$, $n = 0-4$ (compounds **1-5**), referred to as the 4:4:4 phase, can lose one equivalent of Quin ligand to yield a new 1D 4:4:3 phase $[\text{Ag}_4(\text{O}_2\text{C}(\text{CF}_2)_n\text{CF}_3)_4(\text{Quin})_3]$ upon heating at 85-130 °C. The unprecedented solid-state topological transformation is achieved by the dissociation and restoration of Ag-N and Ag-O bonds accompanied by the re-orientation of Quin ligands and perfluoroalkyl chains. The transformation also results in the reinforcement of argentophilic interactions. Notably, this transformation is controllable and leads to a significant change in the dielectric constants from 4:4:4 phase to 4:4:3 phase coordination polymers, which provides a new approach to the high- k materials. Future work will focus on the rational synthesis of the missing 4:4:3 phase coordination polymers and even the possible 4:4:2 phase coordination polymers.

2.5 References

- 1 J. A. Pereira, A. M. Pessoa, M. N. D. S. Cordeiro, R. Fernandes, C. Prudencio, J. P. Noronha and M. Vieira, *Eur. J. Med. Chem.*, 2015, **97**, 664–672.
- 2 Y. V. Kokunov, Y. E. Gorbunova, V. V. Kovalev and S. A. Kozyukhin, *Russ. J. Coord. Chem.*, 2015, **41**, 747–750.
- 3 M. A. M. Abu-Youssef, V. Langer and L. Ohrström, *Dalton. Trans.*, 2006, **4**, 2542–2550.
- 4 G. K. Kole and J. J. Vittal, *Chem. Soc. Rev.*, 2013, **42**, 1755–1775.
- 5 M. Nagarathinam and J. J. Vittal, *Angew. Chem. Int. Ed.*, 2006, **45**, 4337–4341.
- 6 I. J. Vitórica-Yrezabal, G. Míguez Espallargas, J. Soleimannejad, A. J. Florence, A. J. Fletcher and L. Brammer, *Chem. Sci.*, 2013, **4**, 696–708.
- 7 J. S. Wright, I. J. Vitórica-Yrezabal, H. Adams, S. P. Thompson, A. H. Hill and L. Brammer, *IUCrJ*, 2015, **2**, 188–197.
- 8 I. J. Vitórica-Yrezabal, S. Libri, J. R. Loader, G. Míguez Espallargas, M. Hippler, A. J. Fletcher, S. P. Thompson, J. E. Warren, D. Musumeci, M. D. Ward and L. Brammer, *Chem. Eur. J.*, 2015, **21**, 8799–8811.
- 9 C. Romer, MChem Thesis, University of Sheffield, 2015.
- 10 A. B. Rao, MChem Thesis, University of Sheffield, 2014.
- 11 C. M. Reddy, K. A. Padmanabhan and G. R. Desiraju, *Cryst. Growth Des.*, 2006, **6**, 2720–2731.
- 12 C. M. Reddy, R. C. Gundakaram, S. Basavoju, M. T. Kirchner, K. A. Padmanabhan and G. R. Desiraju, *Chem. Commun.*, 2005, **1**, 3945–7.
- 13 G. M. Sheldrick, *Acta Crystallogr.*, 2008, **64**, 112–122.
- 14 O. V Dolomanov, L. J. Bourhis, R. J. Gildea, J. A. K. Howard and H. Puschmann, *J. Appl. Crystallogr.*, 2009, 2008–2010.
- 15 R. H. Blessing, *Acta Crystallogr. Sect. A*, 1995, **51**, 33–38.
- 16 G. M. Sheldrick, *Univ. Göttingen*, 1997.
- 17 L. Krause, R. Herbst-Irmer, G. M. Sheldrick and D. Stalke, *J. Appl. Crystallogr.*, 2015, **48**, 3–10.
- 18 G. S. Pawley, *J. Appl. Crystallogr.*, 1981, **14**, 357–361.
- 19 A. A. Coelho, *TOPAS-Academic, Version 4.1*, 2007, see <http://>

www.topas-www.academic.net.

- 20 H. M. Rietveld, *J. Appl. Crystallogr.*, 1969, **2**, 65–71.
- 21 A. Bondi, *J. Phys. Chem.*, 1964, **68**, 441–451.
- 22 H. Schmidbaur and A. Schier, *Angew. Chem. Int. Ed.*, 2015, **54**, 746–784.
- 23 Y. Gao, J. Cao, Y. Song, G. Zhang, Y. Wang and Z. Liu, *CrystEngComm*, 2013, **15**, 8522.
- 24 J. Y. Wu, C. Y. Chang, C. J. Tsai and J. J. Lee, *Inorg. Chem.*, 2015, **54**, 10918–10924.
- 25 L. Cui, D. Chao, X. Lu, J. Zhang, H. Mao, Y. Li and C. Wang, *Polym. Int.*, 2010, 975–979.
- 26 C. G. Hardy, S. Islam, D. Gonzalez-delozier, J. E. Morgan, B. Cash, B. C. Benicewicz, H. J. Ploehn and C. Tang, *Chem. Mater.*, 2013, **25**, 799–807.
- 27 B. J. Li, S. Il Seok, B. Chu, F. Dogan, Q. Zhang and Q. Wang, *Adv. Mater.*, 2009, 217–221.
- 28 Y. Zhang, Y. Wang, Y. Deng, M. Li and J. Bai, *Appl. Mater. interfaces*, 2012, **4**, 65–68.
- 29 B. Zhou, A. Kobayashi, H. Cui, L. Long, H. Fujimori and H. Kobayashi, *J. Am. Chem. Soc.*, 2011, **133**, 5736–5739.
- 30 P. Jain, N. S. Dalal, B. H. Toby, H. W. Kroto and A. K. Cheetham, *J. Am. Chem. Soc.*, 2008, **130**, 10450–10451.
- 31 G. Xu, L. Zhang, Z. Wang and S. Gao, *J. Am. Chem. Soc.*, 2010, **132**, 9588–9590.

3. Coordination polymers containing silver perfluoroalkylcarbonylates combined with 2-methylquinoxaline: structures and solvent effects

3.1 Introduction

As described in Section 1.4.3 the work reported in this thesis is part of a larger ongoing project to understand the structures, solid-state transformations and trapping of small molecules, such as solvents, by coordination polymers formed by combining silver perfluoroalkylcarboxylates and diimine ligands based on pyrazine and its larger analogues. The aim of the work in this chapter is to investigate whether a slight modification of quinoxaline ligand studied in Chapter 2 would lead to significant changes in the formation of its Ag(I)/perfluorocarboxylate coordination polymers. 2-Methylquinoxaline (2-Me-quin) was thus chosen as the next type of ligand to expand the overall project.

2-Methylquinoxaline is a dark red liquid at room temperature with a strong special smell and it is rarely covered in the literature. In 1986, Ohmori and co-workers reported a method for methylglyoxal (cytotoxic) determination in biological samples by High-Performance Liquid Chromatography (HPLC). As methylglyoxal gave overlapped peaks in HPLC, this method utilized the reaction between methylglyoxal and *o*-phenylenediamine to give 2-methylquinoxaline, which offered identifiable peaks for HPLC determination (**Figure 3.1**).¹

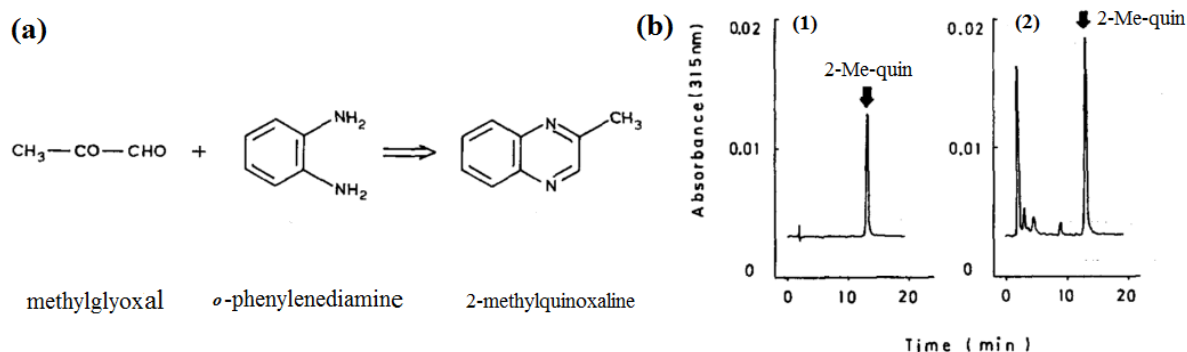


Figure 3.1 (a) Formation of 2-methylquinoxaline from methylglyoxal and *o*-PDA. (b) Identical peaks for 2-Me-quin at the same position in HPLC of (1) an authentic sample of 2-methylquinoxaline and (2) a sample obtained from methylglyoxal in rat liver. (Reproduced with permission from ref.1)

In addition to a few organic or biochemical usages, 2-methylquinoxaline has on rare occasions been reported as a ligand used in inorganic chemistry. The CSD includes only one example of a coordination polymer containing 2-methylquinoxaline. Blake and co-workers have reported the crystal structure of $[\text{HgCl}_2(\text{C}_9\text{H}_8\text{N}_2)]$ in 1989. It was crystallized in a monoclinic space group $P2_1/n$ and the 2D polymeric structure is formed via chloro-bridging interactions linking $\{\text{HgCl}_2\}_2$ dimers along the a -axis and by bridging 2-methylquinoxaline ligands along the second direction (**Figure 3.2**). This leads to stacking of the 2-methylquinoxaline ligands along the a -axis.²

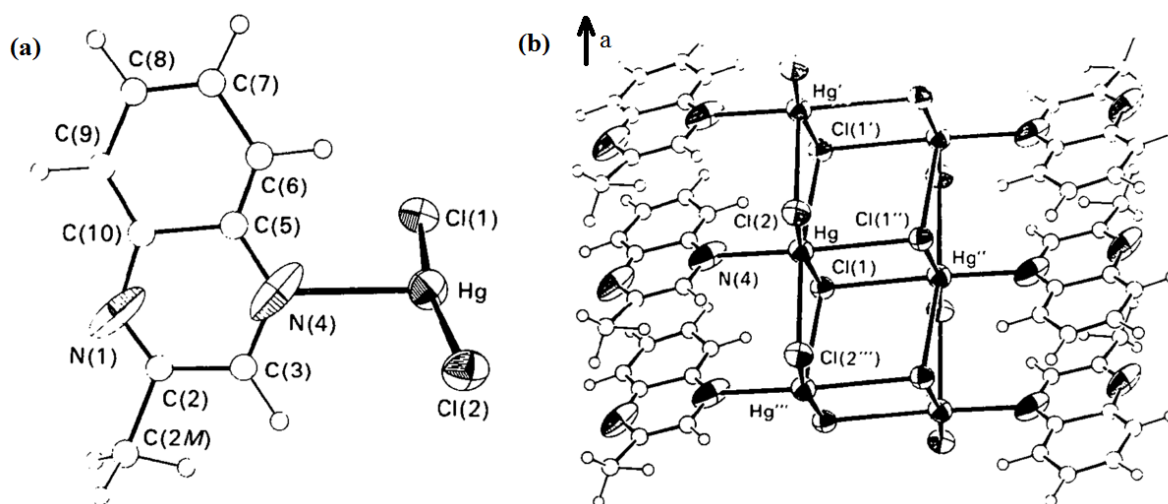


Figure 3.2 View of the asymmetric unit (a) and structure (b) of $[\text{HgCl}_2(\text{C}_9\text{H}_8\text{N}_2)]$. (Reproduced with permission from ref.2)

Solvents can play a very important role in the structural transformation of coordination polymers, for example by the introduction, release and re-introduction of different types of solvents.³ Sumbly and co-workers have recently reported a series of porous silver coordination polymers, $[\text{Ag}(\text{dpzm})]\text{X}$ (dpzm = 2,2'-dipyrazinylmethane; X = PF_6 , ClO_4 , BF_4), which have the property of solid-state breathing and structural transformation. As illustrated in **Figure 3.3**, this single-crystal-to-single-crystal transformation is studied under liquid phase. It starts from placing the large $[\text{Ag}(\text{dpzm})]\text{PF}_6 \cdot \text{DMSO}$ crystal into DCM and the crystal cracks into small pieces but still suitable for X-ray diffraction. Then the smaller crystal is placed into toluene, which replaces the DCM molecules in the cavities and leads to a re-expansion of the crystal and corresponding increase in unit cell volume. Also, the process of introducing toluene and DCM was shown to be reversible.⁴

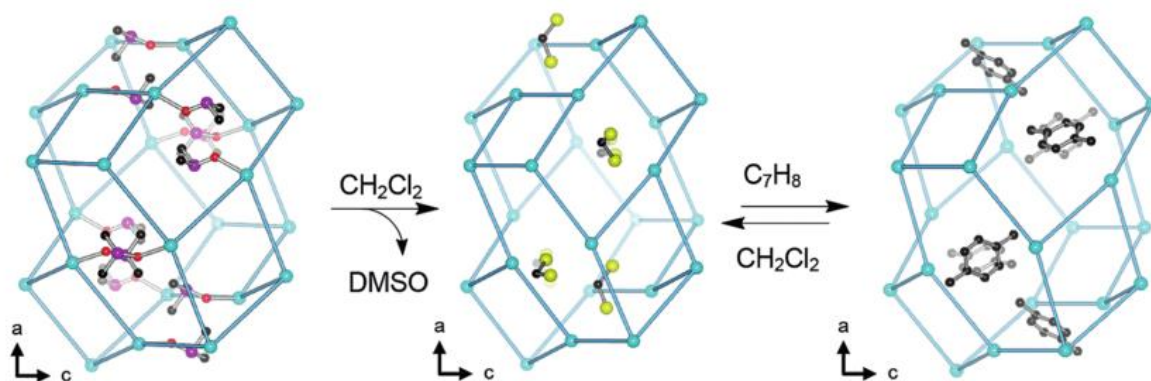


Figure 3.3 The SCSC transformation of [Ag(dpzm)]PF₆ DMSO into [Ag(dpzm)]PF₆ DCM and the reversible transformation of [Ag(dpzm)]PF₆ DCM and [Ag(dpzm)]PF₆ tol (Reproduced with permission from ref.4)

Previous studies in our group on phenazine-containing coordination polymers have shown that they had solvent selectivity among different types of arenes. Compounds were synthesized in mixtures of different combination of these solvents and the preferred solvents in the structure were checked. The results showed a solvent selectivity preference: *p*-xylene > toluene \approx benzene > *o*-xylene > *m*-xylene. However, the structures of these compounds were limited to only two types. [Ag₄(O₂CCF₃)₄(phen)₃] phen arene (phen=phenazine; arene=toluene, *p*-xylene or benzene) were formed as the solvent-containing structure from these three solvents and the solvent-free structure [Ag₄(O₂CCF₃)₄(phen)₂] formed in *o*-xylene and *m*-xylene.⁵

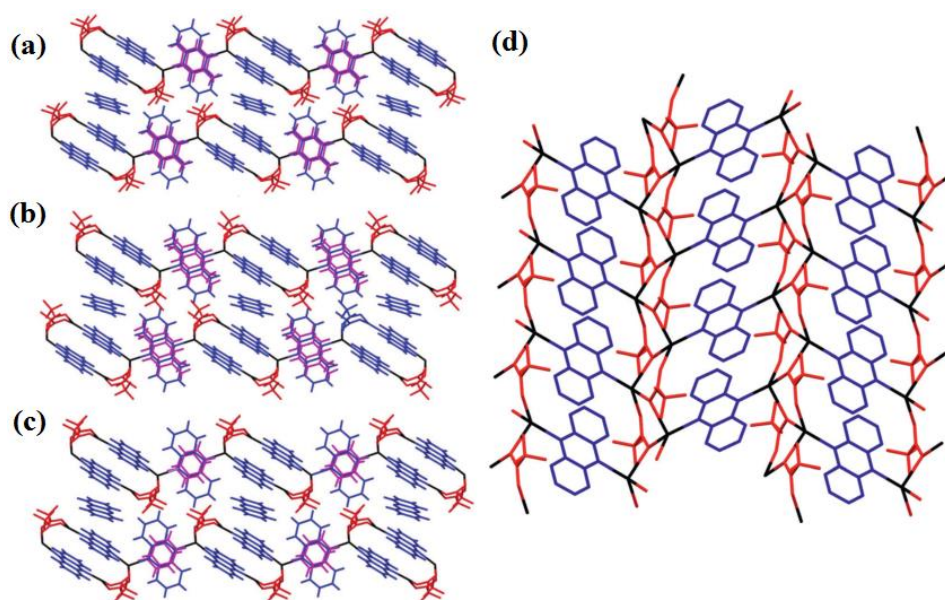


Figure 3.4 View of the structures of [Ag₄(O₂CCF₃)₄(phen)₃] phen tol (a), [Ag₄(O₂CCF₃)₄(phen)₃] phen *p*-xy (b), [Ag₄(O₂CCF₃)₄(phen)₃] phen benz (c) and [Ag₄(O₂CCF₃)₄(phen)₂] (d). (Reproduced with permission from ref.5)

The 2-methylquinoxaline-containing coordination polymers reported in this chapter are different from these phenazine-containing analogues as most of the structures are different to each other (especially the silver pentafluoropropanoate coordination polymers). In this chapter, different structures of coordination polymers formed from silver perfluoroalkylcarboxylates and 2-methylquinoxaline are discussed. It is surprising that these compounds show many new structure types not previously observed in studies of analogous coordination polymers with different diimine ligands. It is particularly notable that a series of structures formed in presence of different arenes suggest a possible solvent effect for these compounds.

3.2 Experimental

3.2.1 Synthesis

All reagents and solvents were purchased from Sigma Aldrich, Alfa Aesar or Fluorochem and used as received. Elemental analyses were carried out by the University of Sheffield, Department of Chemistry elemental analysis service, using a Perkin–Elmer 2400 CHNS/O Series II elemental analyzer. All the coordination polymers were prepared using the “layering synthesis” route described in Chapter 2. For all the solvent-containing coordination polymers (**13-21**) in which aromatic guests were included, crystals formed only after slowly and gradually evaporating the solvents. These crystals typically formed on the wall of the vial during solvent evaporation, and thus needed to be moved back into the solution frequently to prevent degradation of the crystals, presumably from solvent loss. Also, these solvent containing colourless crystals, which is different from the non-solvent containing compounds (**12** and **13**) as these three were red. As none of these solvent-containing compounds were phase pure from PXRD, their elemental analyses were not carried out. Yields for each compound were therefore not calculated and compounds were only identified by SCXRD. Due to the uncertainty of the evaporation, several vials were prepared at the same time. In order to speed up the preparation process, 0.9 M bulk solutions of silver perfluoroalkylcarboxylate salts in acetone were prepared and used during the layering syntheses. Thus, all the reported masses are based on these concentrations of the bulk solution. This approach also minimized the chance of having different amount of silver salts in each vial. Based on the previous results (e.g. Chapter 2), a slight change on the concentration of the reactants could lead formation of different structures. Thus it was important to control this variable when determining the results from using different solvents.

Preparation of [Ag₄(O₂CCF₃)₄(2-Me-quin)₂] (11). 2-methylquinoxaline (64.5 μL, 0.40 mmol) was dissolved in DCM (or ethyl acetate) (4.0 mL) in a 20 mL glass vial and gently layered with DCM (or ethyl acetate) (1.0 mL) and then acetone (1.0 mL). Then an acetone solution (4.0 mL) of silver(I) trifluoroacetate (79.3 mg, 0.36 mmol) was carefully layered onto the buffer layer. The vial was tightly capped and stored in a dark cupboard to minimize the possibility of light degradation of the silver ions. Red crystals of **11** were formed within two days. Yield: 14.6 mg (93%). Anal. Calcd. (%) for C₂₆H₁₆N₄Ag₄F₁₂O₈: C 26.63; H 1.36; N 4.78; found (%): C 26.72; H 1.64; N 4.82.

Some attempted syntheses (both in ethyl acetate and DCM) failed with the formation of a small amount of silver mirror on the wall of the vial, which might be due to the contamination of the acetone (fresh HPLC-grade acetone was used in the successful re-syntheses). SCXRD and PXRD analyses showed that the successful syntheses led to the same compound **11** when prepared in DCM or ethyl acetate.

Preparation of [Ag₆(O₂C(CF₂)₃CF₃)₆(2-Me-quin)₄] (12). Using the aforementioned “layering synthesis” method followed by slow evaporation of solvents, compound **12** was obtained as red crystals within 2 days by using a DCM solution (4.0 mL) of 2-methylquinoxaline (64.5 μL, 0.40 mmol), a buffer layer of DCM (1.0 mL) and acetone (1.0 mL) and an acetone solution (4.0 mL) of silver(I) nonafluoropentanoate (156.7 mg, 0.36 mmol). Yield: 128 mg (76.2 %). Anal. Calcd. (%) for C₆₆H₃₂N₈Ag₆F₅₄O₁₂: C 28.27; H 1.14; N 4.00; found (%): C 28.36; H 1.43; N 3.98.

Preparation of [Ag₄(O₂CCF₂CF₃)₄(2-Me-quin)₃] 1.5(tol) (13) (tol = toluene). Compound **13** was produced as colourless crystals within 3 days by an analogous approach to that used in the isolation of **12**, using a toluene solution (4.0 mL) of 2-methylquinoxaline (64.5 μL, 0.40 mmol), a buffer layer of toluene (0.5 mL) and acetone (1.0 mL) and an acetone solution (4.0 mL) of silver(I) pentafluoropropanoate (97.8 mg, 0.36 mmol).

Preparation of [Ag₄(O₂CCF₂CF₃)₄(2-Me-quin)₃] 2(*o*-xyl) ace (14) (*o*-xyl = *o*-xylene; ace = acetone). Compound **14** was obtained as colourless crystals within 3 days in an analogous manner to that used in the isolation of **12**, using an *o*-xylene solution (4.0 mL) of 2-methylquinoxaline (64.5 μL, 0.40 mmol), a buffer layer of *o*-xylene (0.5 mL) and acetone (1.0 mL) and an acetone solution (4.0 mL) of silver(I) pentafluoropropanoate (97.8 mg, 0.36 mmol).

Preparation of $[\text{Ag}_4(\text{O}_2\text{CCF}_2\text{CF}_3)_4(2\text{-Me-quin})_3] 2(m\text{-xyl})$ (15) ($m\text{-xyl} = m\text{-xylene}$). Compound **15** was yielded as colourless crystals within 2 days by an analogous method to that used in the isolation of **12**, using a *m*-xylene solution (4.0 mL) of 2-methylquinoxaline (64.5 μL , 0.40 mmol), a buffer layer of *m*-xylene (0.5 mL) and acetone (1.0 mL) and an acetone solution (4.0 mL) of silver(I) pentafluoropropanoate (97.8 mg, 0.36 mmol).

Preparation of $[\text{Ag}_4(\text{O}_2\text{CCF}_2\text{CF}_3)_4(2\text{-Me-quin})_4] 2(p\text{-xyl})$ (16) ($p\text{-xyl} = p\text{-xylene}$). Compound **16** was afforded as colourless crystals within 4 days by an analogous method to that used in the isolation of **12**, using a *p*-xylene solution (4.0 mL) of 2-methylquinoxaline (64.5 μL , 0.40 mmol), a buffer layer of *p*-xylene (0.5 mL) and acetone (1.0 mL) and an acetone solution (4.0 mL) of silver(I) pentafluoropropanoate (97.8 mg, 0.36 mmol).

Preparation of $[\text{Ag}_4(\text{O}_2\text{C}(\text{CF}_2)_2\text{CF}_3)_4(2\text{-Me-quin})_3] 1.5(\text{tol})$ (17). Compound **17** was isolated as colourless crystals within 3 days by an analogous method to that used in the isolation of **12**, using a toluene solution (4.0 mL) of 2-methylquinoxaline (64.5 μL , 0.40 mmol), a buffer layer of toluene (0.5 mL) and acetone (1.0 mL) and an acetone solution (4.0 mL) of silver(I) heptafluorobutanoate (120.0 mg, 0.36 mmol).

Preparation of $[\text{Ag}_4(\text{O}_2\text{C}(\text{CF}_2)_2\text{CF}_3)_4(2\text{-Me-quin})_3] 2.5(o\text{-xyl})$ (18). Compound **18** was generated as colourless crystals within 4 days by an analogous method to that used in the isolation of **12**, using an *o*-xylene solution (4.0 mL) of 2-methylquinoxaline (64.5 μL , 0.40 mmol), a buffer layer of *o*-xylene (0.5 mL) and acetone (1.0 mL) and an acetone solution (4.0 mL) of silver(I) heptafluorobutanoate (120.0 mg, 0.36 mmol).

Preparation of $[\text{Ag}_4(\text{O}_2\text{C}(\text{CF}_2)_2\text{CF}_3)_4(2\text{-Me-quin})_3] 0.5(p\text{-xyl})$ (19) and $[\text{Ag}_4(\text{O}_2\text{C}(\text{CF}_2)_2\text{CF}_3)_4(2\text{-Me-quin})_5] n(p\text{-xyl})$ (20). A mixture of compound **19** and **20** was obtained, each as colourless/red crystals, within 5 days by an analogous method to that used in the isolation of **12**, using a *p*-xylene solution (4 mL) of 2-methylquinoxaline (64.5 μL , 0.4 mmol), a buffer layer of *p*-xylene (0.5 mL) and acetone (1.0 mL) and an acetone solution (4.0 mL) of silver(I) heptafluorobutanoate (120.0 mg, 0.36 mmol). Compound **20** was obtained as large needle-like crystals and seems to be the majority phase by observation whereas **19** was plate-like crystals which were occasionally observed under the microscope.

Preparation of [Ag₄(O₂C(CF₂)₂CF₃)₄(2-Me-quin)₃] 1.5(*m*-xyl) (21). Compound **21** was prepared as colourless crystals within 5 days by an analogous method to that used in the isolation of **12**, using a *m*-xylene solution (4.0 mL) of 2-methylquinoxaline (64.5 μL, 0.40 mmol), a buffer solution of *m*-xylene (0.5 mL) and acetone (1.0 mL) and an acetone solution (4.0 mL) of silver(I) heptafluorobutanoate (120.0 mg, 0.36 mmol).

3.2.2 Single Crystal X-ray Diffraction (SCXRD)

Single-crystal X-ray data were collected at 100 K for all the listed compounds (except 150 K for compound **12**) on a Bruker D8 *VENTURE* diffractometer, equipped with a PHOTON 100 CMOS detector (using Cu-K_α radiation, λ = 1.54178 Å). Due to the poor resolution of the solvent-containing crystals, data were collected for a number of crystals of each compound. The collection resolution of some samples was cut to $d_{\min} = 0.9\text{--}1.0$ Å in order to have longer exposure times which fit within the available collection time. The crystallographic data for the best attempt for compounds **11–18** and **21** are presented in Table **3.1**. The crystal structures were solved with direct methods or Patterson method using the *SHELXTL*⁶ or *Olex2*⁷ suites of programs. All the structures were refined against all F^2 values and a multi-scan method (*SADABS*)^{8–10} was used for absorption correction. All non-H atoms were refined anisotropically and hydrogen atoms were added at their calculated positions. Disordered parts in some compounds were modelled with reasonable occupancies for all those atoms and all these atoms were refined isotropically. Disorder of the single bridging 2-Me-ligand in compound **14**, **15** and **19** were modelled with two orientations related by rotation (occupancy for two orientations in each compound: 0.50(4)/0.50(4), 0.50(2)/0.50(2) and 0.61(5)/0.39(5), respectively). Disorder of CF₂CF₃ groups in compound **14** and **15** were modelled with two orientations (occupancy in each compound: 0.531(7)/0.469(7) and 0.599(14)/0.401(14), respectively). Disorder of CF₃ groups in compound **16** was modelled with two orientations (occupancy: 0.507(9)/0.493(9)). Disorder of three CF₂CF₂CF₃ groups in compound **21** were modelled with two orientations (occupancy: 0.508(11)/0.492(11), 0.510(7)/0.490(7) and 0.612(8)/0.388(8), respectively).

Table 3.1 Crystal Data, Structure Solution and Refinement Parameters for compounds **11-18** and **21**

	[Ag ₄ (O ₂ CCF ₃) ₄ (2-Me-quin) ₂] (11)	[Ag ₆ (O ₂ C(CF ₂) ₄ CF ₃) ₆ (2-Me-quin) ₄] (12)	[Ag ₄ (O ₂ CCF ₂ CF ₃) ₄ (2-Me-quin) ₃] 1.5tol (13)
Crystal colour	Red	Red	Colourless
Crystal size (mm)	0.12 x 0.06 x 0.03	0.35 x 0.15 x 0.07	0.17 x 0.14 x 0.03
Crystal system	Monoclinic	Triclinic	Triclinic
Space group, <i>Z</i>	<i>C</i> 2/ <i>c</i> , 4	<i>P</i> -1, 1	<i>P</i> -1, 2
<i>a</i> (Å)	22.3847(8)	7.2951(2)	11.8333(11)
<i>b</i> (Å)	10.0726(4)	13.9088(4)	16.2020(14)
<i>c</i> (Å)	16.7003(6)	21.4931(7)	16.2042(13)
α (°)	90	75.3758(15)	93.051(6)
β (°)	116.7104(15)	81.7834(15)	108.694(5)
γ (°)	90	85.3433(14)	106.232(6)
<i>V</i> (Å ³)	3363.6(2)	2086.19(2)	2790.4(4)
Density (Mg.m ⁻³)	2.314	2.230	1.969
Wavelength (Å)	1.54178	1.54178	1.54178
Temperature (K)	100	150	100
μ (Cu-K α) (mm ⁻¹)	19.532	12.802	12.235
Θ range (°)	4.422 to 66.796	6.136 to 72.476	2.876 to 50.541
Reflns collected	25305	20713	15832
Independent reflns (<i>R</i> _{int})	2997 (0.0577)	7776 (0.0544)	5640 (0.0691)
Reflns used in refinement, <i>n</i>	2997	7776	5640
L.S. parameters, <i>p</i>	245	660	798
No. of restraints, <i>r</i>	0	0	98
<i>R</i> 1 (<i>F</i>) ^[a] > 2.0 σ (<i>I</i>)	0.0302	0.0573	0.0661
<i>wR</i> 2(<i>F</i> ²) ^[a] , all data	0.0649	0.1608	0.1759
<i>S</i> (<i>F</i> ²) ^[a] , all data	1.042	1.035	1.024

Table 3.1 (continued)

	[Ag ₄ (O ₂ CCF ₂ CF ₃) ₄ (2-Me-q uin) ₃] 2(<i>o</i> -xyl) ace (14)	[Ag ₄ (O ₂ CCF ₂ CF ₃) ₄ (2-Me-q uin) ₃] 2(<i>m</i> -xyl) (15)	[Ag ₄ (O ₂ CCF ₂ CF ₃) ₄ (2-Me-q uin) ₄] 2(<i>p</i> -xyl) (16)
Crystal colour	Colourless	Colourless	Colourless
Crystal size (mm)	0.175 x 0.115 x 0.067	0.16 x 0.09 x 0.04	0.21 x 0.05 x 0.03
Crystal system	Triclinic	Triclinic	Triclinic
Space group, <i>Z</i>	<i>P</i> -1, 1	<i>P</i> -1,1	<i>P</i> -1, 1
<i>a</i> (Å)	10.3145(7)	10.0383(4)	10.1598(3)
<i>b</i> (Å)	11.4915(7)	11.3434(5)	11.5836(4)
<i>c</i> (Å)	15.0473(10)	15.0069(7)	15.2399(5)
α (°)	88.367(2)	94.912(3)	92.8952(14)
β (°)	73.653(2)	105.064(3)	91.7363(13)
γ (°)	69.2755(19)	109.379(3)	110.3576(12)
<i>V</i> (Å ³)	1595.67(18)	1528.65(12)	1677.17(9)
Density (Mg.m ⁻³)	1.852	1.886	1.854
Wavelength (Å)	1.54178	1.54178	1.54178
Temperature (K)	100	100	100
μ (Cu-K α) (mm ⁻¹)	10.769	11.205	12.802
Θ range (°)	4.790 to 66.787	4.207 to 55.137	4.648 to 67.679
Reflns collected	20517	15216	15597
Independent reflns (<i>R</i> _{int})	5565 (0.0280)	3836 (0.0664)	5772 (0.0268)
Reflns used in refinement, <i>n</i>	5565	3836	5772
L.S. parameters, <i>p</i>	429	396	462
No. of restraints, <i>r</i>	131	153	0
<i>R</i> 1 (<i>F</i>) ^[a] <i>I</i> > 2.0 σ (<i>I</i>)	0.0505	0.0589	0.0381
<i>wR</i> 2(<i>F</i> ²) ^[a] , all data	0.1256	0.1351	0.0895
<i>S</i> (<i>F</i> ²) ^[a] , all data	1.044	1.038	1.033

Table 3.1 (continued)

	[Ag ₄ (O ₂ C(CF ₂) ₂ CF ₃) ₄ (2-Me-quin) ₃] 1.5(tol) (17)	[Ag ₄ (O ₂ C(CF ₂) ₂ CF ₃) ₄ (2-Me-quin) ₃] 2.5(o-xyl) (18)	[Ag ₄ (O ₂ C(CF ₂) ₂ CF ₃) ₄ (2-Me-quin) ₃] 1.5(m-xyl) (21)
Crystal colour	Colourless	Colourless	Colourless
Crystal size (mm)	0.22 x 0.22 x 0.05	0.16 x 0.07 x 0.04	0.24 x 0.20 x 0.14
Crystal system	Triclinic	Triclinic	Triclinic
Space group, <i>Z</i>	<i>P</i> -1, 2	<i>P</i> -1, 1	<i>P</i> -1, 1
<i>a</i> (Å)	10.3254(3)	10.6093(4)	13.7896(5)
<i>b</i> (Å)	17.7134(5)	17.8108(7)	15.9207(6)
<i>c</i> (Å)	19.5121(5)	19.2036(8)	16.0290(5)
α (°)	101.3006(14)	98.982(2)	91.3536(13)
β (°)	93.8884(13)	90.566(2)	102.1958(14)
γ (°)	96.0988(12)	99.151(2)	109.2333(15)
<i>V</i> (Å ³)	3465.32(17)	3536.4(2)	3231.0(2)
Density (Mg.m ⁻³)	1.777	1.861	1.920
Wavelength (Å)	1.54178	1.54178	1.54178
Temperature (K)	100	100	100
μ (Cu-K α) (mm ⁻¹)	10.103	9.949	11.205
Θ range (°)	2.319 to 63.702	2.331 to 63.995	2.955 to 66.765
Reflns collected	42778	42888	51683
Independent reflns (<i>R</i> _{int})	11122 (0.0448)	11431 (0.0512)	11271 (0.0373)
Reflns used in refinement, <i>n</i>	11122	11431	11271
L.S. parameters, <i>p</i>	891	924	881
No. of restraints, <i>r</i>	41	147	24
<i>R</i> 1 (<i>F</i>) ^[a] <i>I</i> > 2.0 σ (<i>I</i>)	0.0686	0.0800	0.0685
<i>wR</i> 2(<i>F</i> ²) ^[a] , all data	0.2006	0.2253	0.1773
<i>S</i> (<i>F</i> ²) ^[a] , all data	1.041	1.024	1.022

$$[a] R1(F) = \frac{\sum(|F_o| - |F_c|)}{\sum|F_o|}; wR2(F^2) = \frac{[\sum w(F_o^2 - F_c^2)^2 / \sum w F_o^4]^{1/2}}{S(F^2)} = \frac{[\sum w(F_o^2 - F_c^2)^2 / (n + r - p)]^{1/2}}{S(F^2)}$$

The data qualities for all the silver heptafluorobutanoate-2-Me-quin coordination polymers were very poor due to the low resolution and there was no improvement after several attempts. The best attempts for **19** and **20** are shown in **Table 3.2** below.

Table 3.2 Unit cell parameters for compounds **19** and **20**

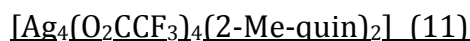
	[Ag ₄ (O ₂ CCF ₂ CF ₃) ₄ (2-Me-quin) ₃] 0.5(<i>p</i> -xyl) (19)	[Ag ₄ (O ₂ CCF ₂ CF ₃) ₄ (2-Me-quin) ₅] <i>n</i> (<i>p</i> -xyl) (20)
Crystal colour	Colourless	Red
Crystal size (mm)	0.14 x 0.07 x 0.03	0.12 x 0.06 x 0.03
Crystal system	Monoclinic	Monoclinic
Space group, <i>Z</i>	<i>P</i> 2 ₁ / <i>c</i> , 2	<i>P</i> 2 ₁ , 4
<i>a</i> (Å)	16.4761(10)	19.6184(11)
<i>b</i> (Å)	7.4371(4)	22.3976(13)
<i>c</i> (Å)	25.5241(16)	21.0946(12)
α (°)	90	90
β (°)	107.216(3)	115.919(3)
γ (°)	90	90
<i>V</i> (Å ³)	2987.4(3)	8336.7(9)
Density (Mg.m ⁻³)	2.080	0.874
Wavelength (Å)	1.54178	1.54178
Temperature (K)	100	100
μ (Cu-K α) (mm ⁻¹)	11.741	7.694
Θ range (°)	2.808 to 54.194	2.329 to 63.540
Reflns collected	22532	84817
Independent reflns (<i>R</i> _{int})	3514 (0.5780)	26656 (0.1757)
Reflns used in refinement, <i>n</i>	3514	26656
L.S. parameters, <i>p</i>	270	437
No. of restraints, <i>r</i>	218	1
<i>R</i> 1 (<i>F</i>) ^[a] / <i>I</i> > 2.0 σ (<i>I</i>)	0.1449	0.2747
<i>wR</i> 2(<i>F</i> ²) ^[a] , all data	0.4377	0.6433
<i>S</i> (<i>F</i> ²) ^[a] , all data	1.860	1.685

[a] $R1(F) = \Sigma(|F_o| - |F_c|) / \Sigma|F_o|$; $wR2(F^2) = [\Sigma w(F_o^2 - F_c^2)^2 / \Sigma w F_o^4]^{1/2}$; $S(F^2) = [\Sigma w(F_o^2 - F_c^2)^2 / (n + r - p)]^{1/2}$

3.2.3 Powder X-ray Diffraction (PXRD)

Powder X-ray diffraction data for phase purity checks were recorded on a Bruker D8 ADVANCE X-ray powder diffractometer at University of Sheffield. The diffractometer was fitted with a focusing Göbel mirror optic and a high-resolution energy-dispersive Lynxeye XE detector and operated in a capillary mode or flat-plate mode and using Cu-K α radiation. For the capillary mode, the sample was packed in a 0.7 mm borosilicate capillary, whereas in the flat plate mode each sample was loaded on a 14 mm silicon zero-background sample disc. Each sample was rotated at 30 rot min⁻¹ to average the sample exposure and was scanned at room temperature. The diffraction patterns were indexed and fitted by Pawley refinement¹¹ using the *TOPAS-Academic* program.¹² Fitted patterns are shown with calculated patterns in red and observed patterns in blue.

For the coordination polymers containing solvent molecules, in order to minimize the solvent loss during collections, these compounds were washed and prepared as a slurry by grinding the samples with the pure aromatic solvent (used in the synthesis) in the mortar. This slurry was then quickly loaded into a 0.5mm kapton tube by using a glass fibre and the tube was sealed at both ends with small amount of wax. PXRD data were then collected in the same manner as that for dry samples loaded in borosilicate capillaries. PXRD measurements were not carried out for silver heptafluorobutanoate-2-Me-quin coordination polymers.



The sample was scanned in capillary mode at a rate of 2 sec step⁻¹, with each detector step size being 0.02°. The unit cell parameters of **11** were used as a starting point for the Pawley refinement, employing 479 parameters (12 background, 1 zero error, 5 profile, 5 cell, 456 reflections). Pawley refinement was converged to $R_{wp} = 0.0791$, $R_{wp}' = 0.1400$. [$a = 22.821(3)$ Å, $b = 10.125(1)$ Å, $c = 17.035(2)$ Å, $\beta = 117.50(1)$ °, $V = 3491.4(9)$ Å³].

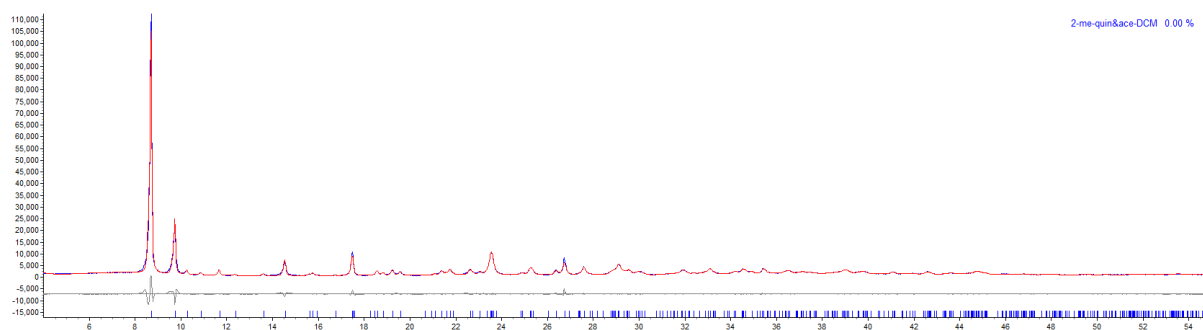


Figure 3.5 Observed (blue) and calculated (red) profiles and the difference plot [$I_{\text{obs}} - I_{\text{calc}}$] (grey) of the Pawley refinement (2θ range 4-55°, $d_{\text{min}} = 1.67$ Å).

[Ag₆(O₂C(CF₂)₃CF₃)₆(2-Me-quin)₄] (12)

The sample was scanned in flat-plate mode at a rate of 1.5 sec step⁻¹, with each detector step size being 0.02°. An indexed unit cell ($[a = 6.9818 \text{ \AA}, b = 15.3767 \text{ \AA}, c = 23.3836 \text{ \AA}, \alpha = 108.531^\circ, \beta = 65.619^\circ, \gamma = 109.419^\circ, V = 2108.5 \text{ \AA}^3]$) was used as the starting point for the Pawley refinement, employing 761 parameters (12 background, 1 zero error, 5 profile, 7 cell, 736 reflections), resulting in final indices of fit $R_{wp} = 0.0547, R_{wp}' = 0.1118$. $[a = 6.989(2) \text{ \AA}, b = 15.344(4) \text{ \AA}, c = 23.437(8) \text{ \AA}, \alpha = 108.46(2)^\circ, \beta = 65.74(2)^\circ, \gamma = 109.44(3)^\circ, V = 2113.1(12) \text{ \AA}^3]$.

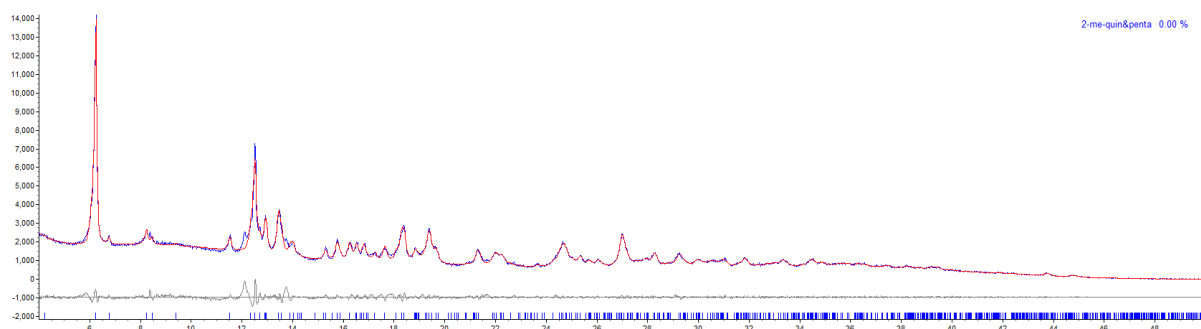


Figure 3.6 Observed (blue) and calculated (red) profiles and the difference plot [$I_{\text{obs}} - I_{\text{calc}}$] (grey) of the Pawley refinement (2θ range 4-50°, $d_{\text{min}} = 1.82 \text{ \AA}$).

[Ag₄(O₂C(CF₂)₃CF₃)₄(2-Me-quin)₃·1.5tol (13)

The sample was scanned in flat plate mode at a rate of 1.5 sec step⁻¹, with each detector step size being 0.02°. The unit cell of the **13** from SCXRD data were used as the starting point for the Pawley refinement, employing 1030 parameters (15 background, 1 zero error, 5 profile, 7 cell, 1002 reflections), resulting in final indices of fit $R_{wp} = 0.0951, R_{wp}' = 0.1042$. $[a = 12.01(5) \text{ \AA}, b = 16.10(9) \text{ \AA}, c = 15.91(4) \text{ \AA}, \alpha = 95.2(3)^\circ, \beta = 108.2(3)^\circ, \gamma = 103.7(1)^\circ, V = 2810(21) \text{ \AA}^3]$.

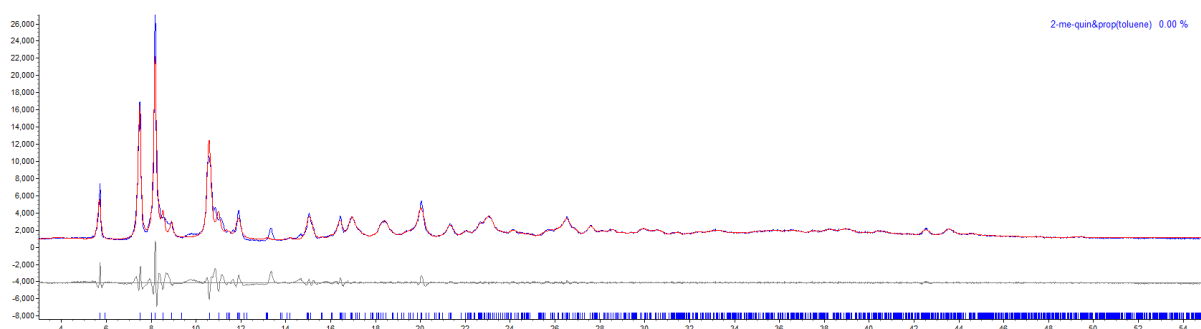


Figure 3.7 Observed (blue) and calculated (red) profiles and the difference plot [$I_{\text{obs}} - I_{\text{calc}}$] (grey) of the Pawley refinement (2θ range 4-55°, $d_{\text{min}} = 1.67 \text{ \AA}$).

[Ag₄(O₂C(CF₂)₃CF₃)₄(2-Me-quin)₃·2o-xyl·ace (14)]

The sample was scanned in capillary mode at a rate of 1.5 sec step⁻¹, with each detector step size being 0.02°. An indexed unit cell ($[a = 10.5019 \text{ \AA}, b = 11.6764 \text{ \AA}, c = 15.0808 \text{ \AA}, \alpha = 87.279^\circ, \beta = 106.849^\circ, \gamma = 67.750^\circ, V = 1612.104 \text{ \AA}^3]$) was used as the starting point for the Pawley refinement, employing 957 parameters (12 background, 1 zero error, 5 profile, 7 cell, 932 reflections), resulting in final indices of fit $R_{wp} = 0.0828, R_{wp}' = 0.1270$. $[a = 10.492(9) \text{ \AA}, b = 11.664(1) \text{ \AA}, c = 15.073(2) \text{ \AA}, \alpha = 87.29(1)^\circ, \beta = 106.910(8)^\circ, \gamma = 68.669(8)^\circ, V = 1606.6(4) \text{ \AA}^3]$.

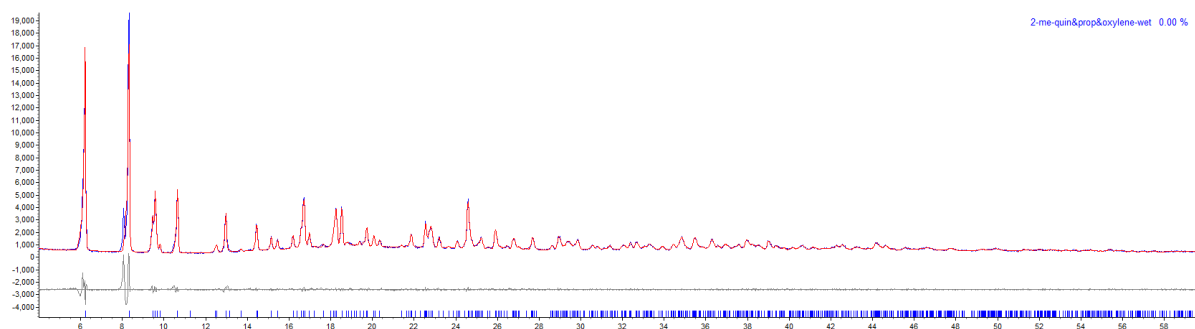


Figure 3.8 Observed (blue) and calculated (red) profiles and the difference plot [$I_{\text{obs}} - I_{\text{calc}}$] (grey) of the Pawley refinement (2θ range 4-60°, $d_{\text{min}} = 1.54 \text{ \AA}$).

[Ag₄(O₂CCF₂CF₃)₄(2-Me-quin)₃·2m-xyl (15)]

The sample was scanned in capillary mode at a rate of 1.5 sec step⁻¹, with each detector step size being 0.02°. An indexed unit cell ($[a = 10.2548 \text{ \AA}, b = 11.6402 \text{ \AA}, c = 15.8569 \text{ \AA}, \alpha = 73.617^\circ, \beta = 67.475^\circ, \gamma = 69.409^\circ, V = 1612.765 \text{ \AA}^3]$) was used as the starting point for the Pawley refinement, employing 928 parameters (12 background, 1 zero error, 5 profile, 7 cell, 903 reflections), resulting in final indices of fit $R_{wp} = 0.0760, R_{wp}' = 0.1760$. $[a = 10.2404(6) \text{ \AA}, b = 11.6173(8) \text{ \AA}, c = 15.844(1) \text{ \AA}, \alpha = 73.644(1)^\circ, \beta = 67.448(7)^\circ, \gamma = 69.463(5)^\circ, V = 1606.4(2) \text{ \AA}^3]$.

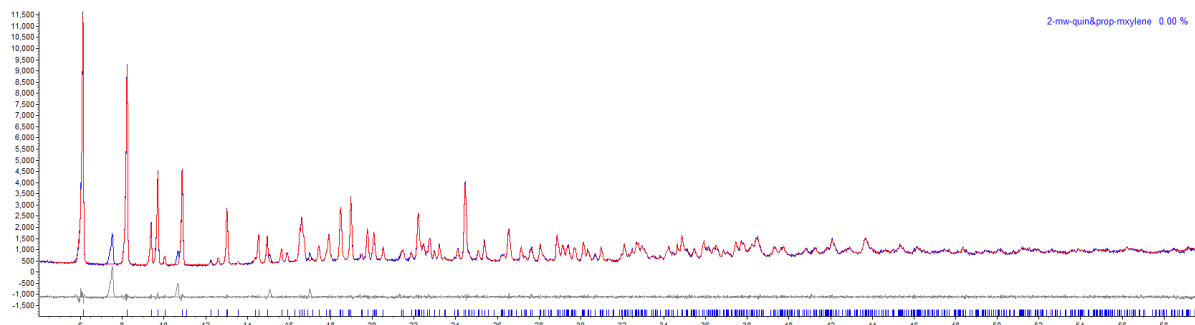


Figure 3.9 Observed (blue) and calculated (red) profiles and the difference plot [$I_{\text{obs}} - I_{\text{calc}}$] (grey) of the Pawley refinement (2θ range 4-60°, $d_{\text{min}} = 1.54 \text{ \AA}$).

[Ag₄(O₂CCF₂CF₃)₄(2-Me-quin)₄]·2p-xyI (16)

The sample was scanned in flat plate mode at a rate of 1.5 sec step⁻¹, with each detector step size being 0.02°. The unit cell of the **16** from SCXRD data was used as the starting point for the Pawley refinement, employing 954 parameters (12 background, 1 zero error, 5 profile, 14 cell, 932 reflections), resulting in final indices of fit $R_{wp} = 0.2245$, $R_{wp}' = 0.3311$. [$a = 10.339(6)$ Å, $b = 11.797(7)$ Å, $c = 15.52(1)$ Å, $\alpha = 93.37(6)^\circ$, $\beta = 91.53(4)^\circ$, $\gamma = 110.56(6)^\circ$, $V = 1769.7(21)$ Å³].

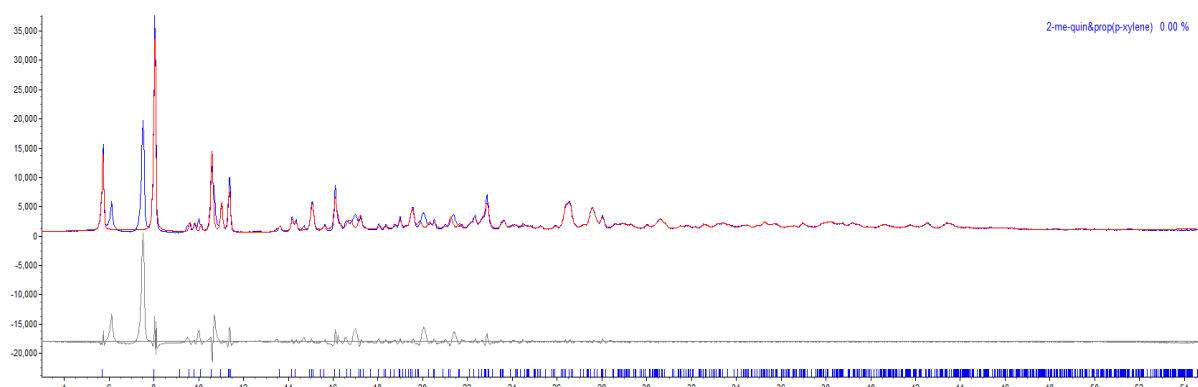
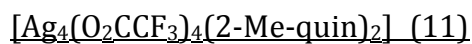


Figure 3.10 Observed (blue) and calculated (red) profiles and the difference plot [$I_{obs} - I_{calc}$] (grey) of the Pawley refinement (2θ range 4-55°, $d_{min} = 1.67$ Å).

3.2.4 Thermogravimetric analyses (TGA)

Thermogravimetric analyses were recorded on a Perkin-Elmer Pyris1 TGA model thermogravimetric analyser. Samples were heated under a flow of dry N₂ gas. Similar to PXRD, none of the solvent-containing coordination polymers were tested as TGA data would be inaccurate due to the rapid solvent loss.



Temperature sweep TGA: Sample was held at 25 °C for 5 mins and then heated to 550 °C at a rate at 2.5 °C/min, followed by holding the temperature at 550 °C for another 5 mins.

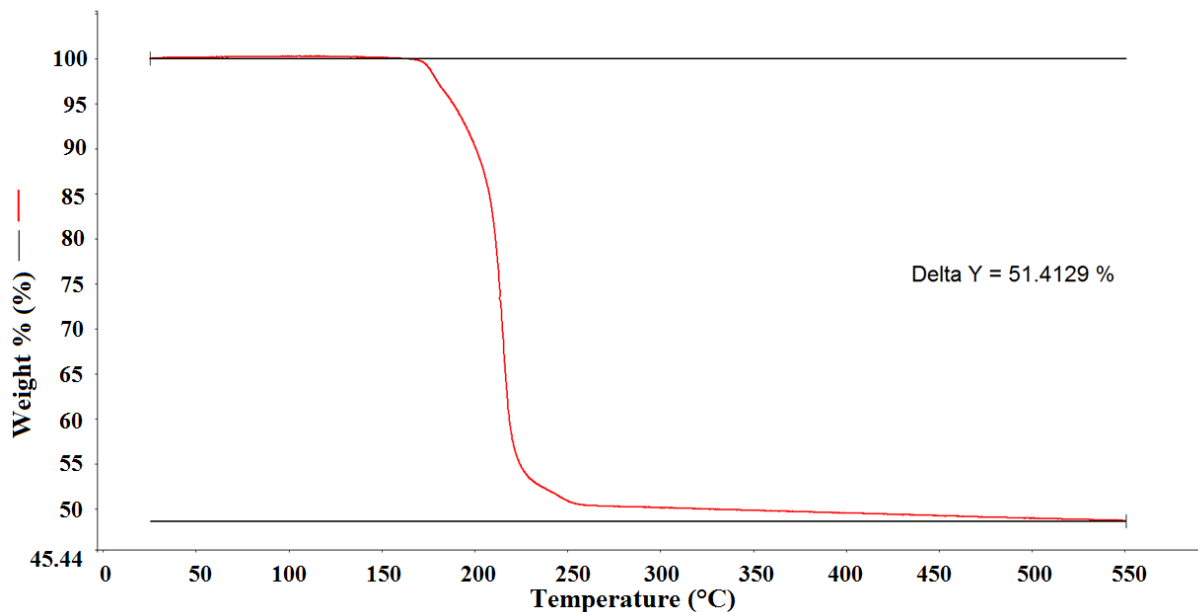
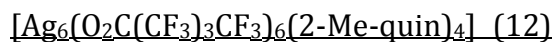


Figure 3.11 TGA for [Ag₄(O₂CCF₃)₄(2-Me-quin)₂] (11) at a scan rate of 2.5 °C/min.



Temperature sweep TGA: Sample was held at 25 °C for 5 mins and then heated to 600 °C at a rate at 5 °C/min, followed by holding the temperature at 600 °C for another 5 mins.

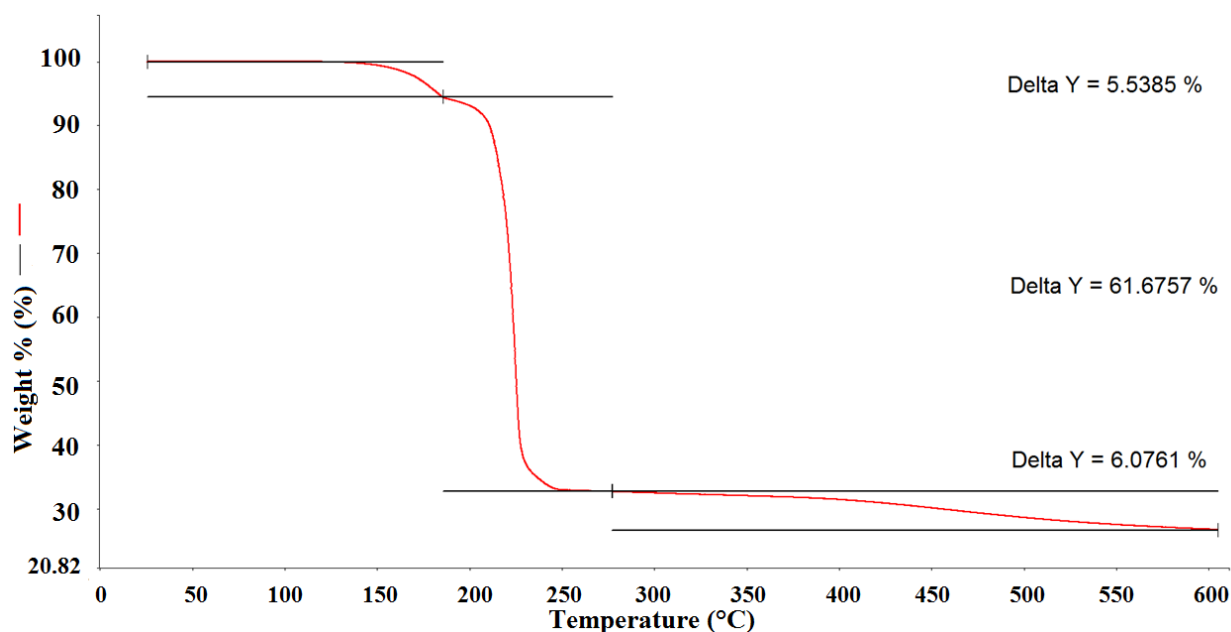


Figure 3.12 TGA for [Ag₆(O₂C(CF₂)₃CF₃)₆(2-Me-quin)₄] (12) at a scan rate of 5 °C/min.

Isothermal TGA: Sample was heated to 150 °C with a heating rate of 10 °C/min and then held at this temperature for 180 mins.

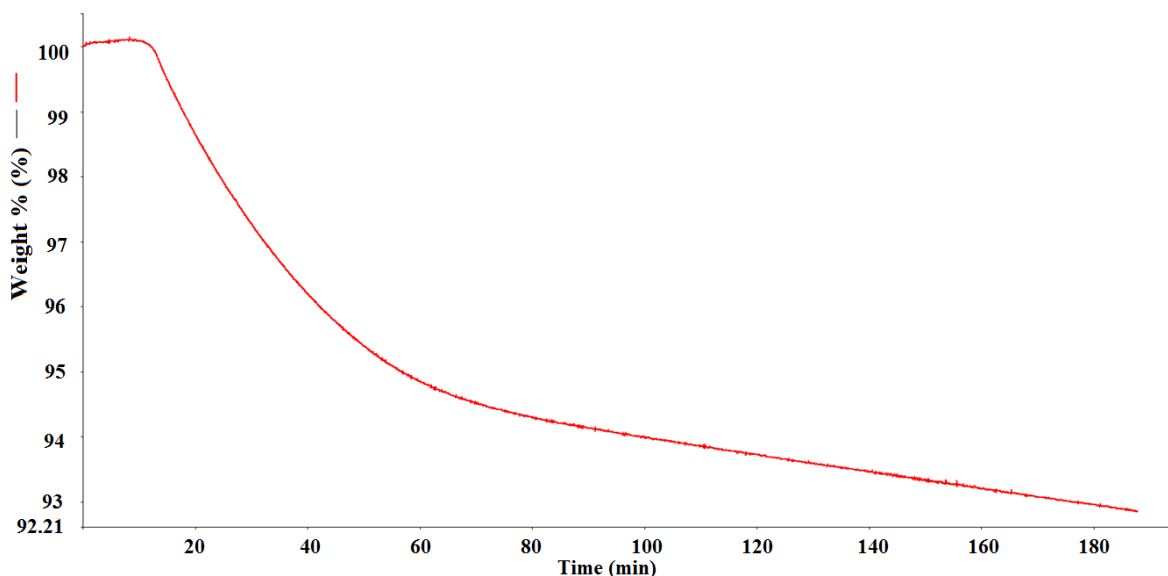
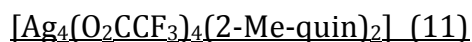


Figure 3.13 TGA for $[\text{Ag}_6(\text{O}_2\text{C}(\text{CF}_2)_3\text{CF}_3)_6(2\text{-Me-quin})_4]$ at a constant temperature of 150 °C

3.3 Results and Discussion

3.3.1 Structure determination

The silver perfluoroalkylcarboxylate coordination polymers with other diimine ligands that have been studied so far seem to share similar structures which only have slight and regular differences due to the increasing of chain lengths. In contrast, the coordination polymers formed with 2-methylquinoxaline as the diimine show abundant new structures, including some not previously observed component ratios such as 6:6:4 for Ag:carboxylate:diimine. Similar to Chapter 2, in order to present the structures clearly in the figures, different components of each structure are coloured in a uniform manner: silver in magenta, oxygen in red, perfluoroalkyl chains in green, 2-Me-quin in blue and solvents in black (or gray if second position or type required). The interplanar distances involving the arene molecules are calculated based on the following method: set one arene molecule as the reference plane and calculate the average perpendicular distance of all the atoms on the second arene to this plane. This allows an estimation of the interplanar separation even if the two arene planes are not precisely parallel to each other.



Compound **11** is crystallized in the monoclinic space group *C2/c* and its asymmetric unit contains half of discrete [Ag₄(O₂CCF₃)₄(2-Me-quin)₂] unit (**Figure 3.14.a**). Each Ag centre is four-coordinated with one N-atom from 2-Me-quin ligand and three O-atoms from two trifluoroacetates. One O-atom from one trifluoroacetate connect two Ag centres to yield a [Ag₂(O₂CCF₃)] unit. This unit is then further linked to its neighbouring equivalents, yielding a 1D backbone chain extending along the *c* axis. Such a chain is connected to its equivalent ones by a double 2-Me-quin bridge to form a 2D herringbone structure propagated along the *bc*-plane (**Figure 3.14.c**). π - π stacking interactions and short Ag-Ag interactions are found in this structure. The 2-Me-quin ligands inbetween chains are face-to-face aligned in an antiparallel manner with a separation of 3.282 Å on average (no disorder for methyl groups). The contact for Ag2'-Ag2'' is 2.938(1) Å. Neighbouring 2D layers are stacked at intervals of 9.998 Å.

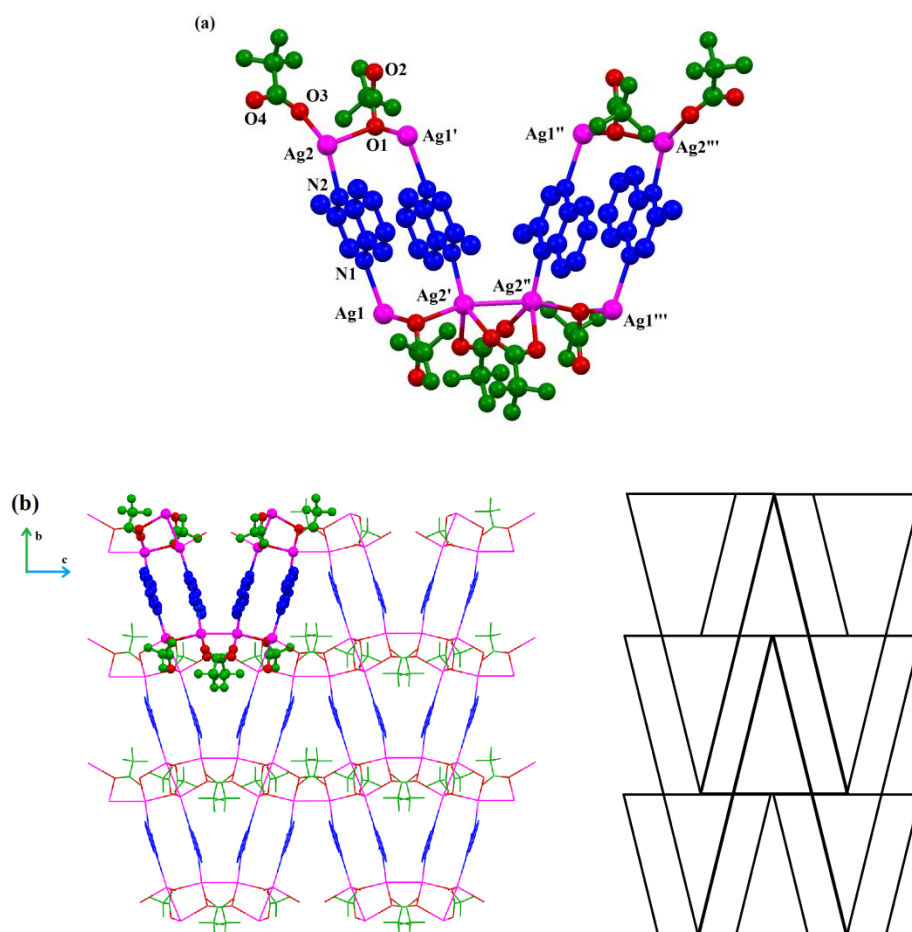


Figure 3.15 Crystal structure of **11** showing (a) single V-shaped arrangement and (b) layer structure along *bc*-plane.

Comparing with other silver/diimine coordination polymers we studied before, compound **11** shows some unique characteristics. Different from other 4:4:2 phases reported before, in this material, rather than having all the diimine ligands lying in parallel, two pairs of double bridges form a V-shaped arrangement and stack relative to each other.

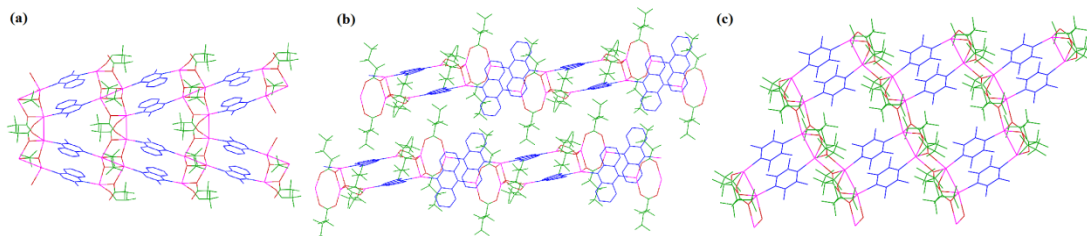


Figure 3.16 Comparison of layer structures of 4:4:2: x (x = number of solvent molecule) ratio coordination polymers: (a) compound **11**, (b) $[\text{Ag}_4(\text{O}_2\text{C}(\text{CF}_2)_2\text{CF}_3)_4(\text{phen})_2]^{13}$ and (c) $[\text{Ag}_4(\text{O}_2\text{C}(\text{CF}_2)_2\text{CF}_3)(\text{TMP})_2]^{14}$.

All other diimine coordination polymers we studied before tended to orient all the fluorinated chains between the layers and interdigitating almost parallel to each other. However, in this case, only half of the chains are interdigitated in this way while the other half are oriented at a 45° angle to the layers (**Figure 3.17a**), which is likely due to the rotation for every four fluorinated chains. Every four pairs of fluorinated chains turn 90° in space along c -axis, forming a periodic alternative silver-trifluoroacetate helix like a trigonometric map (**Figure 3.17.b**).

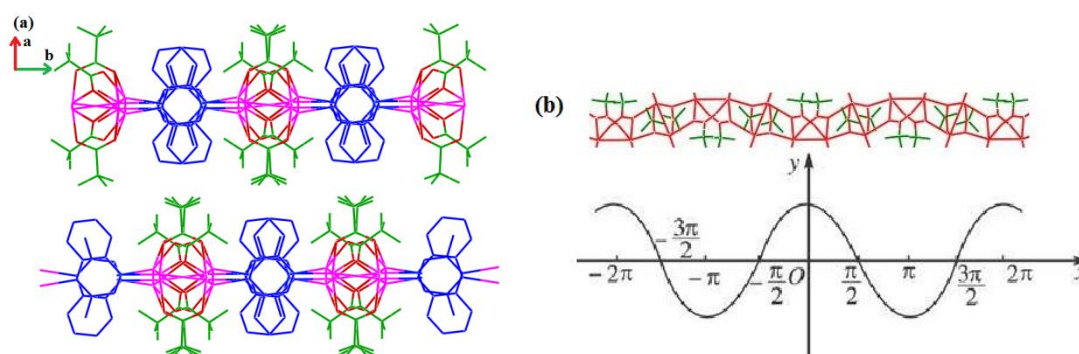
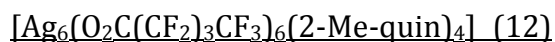


Figure 3.17 Crystal structures of **11** showing (a) interdigitation of fluorinated chains and (b) the helix along the c -axis.



Compound **12** crystallizes in the triclinic space group $P-1$ and its asymmetric unit holds half of $[\text{Ag}_6(\text{O}_2\text{C}(\text{CF}_2)_3\text{CF}_3)_6(2\text{-Me-quin})_4]$ unit. Two types of coordination geometries are found for silver in this compound. Ag1 is four-coordinate with two N-atoms from 2-Me-quin ligands and two O-atoms from two nonafluoropentanoate ligands, whereas Ag2 and Ag3 are only coordinated with one N-atom and two O-atoms, forming a Y-shaped geometry (Ag2) or T-shaped geometry (Ag3). These coordination geometries are much the same as that observed in the $[\text{Ag}_4(\text{O}_2\text{C}(\text{CF}_2)_n\text{CF}_3)_4(\text{quin})_3]$ coordination polymers (Chapter 2) as they all contain singly-bridging ligands. Ag1 and Ag2 are coordinated in the same doubly-bridging mode with their equivalents (**Figure 3.18.a**). Nevertheless, the singly-bridging 2-Me-quin ligand connects Ag1 and Ag3. Thus an extended $[(2\text{-Me-quin})\text{Ag}_2(\text{O}_2\text{C}(\text{CF}_2)_3\text{CF}_3)_2(2\text{-Me-quin})]$ unit is formed by two single-ligand bridges connected via a central $\text{Ag}_2(\text{O}_2\text{CR})_2$ moiety (**Figure 3.18.b**), which is uncommon from what we have studied so far. This extended unit is nearly flat and links between two $[\text{Ag}_4(\text{O}_2\text{C}(\text{CF}_2)_n\text{CF}_3)_4(2\text{-Me-quin})_3]$ unit and this building unit then extends to form a 1D zigzag tape (**Figure 3.18.c**).

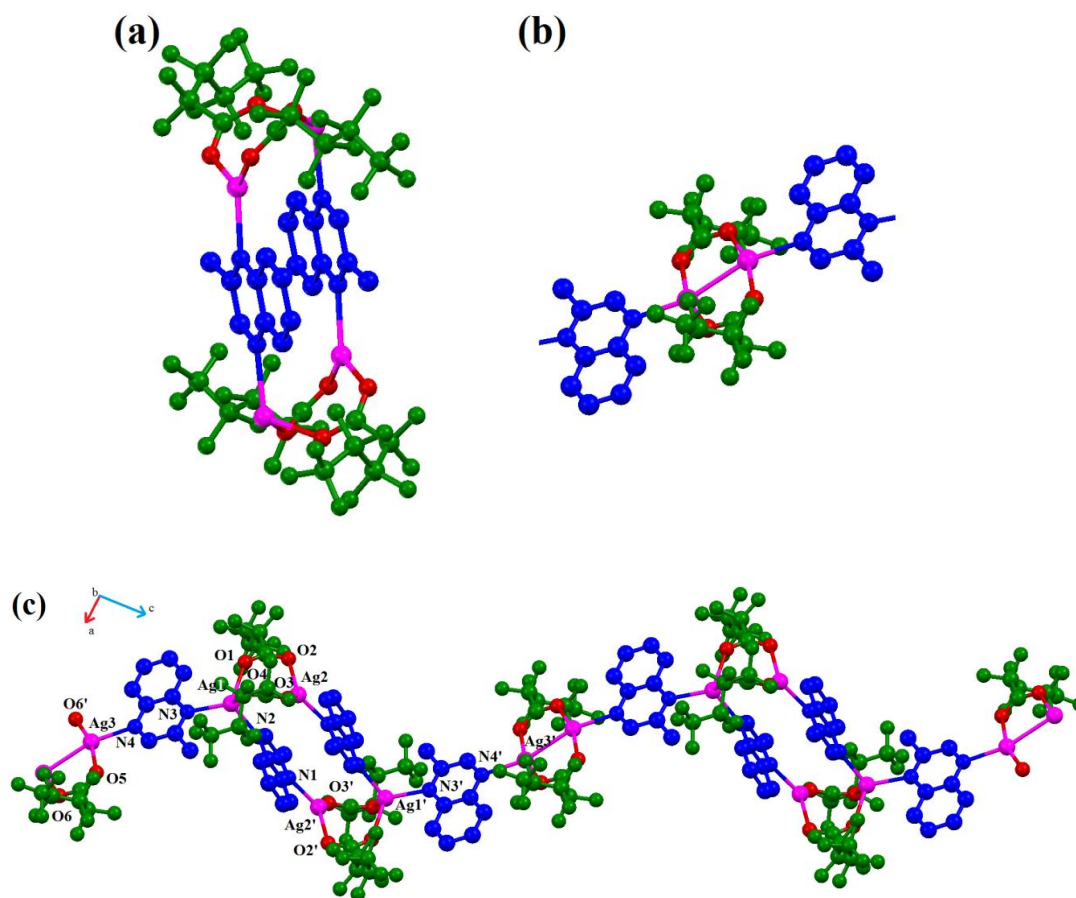


Figure 3.18 Structure of the silver perfluorocarboxylate pairs involved in the (a) doubly-bridging environment, (b) the unique single-pair environment and (c) the 1D zigzag tape structure in compound **12**.

Tapes are then stacked together to afford a layer structure (**Figure 3.19.a**) and neighbouring layers are further stacked with a separation of 13.414 Å (**Figure 3.19.b**). In addition, one short Ag \cdots Ag separation between Ag3 and Ag3' (2.902(1) Å) is observed in this structure.

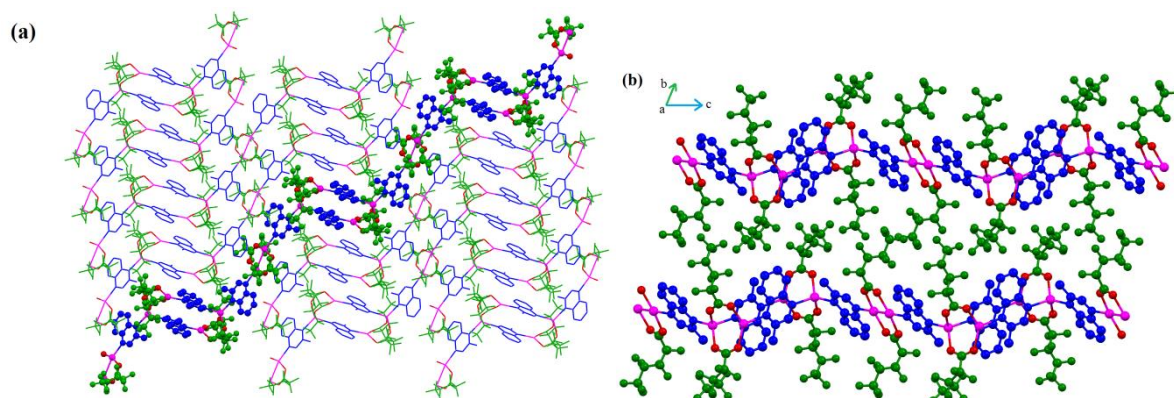


Figure 3.19 Crystal structures of **12** showing (a) stacking of the 1D tapes to form layers and (b) the interdigitation of the perfluoroalkylchains in between layers.

3.3.3 Structures of compounds 13-21, containing trapped arene solvents

Compounds **13-21** were synthesised in solutions containing arene solvents (toluene or xylene) and form structures which contained trapped arene solvent guests. Crystal structures could be determined by single-crystal X-ray diffraction, although in many cases diffraction was quite weak and led to limitations in the structural models, in particular for compounds **19** and **20**. Powder diffraction studies showed that the materials were not phase pure, although in many cases the single crystal structure represented the major product. Discussion of the structures will be focused mainly on their differences resulting from the possible effects of the different solvents.

[Ag₄(O₂CCF₂CF₃)₄(2-Me-quin)₃].1.5(tol) (13)

Compound **13** crystallizes in the triclinic space group *P*-1 and its asymmetric unit has one [Ag₄(O₂CCF₂CF₃)₄(2-Me-quin)₃].1.5(tol) unit (**Figure 3.20.a**). These units are further connected together (between neighbouring N6 and Ag2 atoms) to form a 1D-tape along *c*-axis. This type of 1D-tape structure is similar to those of the 4:4:3 stoichiometry phenazine-containing coordination polymers ([Ag₄(O₂CCF₂CF₃)₄(phen)₃] phen arene) which was introduced in section 3.1 (**Figure 3.4**). However, rather than having all the 1D tapes separate, each pair of neighbouring 1D tapes forms a 1D-dimer-tape in compound **13**. As a result, a distorted hexagonal cavity is formed in every two {Ag₄(O₂CCF₂CF₃)₄(2-Me-quin)₃} units, bounded by two singly-bridging 2-Me-quin ligands, two 2-Me-quin ligands that are part of doubly-bridging {Ag₄(O₂CCF₂CF₃)₄(2-Me-quin)₂} units and two {Ag₂(O₂CCF₂CF₃)₄} moieties that are part of {Ag₄(O₂CCF₂CF₃)₄(2-Me-quin)₂} units. Two toluene molecules can be clearly modelled in the cavity, stacked between the singly-bridging 2-Me-quin ligands, which is one molecule for each asymmetric unit (distance between toluene and singly-bridging 2-Me-quin is 3.43 Å on average). The dimer tapes extend along the *c*-axis and stack along the *b*-axis into a layer structure (**Figure 3.20.b**, referred as Type I). Similar to the [Ag₄(O₂CCF₂CF₃)₄(phen)₃] phen arene structures, one toluene solvent molecule (0.5 tol per asymmetric unit) can also be modelled between the neighbouring 1D dimer-tapes and is stacked between two singly-bridging 2-Me-quin ligands. Neighbouring layers are stacked at intervals of 12.82 Å. No argentophilic interaction is suggested in this structure.

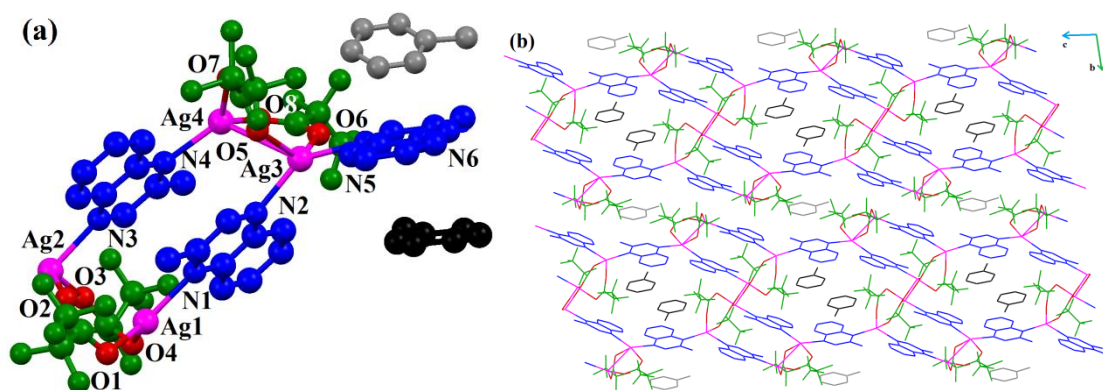
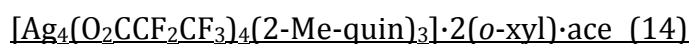


Figure 3.20 Crystal structures of **13** showing (a) the 4:4:3 stoichiometry structure unit and location of the two independent encapsulated toluene molecules and (b) layers consisting of the double tapes showing toluene solvent locations within and between the 1D tapes.



Compound **14** consists of $[\text{Ag}_4(\text{O}_2\text{CCF}_2\text{CF}_3)_4(2\text{-Me-quin})_3]$ repeating unit (**Figure 3.21.a**), which is similar to that of compound **13**. It consists of the same 1D zigzag tapes of $\text{Ag}_2(\text{O}_2\text{CCF}_2\text{CF}_3)_2$ moieties bridged by singly and doubly-bridged 2-Me-quin ligands in alternation as in compound **13**. These tapes are linked in pairs through bridging Ag–O bonds in **13**, but in **14** the tapes are linked through additional bridging Ag–O bonds to form 2D layers (**Figure 3.21.b**, referred as Type II). There are distorted hexagonal cavities, which contain two *o*-xylene molecules that have π - π stacking (3.383 Å interplanar separation on average) with the single-bridging 2-Me-quin ligands around each cavity. Also, the single-bridging 2-Me-quin is disordered in a two-site mode which resembled as a phenazine in pictures. Because of the formation of 2D layers, there is no second cavity for arene guests as found in compound **13**. Interestingly, acetone solvent molecules can be clearly modelled (two-site disorder in **Figure 3.21.c**) on each corner of the unit cell which places them in the gaps between fluorinated chains between the layers (**Figure 3.21.d**). These layers are stacked with a repeat distance of 10.74 Å and again there is no obvious evidence of strong argentophilic interactions.

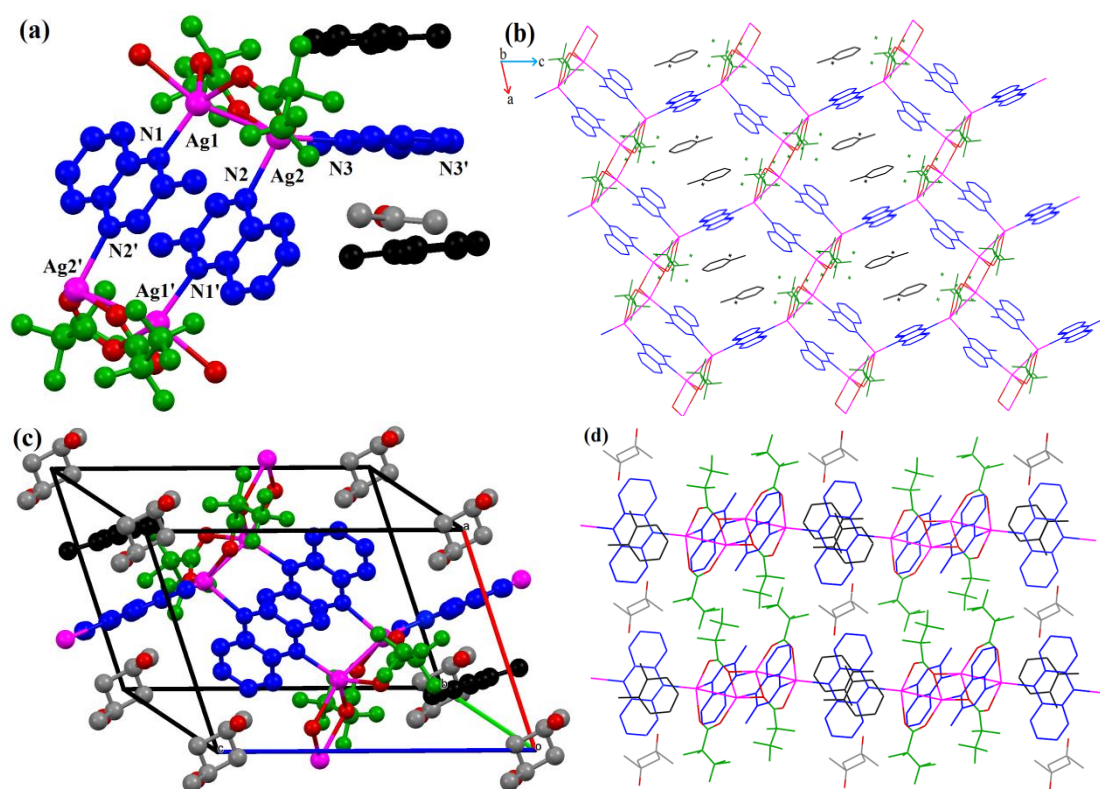


Figure 3.21 Crystal structures of **14** showing (a) the 4:4:3 structure unit and associated solvent guests, (b) one 2D layer with *o*-xylene guests in distorted hexagonal cavities, (c) the acetone solvent molecules at the special positions (disordered about inversion centres) shown for a unit cell and (d) location of acetone guests between the layers.



Compound **15** has a 4:4:3 stoichiometry structure, with a very similar Type II layer structure to that of compound **14** (**Figure 3.22.a**) and a slightly smaller layer-stacking distance of 10.66 Å. Nevertheless, there is a significant difference between two compounds in the way they hold the solvent molecules. For the xylene molecules within the cavity, rather than having π - π stacking along the direction where singly-bridging 2-Me-quin ligands are located (as in compound **14**), the *m*-xylene molecules stack with the doubly-bridging 2-Me-quin ligands (3.358 Å for xylene-quin distance), which is different from all other compounds in this series (**Figure 3.22.b**). There are no extra solvent molecules located at each corner of the unit cell or between layers in **15**.

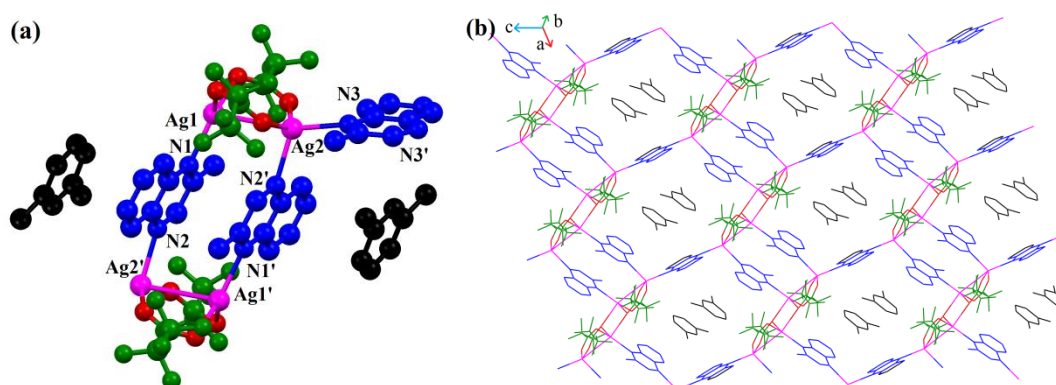


Figure 3.22 Crystal structures of **15** showing (a) the 4:4:3 structure unit with *m*-xylene guest and (b) one 2D layer shown with *m*-xylene guests in distorted hexagonal cavities.



Compound **16** has a unique structure among all of the silver-perfluorocarboxylate-diimine coordination polymers studied so far. It crystallizes in the triclinic space group $P-1$ and the asymmetric unit consists of half of the $[\text{Ag}_4(\text{O}_2\text{CCF}_2\text{CF}_3)_4(2\text{-Me-quin})_4]$ unit and one p -xylene guest (**Figure 3.23.a**). This unit is then extended along the a -axis, forming a 1D tape in which $\text{Ag}_4(\text{O}_2\text{CCF}_2\text{CF}_3)_4(2\text{-Me-quin})_2$ moieties are linked via bridging Ag–O bonds. Unlike all other coordination polymers in this family, in which all diimine ligands are ditopic, only half of the 2-Me-quin ligands in **16** are ditopic while the others bind to only one Ag centre (one N-atom out of two in these ligands is uncoordinated). These monodentate-coordinated 2-Me-quin ligands are π - π stacked along the a -axis with two 2-Me-quin molecules from neighbouring tapes and one p -xylene molecule (**Figure 3.23.b**). The distance between two 2-Me-quin ligands is 3.320 Å while the separation between p -xylene and each of two nearby ligands is 3.375 Å on average. With these π - π stacking interactions, the 1D tapes form a layer in the ac -plane and the layers are further stacked with a repeat distance of 10.85 Å. Similar to compound **14**, extra p -xylene solvent molecules can be modelled on each corner of the unit cell (**Figure 3.23.c**) in **16** and these p -xylenes are entrapped in the gaps between every two pairs of fluorinated chains interdigitated between the layers (**Figure 3.23.d**).

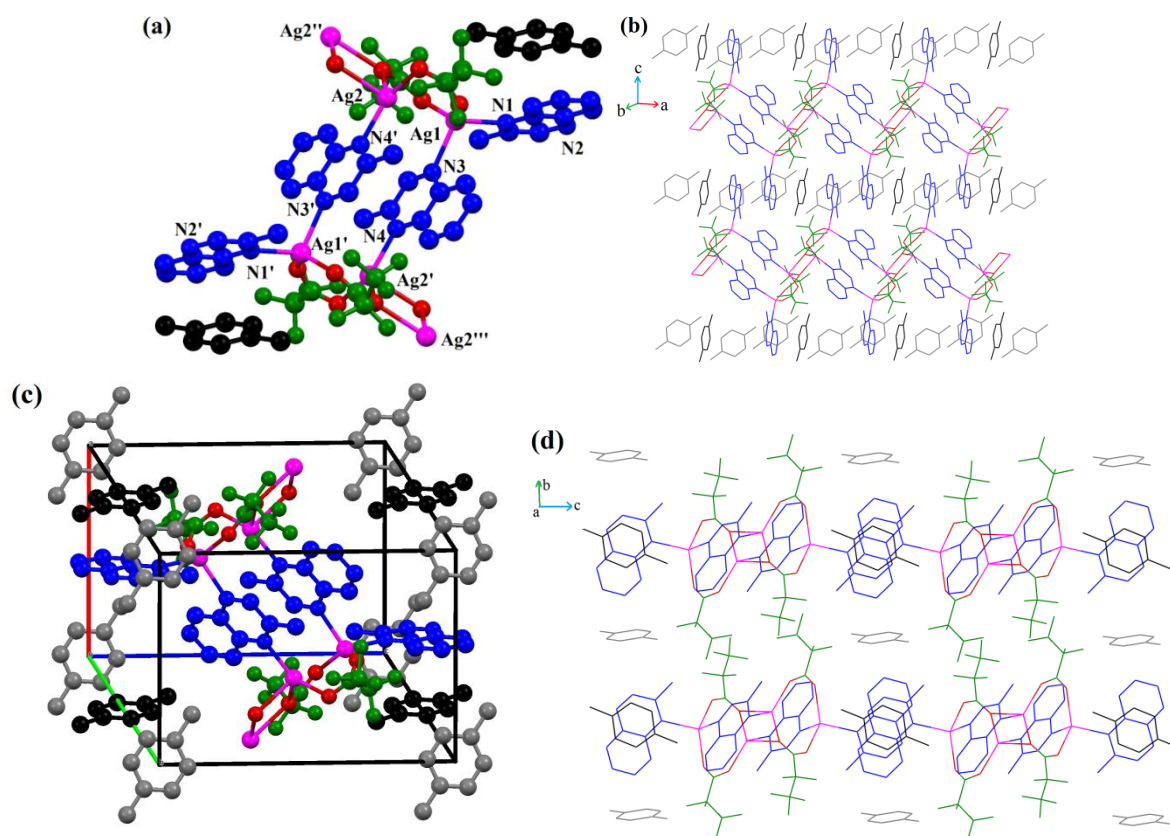


Figure 3.23 Crystal structures of **16** showing (a) the 4:4:4 structure unit and π -stacked p -xylene molecules, (b) layers in the ac plane of the 1D tapes with p -xylene guests, (c) the p -xylene molecules

in the special positions (inversion centres) viewed in one unit cell and **(d)** location of *p*-xylene guests between the layers.

$[\text{Ag}_4(\text{O}_2\text{C}(\text{CF}_2)_2\text{CF}_3)_4(2\text{-Me-quin})_3] \cdot 1.5(\text{tol})$ (17) and $[\text{Ag}_4(\text{O}_2\text{C}(\text{CF}_2)_2\text{CF}_3)_4(2\text{-Me-quin})_3] \cdot 2.5(o\text{-xyl})$ (18)

Again being formed as a 4:4:3 phase, the basic structure of compound **17** is a Type II layer (**Figure 3.24.a and c**) analogous to compound **14**. The arene guest molecules (in black, occupancy 0.5 in **17** and 1.0 in **18** for each) occupy the distorted hexagonal cavities and are π - π stacked with the singly-bridging 2-Me-quin ligands. Compound **18** has an analogous structure to compound **17** but with *o*-xylene guests rather than toluene (**Figure 3.24.b and d**). However, compound **17** holds two extra toluene guests molecules (in grey, occupancy 0.25 each) rather than acetone (in **14**) and similar as for **18** with two *o*-xylene guests in similar positions.

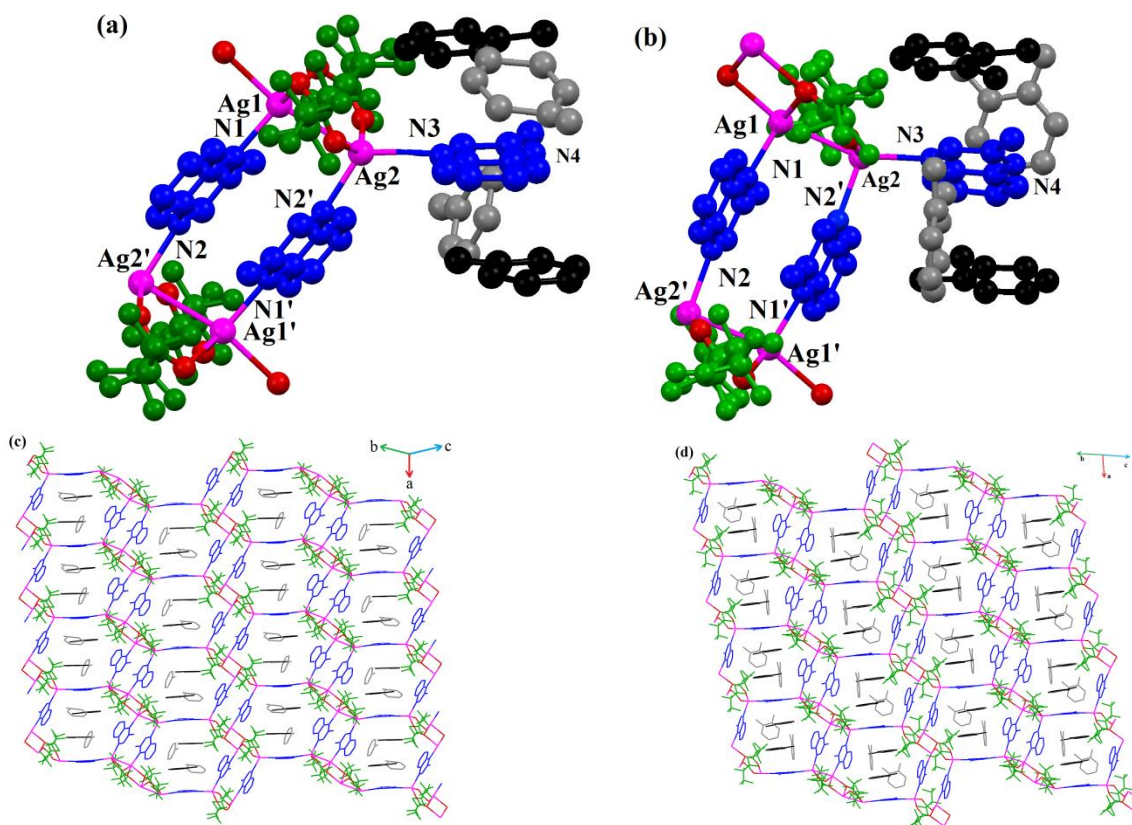


Figure 3.24 Crystal structure of **17** (left side) and **18** (right side) showing **(a-b)** the 4:4:3 structure unit with arene guests and a single layer showing arene guests in the distorted hexagonal channels **(c-d)**.

These extra solvent molecules lie between the perfluoroalkyl groups in the interlayer region (**Figure 3.25.a and b**). Surprisingly these arene molecules have two different orientations in space: either more perpendicular or more parallel to the plane of the layer, which is different from compound **14**. The reason is that in **14**, the 2D layers are relatively flat which leads to a regular interdigitation of fluorinated chains. Thus the sizes of the cavities between chains are the same which means no differences to all the acetone molecules inside (see **Figure 3.21d**). But in **17** and **18**, the layers are slightly wavy if observed along *a*-axis which results in forming cavities with two different sizes. The solvent molecules in larger chambers are more perpendicular to the layers. Those in smaller chambers are compressed into a more parallel orientation to the layers (**Figure 3.25**).

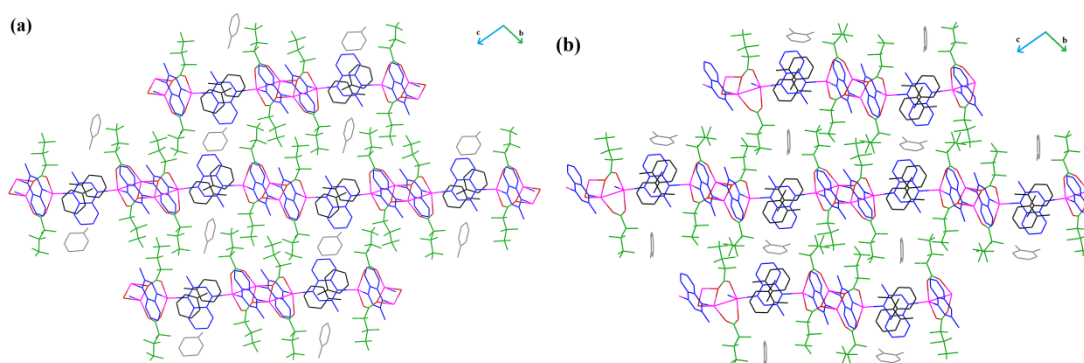


Figure 3.25 Crystal structure of **17** (left side) and **18** (right side) showing (a-b) two layers showing the different orientations of arene guest molecules between layers.

[Ag₄(O₂C(CF₂)₂CF₃)₄(2-Me-quin)₃]_n·0.5(*p*-xyl) (**19**)

The overall structure of **19** contains 1D zigzag tapes similar to those in the quinoxaline-containing 4:4:3 stoichiometry coordination polymers described in Chapter 2 (and those previously reported for diamine ligands phenazine⁵ and TMP¹⁴) that expand from a typical 4:4:3 basic unit, [Ag₄(O₂C(CF₂)₂CF₃)₄(2-Me-quin)₃] (**Figure 3.26.a**). The difference between **19** and previous structures with different diimines is that in **19** the 1D tapes stack in a parallel manner into layers leaving a solvent-accessible space between singly-bridging 2-Me-Quin ligands (**Figure 3.25.b**) rather than forming 2D layers by stacking in an antiparallel manner, which leaves no accessible space (e.g. **Figure 2.52**). In this cavity, two *o*-xylene molecules can be modelled (symmetry generated from one molecule and each of them has an occupancy of 0.25).

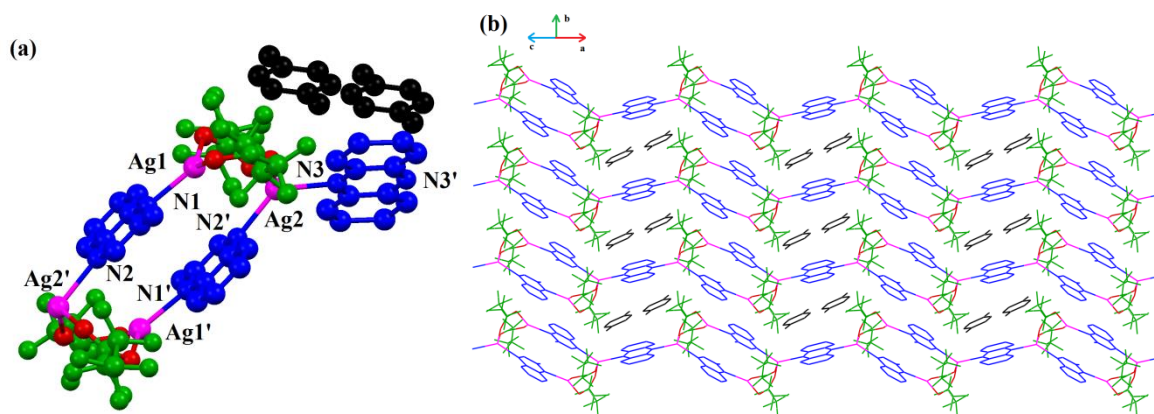


Figure 3.26 Crystal structures of **19** showing (a) the 4:4:3 structure unit and (b) stacking of the 1D tapes.



Because of the poor resolution of the diffraction data, the single-crystal structure of compound **20** was unable to be fully solved. Specifically, the perfluoroalkyl chains of the carboxylate ligands could not be modelled with reasonable positions. Only a backbone structure can be approximately modelled. This suggests the existence of a novel 4:4:5 ratio of the components (**Figure 3.27.a**). Unlike all the other diimine-containing coordination polymers, this structure is the first one which does not contain the $\{Ag_4(O_2CR)_4(\text{diimine})_2\}$ repeating unit with doubly-bridging ligand pairs. Three out of five 2-Me-quin ligands are singly-bridging between the silver centres. The other two 2-Me-quin ligands bind at Ag(I) in a monodentate mode, as observed for compound **15** (prepared in *p*-xylene as well). This 4:4:5 structure unit forms a 1D tape that extends along the *c*-axis (**Figure 3.27.b**) and does not form layers (**Figure 3.27.c**), but instead tapes are packed in a herringbone manner in the *ab* plane. Arene solvent guest molecules may be present in the structure but could not be successfully modelled.

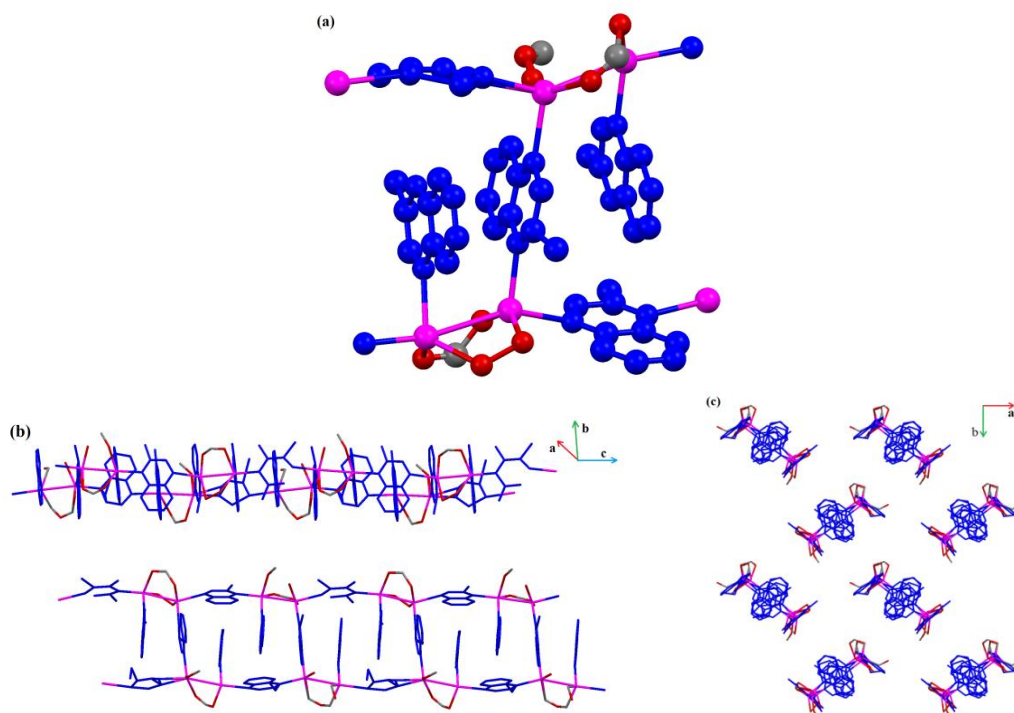


Figure 3.27 Crystal structure of **20** showing (a) the 4:4:5 structure unit, (b) 1D tape structures and (c) the stacking of 1D tapes. Perfluoralkyl chains on the carboxylate ligands could not be modelled crystallographically.



Compound **21** has a Type I layer structure similar to that of **13**, constructed from stacked 1D zigzag tapes. *m*-Xylene solvent molecules are located in the distorted hexagonal cavities within layers and between layers, similar to toluene molecules in **13** (Figure 3.28.a-b).

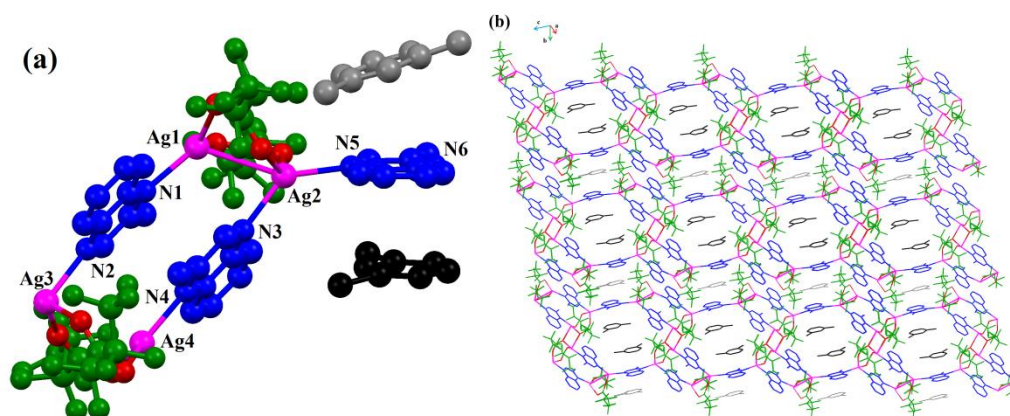


Figure 3.28 Crystal structures of **21** showing (a) the 4:4:3 structure unit with *m*-xylene guests and (b) layers consisting of the double tapes showing *m*-xylene solvent locations within and between the 1D tapes.

In summary, crystal structures for silver-perfluoroalkylcarboxylate-diimine coordination polymers containing 2-Me-quin ligands are far more varied than those of analogous coordination polymers with other diimine ligands. This is especially true for those formed with different arene guests. Although these structures are new but some building blocks in of these structures can be traced back to the previous series of coordination polymers, in particular the common inclusion of the $\{Ag_4(O_2CR)_4(diimine)_2\}$ unit.

For compounds **13-21**, which were synthesised in the presence of arene solvents, the effect of the solvent is most often to direct the structure by inclusion of the arene molecules as guests in their structural frameworks. The reason for their common inclusion appears to be the favoured π - π stacking interactions with the 2-Me-Quin ligands to form a most stabilized structure.

Based on observations using optical microscopy, most of these arene-guest-containing crystals cracked within 5-20 minutes at room temperature even under oil. Unlike the quinoxaline-containing coordination polymers and other 2-Me-quin coordination polymers (i.e. those without arene guests), these compounds (**13-21**) can re-dissolve in pure acetone, thus the pure arene solvents are used when washing is required. These results imply that these crystals are not very stable in the solid state and even in mother liquor as the solvent molecules can escape very quickly.

3.3.2 PXRD data collections

For compound **11** and **12**, their phase purity is confirmed with Pawley fitting of the observed PXRD patterns (**Figure 3.5** and **3.6**), with only slight changes to the unit cell parameters due to the difference of temperature. But for the solvent molecule-containing coordination polymers, none of them were shown to be phase pure. Because the solvent molecules leave the parent crystals very quick, some of the crystals might be able to change their original phases after losing their solvent molecules. Attempts using wet PXRD technique that could minimize the solvent molecule loss provided better quality data. For compound **13-15**, the Pawley fittings suggest that these samples are all very close to a single phase, with only slight amount of other phases. But for compound **16**, more extra peaks are shown from the experimental patterns so attempts are given into finding other phases.



The powder pattern for compound **16** shows small differences compared to the calculated pattern from SCXRD. Two large extra peaks (in the 2θ range 6-8 °) and a few other peaks are observed in the experimental pattern. Attempts to index the whole pattern did not yield reasonable unit cells for a single phase.

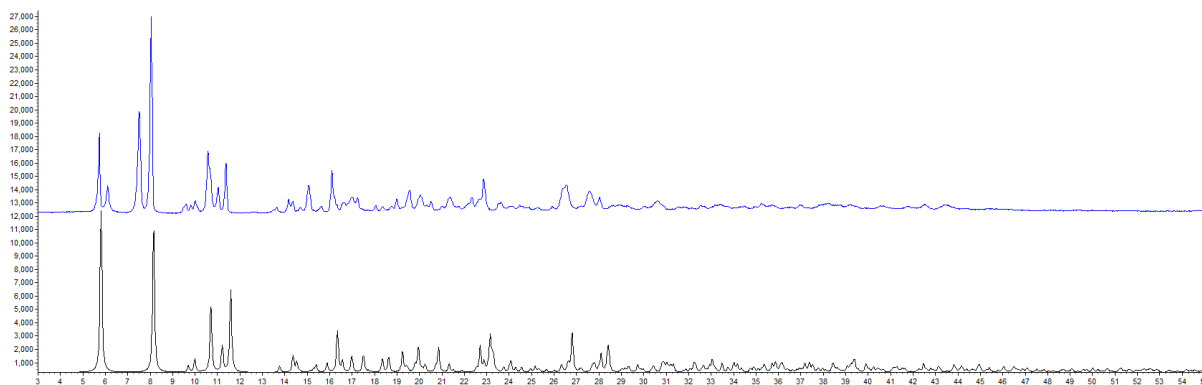


Figure 3.29 Observed (blue) and calculated (black) patterns compared in 2θ range 3-55 °, $d_{\min} = 1.67 \text{ \AA}$.

Attempts to index the extra peaks suggested several smaller unit cells (nearly half of the original unit cell volume) and the Pawley fitting for both two phases at the same time provided a reasonably good overall fit. The unit cell of compound **16** from SCXRD data and a new indexed unit cell ($[a = 5.4874 \text{ \AA}, b = 15.1032 \text{ \AA}, c = 11.7845 \text{ \AA}, \alpha = 91.681^\circ, \beta = 86.767^\circ, \gamma = 73.108^\circ, V = 931.976 \text{ \AA}^3]$) were used as the starting point for the Pawley refinement, employing 1243 parameters (12 background, 1 zero error, 9 profile, 14 cell, 1207 reflections), resulting in final indices of fit $R_{wp} = 0.09081$, $R_{wp}' = 0.11945$. [[**16**]: $a = 10.345(3) \text{ \AA}, b = 11.802(5) \text{ \AA}, c = 15.533(8) \text{ \AA}, \alpha = 92.37(4)^\circ, \beta = 91.53(2)^\circ, \gamma = 110.58(3)^\circ, V = 1772.3(14) \text{ \AA}^3$]; [**Unknown C**]: $[a = 5.493(4) \text{ \AA}, b = 15.30(1) \text{ \AA}, c = 11.928(6) \text{ \AA}, \alpha = 92.88(8)^\circ, \beta = 85.71(15)^\circ, \gamma = 73.15(16)^\circ, V = 954.2(16) \text{ \AA}^3]$.

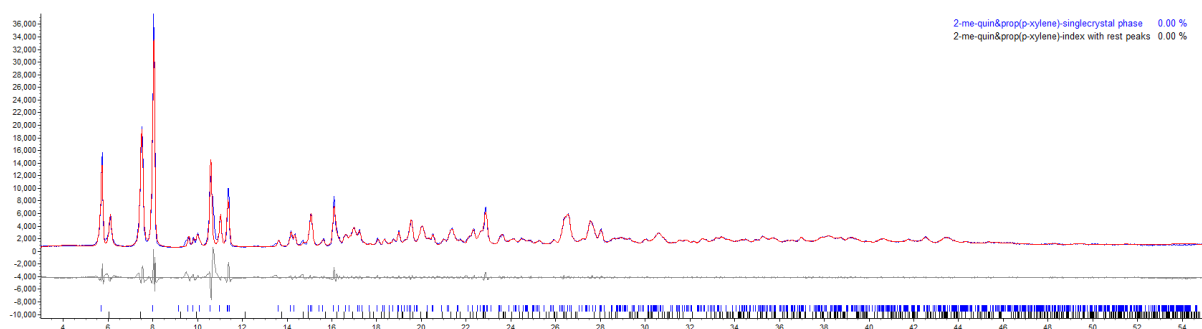


Figure 3.30 Observed (blue) and calculated (red) profiles and the difference plot $[I_{\text{obs}} - I_{\text{calc}}]$ (grey) of the Pawley refinement (2θ range 4-55 °, $d_{\min} = 1.67 \text{ \AA}$).

This indicates that this sample is a mixture of compound **16** and another phase, which could be the desolvated version of compound **16**. By comparing the two unit cells, they indicate that the unknown phase might be transformed from compound **16** by reduction of the *a*-axis by approximately half followed by other transformations. From the single crystal data, the *a*-axis is the direction of the π - π stacking interactions of the monodentate-coordinated 2-Me-quin ligands and the *p*-xylene molecules. Loss of all these *p*-xylene solvent molecules (**Figures 3.31.a**) and joining of the monodentate-coordinated 2-Me-quin ligands with the silver atoms of the adjacent tape (**Figures 3.31.b**), would convert the structure into a 2D-layer 4:4:4 structure. This imaginary structure is different to the known 4:4:4 structures formed from Quin ligands (Chapter 2.3.1.1) as it is not that compressed packing in the layer structure.

Table 3.3 Unit cell parameters for compound **16** and Unknown C

	16	Unknown C
<i>a</i> (Å)	10.339(3)	5.491(4)
<i>b</i> (Å)	11.797(4)	15.29(1)
<i>c</i> (Å)	15.524(7)	11.922(5)
α (°)	93.37(4)	92.85(8)
β (°)	91.53(2)	85.76(13)
γ (°)	110.56(3)	73.14(14)
<i>V</i> (Å ³)	1769.7(12)	952.8(13)

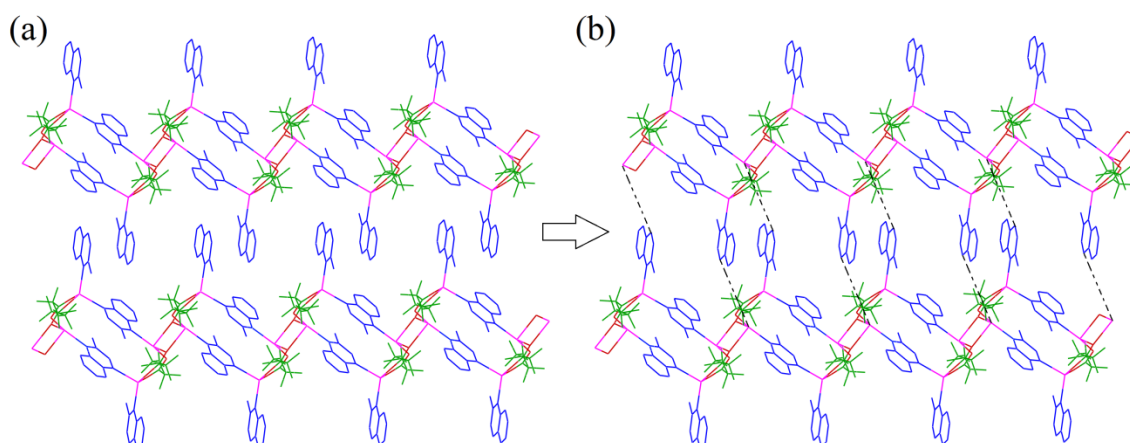
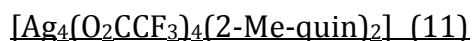


Figure 3.31 Proposed transformation of **16** into **Unknown phase C**: (a) solvent removing step and (b) coordination bonds formation between monodentate-coordinated ligands and silver centres of neighbouring tapes.

Above all, the PXRD patterns have proved the phase purity of the non-arene-containing coordination polymers. Although none of the arene-containing coordination polymers are phase pure, many of them are the majority phase in the mixture and the second phase could result from the desolvation of the compounds. This is consistent with the fact that the crystals lose solvent very quickly once removed from the solvent (5-10 mins even in the oil). The suggestion of minimizing this process could be in transmission as a wet sample to avoid the solvent loss.

3.3.3 Thermogravimetric analyses (TGA)

With the same interest in exploring the possible solid-state transformations, two coordination polymers, **11** and **12**, phase purity of both of which was confirmed, were all examined with TGA. Temperature-sweep TGA plots are shown for compounds **11** and **12** in **Figures 3.11** and **3.12**, respectively. Analyses of the mass changes observed are provided in **Tables 3.3** and **3.4**. Isothermal TGA plots for **12** are shown in **Figure 3.13**.



There is no evidence of ligand loss in stages, which mainly showed a degradation of this material to a silver-containing mixture. The final residue continuously lost some components (which were estimated to be CO₂) during the period of the fixed temperature range (see **Table 3.4**).

Table 3.4 Temperature-sweep TGA mass losses for $[\text{Ag}_4(\text{O}_2\text{CCF}_3)_4(2\text{-Me-quin})_2]$

Onset Temperature (°C)	Lost component	Calculated Mass Contribution (%)	Observed Mass Contribution (%)	Residue
175	degradation	52.93	51.41	$2\text{Ag}_2\text{CO}_3$



In this material, one single-ligand loss stage similar to those found in quinoxaline-containing coordination polymers (Chapter 2) was observed. However, different from the quinoxaline-containing materials, there were no secondary mass loss stages before the degradation (see **Table 3.5**).

Table 3.5 Temperature-sweep TGA mass losses for $[\text{Ag}_6(\text{O}_2\text{C}(\text{CF}_2)_3\text{CF}_3)_6(2\text{-Me-quin})_4]$

Onset Temperature (°C)	Lost component	Calculated Mass Contribution (%)	Observed Mass Contribution (%)	Residue
125	1(2-Me-quin)	5.15	5.53	$\text{Ag}_6(\text{O}_2\text{CCF}_2\text{CF}_3)_6(2\text{-Me-quin})_3$
190	3(2-Me-quin), 6((CF ₂) ₃ CF ₃)	62.27	61.68	$3\text{Ag}_2\text{C}_2\text{O}_4$
275	3CO, 3CO ₂	6.42	6.07	$3\text{Ag}_2\text{O}$

The isothermal TGA did show a 5~6% mass loss which is similar to that provided by the temperature-sweep TGA data. However the intermediate product was not thermally stable, implying that other 2-Me-quinoxaline ligands might leave the structure after the loss of the first ligand.

TGA was not performed for the propanoate/butanoate-containing coordination polymers because none of them could be prepared with phase purity, although different thermal behaviours might be observed for the different phases present. The rapid solvent loss during the sample preparation might complicate the actual total mass of the compound as well. PXRD heating studies were also not performed for these compounds for the same reason. Even for compound **13**, the potential intermediate phase is thermally unstable.

3.4 Conclusion

In summary, the use of 2-Me-Quin ligands has led to different types of structures that have not been observed in previous studies of silver-perfluoroalkylcarboxylate-diimine coordination polymers. Some of them even exhibit new stoichiometric ratios of the three main components, such as 6:6:4 and 4:4:5 for Ag:carboxylate:diimine. These structures, though, still have strong structural relationships to the former structures containing different diimines. For example, all of them still contain the doubly-bridging diamine-ligand connecting mode with $\{\text{Ag}_4(\text{O}_2\text{CR})_4(\text{diimine})_2\}$ units except for **20**. For the structures generated in different arene solvents, although none of those could be shown to be phase pure, they still offer important insights in completing the structural landscape of these silver and diimine ligand coordination polymers. Future studies for this 2-Me-Quin project can be focused on two parts. The first part will be further determination of the structures introduced in this section. Most of them require further optimization of synthetic conditions to improve the quality of the single crystals. Collecting SCXRD data at Diamond Light Source might solve the weak-diffraction problem of crystals as it offers greater X-ray flux. Attempts to modify the ratios of the solvent systems and also the evaporation speed of solvents might be useful in solving the phase purity problem. Secondly, the structures of 2-Me-quin coordination polymers seem to be far more flexible and abundant than any other system we studied before. It will be of great interest to examine other solvent systems (and a variety of combinations) to see whether new phases or structures can be generated.

3.4 Reference

- 1 S. Ohmori, M. Mori, M. Kawase and S. Tsuboi, *J. Chromatogr.*, 1987, **414**, 149–155.
- 2 J. R. Allan, A. D. Paton, A. J. Blake and K. Turvey, *Acta Crystallogr.*, 1989, **C45**, 1422–1424.
- 3 G. K. Kole and J. J. Vittal, *Chem. Soc. Rev.*, 2013, **42**, 1755–1775.
- 4 W. M. Bloch and C. J. Sumbly, *Eur. J. Inorg. Chem.*, 2015, **2015**, 3723–3729.
- 5 J. S. Wright, I. J. Vitórica-Yrezabal, S. P. Thompson and L. Brammer, *Chem. Eur. J.*, 2016, **22**, 13120–13126.
- 6 G. M. Sheldrick, *Acta Crystallogr.*, 2008, **A64**, 112–122.
- 7 O. V Dolomanov, L. J. Bourhis, R. J. Gildea, J. A. K. Howard and H. Puschmann, *J. Appl. Cryst.*, 2009, **42**, 2008–2010.
- 8 R. H. Blessing, *Acta Crystallogr.*, 1995, **A51**, 33–38.
- 9 G. M. Sheldrick, *Univ. Göttingen*, 1997.
- 10 L. Krause, R. Herbst-Irmer, G. M. Sheldrick and D. Stalke, *J. Appl. Cryst.*, 2015, **48**, 3–10.
- 11 G. S. Pawley, *J. Appl. Cryst.*, 1981, **14**, 357–361.
- 12 A. A. Coelho, *TOPAS-Academic, Version 4.1*, 2007, see <http://www.topas-wwwww.academic.net>.
- 13 J. S. Wright, I. J. Vitórica-Yrezabal, H. Adams, S. P. Thompson, A. H. Hill and L. Brammer, *IUCrJ*, 2015, **2**, 188–197.
- 14 I. J. Vitórica-Yrezabal, S. Libri, J. R. Loader, G. Míguez Espallargas, M. Hippler, A. J. Fletcher, S. P. Thompson, J. E. Warren, D. Musumeci, M. D. Ward and L. Brammer, *Chem. Eur. J.*, 2015, **21**, 8799–8811.

4. Conclusions

4.1 Conclusion

In the past years, our group have studied a series of coordination polymers formed with different types of silver perfluoroalkylcarboxylates and diimine ligands ($[\text{Ag}_4(\text{OOCR})_4(\text{diimine})_n]$), referred to as 4:4:n which describes the ratio between the components of silver: perfluorocarboxylate: ligand). We are interested in understanding the relationships within this extensive family of structures, including the structural relationships and transformations (especially under solid-state heating). This project has allowed two new pieces of the overall puzzle to be put in place by describing two new families of compounds involving quinoxaline and 2-methylquinoxaline ligands.

Coordination polymers with silver perfluoroalkylcarboxylate and quinoxaline ($[\text{Ag}_4(\text{OOCR})_4(\text{Quin})_n]$) has been discovered to have two types of basic structural units, referred to as 4:4:4 and 4:4:3 ratio structures. All the structures have been studied and the solid-state thermal transformations from 4:4:4 phases to 4:4:3 phases have been demonstrated with PXRD *in situ* heating studies. This single-ligand loss process is similar to what was reported in the related TMP-containing coordination polymers, although this involved 4:4:3 phase to 4:4:2 phase conversion. It also suggests the possibility of preparing new compounds by losing one ligand per formula unit in the solid-state when solution-phase syntheses do not work.

Coordination polymers formed from silver perfluoroalkylcarboxylate and 2-methylquinoxaline ($[\text{Ag}_m(\text{OOCR})_m(2\text{-Me-quin})_n]$) have been demonstrated to cover the widest range of different structures when compared to families involving other diimine ligands. Rather than having similar structures, most of them are very different to each other when increasing the perfluoroalkyl chain length of the carboxylate ligands. Some novel structures with new component ratios (e.g. 4:4:5 and 6:6:4) and new coordination environments (e.g. monodenate diimine ligands) are found among these structures. Attempts to synthesize coordination polymers in different arene solvents have resulted in a variety of structures which has similar or even same basic structure units but different layer structures or habits in adsorbing solvents. Thus, the results suggest the existence of solvent affect influencing the formation of these structures based on different choice of arenes.

The contribution of the work in this thesis to a larger ongoing project on silver perfluoroalkylcarboxylate and diimine coordination polymers is illustrated in the summary of the compounds studied shown in **Figure 4.1**. These coordination polymers share similar structures and solid-state transformation properties. There are 5 types of basic structure

component ratios identified so far studied. The 4:4:3 phases are the most common phases as all the studies diimine ligands studied form coordination polymers in this phase and the number of structures is the largest.¹⁻³ This type of structure has a common structure unit formed with two pairs silver perfluorocarboxylate coordinated with one pair of doubly-bridging ligand($[(Ag_4(O_2CR)_4(diimine)_2)]$) and another singly-bridging ligand, giving $[(Ag_4(O_2CR)_4(diimine)_3)]$. The 4:4:2 phase is the next common structure type.^{1,3,4} They do not have the singly-bridging ligands compared to the 4:4:3 phases and a solid-state transformation from 4:4:3 phase into 4:4:2 phase by losing these singly-bridging ligands³ has been demonstrated in the TMP-containing coordination polymers. In between these two phases in component ratio, is a so far unique 6:6:4 (4:4:2.667) phase, synthesized with silver perfluoropentanoate and the 2-Me-quin ligand. This is the first structure which does not follow 4:4:n ratio in this family as it contains extra $[(Ag_2(O_2CR)_2]$ units which are not involved in the doubly-bridging coordination with the diimine ligands. The 2-Me-quin ligand results in the greatest diversity of structures types. Apart from 6:6:4 phase, it also forms the only 4:4:5 phase and one 4:4:4 phase, both of which have monodenate ligands in their structures, which are distinctive from all other structures. 4:4:4 phases with a different 2D structure are formed with the quinoxaline ligand and their transformation from 4:4:4 phase into 4:4:3 phases have been demonstrated.

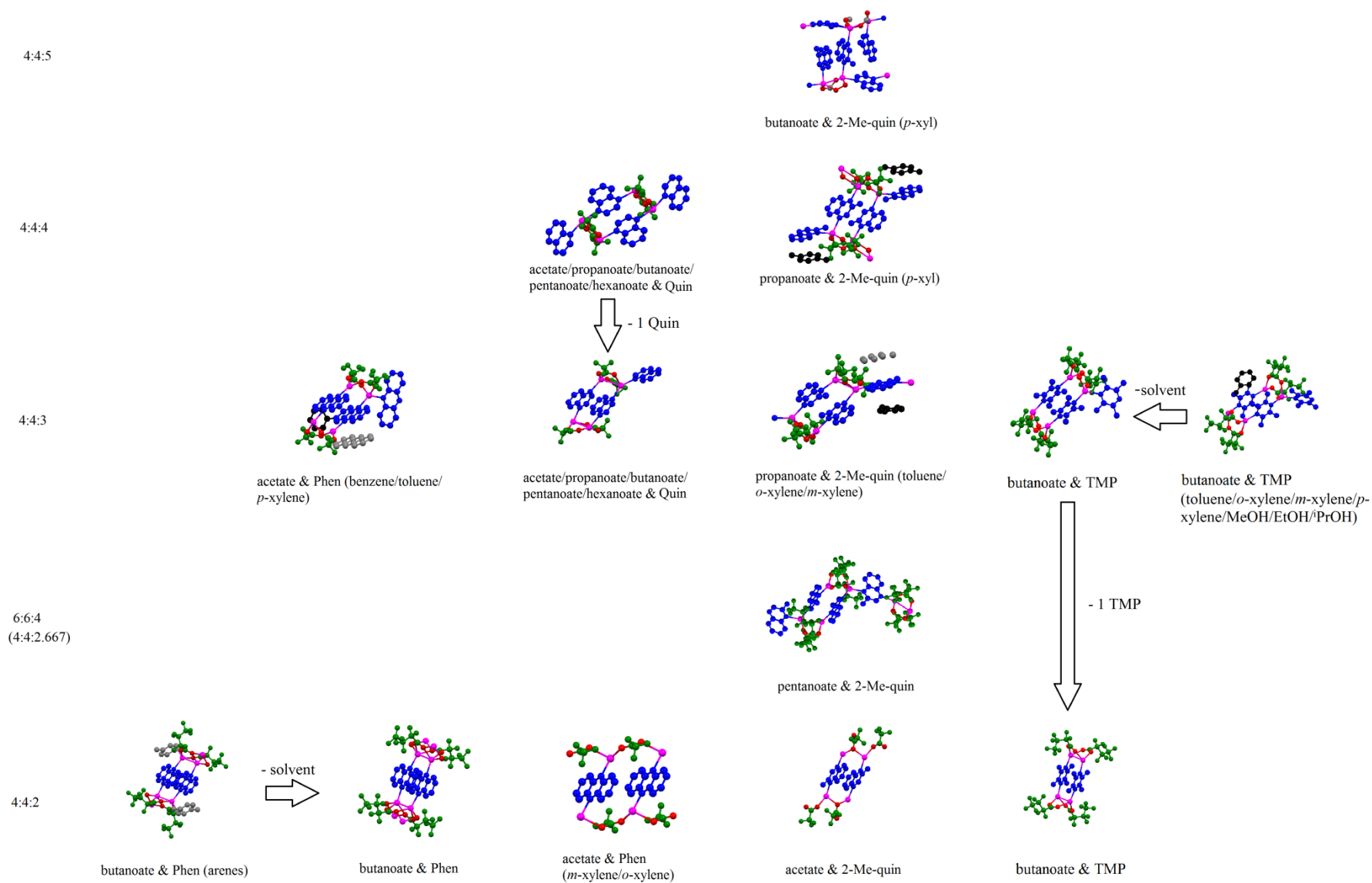


Figure 4.1 Overview of different types of silver perfluoroalkylcarboxylate and diimine coordination polymers. Solid-state transformations are represented by arrows. For each structure the carboxylate(s) and diimine used are noted (Phen = phenazine, Quin = quinoxaline, 2-Me-quin = 2-methylquinoxaline). Trapped solvent indicated in parentheses.

4.2 Future work

Some of the research covered in this thesis could be taken forward in further studies. In the work relating to quinoxaline-containing coordination polymers (chapter 2), the possibility of solid-state transformation from 4:4:3 coordination polymers into 4:4:2 coordination polymers by heating is still uncertain, although TGA results suggest this may be possible. It would be interesting therefore to explore the potential two-step-transformation (4:4:4 \rightarrow 4:4:3 \rightarrow 4:4:2) for some of the coordination polymers in this series. In the work on 2-Me-quinoxaline-containing coordination polymers (chapter 3), a further range of other solvents could be tested in forming potential different types of structures to broaden the scope of the project.

Solid-state transformations for coordination polymers in the literature are mostly related with the guest (solvent/gas) molecules while the solid-state structure transformations by losing ligand molecules under heating are much less common. However, the project demonstrated in this thesis only has only scratched the surface of this topic. Further studies can be focused on finding out the potential principle which explains how and in what preferences do these compounds lose their ligands under solid state. Meanwhile, this will also require further expansion in the diimine ligands to study such as 2,3-dimethylquinoxaline.

4.3 References

- 1 J. S. Wright, I. J. Vitórica-Yrezabal, S. P. Thompson and L. Brammer, *Chem. Eur. J.*, 2016, **22**, 13120–13126.
- 2 I. J. Vitórica-Yrezabal, G. Míguez Espallargas, J. Soleimannejad, A. J. Florence, A. J. Fletcher and L. Brammer, *Chem. Sci.*, 2013, **4**, 696–708.
- 3 I. J. Vitórica-Yrezabal, S. Libri, J. R. Loader, G. Míguez Espallargas, M. Hippler, A. J. Fletcher, S. P. Thompson, J. E. Warren, D. Musumeci, M. D. Ward and L. Brammer, *Chem. Eur. J.*, 2015, **21**, 8799–8811.
- 4 J. S. Wright, I. J. Vitórica-Yrezabal, H. Adams, S. P. Thompson, A. H. Hill and L. Brammer, *IUCrJ*, 2015, **2**, 188–197.